Systematic Tailplane Design for an Aircraft Family Concept

MSc Thesis

Ángel Garmilla Manzano

Delft University of Technology

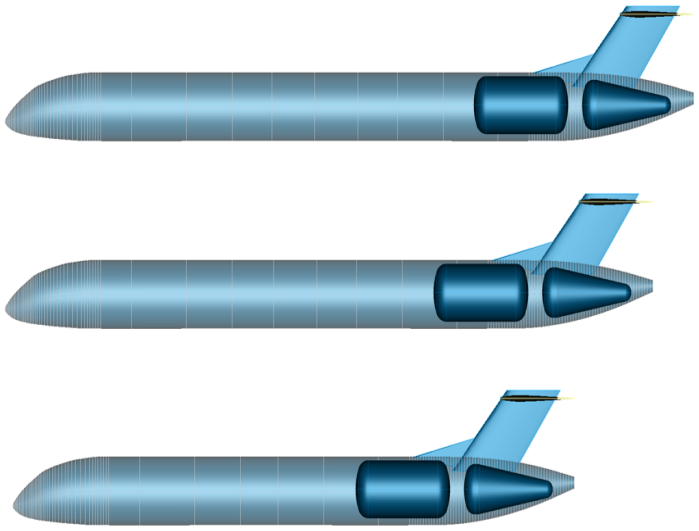

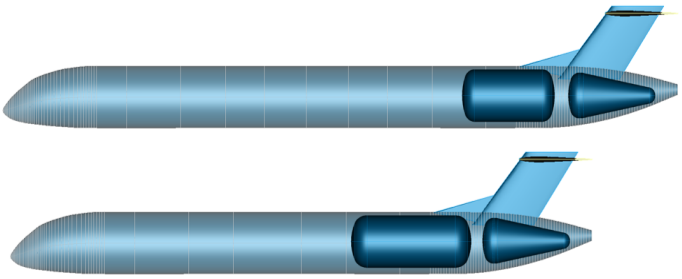

TU Delft

DLR Deutsches Zentrum für Luft- und Raumfahrt

Systematic Tailplane Design for an Aircraft Family Concept

MSc Thesis

by

Ángel Garmilla Manzano

to obtain the degree of Master of Science
at the Delft University of Technology,
to be defended publicly on November 13, 2024 at 1:00 PM.

Student number:	5848768	
Project duration:	February 10, 2024 – November 13, 2024	
Thesis committee:	Dr. ir. R. Vos,	TU Delft, supervisor
	Dr. S. Asaro,	TU Delft, supervisor
	Dr. F. Oliviero,	TU Delft
	Dr. ing. S. Giovani Pereira Castro,	TU Delft
	F. Fritzsche,	DLR-SL, supervisor

An electronic version of this thesis is available at `http://repository.tudelft.nl/`.

TU Delft

DLR Deutsches Zentrum für Luft- und Raumfahrt

Preface

This report presents the outcomes of my MSc graduation thesis, conducted as part of the Flight Performance & Propulsion Track at Delft University of Technology, in collaboration with the DLR Institute for Systems Architectures in Aeronautics in Hamburg. Over this nine-month project, I worked on the conceptual design of liquid hydrogen aircraft families, focusing on tailplane sizing and commonality among family members.

I would like to start by acknowledging everyone at the DLR Institute for Systems Architectures in Aeronautics, particularly the members of the Overall Aircraft Design team, where I began my journey as a research intern in August 2023. Over the past year and a half, this experience has not only accelerated my academic growth but also allowed me to connect with many inspiring and ambitious researchers. Special thanks to my supervisors, Felix Fritzsche and Daniel Silberhorn, for giving me the opportunity to explore liquid hydrogen aircraft design, providing me with essential tools and feedback throughout. I am also deeply grateful to my TU Delft colleague, Petr Martinek, with whom I began this journey. His support during challenging moments has been invaluable.

A heartfelt thanks also goes to my TU Delft supervisors for their time and continued support. I want to especially thank Dr. Salvatore Asaro for supervising me remotely and offering critical feedback on my results. My gratitude also extends to Dr. Roelof Vos for his insightful inputs during our meetings, which greatly shaped the outcome of this project.

I am immensely thankful for these two years in both Delft and Hamburg, where I met incredible people who have become lifelong friends. While I do not know where our ambitions will lead us, I will always carry the memories of these two places and the amazing people I met in my heart.

Por último, me gustaría expresar mi más profundo agradecimiento a mis padres por todo su amor, apoyo moral y económico durante mi estancia en Delft y Hamburgo. A pesar de la distancia, que no ha sido fácil, siempre han estado ahí para mí. También quiero agradecer a mis hermanos Jaime y Juan por su apoyo constante. Su presencia, aunque desde lejos, ha sido una fuente de fortaleza y motivación a lo largo de este camino.

Ángel Garmilla Manzano
Hamburg, October 2024

Abstract

Liquid Hydrogen (LH2) appears as one of the leading solutions for sustainable aviation, especially as the industry anticipates significant growth in the coming years. Multiple academic studies demonstrate the feasibility of LH2 aircraft designs, with rear-fuselage tanks being one of the preferred options for fuel integration in conventional tube & wing aircraft configurations. Most conceptual aircraft design studies follow a point design approach, where components are sized for a specific aircraft. This approach has revealed limitations in the aforementioned concepts, particularly highlighting the large horizontal tailplane (HTP) needed to maintain feasible operations due to the increased longitudinal center of gravity (CG) travel. However, few studies adopt the industry approach of the family concept, where programs are developed to produce multiple aircraft designs with a high degree of commonality, grouping them into the same aircraft family. In conventional aircraft families, the empennage is typically shared across members, even though each aircraft has an optimal size due to variations in lever arm. Studies have shown that the benefits of commonality outweigh the associated performance penalties.

This thesis examines the effect of this industry decision in conceptual aircraft design studies involving LH2 aircraft with rear-fuselage tanks. The report outlines the general trends observed for tailplane sizing in an LH2 aircraft family, with a special focus on horizontal tailplane sizing and its comparison to the traditional kerosene designs regarding the commonality penalties incurred. A methodology was developed which sizes an aircraft influencing the design of the horizontal and vertical tailplanes (HTP and VTP) by the definition of two potential shorter family members. All three aircraft are designed simultaneously, resulting in a converged family with a common empennage size. Special emphasis is placed on the HTP sizing routine. The aircraft sizing workflow has been validated against publicly available data for the A320neo family. In this family design, a trade-off is given between payload and range, while fuel capacity remains constant. The results align with the expected behavior for kerosene-fueled aircraft: reducing the fuselage length leads the smallest aircraft to determine the size of both the HTP and VTP due to its shorter lever arm. The same tailplane is used across all members of the aircraft family, with the associated commonality penalties being considered as a reasonable trade-off.

In the context of LH2 aircraft concepts featuring rear tanks, notable trends have emerged concerning the tailplane sizing process. As anticipated, the horizontal tailplane for these designs is considerably larger than that of kerosene-powered aircraft. Conventional volume coefficient statistics are no longer useful for estimating the HTP size of these designs, which require a value 40%-50% bigger. The aft landing gear position due to the cryogenic tanks reduces the tail lever arm, making the take-off rotation requirement the primary factor in the sizing process.

Regarding the commonality of the empennage among family members, a general trend is observed in a family in which payload is reduced to increase range while maintaining the same fuel capacity. The optimum HTP size for each family member is much closer than in a kerosene aircraft family. This is due to the shorter CG range in the case of the shorter family versions, which compensates for the shorter lever arms. Consequently, for an LH2 family of these characteristics, a smaller performance penalty due to empennage commonality is given than for kerosene designs. However, other LH2 family design strategies that involve increasing the fuselage length—whether by raising the payload, fuel capacity, or both—have a significantly larger impact on tailplane commonality, in contrast to what is observed for kerosene designs. An increase in the fuselage length increases the relative distance of the tank to the wing, and thus the CG range, which is critical for the final HTP size of the family.

Contents

List of Figures

List of Tables

Nomenclature

Abbreviations

Abbreviation	Definition
ADAS	Aircraft Design Analysis Software
AP	Airport Conditions
AR	Aspect Ratio
ac	Aerodynamic Center
BF	Block Fuel
BWB	Blended Wing Body
CAD	Computer Aided Design
ceo	Current Engine Option
CFD	Computational Fluid Dynamics
CFRP	Carbon-fiber Reinforced Polymer
CG	Center of Gravity
CPACS	Common Parametric Aircraft Configurations Schema
DLR	Deutsches Zentrum für Luft-und Raumfahrt
DLR-SL	DLR - System-architekturen in der Luftfahrt
DOE	Design of Experiments
DPR	Dynamic Pressure ratio
EASA	European Union Aviation Safety Agency
ECS	Environmental Control Systems
EIS	Entry Into Service
ER	Extended Range
EXACT	Exploration of Electric Aircraft Concepts and Technologies
FEM	Finite Element Methods
FLOPS	Flight Optimization System Weights Estimation Method
GH2	Gaseous Hydrogen
HTP	Horizontal Tailplane
IAS	Indicated Air Speed
ISA	International Standard Atmosphere
LH2	Liquid Hydrogen
LR	Long Range
MAC	Mean Aerodynamic Chord
MDO	Multidisciplinary Design Optimization
MFM	Mission Fuel Mass
MLI	Multi-Layer Insulation
MLM	Maximum Landing Mass
MTOM	Maximum Take-Off Mass
MZFM	Maximum Zero-Fuel Mass
NASA	National Aeronautics and Space Administration
neo	New Engine Option
NOx	Oxides of nitrogen

Abbreviation	Definition
NP	Neutral Point
OAD	Overall Aircraft Design
OEI	One-Engine Inoperative
OEM	Operating Empty Mass
PASS	Program for Aircraft Synthesis Studies
PBD	Point-Based Design
RANS	Reynolds Average Navier-Stokes
RCE	Remote Component Environment
SAF	Sustainable Aviation Fuel
SBD	Set-Based Design
SL	Sea Level
SM	Static Margin
SMR	Short-Medium Range
TAS	True Air Speed
TET	Turbine Entry Temperature
TOC	Top-of-Climb
THS	Trimmable Horizontal Stabilizer
TLARs	Top Level Aircraft Requirements
TOFL	Take-off Field Length
T & W	Tube & Wing
VLM	Vortex Lattice Method
VTP	Vertical Tailplane
XML	Extensible Markup Language

Symbols

Symbol	Definition	Unit
a	Speed of sound	[m/s]
AR	Aspect ratio	[-]
b	Wingspan	[m]
b_f	Fuselage width	[m]
c	Section chord length	[m]
$c^{'}$	Section chord length with flap	[m]
$\overline{c}$	Mean aerodynamic chord (MAC)	[m]
c_{HT}	Horizontal tail volume coefficient	[-]
c_{VT}	Vertical tail volume coefficient	[-]
c_L	2D lift coefficient	[-]
C_D	Drag coefficient	[-]
C_{D0}	Zero-lift drag coefficient	[-]
C_L	Lift coefficient	[-]
$C_{L\alpha}$	Lift curve slope	[rad^{-1}]
$c_{m,ac}$	2D pitching moment coefficient around the aerodynamic center (or zero-lift pitching moment coefficient)	[-]
C_m	Pitching moment coefficient	[-]
$C_{m,ac}$	Pitching moment coefficient around the aerodynamic center	[-]
D	Drag force	[N]
dm_f/dl_f	Change in fuselage mass per meter of cabin section	[kg/m]
e	Oswald factor	[-]
g	Gravitational constant	[m/s^2]
h_f	Height of the fuselage	[m]
I_{yy}	Mass moment of inertia around the y-axis	[kg·m^2]
i_h	Horizontal tail incidence angle	[rad]
i_w	Wing incidence angle	[rad]
k	Airfoil efficiency factor	[-]
l_f	Length of the fuselage	[m]
l_h	Horizontal tail lever arm	[m]
l_v	Vertical tail lever arm	[m]
L	Lift force	[N]
m	Mass	[kg]
M	Pitching moment	[N·m]
$Mach$	Mach number	[-]
n	Number of	[-]
N	Normal force	[N]
q	Dynamic pressure	[Pa]
R	Reaction force	[N]
S	Reference area	[m^2]
S_{net}	Net wing reference area	[m^2]
V	Velocity	[m/s]
T	Thrust	[N]
x	Longitudinal distance measured along the x-axis, starting from fuselage nose	[m]
$\overline{x}$	Dimensionless x distance with MAC	[-]
xsi_{mg}	Main landing gear dimensionless position along the wing chord	[-]
W	Weight	[N]
z	Vertical distance along z-axis, measured from fuselage center line	[m]
α	Angle of attack	[rad]

Symbol	Definition	Unit
β	Prandtl-Glauert compressibility correction factor	[-]
Δ	Increment	[-]
Δl_{VTP}	change in fuselage length due to sections added behind the wing	[m]
δ	Control surface deflection angle	[rad]
ε	Downwash angle	[rad]
ε_t	Wing twist	[rad]
λ	Taper ratio	[-]
Λ	Sweep angle	[rad]
μ	Runway friction coefficient	[-]
ρ	Density	[kg/m^3]
$\ddot{\theta}$	Angular acceleration	[rad/s^2]

Subscripts

Symbol	Definition
ac	aerodynamic center
$c/4$	quarter chord position
$c/2$	mid chord position
$cabin$	relative to the cabin
e	elevator
cg	center of gravity
$clean$	clean configuration
CP	center of pressure
E	due to the engine thrust
f	relative to the fuselage
$fuel$	relative to the fuel
$flap$	due to flap deflection
$flapped$	affected by flaps
h	relative to the horizontal tail
LE	leading edge
$long$	relative to the long family member
m	relative to a mass
$main$	relative to the main aircraft family member
max	maximum of the value assigned to
mg	relative to the main landing gear
$misc$	miscellaneous
mu	minimum unstick
np	neutral point
r	rolling
$root$	wing root station location
R	rotation
S	stall
$sizing$	relative to the sizing family member for the HTP/VTP
sys	relative to the aircraft systems
tip	wing tip station location
v	relative to the vertical tail
$version$	relative to an aircraft family version
w	wing
wf	wing fuselage

1 Introduction

Aviation must shift to alternative energy sources to meet the 2050 zero-emission goals, as fossil fuels and efficiency improvements are no longer sufficient [1]. With passenger traffic projected to grow by nearly 4% annually [2], the need for alternative propulsion methods is critical. Liquid hydrogen (LH2) has emerged as one of the leading solutions, supported by numerous studies [1] [3]. Although not a new concept, advances in technology and government incentives have reignited the interest in LH2-powered aircraft. While real-world demonstrators, such as Airbus' ZeroE project [4], are underway, most of the interest is reflected in the growing number of academic publications focused on the conceptual design of such vehicles.

The research objective of this thesis is to explore the design space for LH2-powered aircraft families, with a special focus on the tailplane sizing process and its commonality among family members. The motivation, research questions, and structure of the work are outlined in the following sections.

1.1. Motivation & Research Questions Definition

Most academic publications on conceptual aircraft design use a point-based design (PBD) approach, focusing on individual aircraft requirements without accounting for potential family members. This contrasts with industry practices, where the family concept is widely used.

The horizontal and vertical tailplanes (HTP and VTP) are among the most impacted components when stretching or shrinking the fuselage in an aircraft family. Changes in fuselage length alter the moment arms, requiring adjustments to the moment equilibrium to meet the trim, stability, and control requirements [5]. Ideally, each family member would have a tailored empennage size for optimal weight and drag. However, to increase commonality, the empennage is shared across family members, resulting in oversized lifting surfaces and a trade-off between performance and commonality.

The first goal is then to develop a new methodology for conceptual aircraft design to systematically size an aircraft while considering potential family members, aligning with industry practices. Special attention is given to the empennage, as both HTP and VTP are affected by aircraft family design. In this context, the first research question for the study arises: **How well can we estimate the size of the vertical and horizontal tailplanes of an aircraft during the conceptual design phase, when potential family members are already considered in the design loop, defined by their top level aircraft requirements (TLARs)?**

Historically, using a common empennage across family members has proven feasible, offering benefits in commonality despite some performance penalties. However, this approach may need to be reevaluated for future generations of aircraft.

As mentioned before, LH2 is emerging as one of the leading solutions for a new energy carrier. Among the preferred designs are aircraft that feature rear fuselage-mounted LH2 tanks [6] [7]. Nevertheless, these concepts pose challenges for aircraft longitudinal stability and control, impacting HTP design. The presence of rear tanks significantly affects mass distribution, leading to increased longitudinal center of gravity travel and, consequently, larger HTP size. Several studies agree that for LH2 aircraft with rear-fuselage tanks, the HTP becomes critical due to the substantial surface area required [8] [9] [10]. However, no study to date has specifically addressed how the sizing process of this component operates within an aircraft family and the performance penalties associated to its commonality. From this claim, the second research question arises: **What are the performance penalties in an LH2 aircraft family when the same horizontal tailplane is shared among all family members, as has been traditionally done for kerosene aircraft?**

Moreover, the LH2 aircraft family design space is still largely unexplored. There are very few publications that examine how the added degree of freedom introduced by the cryogenic tanks affects the family design. It remains to be seen how the tank and its commonality can affect the performance and the tailplane commonality, when different design strategies are used; i.e. varying payload, or varying fuel capacity among family members. From these claims, the last research question arises: **How do different strategies for LH2 aircraft family design influence the commonality of the tailplane?**

1.2. Thesis Outline

The thesis aims to integrate the three concepts discussed in the introduction—tailplane sizing, aircraft family design, and LH2 aircraft—within the framework of a conceptual aircraft design study. The document is structured in the following way to find an answer to the research questions stated above.

Chapter 2 reviews the state-of-the-art in the three areas: horizontal tailplane sizing during the conceptual aircraft design phase, the aircraft family concept, and LH2 aircraft. In Chapter 3, the methodology is explained. A DLR-developed conceptual aircraft design workflow has been enhanced and modified to address the research questions. The improved workflow is able to systematically size an aircraft, with special emphasis on its tailplane, considering not only the given TLARs but also potential family members. A special section is dedicated in this chapter to further detail the methodology used for HTP sizing. Additionally, the reference and baseline aircraft, together with the LH2 aircraft concepts of the study are outlined in this third chapter

Note that significant emphasis is placed on the horizontal tailplane sizing methods used, in both the literature review and methodology chapters. This focus is justified by the substantial impact that rear-mounted LH2 tanks have on the HTP, which requires a higher level of fidelity to accurately capture its sizing. In contrast, a simpler empirical formula is used for vertical tailplane sizing, as further discussed in Chapter 3. While this approach offers a lower level of fidelity, it still effectively captures the differences in VTP size among the various family members.

Chapter 4 outlines the validation and verification procedures followed for the methodology, using the D239 reference aircraft [11], the DLR interpretation of the A321neo. In Chapter 5 the methodology is used for the family design of two DLR aircraft concepts that were results of the EXACT project [12]: the D250 [11] and D250-LH2 [13]. Moreover, a design space exploration is carried out for different LH2 aircraft family design strategies, addressing the impact of each of them on the tailplane commonality. Chapter 6 concludes the report, summarizing the general trends identified for tailplane sizing and its commonality, and providing some first guidelines for the design of LH2 aircraft families with rear-fuselage tanks.

2

State of the Art

This chapter showcases the state of the art of the three disciplines that are interconnected in the thesis work. Section 2.1 presents a summary of the current methodologies available for horizontal tailplane sizing, and are used during the aircraft conceptual design phase. Section 2.2 dives into the topic of aircraft family, and how this concept can be considered since the early stages of the aircraft design process. Section 2.3 reviews the state of the art of LH2 aircraft concepts.

2.1. Horizontal Tailplane Sizing in Conceptual Aircraft Design

2.1.1. Aircraft design process: Conceptual aircraft design

The conceptual aircraft design phase is the first step in every aircraft design project. The process starts with a given set of requirements, often referred to as Top Level Aircraft Requirements (TLARs). These either come from a prospective customer or a market study done by the company. These requirements lead to the first definition of the aircraft layout, the geometry and position of the different components, and the adequate technologies to include in the design. Basically after this stage, the main questions regarding configuration, weight, size, costs, aerodynamics, propulsion, performance, and technology have to be answered [14].

During the conceptual design, multiple configurations and alternative designs are compared. Trade-off studies are conducted, to determine which configuration performs better for the given set of requirements. The concept evolves continuously through an iterative design process, in which optimization techniques are used to come up with the most cost-efficient design [14].

The expected outcome is an aircraft concept that is "frozen" and can go on to the next stage of the design, the preliminary design phase. During the preliminary design phase, more changes are expected to be made to the concept. Nevertheless, major changes in the configuration are not expected to come up, if everything has been done correctly during the first stage of the design. The final conceptual design is now analyzed more in detail with more complex methods, and optimized again and again. The final product from the preliminary design will go to the third design phase, the detail design. In this phase, the actual parts get designed and manufactured, including all components from all systems and subsystems [14]. The three design phases for a front wing spar can be visualized in the example from Figure 2.1.

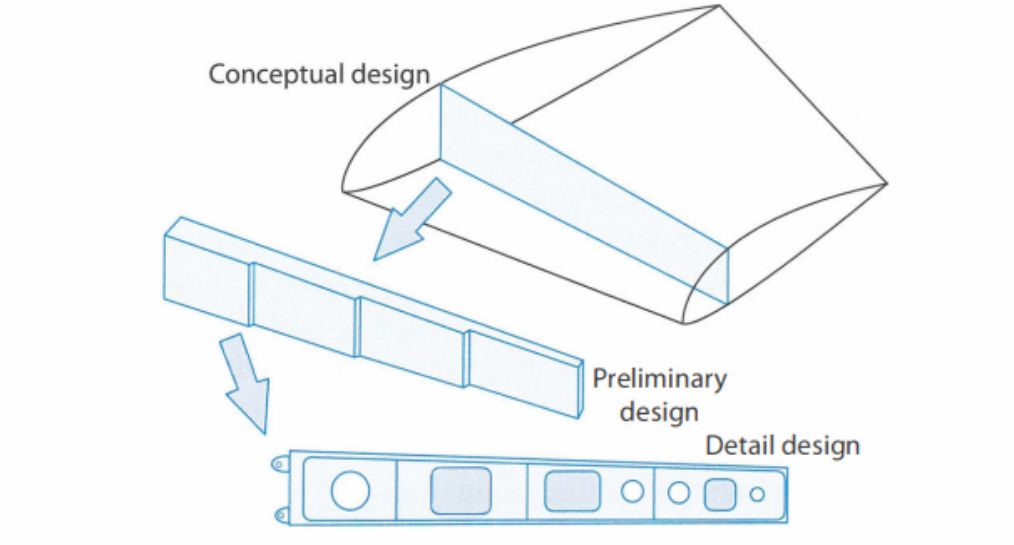

Figure 2.1: Design phases for a front wing spar [14]

Consequently, the design choices made during the aircraft conceptual design phase will govern the progress and outcome of the project, as well as its profitability. It is also a crucial phase in the sense that there is a lot of uncertainty attached to most of the assumptions and methodology used [15]. As stated by Daniel Raymer in his book *Aircraft Design: A Conceptual Approach* (2018): "Aircraft conceptual design is a separate discipline, with its own history, methods, and rules of thumb. It's a skill that takes education and experience to perfect" [14].

During the conceptual design, most methods used are semi-empirical or statistical. These methods are simple mathematical formulas, that come either from theoretical assumptions, from simple physics models, or from curve-fitting on experimental evidence. Aircraft design books like [5] [14] [16] and results from wind tunnel experiments like [17] are some examples. Their simplicity and computational efficiency allow for the evaluation and optimization of multiple designs in a short period, making them suitable for the conceptual design phase [18].

These low-fidelity methods that help the designer to study the aircraft's performance while its geometry is not yet well defined, evolve into more advanced mid and high-fidelity methods during the following design phases. More advanced Computer-Aided Design (CAD), Computational Fluid Dynamics (CFD), and Finite Element Method (FEM) tools, as well as wind tunnel testing, are used as the design advances, and significant changes in the configuration start to become costly [14].

2.1.2. Horizontal tailplane sizing process

"During the preliminary design stage, the tail surfaces may present one of the most difficult problems in the dimensioning of the main parts of the aircraft, and this, in turn, may lead to many iterations," as Egbert Torenbeek highlights in his book Synthesis of Subsonic Airplane Design (1982) [5]. This statement underscores the complexity of the aircraft´s tail surfaces design process.

The design of the empennage is closely related to all disciplines involved in the aircraft design. A good aerodynamic and engine model, an accurate mass distribution and moments of inertia calculation, and even aeroelastic considerations; are all needed to have a good estimation of the required horizontal and vertical tail size. The final design will have to satisfy several control and stability constraints, that are to be evaluated around the whole operating flight envelope of the aircraft [5].

The empennage in a conventional transport aircraft is divided into two lifting surfaces. Both vertical and horizontal tails are responsible for three main functions: providing static as well as dynamic stability; providing aircraft control through its movable control surfaces (elevator and rudder); and allowing to

reach a state of equilibrium (trim) for a given flight condition. As a result, its size is determined by stability and control requirements [18]. Based on the aircraft design purpose, the lifting surfaces can be arranged into different configurations, as shown in Figure 2.2.

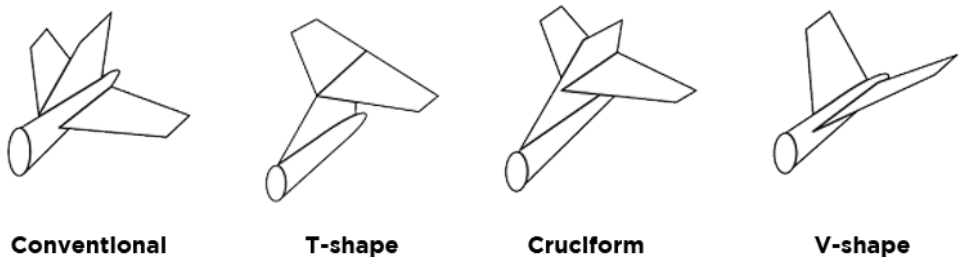

Figure 2.2: Different tail configurations [19]

The most common configuration for conventional transport aircraft is the conventional tail, followed by the T-Tail [14]. In the T-Tail configuration, the HTP is positioned high on the vertical stabilizer, keeping it clear of the disturbed airflow from the wing wake, which increases its efficiency and reduces the required size. However, this design also introduces the risk of a deep stall. A deep stall occurs when the wing´s airflow separates due to high angles of attack. This separation generates a turbulent wake that can envelop the T-Tail, making it ineffective for pitch control. In such a scenario, the aircraft may lose the ability to pitch-down and recover from the stall [19].

In the following subsections, a summary of the basic requirements currently considered for sizing the horizontal tail during the conceptual aircraft design phase is presented. As highlighted in Chapter 1, the thesis emphasizes the sizing of this component, as it has proven to be critical due to its large size in emerging LH2 aircraft concepts with rear fuselage integrated tanks [7] [8] [9]. These sections will serve as the baseline for the definition and justification of the methodology that will be used in this work for preliminary sizing the HTP.

2.1.2.1. Requirements for horizontal tailplane sizing

The horizontal tailplane must achieve equilibrium in steady flight (trim), ensure stability and effective damping of disturbances, and generate sufficient aerodynamic forces for control and maneuvering, especially during low-speed conditions, takeoff, and landing. It must do so with acceptable control forces [5]. These functions align with the certification specifications set by aeronautical bodies. These focus on control (CS-23.143/CS-25.143), trim (CS-23.161/CS-25.161), and stability (CS-23.171/CS-25.171) across all flight phases. More details can be found in EASA's (European Union Aviation Safety Agency) Certification Specifications and Acceptable Means of Compliance, for both large (CS-25) [20] and small aircraft (CS-23) [21].

The horizontal tail configuration for a conventional transport aircraft often includes a trimmable horizontal stabilizer (THS), together with the elevator [22]. The THS allows for the variation of the incidence angle at the tail. The tail will change its angle of attack, and with it, the resulting pitching moment to trim the aircraft and compensate for changes in the moment balance around the center of gravity (CG) during the different flight phases. On the other hand, the elevator is only used to control the aircraft in pitch. In the case of a fixed horizontal tail, the elevator will be responsible for both trim and control of the aircraft [22].

To model the aforementioned certification specifications, the following requirements have been found in literature. Each of them is used to size the HTP focusing on a given function of the lifting surface. The minimum tail size needed to trim and have a stable aircraft for all flight conditions is always pursued for a point design, to obtain the minimum drag and weight penalty [5]. These requirements also dictate the allowed forward and aft center of gravity position of the aircraft. The larger the tail, the larger the allowed longitudinal travel of the center of gravity [22].

- **Longitudinal control of the aircraft**
  The sizing requirement is based on the moment equilibrium around the center of gravity position (CG) of the aircraft [5] [23]. There must be a longitudinal equilibrium of all forces, that results in a moment equal to zero around this point. In this situation, the aircraft is said to be trimmed [24]. A representation of the forces and moments acting on the aircraft is shown in Figure 2.3. For a given aircraft configuration, the combination of lift from the wing-fuselage (L_{wf}) and the zero-lift pitching moment ($M_{ac_{wf}}$), along with the horizontal tail lift (L_h), must ensure that the total aircraft moment around the center of gravity is zero [5]. Some sources account also for the thrust (T) contribution [23]. Others like the drag are often neglected in most models in the literature.

  The tail will change its incidence angle and elevator deflection to compensate for the change in the flight conditions [24]. This requirement is referred to in [5] as the "Control capacity required to stall the aircraft". Among all flight conditions, the most critical from the control point of view usually will be the one when flying at maximum lift coefficient with full flaps deflected, and the center of gravity in its most forward position. The aircraft must be able to be trimmed in this scenario with reserve control capacity available for further maneuvering [5]. The expression for the calculation of this requirement is further discussed in Section 3.2.

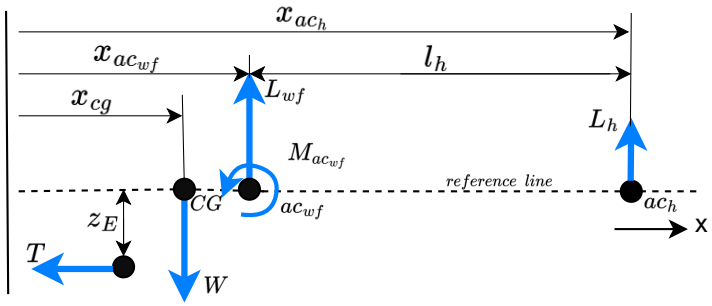

Figure 2.3: Schematic of the forces and moments acting on an aircraft considered for the calculation of the trimmed state [5] [23]

- **Longitudinal static stability of the aircraft**
  The second function of the HTP entails ensuring the stability of the aircraft during all flight phases. The longitudinal static stability is related to the capability of the aircraft to create the corresponding restoring pitching moment, as a response to steady perturbations (for instance the change in aircraft angle of attack due to a gust) [24]. A state of equilibrium must always be achieved by adjusting either the THS or the elevator [5]. The condition for static stability translates into the requirement that any change in the aircraft's pitching moment due to a positive angle of attack must result in a restoring moment that brings the aircraft back to its original attitude. Mathematically, this is expressed as $dC_m/d\alpha < 0$, where a negative value of the derivative of the pitching moment coefficient (C_m) with respect to the angle of attack (α) ensures a pitch-down attitude that opposes to the increase of the angle of attack.

  A disturbance in the longitudinal attitude of the aircraft ($\Delta\alpha$), creates an increment in the lift generated (ΔL). The resultant of this force is applied in the so-called neutral point (NP) along the longitudinal axis of the aircraft. A sketch based on the model from [5] is shown in Figure 2.4.

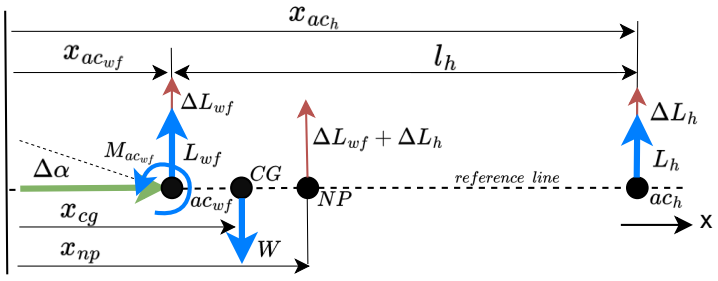

Figure 2.4: Geometric definition of neutral point (NP) [5]

If moment equilibrium around the center of gravity is taken for a given disturbance from the trimmed state (ignoring drag forces, propulsion forces and aeroelastic effects, and a constant control surface deflection), equation (2.1) results [5] [24]

$$C_m = C_{m,ac_{wf}} + \left[C_{L_{wf}} + C_{L_h} \frac{S_h}{S} \left(\frac{V_h}{V} \right)^2 \right] \cdot \frac{(x_{cg} - x_{np})}{\overline{c}} \tag{2.1}$$

The pitching moment coefficient around this point (C_m) equals the sum of the zero-lift pitching moment coefficient from the wing-fuselage ($C_{m,ac_{wf}}$) and the the wing-fuselage and HTP lift contributions. These are indicated by their respective lift coefficients, $C_{L_{wf}}$ and C_{L_h}. The later coefficient is adjusted with the surface ratio (S_h/S) and dynamic pressure ratio ($(V_h/V)^2$ or DPR) of the HTP to the wing. The arms are defined with respect to the position of the CG (x_{cg}), and the disturbances are applied on the NP (x_{np}). Both are normalized using the mean aerodynamic chord of the wing (MAC or $\overline{c}$). Deriving (2.1) with respect to the angle of attack results in:

$$\frac{\partial C_m}{\partial \alpha} = 0 + \left[C_{L\alpha_{wf}} + C_{L\alpha_h} \cdot \left(1 - \frac{\partial \varepsilon}{\partial \alpha} \right) \frac{S_h}{S} \left(\frac{V_h}{V} \right)^2 \right] \cdot (\overline{x}_{cg} - \overline{x}_{np}) \tag{2.2}$$

The values for $C_{L\alpha_{wf}}$ and $C_{L\alpha_h}$ are the lift curve slopes of the wing-fuselage and the HTP respectively, and $\partial\varepsilon/\partial\alpha$ represents the downwash gradient. Looking at equation (2.2), the stick-fixed neutral point represents the centre of gravity position for which the moment coefficient change with respect to angle of attack is zero. Positioning the center of gravity forward results in a negative value for the derivative, thus a longitudinally statically stable aircraft. Note that the value in brackets is always positive. The expression used for this requirement is further discussed in 3.2.

This tail sizing requirement behaves as a constraint for the most aft position of the center of gravity. It has to be evaluated especially at high Mach number conditions, i.e. cruise speed. The effect of compressibility on the aerodynamic coefficients involved has to be considered during the stability analysis. Although these effects are complex and difficult to model, it has been observed that the Mach number has a destabilizing effect. This effect is generally translated to a forward shift of the neutral point at sub-critical speeds (no presence of shock-waves) [5].

- **Low-speed manoeuvres**
  Three low-speed maneuvers represent special cases of the controllability requirement.

  During take-off, the tail needs to be able to produce enough downforce, generating the nose-up moment required to rotate the aircraft around the landing gear position, with an acceptable angular velocity and acceleration [5]. The most critical scenario corresponds to the aircraft weight configuration that generates the biggest nose-down moment with respect to the landing gear position. This usually corresponds to the most forward position of the aircraft´s center of gravity. The moment due to the aircraft´s weight is maximum at this position, thus critical for tail size [5]. Figure 2.5, sketches all forces and moments acting on the aircraft at the moment of rotation. The expression for this requirement is derived from Figure 2.5 and discussed in Section 3.2.

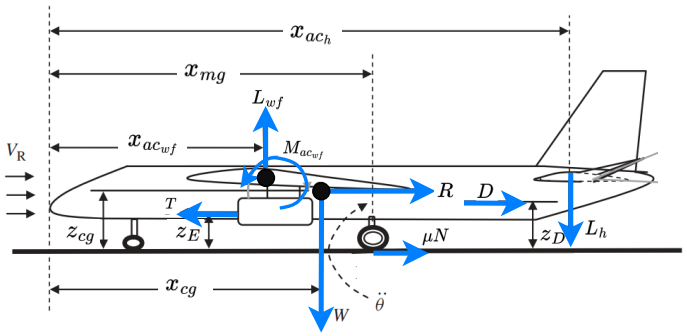

Figure 2.5: Schematic of the forces and moments acting on an aircraft during take-off rotation [25]

Landing flare is also mentioned in [5]. The requirement is similar to the take-off rotation one. In this case, the aircraft rotates around the center of gravity, not the landing gear. The tailplane has to be able to generate sufficient force, obtaining the pitch-up moment required to flare the aircraft at landing with an acceptable angular acceleration. The forces and moments acting on the aircraft at the moment of landing can be considered the same as the ones shown in Figure 2.3. The most critical position for the center of gravity is again the most forward position, as for the control requirement.

A third low-speed requirement, which is modeled in [26] and [27], is the requirement for minimum unstick speed (V_{mu}). The minimum unstick speed is defined as the minimum speed needed to lift off the aircraft from the ground, when the aircraft fuselage is pitched up to the maximum geometrically allowed angle (tail touching the runway) [28]. A similar expression to the one for the take-off rotation requirement can be derived [26]. Again, this requirement is usually critical for the most forward center of gravity position.

- **Other considerations**
  Besides the requirements above, there are still other considerations that can be included during the conceptual sizing of the HTP. Although these probably are out of the scope of the thesis work, they are still worth mentioning in this chapter.

  Out of trim conditions are included in [5], as another control requirement to be fulfilled by the horizontal tail. Local flow-field fluctuations at the tailplane due to excursions from the trimmed state, should not lead to the stall of the lifting surface. There are multiple out-of-trim manoeuvres. Thus, a detail study of the different flow conditions that result at the tail, makes more sense during a later stage of the design [5].

  The above-stated stability requirement, just focuses on the static longitudinal stability of the aircraft. It sizes the HTP so that the most aft center of gravity is never located behind the neutral point position. Additionally, expressions identified in [5], may assist in modelling the dynamic stability characteristics of the aircraft at an early design stage.

2.1.2.2. Horizontal tailplane sizing requirements calculation methods

The previous section showcased the multiple requirements that are often considered during the preliminary sizing process of the HTP. The way of modeling each of the above-stated constraints, dictates the accuracy of the final tail size estimate. This section provides a summary of the various methods identified in the literature.

- **Volume coefficient and statistics**
  The horizontal tail volume coefficient is a dimensionless parameter that relates the horizontal tail geometry to the wing geometry, see expression (2.3) [25].

$$c_{HT} = \frac{S_h l_h}{S\bar{c}} \tag{2.3}$$

  The term S_h/S represents the ratio of the surface area of the HTP to the surface area of the wing, while $l_h/\bar{c}$ represents the length ratio of the HTP lever arm to the mean aerodynamic chord of the wing. For a fixed aircraft geometry; i.e. constant wing area, tail lever arm, and mean aerodynamic chord; the bigger the volume coefficient, the bigger the tail size. Some aircraft design books suggest tabulated values based on previous aircraft designs. For example, 0.9 is suggested in [25] for a typical twin turboprop aircraft.

  The volume coefficient does not directly evaluate the stability and control requirements of the aircraft. Consequently, this parameter is normally used as an initial guess for the HTP size during the iterative tail sizing process [29]. With it, a first approximation of the aircraft´s mass distribution is found. After, the control and stability requirements can be evaluated, recalculating the HTP size [29]. There are even some studies like [22] or [30], that focused on having a better first estimate for this parameter to speed up the iterative process.

  Nevertheless, there are other publications in which the horizontal tail is sized purely based on a value for the volume coefficient. Its magnitude comes from a simple empirical expression. The

similarities in the design of an aircraft with a tube & wing (T & W) configuration allow to easily draw correlations between different aircraft design parameters.

- In [31], a methodology is presented, that estimates the volume coefficient just by looking at the aircraft maximum take-off mass (MTOM), fuselage shape, design range, and passenger capacity [31]. In this paper, a database was generated based on multiple geometric parameters from existing aircraft. A methodology was developed based on statistical data and the correlations between the multiple parameters studied.
- The Flight Optimization System Weights Estimation Method by NASA ("FLOPS") is a code used for conceptual aircraft design. It gives a first estimate of the size of major components and aircraft systems, including the HTP [32]. The method implemented consists on a simple empirical formula that has been derived from historical data coming from 17 transport aircraft and 25 fighter aircraft. This method is used for example in the aircraft design study by Riaz et al. [33].

These expressions allow to have a quick and realistic value for the tail size. However, it has to be taken into account that no control nor stability requirements are evaluated for the new design itself. The result is only dependant on statistical relations derived from previous aircraft designs.

- **Scissors plot**
  The scissors plot is the most used methodology to size the HTP during the conceptual aircraft design phase. This plot is also referred to as X-Plot or S_h/S vs $x_{cg}/\overline{c}$ plot [5]. It evaluates the stability and control of the aircraft, and gives a visual representation of the required horizontal tail size for a given longitudinal range of the aircraft´s center of gravity.

  The x-axis represents the allowed center of gravity longitudinal travel, as a percentage of the length of the mean aerodynamic chord (MAC). In the y-axis, the tail-to-wing surface ratio is plotted. Multiple lines are drawn in the graph. Each of these lines represents a distinct control and stability constraint, establishing limits for the most forward and aft center of gravity positions. An example of this plot is shown in Figure 2.6. Based on a given center of gravity longitudinal travel (or HTP surface), the plot helps to determine the minimum horizontal tail size required (or allowed center of gravity range).

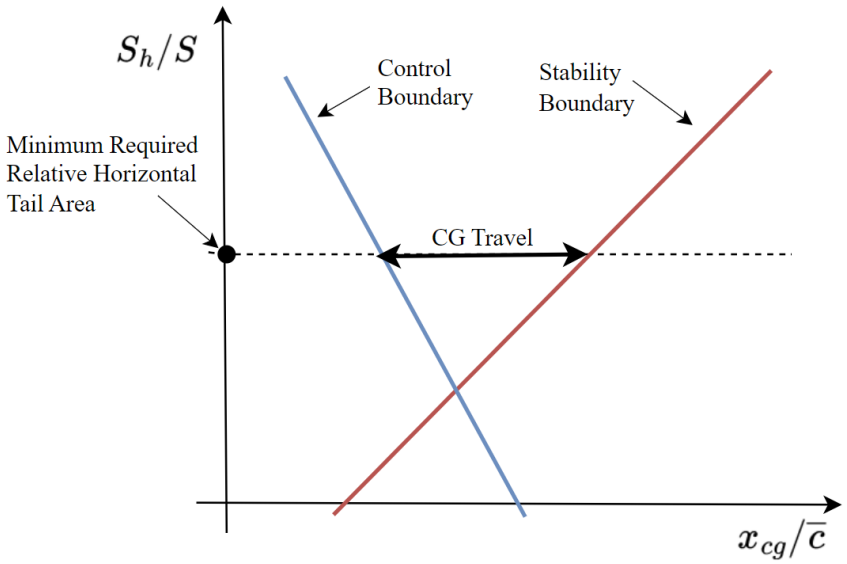

Figure 2.6: Scissors plot example [23]

The tail sizing requirements included in the scissors plot can change. The example from Figure 2.6 represents only the control and stability boundaries. These are the two main requirements and are always included when using this methodology, see [5] [23] [34] [35][36] ... . Studies from

above such as [34] or [35] and books like [5] or [25] do also include in their plot the line for the the take-off rotation constraint. This requirement is often more complex to estimate, due to the uncertainties and complexity of the aerodynamics in ground effect [27]. The same thing occurs with the landing flare and the minimum unstick speed requirements (explained more in detail in [27]), which are usually overlooked in most of the conceptual aircraft design studies using this method.

When an aircraft is designed, the minimum weight, drag, and thus fuel consumption is pursued. This philosophy also applies to the design of the HTP. The scissors plot method can be used to find the minimum size for the horizontal tail surface. This is achieved by shifting the wing position iteratively as described in [24]. For this routine, the scissors plot is combined with a plot that represents the aircraft´s change in center of gravity range with the wing position along the fuselage length ($x_{LE,MAC}/l_f$), see Figure 2.7.

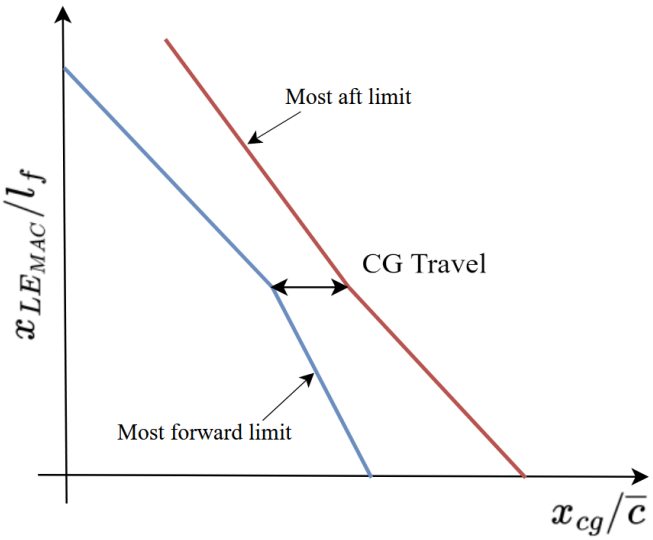

Figure 2.7: Change in the longitudinal center of gravity travel with wing position along the fuselage length [24]

If the wing is positioned too far aft of the fuselage, the relative position of the center of gravity to the MAC shifts forward. A big HTP is needed to compensate for the forward center of gravity position. In the scissors plot, this is shown as the most forward center of gravity being just on the limit, whereas the most aft center of gravity is far ahead of the stability boundary [24].

On the other hand, if the wing is positioned too far forward, the relative position of the center of gravity to the MAC moves aft. The tail has to be big enough, in this case, to compensate for the stability requirement. This is shown in the scissors plot as the most aft center of gravity being just on the limit, whereas the most forward is far behind the controllability boundary [24].

The optimum horizontal tailplane size is obtained for the wing position that results in a center of gravity range that lies perfectly between the two limits of the scissors, as shown in the example picture from Figure 2.6. Note that this explanation only considers the stability and control requirements in the scissors plot. The influence of new requirements on the optimum wing position, such as the take-off rotation requirement, is further discussed in Section 3.2 of the document.

As depicted in Figure 2.6, each tail sizing requirement is represented by a line in the plot. The equations for these lines come from the forces and moments equilibrium of the aircraft for a given fight condition. Thus, these expressions contain multiple aerodynamic coefficients (C_{L_h}, C_{L_α}, $C_{m_{ac}}$...), that are normally difficult to estimate during the conceptual design phase. The complexity of the flow-field [5], and the presence of the ground effect in some manoeuvres [27] makes it a difficult task. Two main approaches are identified in the literature, that are used for estimating their values:

– Semi-empirical methods:
As explained in the introduction of this section, semi-empirical formulas are widely used during the conceptual design phase of an aircraft. These mathematical formulas; which either come from theoretical assumptions or from simple physics models and curve-fitting on experimental evidence; are simple and computationally efficient [18].
Aircraft design books like [5] [14] [16], as well as manuals and databases like [17] or [37], contain multiple semi-empirical formulas that can be used to estimate these values. Most of the available aircraft design studies rely on semi-empirical expressions for tail sizing. Examples of this methodology are the Aircraft Design Analysis Software (ADAS) [38] used in [34], or the method used in [36].

– Computational Fluid dynamics (CFD):
The use of CFD to support the aircraft design process started during the 60´s. These tools were introduced to partially substitute costly and time-consuming wind tunnel experiments. Some studies were found that showcase the behaviour of CFD codes with different levels of fidelity in the context of tail sizing.
In [34], a VLM (Vortex-Lattice Method) code is compared with the results obtained with the semi-empirical expressions from USAF-DATCOM (see [17]). The results were contrasted with wind tunnel test data. The comparison showed that the VLM accurately predicted the values for the stability derivatives and downwash of the aircraft, with a relatively small error. Nevertheless, for parameters such as the lift curve slope or the down-wash gradient, the results from the semi-empirical formulas showed a lower error when compared to the wind tunnel data [34].
In [18], a study is presented that incorporated RANS (Reynolds-Averaged Navier-Stokes) simulations to model the aerodynamics of the vertical tailplane. The main motivation of the work was that the wind tunnel experiments that yielded the results and expressions from [17] or [37], were done during the 50s, using aircraft models that do not represent the current reality of conventional transport aircraft (see Figure 2.8). An updated semi-empirical methodology is presented, building on the results of CFD RANS simulations conducted on various aircraft configurations that closely resemble current aircraft designs. The methodology was validated using wind tunnel data, demonstrating improved accuracy over the results obtained with the USAF-DATCOM [18].

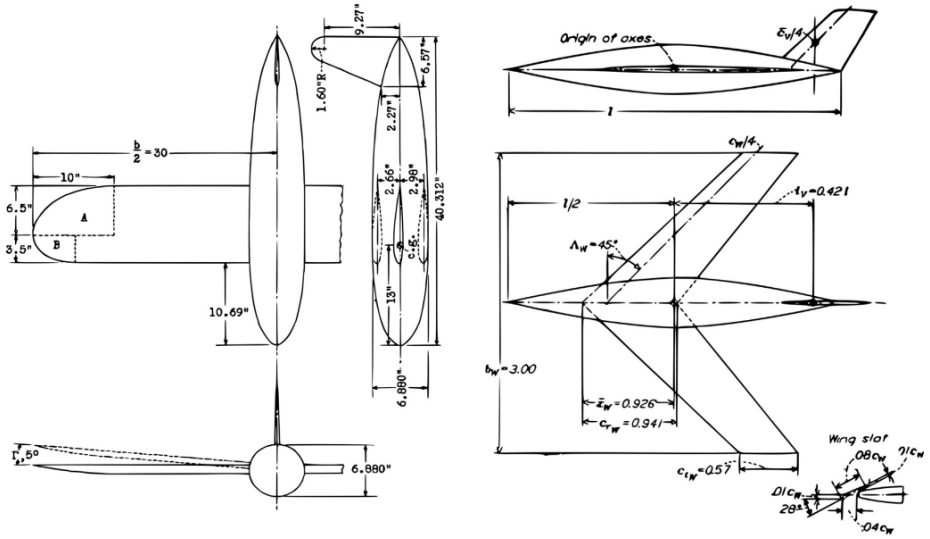

Figure 2.8: Aircraft models investigated by NACA during the 50´s [18]

- **Optimization of tailplane size including other aircraft design disciplines**
Most of the aforementioned aircraft design studies size the horizontal tailplane using an iterative

process, resizing the tail and repositioning the wing after each design iteration to ensure stability and control throughout all flight phases. However, other studies propose optimization approaches to achieve a more efficient solution for horizontal tail sizing, see [31] [39].

For instance, in [39], a multidisciplinary design optimization (MDO) framework is developed to better merge the disciplines of flight dynamics and control surface integration, with the traditional disciplines considered in an aircraft sizing process. Conventional tailplane sizing methodologies are limited when assessing these disciplines, which can only be taken into account later during the design process. As a result, this sequential process might not lead to finding the better optimum for the tail surface [39]. In [39], a multidisciplinary design optimization of the tail is conducted, incorporating control surface sizing and feedback for the flight control systems. The objective is to more accurately model the relationships and interactions between the size of the control surfaces, the control systems, and the aircraft's dynamic behavior, to find an optimum for the HTP size.

Some of the advantages of the optimization methods are highlighted in this section. However, the focus of this thesis is on estimating the required HTP size for a given aircraft configuration, rather than optimizing the entire aircraft design around this component. Therefore, optimizing the horizontal tail for the most efficient configuration is beyond the scope of this study and would not contribute to addressing the main research questions.

2.1.3. Methodology down-selection for horizontal tailplane sizing

After reviewing the state of the art in horizontal tailplane sizing for conceptual aircraft design, the methodology used in this thesis is defined and justified based on the available literature and the study's scope, ensuring it effectively addresses the research questions.

The scissors plot appears as the most used alternative. Simple methods like semi-empirical formulas based on statistics are especially critical for hydrogen aircraft. There is no data for these new aircraft configurations, and using kerosene aircraft data might result in an overestimation of the stability of the vehicle due to the impact of the rear tanks not being reflected in the data. This methodology also does not account for the possible oversizing of the HTP due to potential family members.

The tail surface area will be considered as the main design parameter. It is directly linked with the capability of the surface to generate lift. Besides this, it allows to have a quick estimate of the weight and thus production and manufacturing costs, especially important for family commonality to performance trade-off studies. Other horizontal tail design parameters affecting its aerodynamics; such as the aspect ratio, taper ratio, sweep, or span; do not offer further information for the purpose of the study and will not be considered. The HTP shape is quite similar between aircraft. Values for the aspect ratio and taper ratio will be chosen from a reference aircraft, and fixed for the derived kerosene and hydrogen concepts.

When comes to the requirements modeled in the plot, most studies only include stability and control [36] [38] [40]. The take-off rotation requirement is often also included [34] [35]. Consequently, these three requirements will be considered for the analysis. Others mentioned in this chapter, such as landing flare, were not even included in the conceptual aircraft design studies reviewed. The literature does not identify this requirement as critical for a conventional tube & wing aircraft design. Dynamic requirements are also not considered at this early stage of the design, where the goal is to get a first estimate of the horizontal tailplane size.

To estimate the aerodynamic parameters required for defining the requirements in the scissor plot, a semi-empirical approach is considered the most suitable option. The DATCOM 1978 [17] will be used as the main source. The configurations to be analyzed, while differing slightly in geometry, remain consistent with the tube & wing designs tested in the 1950s and used to derive these models [17]. Therefore, the existing expressions are considered adequate for capturing the primary aerodynamic effects of this type of aircraft configuration. However, for novel designs such as Blended Wing Bodies (BWB) or truss-braced wings, this approach would be inadequate. In such cases, methods like those presented in [18] or [34] would be employed instead.

2.2. Aircraft Family Concept

The second section of the chapter focuses on the concept of aircraft family. Firstly, the definitions of product family, commonality, and reserve in the aircraft design context are presented. Then, the different strategies for family creation are summarized. Lastly, a review is made on multiple studies that have considered the family concept since the early stages of the aircraft design process.

2.2.1. Product family and commonality

The aircraft design process starts from a series of requirements that come from potential costumers or market research. In order to meet the multiple and diverse desires from aircraft costumers, big aircraft manufactures have introduced the concept of aircraft family [41].

For a given product, in this case, an aircraft, a product family is a set of products that are developed with similar characteristics from the same base or platform product. They have similar parts and characteristics, but each of them is able to address specific needs in order to cover a wider market segment [41]. The aircraft family is based on the concept of commonality, which leads to the reduction in the development and operation costs of the product, as well as improves its residual value [41].

Commonality can be understood as the action of reusing and sharing different parts, functions, or technologies, between the different members of a product family [42]. Boeing first stated that commonality brings multiple benefits from both manufacturers as well as the costumer perspective, reducing the manufacturing costs and improving as a result the quality of the final product [42]. Airbus, on the other hand, focused its definition of commonality more towards the benefits that similarity between products in the cockpit layout and operation can bring to the pilots [42]. In conclusion, commonality benefits all stages of the aircraft design process. It lowers design and research costs during the initial phases, streamlines manufacturing by minimizing expenses associated with new techniques and equipment, and reduces operational costs by decreasing training expenses [42].

2.2.2. Design strategies for conventional aircraft families

When talking about aircraft, an aircraft family represent a series of aircraft products that were created under the same program, sharing common components and manufacturing processes [43]. Inside an aircraft family there are multiple aircraft versions. However, two types can be identified. The "Basic version of the family" is the main aircraft model that serves as the base or reference model for the creation of the rest of the family members. An example could be the 747-100 for the Boeing 747 family [43], or the Airbus A320 in the A320 family [33]. The rest of the family members that come from this basic version, are called "modified versions" or "family versions" [43].

Aircraft manufacturers have followed different strategies when creating an aircraft family. Two classifications can be identified [33] [43]. The first one classifies the aircraft family based on the differences in performance between family members. The latter one classifies the family based on when each member was developed in time.

2.2.2.1. Performance trade-offs

By plotting payload versus range specifications for existing aircraft families and analyzing the trends, the results can be categorized into three distinct family strategies [33]. This is shown in Figure 2.9.

- **Constant fuel capacity:** a trade-off is made between range and payload. The fuselage can be either stretched or shrinked. This modification enables an increase or decrease in passenger capacity, and as a result less or more range, for a fixed fuel capacity for the family [33]. This example can be seen in the A320 family [44], represented in red in Figure 2.9.
- **Constant payload:** in this case the fuselage length stays equal among the family members. A higher fuel capacity and/or improved engines can be introduced in order to obtain a longer range when compared with the base family member [33]. An example of this approach are the extended range (-ER) versions from the Boeing 777 family [45], represented in green in Figure 2.9.

- **Varying payload and fuel capacity:** this strategy combines both above stated. The fuselage is stretched to increase the payload. Aerodynamic or engines improvements and extra fuel capacity are added to the base design to further increase the range and compensate for the increase in MTOM [33]. An example of this trend is the Boeing 777-300, represented in blue in Figure 2.9. It has a longer fuselage as well as a higher fuel capacity, when compared to the main (base) family member, the 777-200 [45].

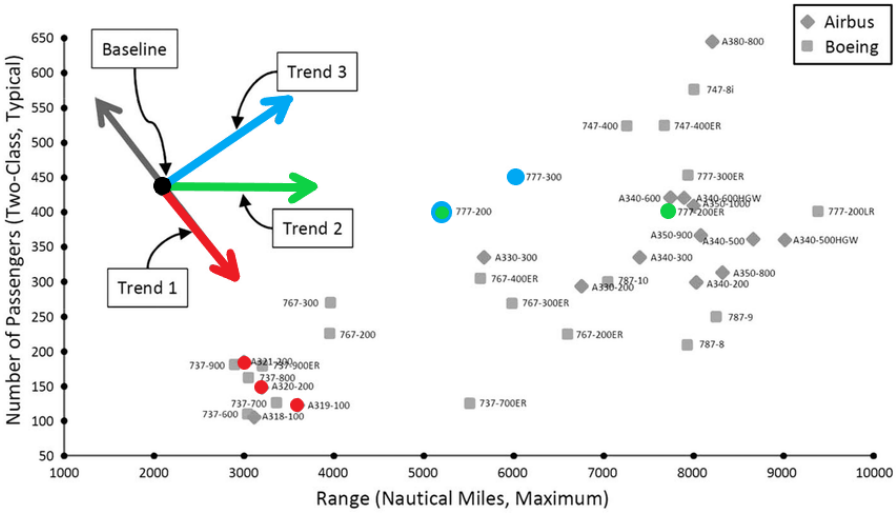

Figure 2.9: Transport aircraft family design trends [33]

2.2.2.2. Simultaneous design vs Sequential design

The creation of an aircraft family has two different approaches, based on the moment in time in which each of the family members is designed [33].

- **Sequential family design:** this design approach is the most simple, and thus less optimum. In this case, the main family member is designed first, deriving the family versions after. This methodology was adopted at the beginning by aircraft manufacturers [33]. The sequential design is especially used when comes to unplanned family versions [43]. Sometimes, the aircraft manufacturer has to develop a modified version of the main aircraft, as a response to the market needs. Most of the characteristics and performance of this so-called unplanned version are not known during the design stages of the basic family version [43]. An example is the A320 family from Airbus. The Airbus A320 was first delivered during the 80s, while the stretched (A321) and shrinked (A319) versions came a decade and two decades later respectively [46].

  The concept of reserve is introduced in this case. It consists on multiple design decisions that are applied during the design of the main family member [43]. These have the goal to minimize the change in the aircraft components and structure, maximizing the commonality and thus the benefits it implies [42]. However, selecting a big value of the reserve, especially for some aircraft components, can led to performance issues. A trade-off is then made. The following reserves can be applied to some shared components during the main aircraft design:

  - To maintain a similar field length between aircraft variants, modifications can include increasing the wing area, enhancing high-lift devices, or down-rating the engine while using the same propulsion system [47]. Reserves in wing area are often used due to the complexity of increasing the wing area for future modifications of the base aircraft [43].
  - To account for future stretched versions with a longer fuselage, a longer landing gear can be mounted than needed for the basic family version [43].
  - Another example of reserve that is observed in multiple existing aircraft (A320 family [48] [49] [50] or A350 family [51]), is the one applied for the VTP and HTP. These components are one of the most affected by the stretch or shrink of the fuselage in an aircraft family. The

difference in fuselage length among the family members results in a change in the moment arms, and consequently a different moment equilibrium for each member. The tailplane is usually shared between members.

- **Simultaneous family design:** the main family member is designed in parallel with the rest of the family versions. In this case, all family versions are known beforehand and their performance characteristics are defined. Considering all aircraft family members since the early stages of the design results in a better optimal design as showcased in [52]. The shared components will be optimized for each member. Then, the most critical one will be selected and shared among the rest of the members for commonality. Thus, the reserve value is minimized.

2.2.3. Consideration of the family concept during conceptual aircraft design

Both sequential and simultaneous design approaches have been studied multiple times concerning its applicability during conceptual aircraft family designs. Methods for sequential design are presented in [43], by introducing reserves in some of the components of the base product. However, this methodology was proved to be weaker in a study from Willcox and Wakayama [52]. In this publication, both methodologies were compared for the design of a Blended-Wing-Body (BWB) aircraft family, showing that simultaneous design yields to substantial savings in structural weight [52].

The approach of firstly designing and optimizing a family member was also questioned by Fujita et al. [53]. The result from the optimization of the main aircraft might not satisfy all the constraints of the other family members. An example of this could be the tail size. If the base aircraft is optimized, the resulting tail size might not be enough to provide stability and control for a shorter version. This effect is aggravated when more family members are added. In the end, a sub-optimal family results [53].

This section presents the two main methodologies that are found in the literature to simultaneously design an aircraft family. Simultaneous family design has been proved to be a more effective methodology than sequential design [52]. Not only most research work focuses on it, but also it is the direction adopted by the big aircraft manufacturers like Airbus for the development of their latest transport aircraft families, like the Airbus A350 family [54].

2.2.3.1. Optimization based approach

The commonality level is only one of the multiple weights that take part in the global optimization problem of an aircraft family design [42]. Commonality brings multiple benefits to the costumer. However, compromises are often made with other objectives like the aircraft performance. These have as a goal to maximize the overall product value, an thus customer satisfaction [42].

The conceptual aircraft family design is often viewed as a multi-objective optimization problem, requiring a balance between the level of commonality among family members and the performance penalties associated with it. Several studies address this issue. In addition to the study by Wilcox and Wakayama [52], other research focused also on formulating such optimization problem [15] [36] [55] [56] [57]. One of the most important tasks in these studies is the definition of the objective functions for the multi-objective optimization problem. Normally, two objective functions are defined. The aircraft performance objective function that aims to be maximized (usually modeled as block fuel weight [36] [55] or maximum take-off weight [36] [56]), and a cost analysis function including the whole aircraft life cycle. This latter function is minimized by maximizing the commonality degree between members.

2.2.3.2. Set-Based Design approach

The second methodology that is found in the literature for simultaneous aircraft family design is the so-called Set-Based Design (SBD). In a study by Riaz, Guenov, and Molina-Cristobal [33], the SBD methodology is presented as a better option than the multi-objective optimization approach.

The optimization is claimed to be less flexible when comes to changes in the design requirements. These changes in the product definition are likely to occur, especially during the conceptual design

phase. If modifications are introduced, the whole optimization problem will have to be redefined [33]. Another advantage stressed in [33], is that the SBD approach considers system architecture analysis in the conceptual design phase. Traditionally, the system architectures are optimized separately, resulting in a sub-optimal solution. The system architecture optimization is not considered inside the main optimization problem. Thus, the interactions and their impact on the whole aircraft design are usually overlooked [33]. This latter drawback of the optimization approach has already been addressed in projects such as AGILE [58] and AGILE 4.0 [59]. For instance, in [60], the optimization of system architectures for environmental control systems (ECS) and flight control systems was integrated with the overall aircraft design from a family concept perspective.

During the conceptual design phase designers often select a concept that is iteratively refined and modified. Multiple design decisions are taken until the final solution that satisfies all the constraints. This approach is usually referred to as point-based design (PBD). The Set-Based Design (SBD) methodology can be defined as the opposite. In this case, multiple designs are analyzed at the same time, in parallel. No critical design decisions are taken at the beginning, delaying them for later stages. As the design process advances, more designs are discarded, as the problem begins to be more understood. In other words, instead of considering only one solution to the problem, in the SBD multiple are studied, eliminating the worst and unfeasible ones. This approach helps to understand better the design space of the problem, getting a better overview of all trade-offs since the early stages of the design [33].

In [33], the SBD methodology was tested with a tube & wing configuration aircraft family with three variants: short, base, and long. The wing and empennage were shared and different engines, fuselage, and landing gear were used for each member [33]. To generate the multiple family combinations, a design of experiments (DOE) full factorial approach was used. This is the simplest but most computationally expensive methodology that requires discretization of the continuous design variables [33]. The DOE resulted in 30720 possible aircraft families. This methodology indeed helps to explore wider design spaces. However, it can get too computationally expensive. As a result, the PBD is still seen as a good option for conservative design problems, whereas SBD is seen more for innovative designs, where there is still little knowledge about the design space [33].

2.2.4. Methodology down-selection for aircraft family concept

After reviewing the state of the art in conceptual aircraft family design, this thesis adopts the simultaneous design approach due to its advantages over the sequential method.

In literature, the simultaneous design problem is typically addressed through multi-objective optimization or set-based design studies. However, the design of an aircraft family from scratch, as done in these articles, exploring various levels of commonality to minimize performance impacts, is beyond the scope of this study. Instead, the thesis will focus on testing aircraft designs that are derived from already existing DLR concepts. The developed methodology will be applied to define an aircraft family, using these concepts as the main member and following a simultaneous design approach. Different aircraft families will be derived to address the primary objective of the thesis regarding HTP commonality in a hydrogen aircraft family and its penalties. Consequently, a special focus is put on the methodology used to size this component, in contrast to what is done in the aforementioned studies, which only aimed to demonstrate the methodology's functionality. These latter studies used simpler tools based on semi-empirical formulas, like FLOPS [32] used in [33] or PASS [61] used in [57].

Although neither of the previously mentioned approaches will be used in this thesis, the adopted methodology, as will be depicted in Chapter 3, resembles a simplified version of set-based design (SBD) [33]. To explore the design space for LH2 aircraft families, different levels of commonality for the various components, together with different aircraft TLARs, will be defined for the different family members. Several conceptual aircraft families are generated to address the impact of tailplane commonality in each of them. The computational cost is assumable, as no DOE is performed. The number of points tested in the design space is limited. Only a few TLARs and the degree of commonality of certain components will be varied, as most of the aircraft design is already fixed based on existing DLR concepts. More information about the design space exploration and the concepts studied is provided in Chapter 3.

2.3. Hydrogen Aircraft Concepts

2.3.1. Liquid hydrogen as an energy carrier

Aviation urgently needs to shift to alternative energy sources to meet the goals for zero-emission established for 2050 [1]. Improvements on current aircraft efficiency are not enough, as the industry still relies on fossil fuels [1]. The yearly passenger traffic growth of almost 4 % predicted by the big aircraft manufactures like Airbus [2], showcases the need to go towards alternative ways of powering aircraft to meet the decarbonization objectives. The emission projection for the aviation industry until 2050, is shown in Figure 2.10.

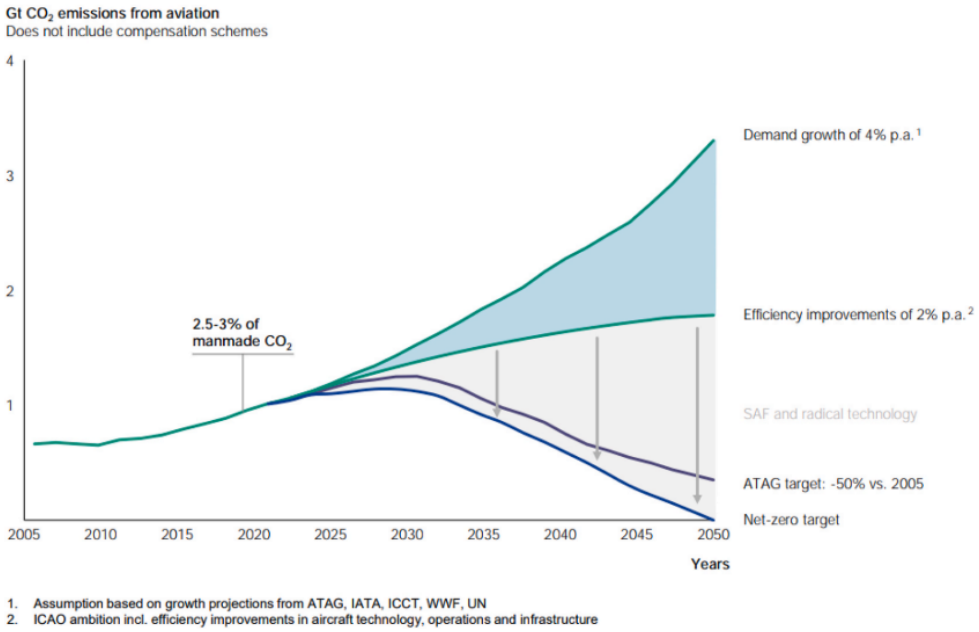

Figure 2.10: Emission projection in the aviation industry until 2050 [1]

Multiple studies show hydrogen as one of the leading solutions [3]. It offers multiple advantages against Sustainable aviation Fuel (SAF) or electric batteries [1] [3]. The technology for batteries is not developed yet, and the current state of the art for energy densities is far below the values required to be used on aircraft [1]. Regarding SAF, CO_2 emissions are only reduced by 70 %. Besides this, production is costly and the supply is limited due to required large amount of land [1].

Although LH2 aircraft are a current trend, it is not the first time in history that hydrogen has been seen as a potential solution. Several projects were carried out in the United States during the 50s and 70s [3], and later in Europe during the 2000s with the Cryoplane project, led by Airbus (see Figure 2.11) [8]. Although many concluded that this technology was feasible, no real efforts were put together to build a hydrogen transport aircraft to be put into service [1] [3]. Government incentives to meet the 2050 goals and the technological advances in green propulsion are pushing this trend again among scientists [1] [3]. There are even plans for the entry into service of this kind of technology in the coming years. The ZeroE project from Airbus [4] is an example.

2.3.2. Liquid hydrogen preliminary tank sizing

The storage of hydrogen can be classified into two big groups, physical-based storage using tanks; either in liquid, gaseous stage, a mix, or cryo-compressed; and material-based storage [1]. This latter is not suitable for aircraft, because of the additional weight needed for the systems that transform the material where hydrogen is stored (metal hydrides, metal-organic frameworks...), back into hydrogen [1]. Between the different ways of physical storage, liquid hydrogen (LH2) is found to be the most feasible solution for aerospace applications [1]. This choice mainly depends on the bigger density and

the higher tank gravimetric efficiencies that can be achieved, i.e. the ratio between the fuel mass and the total mass of the tank. This is partially due to the lower pressure required when compared with gaseous hydrogen (GH2) [1].

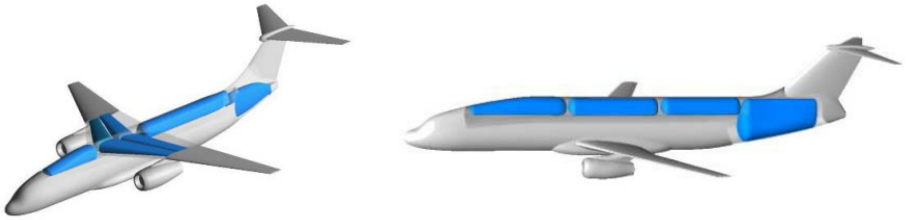

Figure 2.11: Cryoplane project short-medium range (SMR) concepts. First proposal (left) and revised configuration (right) [8]

Liquid hydrogen possesses a specific energy density (per mass unit) that is 2.8 times bigger than the one from kerosene [62]. On the other hand, the volumetric energy density is much lower than in the case of kerosene, and tanks four times bigger are required to carry the same amount of energy [62]. This presents unique challenges for hydrogen storage and the integration of the tanks, identified as the main showstopper for this new technology. The specific requirements for aviation, mainly low weight and low boil-off rates, call for a more mature technology than the one available used for cars and space applications [6]. Durable, low-weight, and highly insulated cryogenic tanks are seen as the key enablers to allow hydrogen to be the future of aviation [63].

Multiple studies have proposed methodologies for preliminary sizing a hydrogen tank to be used for an aircraft mission [6] [9] [64] [65] [66]. The following design variables have to be taken into account.

- **Shape:** the minimum area-to-volume ratio is pursued for the design. This minimizes the boil-off of the fuel due to heat transfer from the outside [6]. Consequently, the best shape for an LH2 tank is a sphere. Normally, the shape studied is more similar to the one of a cylindrical tank with hemispherical end caps, which still has an acceptably low surface-to-volume ratio, while allowing for a better integration within the aircraft´s fuselage [7] [64] [66]. Integrating the tanks in the wings is no longer feasible, as identified in many design studies like the Cryoplane project [8]. In this project the concept with wing mounted tanks was discarded as shown in Figure 2.11.
- **Tank wall material:** the material that is usually considered in most studies, is aluminum [6]. It presents good mechanical properties; i.e. high strength, fracture toughness, and stiffness, together with low density and resistance to hydrogen permeation [6]. The thickness of the tank wall depends directly on the material chosen. It should be able to withstand the pressure rise inside the tank due to the fuel boil-off. If thanks are integrated within the fuselage structure, loads will also have to be taken into account [6].
- **Insulation material:** there are mainly two different materials that are being considered by scientists: multilayer insulations (MLI) and low-density foams (either flexible open-cell polyimide or polyurethane foams) [6]. MLI thermal performance has proved to be superior to that of foam tanks. However, MLI requires a double tank wall to operate safely and ensure the vacuum working conditions that it requires [6]. A study from Verstraete et al. [6], showcased that the better thermal behavior of the MLI was outweighed by the double layer needed. Theoretically, a higher gravimetric storage energy density can be obtained with a foam tank, despite its thicker walls.
- **Tank operating conditions:** the tank fill and venting pressures are both important design parameters. The fill pressure is normally set to values between 1.2 to 1.4 bar [67]. The selected tank venting pressure is the maximum allowed pressure inside the tank. It dictates both the volume and also influences the tank wall and insulation material thickness. The bigger the venting pressure selected, the bigger the tank volume [6]. The venting pressure also represents a trade-off between tank wall thickness and insulation thickness (if foam is used as insulation) [6].

An LH2 tank sizing methodology consists on an iterative process. Multiple effects and parameter interactions have to be considered in order to arrive to the optimum tank solution. The best compromise between shape, tank material, tank wall thickness, insulation type, insulation thickness, and operating conditions is pursued for the given mission to obtain the highest gravimetric energy density. There are

three calculation blocks that are included in most of the preliminary tank sizing methodologies found in the literature. All these design blocks are coupled in an iterative design loop:

- **Geometrical and mechanical sizing:** aluminum 2219 is normally used for the tank walls [67]. Simple expressions are applied to determine the tank wall thickness based on the maximum pressure difference, tank size, material properties, and safety factors. Similar expressions and some examples can be found on [9], [64], [66], or [68].
- **Thermal design:** this block contains the methodology for estimating the heat transfer in the tank, and thus the resulting pressure rise due to boil-off. Similar methodologies are found in all studies. For example, in [6], [9], [64], or [66], an expression based on the first law of thermodynamics and mass conservation models the pressure fluctuation in an elastic tank considering the fuel as a homogeneous liquid. In [65], a model from [69] is used, which has a similar behaviour. No more detailed explanation and comparison of the models is presented, as it is considered to be out of the scope of the study.
- **Mission study:** the pressure inside the tank changes during the mission. Hydrogen boils off increasing the pressure inside the tank at the same time that fuel is used, decreasing it [6]. The thermodynamic behavior of the fluid has to be analyzed throughout the whole mission. If the pressure in the tank goes above the maximum, hydrogen will need to be vented. If it drops below the fill pressure, heat will have to be added [6]. A value that is also important to take into account is the amount of fuel that is left in the tank at the end of the main mission, i.e. the reserve fuel.

2.3.2.1. LH2 tank insulation type selection

A key distinction in the methodology across various studies on preliminary LH2 tank sizing is the design decision related to tank insulation. Most studies typically differentiate between foam-insulated tanks and Multi-Layer Insulation (MLI) insulated tanks. For this thesis, MLI-insulated tanks have been selected. The methodology outlined by Tim et al. [65] will be used. The design process integrates the same blocks as discussed earlier: firstly the geometry, structure, and mass are defined, followed by the simulation of the thermodynamic behavior of the fuel during the aircraft mission profile [65]. Further details on the working principles are provided in the methodology chapter in Section 3.1.1.1.

In the case of MLI tanks, the venting pressure can be kept relatively low. The thermal properties are superior to the foam and boil-off will likely not happen. Moreover, the insulation thickness of the MLI can be considered constant, as it is defined by the vacuum layer [6]. Thus, for an MLI-insulated tank, neither the venting pressure nor the insulation thickness significantly affects the final weight of the system [6]. However, for foam-insulated tanks, the venting pressure represents a crucial design variable [6]. The optimum value represents the perfect compromise between the tank wall and insulation thickness, which minimizes the tank mass. Consequently, the methodology for sizing these type of tanks is slightly different and more complex than that for MLI-insulated tanks.

Theoretical studies, like the one from Rompokos et al. [64] and Winnefeld et al. [66], present a workflow for the design of a foam-insulated aluminum LH2 tank. A first iterative loop is introduced to optimize the tank wall thickness. The pressure evolution is calculated during the mission, together with the leftover fuel. This is done for a fixed insulation thickness and tank fill pressure. If the remaining amount of fuel at the end of the mission is lower than the required, the volume is increased. At the same time, the tank walls are resized to withstand the maximum pressure difference that results from the analysis. The process is repeated until convergence, achieving the optimum wall thickness with enough reserve fuel. This methodology reduces the tank thickness and thus weight, but it is calculated assuming a constant insulation thickness. To find a global optimum, a compromise has to be found between insulation thickness and maximum pressure inside the tank, that gives the highest gravimetric efficiency. The higher the insulation thickness, the lower the tank wall thickness and vice-versa. A second external iterative loop is needed, that searches for an optimum by changing the insulation thickness [64] [66].

Foam has been theoretically proven to be a better solution than MLI, resulting in tanks with up to 3 % higher gravimetric efficiency [6]. However, if the whole aircraft operation is considered including stays on the ground at the airport with full tanks, the fuel consumption advantages are not that clear. The vented hydrogen due to boil-off at the ground for the foam tank is much bigger than for MLI

[65]. This results in the end in a lower overall fuel consumption for the MLI tanks, being foam tanks only beneficial when the airport infrastructure is equipped with hydrogen capturing technology [65]. Additionally, although theoretically possible, optimizing a foam-insulated tank for minimum weight is a highly complex task in practice. In the end, MLI tanks are selected for the study. The methodology from [65] can also be used for foam tanks. However, the insulation thickness is fixed and not optimized for minimum tank weight [65].

2.3.3. Liquid hydrogen conceptual aircraft design studies

2.3.3.1. Impact of hydrogen in the overall aircraft design and performance

Based on a classical tube & wing configuration, the following differences can be observed in an LH2 concept when compared with a conventional kerosene aircraft design [1] [3] [9].

- **Mass:** the concept of tank gravimetric efficiency compares the weight of the fuel inside the tank, with the added weight of the fuel plus the empty tank. It quantifies the weight penalty due to the use of hydrogen as an energy carrier, so the higher the better [3]. This value equals to 100 % for a conventional kerosene tank. The integration of the bulky LH2 tanks inside an aircraft, results already in a weight penalty, with an increase in the operating empty mass (OEM) of the aircraft. Recent studies consider an increase between an 8-15 % with respect to the kerosene baseline aircraft [40] [70].
  On the other hand, the maximum take-off weight is expected to decrease. This is mainly due to the much higher gravimetric energy density of hydrogen [8] [40] [70].
- **Wings:** for LH2, a small surface-to-volume ratio is pursued for the tanks. Thus, wings are not the ideal option to store them [3]. The resulting wing will then no longer benefit from the load alleviation coming from the fuel mass. A heavier structure will have to be designed to deal with the aerodynamic loads [3].
- **Fuselage:** although there have been some proposals regarding external tanks mounted over the wings; like a modification of a B-57 bomber [1] or the concept *LR-GKN2* by GKN and Chalmers [71]; most of the designs proposed include tanks mounted inside the fuselage. The different solutions are discussed further in this chapter. However, regardless of the tank configuration, the fuselage will experience some kind of changes in its length, shape, and weight, influencing the overall weight and aerodynamic performance of the aircraft.
- **Center of gravity range:** conventional kerosene aircraft carry most of the fuel mass inside integral tanks that are located inside the wing structure. For LH2, the preferred solution is distributing the fuel mass in tanks along the fuselage length. This has a huge impact on the longitudinal aircraft center of gravity travel during the mission, and thus the longitudinal stability of the aircraft [9].
- **Horizontal tailplane:** the increase in the longitudinal center of gravity travel for an LH2 design is directly linked with the HTP [5]. In the end, a bigger range for the center of gravity results in a bigger horizontal tail. This is specially critical for tanks mounted in the rear fuselage. Some solutions to limit the HTP size are:
  - Divide the fuel mass into two tanks. One is positioned in the back after the pressure bulkhead and one in the front, between the cabin and the cockpit [6] [8].
  - Tanks mounted above the passenger cabin, as shown in [72], as well as in some concepts from [6] and [8]. This solution and the one above are especially used for long-range aircraft, where the mission fuel mass is big.
  - Operational limitations. In [7], some on-ground operational constraints are discussed to limit the aft travel of the center of gravity, and thus the HTP size.
- **Landing gear:** some design challenges have been identified for the landing gear, specially for configurations with rear LH2 tanks [40]:
  - Due to the aft center of gravity position, the main gear will have to be positioned further aft to avoid tip-over. It will have to be integrated in the fuselage, resulting in integration and structural challenges together with increased weight and drag [7] [40].
  - Weight is expected to be higher, due to longer fuselages [40].
  - Ground operations can be critical, regarding sufficient load at the nose landing gear [40].

- **Aircraft performance:** results from the Cryoplane project [8] already predicted an increase in the aircraft energy consumption, and thus in the direct operating costs of an LH2 aircraft when compared to the kerosene reference. This change is due to the increase in the mean mass of the aircraft during the cruise phase, together with the higher drag penalty coming from larger fuselages or tails [40].

2.3.3.2. Hydrogen tank integration

Liquid hydrogen aircraft incorporate a new degree of freedom in the design of the vehicle. The main difference between the concepts found in the literature relies in the integration of the tanks inside the aircraft. Based on the tank positioning, the published studies on LH2 aircraft concepts can be classified into four groups. Most of them follow the classical kerosene aircraft tube & wing configuration. This is shown in Figure 2.12, where the tank is located at different positions along the fuselage. Novel aircraft configurations have also been studied as possible solutions to the tank integration problem.

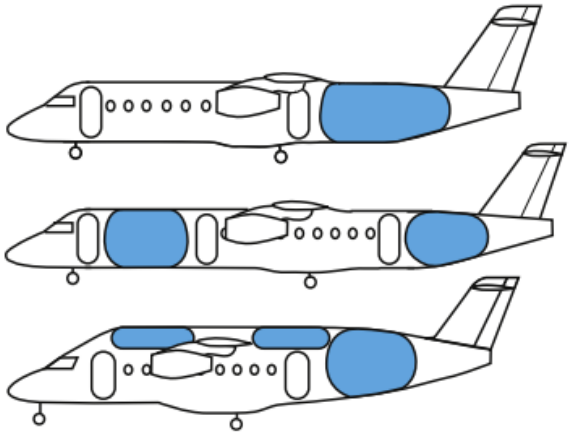

Figure 2.12: LH2 tank integration concepts for a conventional short-medium range (SMR) transport aircraft [6]

- **Tanks in the rear fuselage:** tanks are positioned behind the cabin pressure bulkhead. From a weight perspective, this configuration results in the lowest increase in MTOM and OEM [6] [40]. However, it has an important drawback. The excessive aft travel of the center of gravity results in a huge HTP size required for the design [40].
- **Tanks in the front and rear fuselage:** the forward tank is seen as a solution for the previous problem. This especially makes sense for long-range (LR) aircraft, due to the bigger mission fuel mass. As concluded by most studies [6] [7] [40], this configuration leads to higher weight penalties than a single tank in the back. Besides this, the access from the cabin to the cockpit is restricted, and the creation of a small corridor to connect both areas accentuates, even more, the weight penalties [6]. However, the fuel consumption can be partially reduced. Friction, as well as trim drag, are lower, together with the lower weight of the smaller HTP [40].
- **Tanks on top of the fuselage:** this idea was introduced by the Airbus Cryoplane project [8]. Some more recent studies also propose this approach [72] [6]. However, conclusions from these studies stress the performance penalties of this configuration. The diameter of the tanks highly influences the gravimetric efficiency. Tanks positioned on the top of the fuselage have high area-to-volume ratios, requiring from thick insulation layers to avoid boil-off. Moreover, there is an added drag and weight penalty due to the fuselage extension to allocate the tanks [6] [72].
- **Non-conventional configurations:** other configurations have been also studied. Some examples are blended wing bodies (BWB), conventional aircraft with extended wing surface at the root section [71], or even the integration of the tanks as pods mounted behind the propellers [68], or under the wings [70]. However, the level of maturity of these technologies compared with the common tube & wing is much lower. The technological challenges extend from the tank integration to the performance of the entire aircraft configuration.

In summary, based on the concepts discussed, a tube & wing configuration with either rear-mounted tanks or both front and aft tanks emerges as the most viable option for LH2 aircraft design. According to Wöhler et al. [7], aft-mounted tanks offer the most fuel-efficient solution, resulting in lower tank weight and reduced fuselage mass due to the shorter length. Additionally, the shorter fuselage facilitates the integration of a more compact landing gear, which incurs a reduced weight penalty [7]. On the other hand, in the study by Onorato et al. [40], the front and aft tanks configuration showcased a better performance. The weight penalty due to the heavier tanks and longer fuselage, was compensated by the reduction in horizontal tail size and consequent lower parasite and trim drag during cruise [40].

Both configurations show multiple trade-offs. In the end it cannot be concluded which one is better, as it mostly depends on the type of aircraft analyzed, as well as the methods, assumptions, and levels of fidelity used to analyze each component. The first study did not account for the effects of the HTP on performance, while the study by Onorato et al. did not consider the impact of landing gear integration on the design. For the purpose of the study, it has been decided to focus on the rear tank configuration. In the end, the goal of the study is to address the commonality penalties of the tailplane in an LH2 aircraft family. Thus, analyzing this critical configuration is the logical approach as it will showcase better the differences between a conventional and an LH2 aircraft family regarding the HTP size.

2.3.3.3. LH2 aircraft family concept

After the literature review, not many studies were found that tackle the problem of different design strategies (as shown in 2.2.2.1 for kerosene aircraft) for an LH2 aircraft family. The different tank position changes slightly the family concept that is widely understood for conventional kerosene aircraft. The commonality degree of components like the tanks and empennage, and the performance trade-offs are still to be studied. Looking at the few publications available, a few hypothesis can be made:

- The LH2 tank is commonly sized for the design mission. Consequently, payload-to-range flexibility is reduced for LH2 aircraft families that share this component [8]. Tank commonality might no longer be possible for some cases, which might also have an impact on empennage commonality.
- The fuselage length increases more in the case of an LH2 family with increased range and payload. The bigger tank further increases the length, which does not happen in a kerosene design.
- The same fuselage length could be used for all members in the case different payload values are defined for each family member [73] as shown in in Figure 2.13. For kerosene families different fuselage lengths are needed.

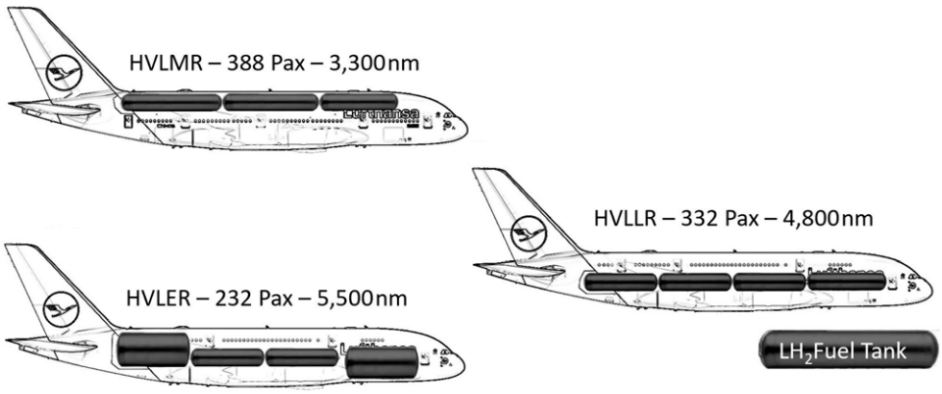

Figure 2.13: LH2 aircraft family concept for trade-off between range and payload [73]

To sum up, in the next chapter a methodology is developed to simultaneously size an aircraft family. The main goal will be to address the questions in Chapter 1 concerning the degree of commonality of the tailplane for both kerosene and LH2 aircraft families with rear-fuselage tanks. The D250-LH2 aircraft concept developed by DLR during the EXACT project [11] [13] will be used as the starting point for the different family studies involving hydrogen aircraft. It consist of a short-medium range (SMR) LH2 concept with MLI-insulated rear fuselage-mounted tanks.

3

Methodology

This chapter details the methodology used for conducting the various aircraft design studies in the thesis. Section 3.1 outlines the key components and working principles of the conceptual aircraft design workflow, with special emphasis on the modifications introduced compared to the baseline workflow. The baseline methodology was originally developed by the DLR and utilized in the EXACT project [12] to produce multiple LH2 aircraft concepts and trade-off studies [11] [13] [65] [68] [74]. A dedicated section in Section 3.2 focuses on the enhanced HTP sizing methodology, which represents one of the key additions to the baseline workflow.

The second part of the methodology focuses on detailing the different aircraft designs to be evaluated using the workflow. Section 3.3 outlines the procedure for recalibrating the reference and baseline aircraft for the study. The reference aircraft is employed to validate the methodology, while the baseline aircraft serves as a basis for developing and comparing the LH2 concepts within the design study. Finally, Section 3.4 outlines the LH2 aircraft concepts to be tested and sets out the plan for design space exploration, focusing on the family concept applied to this technology.

3.1. Aircraft Sizing Workflow

The EXACT project, which stands for Exploration of Electric Aircraft Concepts and Technologies [12], is a DLR internal project joining more than 20 research institutes. It started in 2020 and had as its main goal to get to the best possible design solution for climate-neutral transport aircraft. This not only includes aircraft design, but also global fleet assessment and climate impact, considering the entire life cycle of an aircraft and the different energy sources [12].

The aircraft design work package of the project focused on exploring the design space of future aircraft concepts, to identify the most promising solutions and configurations. The fleet concept consists of regional, short-range, and medium-range aircraft. A wide range of propulsion systems are used, from distributed electric propulsion to turboprop and turbofan drives. These latter are operated both hybrid-electrically using hydrogen fuel cells and by direct combustion of hydrogen, or using Sustainable Aviation Fuel (SAF) [12]. The overall aircraft design team at the DLR-SL institute developed the EXACT workflow, used as the main tool for the studies conducted during the project [11] [13] [65] [68] [74].

For the thesis study, the existing EXACT workflow was adapted to suit the thesis specific objectives. Two key limitations were identified in the baseline methodology, which required modifications to

effectively address the research questions. The improvements applied with respect to the baseline workflow are highlighted in red in Figure 3.1, which represents the final version used for the study.

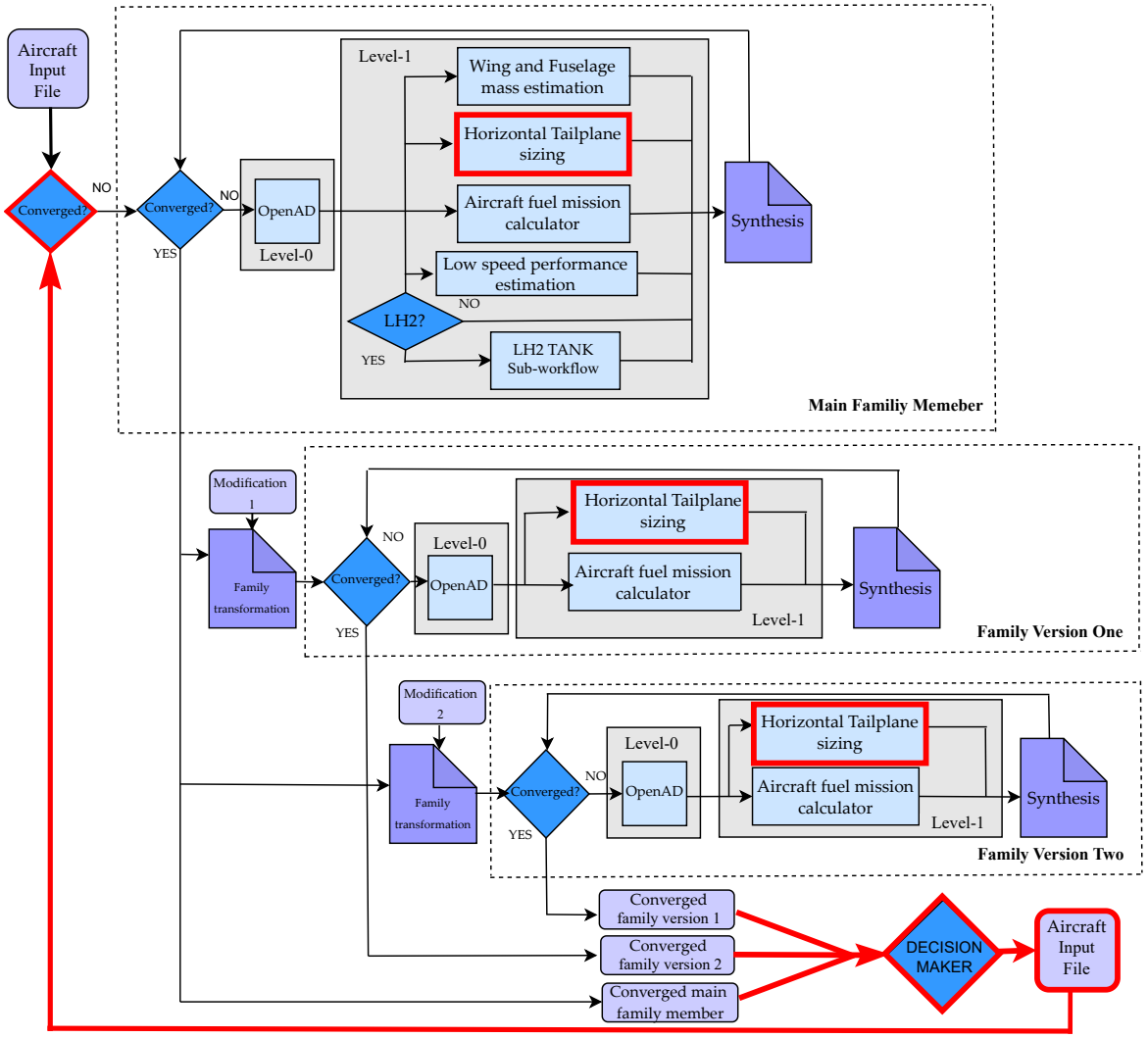

Figure 3.1: Modified EXACT workflow sketch

The final goal was to derive a methodology that is able to size an aircraft, together with its family versions, with a special focus on the horizontal tailplane sizing process. Both HTP and VTP of the main family member will be sized not only considering its stability and control requirements, but also potential family members defined by their TLARs. The three main changes introduced are explained below:

- **A new tool for HTP sizing** has been integrated within the workflow which is based on the scissors plot methodology [5] [23]. The working principles are further explained in in Section 3.2 of this chapter. The new tool performs a more in detail flight mechanics analysis to size the HTP, repositioning the aircraft wing for minimum horizontal tail size.
  Previously, there was no dedicated tool within the workflow that focused exclusively on horizontal tailplane sizing. OpenAD (see Section 3.1.1) was responsible for this task, relying on two simple formulas for take-off rotation and controllability requirements taken from Chapter 9 of [5]. No different flight conditions or mass configurations were accounted for. Moreover, OpenAD did not implement a routine to systematically shift the wing position to get to the minimum HTP size.

- **A decision maker block** has been added at the bottom of the workflow. As shown in Figure 3.1, the sizing workflow consists of three individual aircraft sizing loops. This process generates three

family members: one main family member and two derived versions, which are based on the results of the primary design. To transition from the main design to the family versions, the main output file undergoes the "Family transformation" scripts. These scripts apply modifications (such as changes in fuselage length, TLARs, etc.), which are further detailed in Section 3.1.2. However, the resizing of both HTP and VTP was not considered. This means that the methodology did not account for the possibility of the family versions being critical for the empennage size, assuming for this value the result from the main family member.
The methodology has been modified so that firstly both the HTP and VTP are independently sized for each family member. Once all design are converged, the goal of this decision-maker block is to identify the sizing member for the empennage by comparing all members.

- **An external convergence loop for the empennage size of the aircraft family** is the last modification introduced. The ultimate goal of the workflow is to design the main aircraft, along with its family versions, with a common minimum VTP and HTP size. After the initial iteration, three aircraft are sized with varying empennage dimensions. Once the decision-maker identifies the sizing member, the input file is rerun with this result set as a fixed input. All family members are then resized until a common tail size is obtained. A more detailed explanation of the sizing routine and the potential scenarios that may arise is provided in Section 3.1.2.

The following subsections dive more into the tools and the working principles of the methodology.

3.1.1. Workflow design tools

The rectangles in light blue represent each of the design tools. In the workflow, two different levels of fidelity are identified. Level-0 methodologies are based on handbook methods. These are mainly statistical or empirical expressions that allow for the exploration of the design space at a low computational cost [75]. The Level-1 tools focus on a specific discipline within overall aircraft design. These are based on simplified physics models, that are applicable to simple extensions of the design space [75]. A Level-2 methodology, which is not considered for the study, relies on a more accurate physical representation of both the geometry and physics of the problem. This comes with a high computational cost, which is not suitable for conceptual aircraft design purposes [75].

The workflow couples all the following tools to generate the final aircraft design. A brief explanation of each of them, including their main functions and fidelity levels, is provided below.

- **Overall aircraft design tool:** OpenAD is a software that has been developed at DLR-SL. It is the tool for conceptual aircraft design based mainly on publicly available handbook methods [76].
- **Aircraft fuel mission calculator:** this tool has also been developed at DLR-SL. It solves the equations of motion for an aircraft at every time/mass step based on the aerodynamic polars and the engine maps from OpenAD. The result is the fuel consumption for the design and reserve missions [7] [65].
- **Low-speed performance calculation:** this sub-routine allows for a more elaborate take-off and landing calculations [77]. The engine thrust required is adjusted for a given take-off field length.
- **Wing and fuselage mass estimation:** a more detailed load analysis that takes into account the rear integrated tanks and systems is used [78]. Based on these loads, a sub-workflow is used to calculate the fuselage and operator items mass [79] and the wing mass. More detailed description of the methods for wing and fuselage can be found in [80] and [81].
- **Horizontal tailplane sizing tool:** a dedicated section of the document, found in 3.2, provides further details on this tool.
- **LH2 tank sizing sub-workflow:** a more in detail explanation is done in Section 3.1.1.1.

3.1.1.1. LH2 tank sizing sub-workflow

A specific subsection is dedicated to the LH2 tank sizing sub-workflow. The sizing routine was developed at DLR-SL and is further explained in [65]. In Figure 3.2, a more detailed schematic of the different blocks and the connections of the sub-workflow is shown.

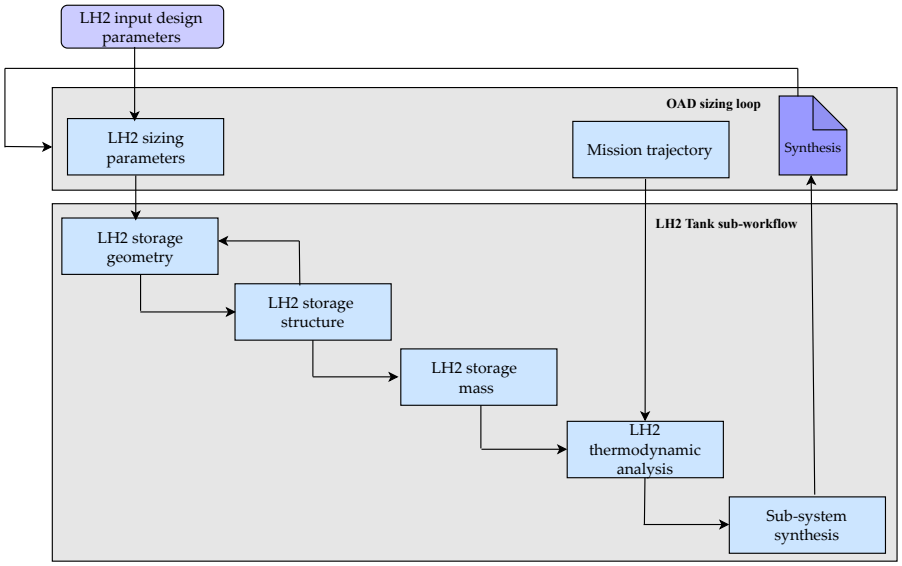

Figure 3.2: LH2 tank sizing sub-workflow schematic from [65]

The sub-workflow is integrated as a parallel branch within the overall aircraft sizing loop, together with the rest of Level-1 fidelity tools, as shown in Figure 3.1. The LH2 design process starts setting some parameters fixed from the input file. These are for instance the integration and location of the tanks, architectural decisions, and other assumptions such as the minimum ullage volume [65]. These inputs are taken into the sub-workflow, together with some other sizing parameters that come from the overall aircraft design (OAD) loop. Values like the fuselage diameter or the mission fuel mass, are used to determine the tank volume and constraint its geometry [65]. These inputs are used to generate a first estimate of the tank geometry, including the structural elements and its mass [65].

The physical description of the tank is then simulated during the mission trajectory of the aircraft. The thermodynamic behavior of the LH2 storage tank is analyzed to see if the required fuel mass for the mission is matched [65]. If the tank size is small, and not enough fuel is carried to complete the mission, the tool will fail. After the mission analysis, the results from the sub-workflow are synthesized and feedback into the OAD design loop.

3.1.2. Working principle

The methodology employed in the EXACT workflow enhances the integration between disciplinary tools, allowing for easy expansion of the workflow by incorporating additional disciplines and fidelity levels. This framework is supported by two primary pillars: the Remote Component Environment (RCE) [82], which is used to set up the workflow, and the Common Parametric Aircraft Configurations Schema (CPACS), which facilitates data exchange between tools [83] [84].

CPACS is the DLR's standardized aircraft design language, essentially an XML format that can store data from various disciplines involved in the aircraft design process [84]. The different design tools are able to read from the CPACS schema, outputting their results also in this format. This common language then allows for the easy interconnection of different tools to create complex multi-disciplinary and multi-fidelity design workflows, under the common framework of the RCE environment [82]. This open software allows for the integration of local, as well as sever tools. It contains multiple self-built components, such as convergers, XML file mergers, or switches. This allows the user to integrate the design tools and connect them in the desired way to generate the final design workflow [85].

As depicted in Figure 3.1, the workflow consists of 3 aircraft sizing loops. The upper one is run first and is used to generate the **main family member** design. The number of tools and level of complexity of this design loop is the highest. Once the main design is converged, some transformations are applied

to the output, deriving from it another two **family versions**. These aircraft are sized with a simplified version of sizing loop above. In the end, three family members are generated. The process can be decomposed in the following steps:

1. The input for the workflow consists of the aircraft design specifications, provided in an XML file. The design is based on a set of fixed values and factors. The fixed values primarily include the TLARs (such as range, payload, and wingspan). Additionally, geometric inputs like fuselage length and architectural decisions such as the type of wing or the number of engines are also specified. Other parameters, such as the aircraft´s maximum take-off weight, required tail size, or the wing position, along the fuselage, are a result of the workflow calculations.

   However, some aircraft parameters do not receive a direct input but a factor is applied instead. These factors are calibrated to a reference aircraft. For every conceptual aircraft design study, a reference aircraft is required. This aircraft model is used for the calibration of the methods and serves as the starting point to derive new aircraft designs and compare the obtained results [86]. The reference is initially sized using the workflow selected for the study. A calibration process is followed. During calibration, adjustment factors are applied to specific design parameters in the input file to ensure that the reference aircraft's publicly available data—such as geometry, weight, aerodynamics, and engine performance—aligns with the results from the aircraft sizing workflow. These same factors are then applied to other aircraft designed using the same methodology. Section 3.3 showcases a more detailed explanation of the calibration process followed.

   The input file also contains the definition of the potential family versions. This consists on the following values: the change in total fuselage length (Δl_f), the change in length due to sections added behind the wings (Δl_{VTP}), the maximum number of passengers, the design and maximum payload, the design range, the change in mass per meter of cabin section (dm_f/dl_f), and the change in wing mass (Δm_w). All values are defined with respect to the main family design.

2. The workflow starts running and the input file goes through OpenAD. The tool converges producing the first attempt of the design. The output from this tool needs refinement, as it ranks as a Level-0 fidelity tool. Some of its results will be recalculated using a higher fidelity design tool.

3. As depicted in Figure 3.1, there are 4 parallel branches (5 in the case of a hydrogen aircraft). These branches have tools with a higher level of fidelity. Each of them carries out a disciplinary calculation taking as an input the OpenAD output. The function of each tool is explained in Section 3.1.1.

4. The rectangles with cut corners represent Python scripts. These scripts receive a CPACS XML file from the preceding tools. The code within reads the output, modifies specific parameters, adapts the file, and makes certain design decisions accordingly.

   The so-called "Synthesis" script is at the end of the workflow. Its function is to read the output of the higher fidelity tools and overwrite some of their calculations into the OpenAD input. For the next iteration of the design, OpenAD "Synthesises" all the outputs coming from the higher-fidelity tools into a new aircraft design. The values that are overwritten include block, reserve, and mission fuel masses, wing and fuselage structure mass, engine sizing factors, as well as HTP size and wing position.

   In the case of an LH2 design, the main results from the LH2-sub-workflow (see Section 3.1.1.1) are also feedback into the OpenAD input through the "Synthesis" script. These parameters include the center of gravity position of the fuel mass, the recalculated fuselage and cabin lengths, and the masses and center of gravity positions of the tank, crash structure, and other systems. These last masses are combined into a single miscellaneous mass with its corresponding center of gravity.

5. The operating empty mass (OEM) and aircraft maximum take-off mass (MTOM) are used as the convergence criteria for the design. For every iteration, OpenAD recalculates these values. Thus, the convergence of all aircraft disciplines (fuel mass, structural mass ...) is done in parallel. If the change in the overall aircraft weight is below a threshold, the design is considered to be converged.

6. Once the main family member design is converged, the "Family transformation" scripts are run. These take as input the converged main design, and generate two new input files for the family versions. The following transformations are done in the script:

   - Adjusts the performance parameters based on the range and payload defined for the versions.
   - Adjusts the fuselage length and mass (l_f and m_f), wing mass (m_w), systems position ($x_{cg,sys}$) (including LH2 for the miscellaneous and fuel masses), and landing gear relative position to the wing chord (xsi_{mg}). The expressions below are used to go from the **main family member** to the **family versions**:
     - $l_{f_{version}} = l_{f_{main}} + \Delta l_f$
     - $m_{f_{version}} = m_{f_{main}} + \frac{dm_f}{dl_f} \cdot \Delta l_f$
     - $m_{w_{version}} = m_{w_{main}} + \Delta m_w$
     - $x_{cg,sys_{version}} = x_{cg,sys_{main}} + \Delta l_f$
     - $x_{cg,misc_{version}} = x_{cg,misc_{main}} + \Delta l_f$
     - $x_{cg,fuel_{version}} = x_{cg,fuel_{main}} + \Delta l_f$
     - $xsi_{mg_{version}} = xsi_{mg_{main}}$

     The LH2 sub-workflow is only part of the main aircraft design loop (see Figure 3.1). For the family versions, the same tank is used, which is sized for the main family member. Two simple modifications are included in the family transformation scripts. Both the centers of gravity of the fuel ($x_{cg,fuel}$) and the miscellaneous mass ($x_{cg,misc}$) are shifted based on the change in fuselage length for each version. The change in the position for the rest of the systems ($x_{cg,sys}$) is done the same way.
     The same wing is shared among family members. To ensure wing-box commonality, the main gear must be integrated at the same relative position along the wing for all family members. This position is referred to as xsi_{mg} and is kept constant.
     Note that the expressions above are valid for the main family member being either the short, the medium, or the long aircraft. The only thing that has to be considered is to define the Δ with the correct sign (positive if the fuselage length is increased).

7. The two generated input files are run in parallel. The design loops for the family versions are a simplified variant of the main design loop. They still contain OpenAD together with the tool for the fuel estimation. Nevertheless, the rest of the tools are omitted and some results are taken directly from the main aircraft design. Thus, it is important to note that the main aircraft results affect the family versions, particularly in terms of fuselage and wing masses (see expressions above), as well as engine size and performance, since no transformations are applied to the results obtained in the main design loop. The OEM and MTOM values are also checked for convergence.

8. Step 7 concludes the **point-design phase**, resulting in three converged aircraft designs. Each design features independently sized tailplanes and wings positioned to achieve the minimum HTP size in each case. The three designs go then into the decision-maker block. Here, the sizing members for the empennage are identified. The critical HTP size is taken and fixed as an input for the next iteration of the main aircraft design. The same is done for the VTP.

   For every point design, the minimum HTP size is found, freely changing the wing position along the fuselage length. However, when a family is designed the wing position cannot be arbitrarily defined. This parameter is related to all family members based on the change in fuselage length (Δl_f) and the number of sections that are added or removed in front and behind the wing (Δl_{VTP}) (see Figure 3.3). Ideally, the wing position of the main family member should be chosen such that, when adjusting the fuselage sections by adding or removing the required segments, the resulting wing position for the most critical family member aligns with the optimal position for minimizing the size of the HTP. In other words, in the decision-maker block the wing position for

the "main" aircraft is determined based on the wing position of the member that dictates the size of the HTP, referred as "sizing". Expression (3.1) is used to reverse engineer the wing position for the main family member and fix it together with the empennage size for the next iteration. In the expression, the wing position is indicated by the distance from the aircraft's nose to the leading edge of the wing's root chord ($x_{root_{LE}}$).

$$x_{root_{LE,main}} = x_{root_{LE,sizing}} + \Delta l_f - \Delta l_{VTP} \tag{3.1}$$

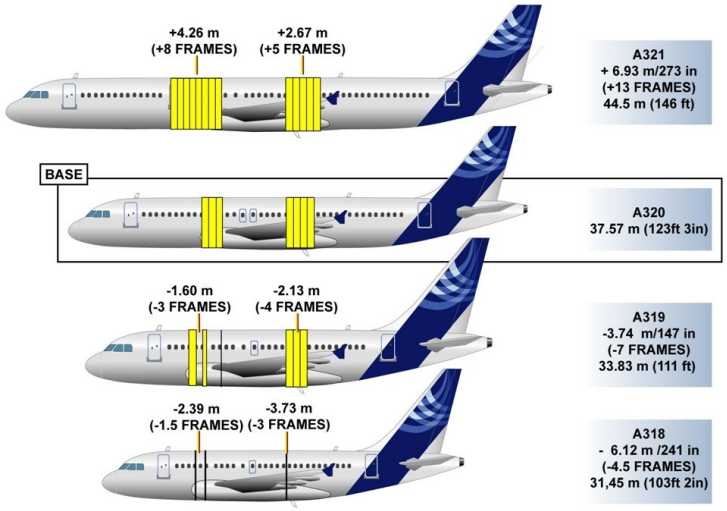

Figure 3.3: Change in fuselage length and wing position for the Airbus A320 family [87]

9. The new input file with updated values for wing position, VTP and HTP sizes, is feedback into the main workflow. Steps 2-8 are run again. The so-called **family-design phase** starts, with the ultimate goal of achieving a converged aircraft family that shares a common empennage and has the wing positioned to minimize the size of the HTP. Based on the aircraft member that drives the size of the HTP, and consequently the wing position, there are two potential design outcomes:

   (a) The main aircraft design is sizing for the HTP: in this case, the main design will remain unchanged from the first iteration. Both HTP and wing position resulting from the point design phase, will be fixed for the family design.
   The family versions will have to be redesigned. This time, a fixed value for the HTP will be used, coming from the main family member. The wing will be positioned based on the result from the long family member using the same expression as in (3.1). The design function from the HTP sizing tool is now deactivated for the family versions. However, it will still run as an analysis tool. In this way the workflow can still detect if the tail is being undersized based on the new wing position of the family versions, stopping the iterative process.

   (b) One of the family versions is sizing for the HTP: in this scenario the design of the main family member is affected due to the retrofitted HTP (and VTP) size coming from one of the family versions. The wing position is fixed as well, calculated using expression (3.1). The main aircraft will converge to a slightly different design due to these changes:
   - When a bigger VTP and HTP are fitted, the engine weight increases as the aircraft becomes heavier.
   - The center of gravity travel will slightly change, due to the new empennage size and wing position. This will affect the location of the main gear of the aircraft.
   - The new engine and empennage masses may influence the wing and fuselage masses of the main family member, potentially causing deviations from the results obtained in the point-design iteration.

   Note that in step 6, the fuselage and wing mass results from the main family member are utilized to calculate the corresponding values for the other family variants. Additionally,

the same engine mass and landing gear position are assumed across all family versions. Consequently, the above mentioned changes in the main aircraft design have also an impact on the family versions, and thus on the critical tail size of the family. The family version that is sizing for the HTP will be redesigned, obtaining a new critical HTP size and wing position for the next iteration.

The family version that is not sizing will have its tail fixed, as done for the main design. The wing position will be derived from the main family member design using a similar expression to (3.1). The HTP sizing tool will still run in the background as an analysis tool for both cases that are not sizing to detect any inconsistencies in the process.

The methodology also considers resizing both family versions' horizontal tailplanes. This is done when the point design results have a difference lower than 1 m^2. In this case, it is considered that the changes in the main aircraft design can lead to changes in the sizing member from one iteration to another. Although this is usually not the case, it is still considered to make the methodology more robust.

The VTP size is converged in parallel with the HTP size. The VTP size of the most critical family member will be recalculated after every iteration, accounting for the changes in the main aircraft design as done for the HTP. The calculation method for the VTP size is much simpler. An empirical expression is implemented in OpenAD [76] that calculates the vertical tail volume coefficient (c_{VT}) based on the aircraft wingspan (b), fuselage length (l_f) and height (h_f), and wing area (S), see equation (3.2).

$$c_{VT} = \frac{S_v l_v}{Sb} = 0.0325 + 0.3375 \cdot \frac{{h_f}^2 \cdot l_f}{Sb} \tag{3.2}$$

The VTP size is therefore viewed as a result of the overall aircraft geometry. Unlike the HTP, the VTP size has a relatively minor influence on the aircraft design. The empirical equation used is considered sufficient for the purpose of the thesis to account for the variations in VTP size among the different family members, differentiating between the point and family design phases.

10. The family design phase will proceed through steps 2-8 iteratively until a final, converged family with a common empennage size is achieved. The stopping criteria for the outer convergence loop is based on the reference area of both lifting surfaces. The convergence threshold will be directly linked to the weight tolerance within the inner aircraft design loops. The specific values chosen for the study will be detailed in Chapter 4.

    Convergence for the family design phase is expected to require one additional iteration of the outer convergence loop if the main family member is sizing for the HTP (9.a). In this case, the design of the main family member will remain unchanged from the point-design phase. Only the two family versions have to be resized based on the updated empennage size.

    However, if one of the family versions is sizing for the HTP (9.b), the outer loop is expected to take more than two iterations to converge. The main aircraft is redesigned after every iteration, which affects the final HTP size of the family. The design typically converges quickly (3 to 4 iterations) since changes in mass and landing gear position are generally minimal.

Note that the methodology, as described in this document, can only be used to size a family if the aircraft that is considered as the main family member is the stretched version. The "Family transformation" scripts take the converged main design and adjust the position of the aircraft components and their centers of gravity based on the change in fuselage length for each family version. Besides this, the workflow considers the resizing of the HTP and VTP for each family version.

However, the resizing of other components, such as the engine, is not considered. This component is shared among family members and is typically sized for the largest family member, i.e., the heaviest one, which has the lowest thrust-to-weight ratio. This logic applies to most aircraft components except the horizontal and vertical tailplanes. Consequently, only the long family member, which has already been established as the sizing case for the engines and other shared components, is used as the main aircraft input, as only the VTP and HTP are resized for the family versions.

3.2. Horizontal Tailplane Sizing Tool

This thesis focuses mainly on the horizontal tailplane sizing and the commonality of this component among family members. Thus, it makes sense to dedicate a special section in the methodology to describe more in detail the methods implemented for sizing this aircraft component. The tool was developed to be used within an overall aircraft design context. It is able to find the minimum horizontal tailplane size for a conventional transport aircraft, influencing the wing position. This includes wing-mounted engines as well as fuselage-mounted engines; conventional tail or T-tail configurations; turbofan or turboprop engines; and irreversible flight controls. It is based on the moment equilibrium of the aircraft needed for stationary flight and low-speed manoeuvres, according to [5], [23], and [25].

Firstly, the working principles of the tool are described. Here the tool is presented as an analysis tool, in the sense that it does not influence the overall aircraft design process. Once the working principles have been established, the implementation of the tool inside the DLR tool environment is discussed. The coupling between the tool and OpenAD is presented.

3.2.1. The tool as an analysis instrument

The development of the tool as an analysis instrument was part of an internship task. The thesis work focuses then on its implementation inside the DLR tool landscape and the EXACT workflow. A short description of the requirements included and some further improvements is presented below. For a more detailed documentation of the analysis process, please refer to Appendix A, where an updated version of the internship report is attached.

As explained during the literature review in Section 2.1.3, the tail sizing methodology is based on the so-called X-plot or scissors plot [5]. This graph represents the area ratio of the HTP to the wing (S_h/S) as a function of the longitudinal center of gravity range, commonly shown as a percentage of the length of the mean aerodynamic chord ($x_{cg}/\overline{c}$ or $\overline{x}_{cg}$). On this graph multiple lines are drawn. Each of them represents a given tail sizing requirement. In this case three requirements are considered: take-off rotation, controllability, and stability. All lines are plotted together, defining a region inside with the shape of an X or scissors. This region represents all combinations of center of gravity ranges and HTP surfaces that fulfill all sizing requirements.

The input for the tool is a CPACS file with a fully defined aircraft model. This includes its geometry, masses, center of gravity range, and the aerodynamic and engine performance maps. The tool analyses the file content as follows:

1. The aircraft flight envelopes are defined and discretized in several flight points. Each of them has associated an altitude and a flight Mach number, together with a flap setting. Three aircraft configurations are studied, with clean wing configuration, take-off, and landing flap settings. A more detailed explanation of the definition of the envelopes can be found in Appendix A.
2. The stability and control requirements are calculated along discretized points in the flight envelopes. On the other hand, the take-off rotation requirement is only calculated at the moment of take-off. What is changed in this case is the weight configuration of the aircraft.
3. The most critical flight condition for each sizing requirement is selected, and all of them are plotted together to create the final scissors plot.
4. Based on the resulting lines from the scissors, and the center of gravity range of the aircraft, the user can visualize if the tail of the aircraft is either undersized, oversized, or perfectly sized.

A more in detail description of the requirements, and its calculation methods is presented below.

3.2.1.1. Horizontal tailplane sizing requirements

Three requirements are modeled in the tool and represented in the scissors-plot, together with the aircraft´s longitudinal center of gravity travel. These are the controllability, stability, and take-off rotation requirements. This approach is comparable to other aircraft conceptual design studies that use also this methodology for HTP sizing (see Section 2.1.3 of the document). Literature suggests

many different ways for the calculation of the sizing requirements. In the end, all equations used are based on the moment equilibrium of the different forces acting on the aircraft during flight and ground manoeuvres.

- **Controllability requirement:**
  This requirement is based on the premise that the tail should be able to generate a moment in a way that ensures a longitudinal equilibrium of all forces, that in the end, results in a moment equal to zero around the center of gravity of the vehicle. At this point, the aircraft is said to be trimmed [24]. If moments are taken around the center of gravity, and the resulting expression is rearranged with the form of the equation of a straight line, equation (3.3) is found. The values for $C_{L_{wf}}$ and C_{L_h} are the lift coefficients of the wing-fuselage and the HTP respectively. The value of $C_{m,ac_{wf}}$ represents the zero-lift pitching moment coefficient. The tail lever arm (l_h) is normalized with the value for the MAC ($\overline{c}$), as done as well for the position of the aerodynamic center of the wing-fuselage ($x_{ac_{wf}}$). The dynamic pressure ratio at the tail is $(V_h/V)^2$ also referred as DPR.

$$\frac{S_h}{S} = \frac{1}{\frac{C_{L_h}}{C_{L_{wf}}} \cdot \frac{l_h}{\overline{c}} \cdot \left(\frac{V_h}{V}\right)^2} \cdot \overline{x}_{cg} + \frac{\frac{C_{m,ac_{wf}}}{C_{L_{wf}}} + \frac{C_{m_E}}{C_{L_{wf}}} - \overline{x}_{ac_{wf}}}{\frac{C_{L_h}}{C_{L_{wf}}} \cdot \frac{l_h}{\overline{c}} \cdot \left(\frac{V_h}{V}\right)^2} \tag{3.3}$$

  This expression accounts for the effect of the thrust on the equilibrium around the center of gravity position (C_{m_E}), as depicted in [23]. This is the main difference with respect to other similar equations that are found in [5] or in [24]. As discussed in Section 2.1.2.1 of the document, the most critical condition for trimming is normally achieved in landing configuration and imposes a **limit to the most forward position of the center of gravity**. Figure 3.4 shows an example for the calculation of this requirement in the tool. Each line represents a different flight condition. The colors are associated with different aircraft flap settings, being landing the limiting condition.

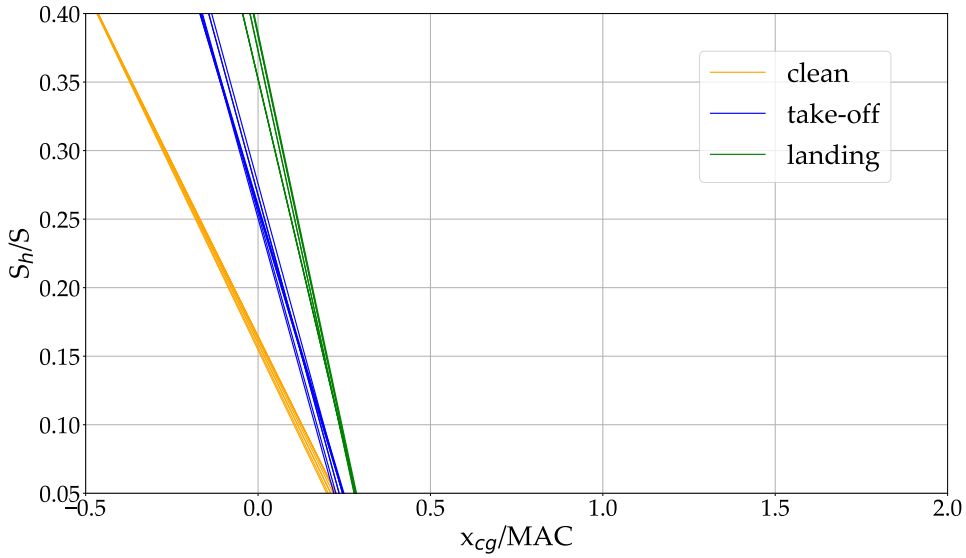

Figure 3.4: Example of control requirement limit for different aircraft flap settings

- **Stability Requirement:**
  During flight, the aircraft should be longitudinally statically stable for all its center of gravity positions. This translates into the derivative of the pitching moment coefficient with respect to the angle of attack being negative [5]. Expression (3.4) depicts the neutral point position as a function of the aerodynamic center of the aircraft less tail [5] [24].

$$\overline{x}_{np} = \overline{x}_{ac_{wf}} + \frac{C_{L\alpha_h}}{C_{L\alpha_{wf}}} \cdot \left(1 - \frac{d\varepsilon}{d\alpha}\right) \cdot \frac{S_h l_h}{S\overline{c}} \cdot \left(\frac{V_h}{V}\right)^2 \tag{3.4}$$

The values for $C_{L\alpha_{wf}}$ and $C_{L\alpha_h}$ are the lift curve slopes of the wing-fuselage and the HTP respectively, and $\partial\varepsilon/\partial\alpha$ represents the downwash gradient. The neutral point ($\overline{x}_{np}$) and aerodynamic center ($\overline{x}_{ac_{wf}}$) positions are again normalized with the MAC value.

For an aircraft design the neutral point is not usually set as the most aft position for the center of gravity. A safety factor is defined as the so-called static margin (SM). It is the distance, referenced to the mean aerodynamic chord length, between the neutral point and most aft allowed center of gravity position [5]. Expression (3.5) can be obtained when the definition of static margin ($SM = \overline{x}_{np} - \overline{x}_{cg}$) is substituted in equation (3.4), and rearranged as a straight line [24].

$$\frac{S_h}{S} = \frac{C_{L\alpha_{wf}}}{C_{L\alpha_h} \cdot \left(1 - \frac{d\varepsilon}{d\alpha}\right) \cdot \frac{l_h}{\overline{c}} \cdot \left(\frac{V_h}{V}\right)^2} \cdot \overline{x}_{cg} + \frac{C_{L\alpha_{wf}}(-\overline{x}_{ac_{wf}} + SM)}{C_{L\alpha_h} \cdot \left(1 - \frac{d\varepsilon}{d\alpha}\right) \cdot \frac{l_h}{\overline{c}} \cdot \left(\frac{V_h}{V}\right)^2} \tag{3.5}$$

High-speed conditions are usually the most critical from a stability point of view, and generally **limit the most aft center of gravity position of the aircraft.** This is depicted in Figure 3.5.

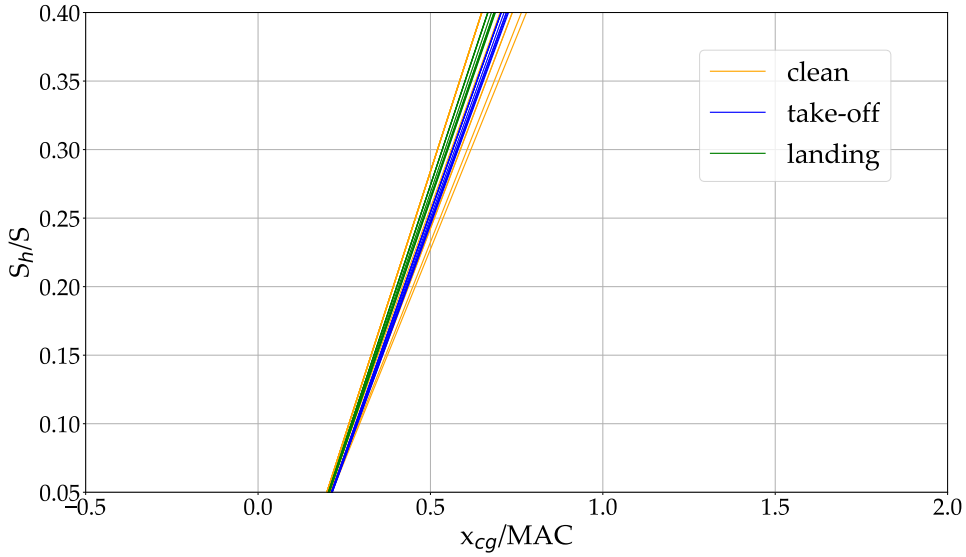

Figure 3.5: Example of stability requirement limit for different aircraft flap settings

- **Take-Off Rotation Requirement:**
  The expression used for take-off rotation has been taken from chapter 12 in [25] (see equation (3.6)). It represents the moment equilibrium around the position of the main landing gear of the aircraft. The forces and moments acting on the aircraft during rolling are shown in Figure 2.5.

  The forces involved include the lift generated by the wing-fuselage (L_{wf}) and the tail (L_h), the drag (D), the thrust (T), the weight (W), and the reaction force (R). Note that this last force is an inertial force, acting backward due to Newton's third law as a reaction to the vehicle's acceleration. The different moment arms are defined with respect to the main landing gear position (x_{mg} and z_{mg}), from the positions of the center of gravity (x_{cg} and z_{cg}), aerodynamic center of the wing-fuselage ($x_{ac_{wf}}$ and $z_{ac_{wf}}$) or tail (x_{ac_h} and z_{ac_h}), and engine (x_E and z_E). The $M_{ac_{wf}}$ term stands for the zero-lift pitching moment of the wing-fuselage. The sum of all moments around the main gear position has to overcome the inertia of the aircraft ($I_{yy,mg}$), rotating the vehicle at a certain angular acceleration ($\ddot{\theta}$).

$$\begin{aligned} I_{yy,mg}\ddot{\theta} = &-W(x_{mg} - x_{cg}) - T(z_E) + D(z_D) \\ &+ L_{wf}(x_{mg} - x_{ac_{wf}}) + L_h(x_{ac_h} - x_{mg}) + M_{ac_{wf}} + R(z_{cg}) \end{aligned} \tag{3.6}$$

The calculation for the wing-fuselage lift, tail lift, drag, and reaction force, follow from equations (3.7), (3.8), (3.9) and (3.10) respectively. The speed of the vehicle during the rotation manoeuvre equals the so-called rotation speed (V_R).

$$L_{wf} \cong \frac{1}{2}\rho V_R^2 S C_{L,r} \tag{3.7}$$

$$L_h = \frac{1}{2}\rho V_R^2 S C_{L,max_h} \frac{V_h^2}{V_R^2}\frac{S_h}{S} \tag{3.8}$$

$$D \cong \frac{1}{2}\rho V_R^2 S C_D \tag{3.9}$$

$$R \cong T - D - \mu N = T - D - \mu(W - L_{wf}) \tag{3.10}$$

During the rotation maneuver, the aircraft's weight is not entirely supported by the wings. Thus, the lift coefficient during rolling ($C_{L,r}$) is used in (3.7). Part of the weight is still supported by the wheels. The friction force in equation (3.10), which equals the runway friction coefficient (μ) times the normal force (N), accounts for the portion of the weight that remains on the landing gear. The value of C_{L,max_h} is used in (3.8), as the tail must generate enough lift to rotate the aircraft in all configurations. Since the sizing is based on the most critical condition, the tail will be operating at its maximum lift capacity. For expression (3.6), all distances are defined in a way that the resulting arm is always positive. The sign of the moment is given by the sign in front, being nose up positive.

The requirement is calculated for the aircraft taking-off at 5 different weight configurations. All configurations tested are further explained in Appendix A. An example of the resulting plot from the calculation is shown in Figure 3.6. **Among all weight configurations** chosen, there will be **one that requires the biggest tail to rotate.** This is **normally the weight configuration represented by the most forward center of gravity.** In this situation, the weight moment ($-W(x_{mg} - x_{cg})$) is the biggest due to the long lever arm to the main gear position. A more detailed explanation is found in Appendix A. The calculation procedure will be repeated for two take-off conditions: one at sea level (SL) (Figure 3.6), and another one at the so-called "airport conditions" (AP) or "hot and high conditions". These airport conditions represent a scenario with lower air density in which the aircraft can still take-off. The aerodynamic and engine performance will be affected.

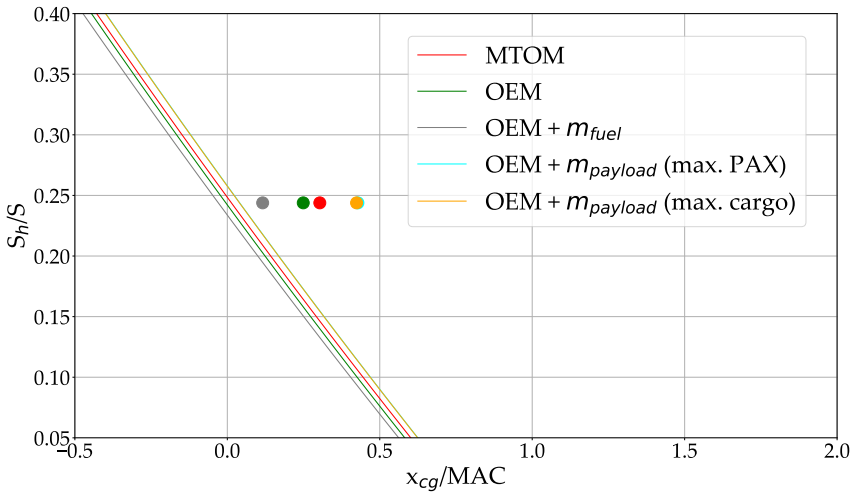

Figure 3.6: Example of take-off rotation requirement limit for different aircraft weight configurations

The final scissors plot consolidates the most critical conditions from all the figures above. The most critical condition in Figure 3.4 represents the limit for the most forward CG. Meanwhile, the most critical condition from Figure 3.5 defines the limit for the most aft CG. In Figure 3.6, the most critical mass configuration for rotation at sea level (same for airport conditions) is defined, typically coinciding with the most forward on-ground CG position. It is important to note that this position usually differs from the in-flight forward CG limit used to assess the controllability requirement, as discussed further below [88]. In total, **the final scissor plot features four lines and three CG positions.** Examples of the final plot and its interpretation are provided in Figures 3.8 and 3.9 in the next section.

3.2.1.2. Aerodynamic, geometric, and engine parameters calculation methods

The expression for each tail sizing requirement includes multiple aircraft geometric, aerodynamic, and engine performance parameters. The calculation methodology is described more in detail in Appendix A, using the USAF-DATCOM [17] as the main source.

3.2.2. The tool as a design instrument

The previous section described the calculations that are carried out inside the tool to generate the scissors plot. The plot can be used to analyze the tail size of a given aircraft design.

However, the tool on its own is merely an analysis instrument and cannot determine the minimum HTP size for a given aircraft design. To address this limitation, one of the primary objectives of this thesis has been to integrate the previously described analysis tool with OpenAD. This subsection explores the connection between OpenAD and the HTP sizing tool as part of the EXACT workflow, as shown in Figure 3.1. As explained in Section 3.1.2, the OpenAD input is adjusted using the results from the HTP sizing tool in an iterative process. The ultimate goal is to obtain the minimum horizontal tailplane size for a given aircraft design. The implemented algorithm for HTP sizing is described below:

1. OpenAD runs first. A first attempt of the aircraft design is obtained with a given center of gravity longitudinal travel and wing position.

2. The HTP sizing tool re-calculates the required tail size based on the scissors plot methodology. The wing position is also adjusted based on the scissors plot of the current design. There are two possible outcomes based on [24]:

   - **Wing is too far aft:** the situation is identified in the scissors plot with the most aft center of gravity being far in front of the stability limit. The control requirement is oversizing the HTP, being the most forward CG over the controllability boundary. In this case, the wing is shifted forward to reduce the HTP size [24]. In some cases, the most forward center of gravity is constrained not by the controllability but by the take-off rotation requirement. This scenario appears in the scissors plot with the most forward center of gravity aligned with the take-off rotation limit, while the most aft CG lies again ahead of the stability limit. Although not explicitly discussed in [24], this situation is a variation of the same case. For rotation, the minimum HTP size is achieved when the wing position maximizes the tail lever arm and minimizes the aircraft's weight lever arm relative to the main gear position. It has been observed that generally shifting the wing forward results in a smaller tailplane for rotation.

     It is important to note that there is generally a distinction between the most forward CG limits for control during flight and for take-off rotation. The difference is depicted in Figure 3.7.

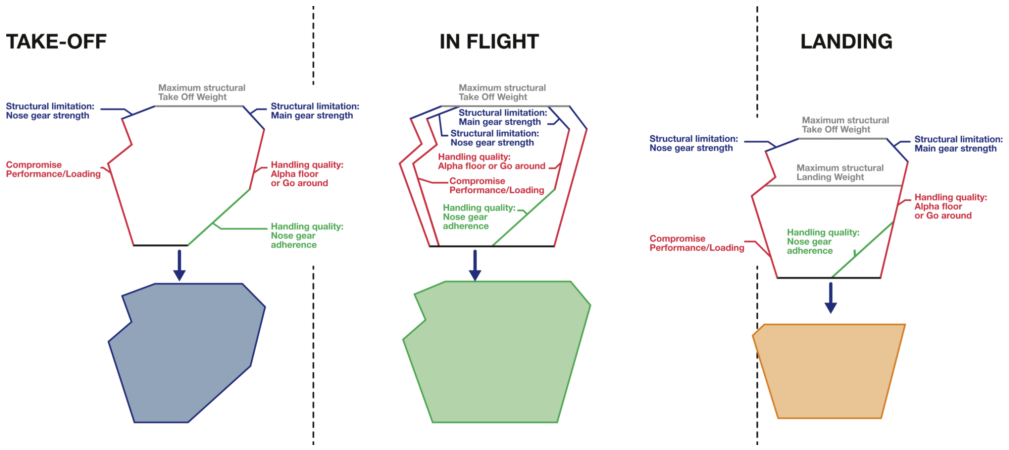

Figure 3.7: Center of gravity (CG) limitations envelope for different aircraft flight phases [88].

Both of these limits define the forward CG boundary of the aircraft, but they apply to different conditions: one for in-flight operations and the other for on-ground operations. The most forward CG limit for flight control addresses the aircraft's maneuverability in the air, whereas the CG limit for take-off rotation refers to ground handling during take-off and landing manoeuvres. For conventional transport aircraft, on-ground limits are typically more restrictive than those in flight. This is because ground operations impose tighter constraints on the allowed CG travel as depicted in Figure 3.7. In flight, the CG range is wider due to factors like fuel burn and the dynamic nature of flight. As a result, a small margin, usually a few percentages of the MAC, exists between both the forward and aft CG limits for ground operations with respect the overall in-flight CG limits of the aircraft [88].

- **Wing is too far forward**: this situation presents a scissors plot where the most forward center of gravity is positioned behind the controllability and take-of rotations limits, with the stability requirement acting as the constraint on the HTP size. To reduce the required HTP size, the wing is shifted backwards [24].

The algorithm implemented computes the distance between the most forward and aft centers of gravity and their corresponding limits. This allows for the identification of the relative position of the CG range within the boundaries of the scissors plot. Based on the results, one of the above mentioned wing shifts is applied. The magnitude of the step chosen for the wing shift is adapted according to the distance between the CG range and the plot boundaries, with larger steps used for greater distances to accelerate convergence. A minimum step is established which is calibrated based on a reference aircraft and the desired level of accuracy, as detailed in Section 4.1.1.

3. The recalculated HTP area and wing position are feedback to OpenAD trough the "Synthesis" script and set as fixed inputs for the next iteration.

4. OpenAD runs again, generating a new aircraft design with recalculated center of gravity range for the new wing position and horizontal tail size.

5. The tail sizing tool repeats its calculations for the new design, adjusting once more both the HTP size and the wing position.

6. The process continues until the aircraft weight is converged, meaning that the HTP size and the wing position are no longer changing. In this situation, the minimum size for the HTP is achieved. There are two possible outcomes:

   - **Minimum horizontal tail size for control and stability:** the in-flight center of gravity range lies perfectly between the control and stability requirements. An example is shown in Figure 3.8. All requirements are met, and the minimum HTP size is determined.

     However, the tail is oversized for take-off rotation, as the on-ground forward CG limit lies behind the take-off rotation requirement line. Adjusting the wing position to optimize the tail size for rotation results in the other two requirements not being fulfilled automatically, leading to the need for a larger HTP size than the one depicted in Figure 3.8.

   - **Minimum horizontal tail size for stability and take-off rotation**: in this case the most forward center of gravity for on-ground operations lies over the take-off rotation limit. This is represented in Figure 3.9. Once again, the minimum HTP size is determined to satisfy all requirements.

     In this case, the tail is oversized for control, being the controlabillity boundary slightly ahead the most forward (in-flight) CG limit of the aircraft. However, if the wing is shifted aft to approach the control boundary, the take-off rotation requirement would no longer be met, necessitating a larger tail than the result in Figure 3.9.

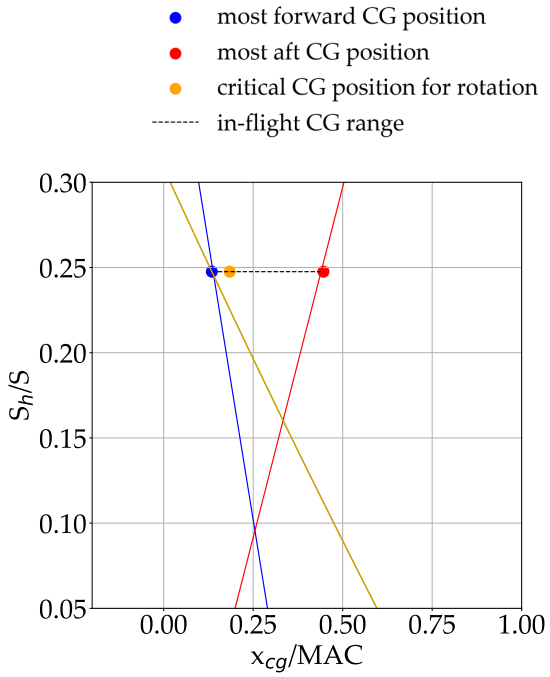

Figure 3.8: Example of minimum HTP size for control and stability

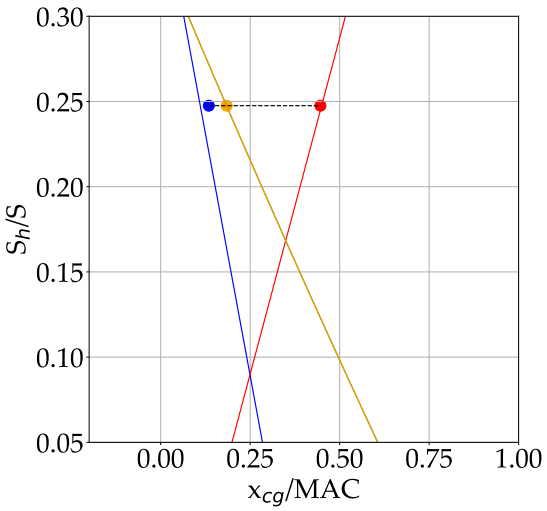

Figure 3.9: Example of minimum HTP size for stability and take-off rotation

Note that the green line corresponding to the take-off rotation requirement at sea level (SL) in both figures coincides with the take-off rotation requirement at airport conditions (AP).

3.3. Definition of the Reference and Baseline Aircraft Models

For every conceptual aircraft design study, it is essential to have a reference aircraft [86]. The reference aircraft data is used as a basis to calibrate the methodology applied during the aircraft design study, serving at the same time as a model for comparison, sensitivity studies, and further development into other aircraft designs with incorporated novel technologies [86].

The concept of baseline aircraft is also widely used in the overall aircraft design context [70] [72]. The baseline aircraft represents an evolved version of the reference aircraft. Technology factors are applied that account for aircraft performance improvements in different disciplines, such as lighter structural mass or better combustion technologies [70]. In other words, the baseline represents a conventional aircraft configuration at the same expected entry into service (EIS) as the new technology that aims to be studied. As its name indicates, the baseline is used as a base for the development of new aircraft concepts and to compare the obtained results.

This section goes through the calibration process followed in order to obtain a solid reference and baseline aircraft models for the aircraft design study conducted in the thesis.

3.3.1. Reference aircraft: D239

A consistent reference aircraft is indispensable to evaluate the impact that the integration of new technologies has on the overall aircraft design. All disciplines involved in the design process of the reference, i.e. masses, aerodynamic and engine performance, or aircraft geometry, have to be as close as possible to the real aircraft data. Nevertheless, this is hardy ever achievable, as the amount of data available to be used for research coming from the industry is fairly limited [86].

For this research project the chosen reference is the DLR D239 aircraft concept. This concept consists of the DLR interpretation of the Airbus A321neo with technology factors from 2016. The same model

was used as the reference for the EXACT project short-medium-range class aircraft concepts. Table 3.1 summarizes the main TLARs. These values have been taken from the final report of the EXACT project [89], and are also published in the study by Atanasov et al. [11].

Table 3.1: D239 reference aircraft concept TLARs [11]

TLAR	Value	Units
Design Range	2500	[NM]
Design PAX (single class)	239	[-]
Mass per PAX	95	[kg]
Design Payload	25000	[kg]
Max. Payload	25000	[kg]
Cruise Mach number	0.78	[-]
Max. operating Mach number	0.8	[-]
Max. operating altitude	40000	[ft]
Approach speed	136	[kt]
TOFL (ISA +0K SL)	2200	[m]
Rate of Climb @ TOC	>300	[ft/min]
Wing span limit	$\leq$ 36	[m]

With the new horizontal tail sizing tool in the design loop, some reference aircraft parameters have to be re-calibrated for the scissors plot methodology to work properly. The following values have been identified as critical. Having a good match of these parameters with the reference aircraft dictates the accuracy of the whole tail sizing process.

- **Aircraft geometry:** the requirements implemented on the scissors plot are all based on flight mechanics and the forces and moments equilibrium of the aircraft. Therefore, it is crucial to align the positions of the aircraft's lifting surfaces and the aerodynamic centers of the wing and horizontal tail with the actual geometry of the reference aircraft.
- **Main landing gear position:** this parameter is especially relevant for the take-off rotation requirement. Moments are taken with respect to this position to evaluate the tail surface required for rotation. The equation for the method is really sensitive to this parameter.
- **Aircraft center of gravity range:** the allowable longitudinal center of gravity travel for a given aircraft ultimately determines the required HTP size, based on the scissors plot method. Normally, the most aft and forward center of gravity positions correspond to concrete aircraft weight configurations. It has been observed that for a kerosene aircraft the most forward usually corresponds to the ferry flight configuration, i.e. OEM + maximum fuel mass. The most aft center of gravity position is normally the one for the OEM + payload.

The input file for the reference aircraft has been modified and re-calibrated to match the critical parameters that are summarized above. The airport planning manual for the reference aircraft has been used as the main source for the calibration process. Airport planning manuals are available online for all Airbus aircraft, including the one for the A321neo [50]. These manuals contain information regarding the aircraft different weight variants, together with a definition of the aircraft geometry. The geometric parameters that have to be matched and the aircraft dimensions are taken from this source.

In addition to this, airport planning manuals also provide diagrams for ground landing gear loading on pavement which illustrate the most forward and aft limits for the CG on-ground to ensure stable aircraft operations. These limits serve as a reference for the definition of the overall in-flight CG limits of the D239 concept. As depicted in Figure 3.7 it is typically observed that the on-ground CG limits are more restrictive than the in-flight limits. A small margin is applied to determine the final values for the in-flight CG limits.

Based on the data from [50], the on-ground center of gravity range for the A321neo weight variant WV053 extends from 17 % to 37 % of the mean aerodynamic chord (MAC). This corresponds to a center of gravity travel of 20 % of the MAC. For the A320, the actual CG travel is approximately 30 % of the MAC [88]. Since no additional data is available, this 30 % value is also applied to the A321neo, as both aircraft belong to the same family. As a result, a margin of 5 % is added both forward and aft of the on-ground CG limits, defining the overall CG travel for the reference aircraft model. The final in-flight range used for the calibration goes from 12 % to 42 % of the MAC.

The reference aircraft input file was modified by applying factors to some of the aircraft parameters. The following values were modified with factors to match the publicly available data found for the aircraft regarding its geometry and center of gravity range:

- **Calibration of the aircraft center of gravity longitudinal travel:** factors were applied to certain aircraft masses. This shifted their longitudinal position along the fuselage length. The goal was to match the center of gravity limit values from [50], considering also certain margin for the in-flight limits as explained above. The following masses were adjusted:
  - Passenger mass center of gravity: this factor was used to shift the most aft center of gravity position. This usually corresponds to the OEM + payload weight configuration. OpenAD assumes the passenger mass center of gravity to be positioned in the middle of the fuselage cabin. Each passenger is assumed to be 95 kg, including in this value the weight of the checked luggage. This mass does not necessarily have to be loaded in the middle of the cabin. Moreover, the different cabin layouts, and the location of the galleys and emergency exits, also have an impact on the real position of the passenger center of gravity. Based on these statements, it seems logical to assume the center of gravity of the passenger mass to not be exactly located in the middle of the cabin.
  - Operating empty mass center of gravity: this factor was used to shift both the maximum and minimum allowed center of gravity positions of the aircraft (usually OEM + fuel and OEM + payload respectively). It accounts for inaccuracies in the calculation of the center of gravity of the different aircraft components, such as the fuselage structure, wing, and other systems.
  - Fuel mass center of gravity: this factor was used to shift the most forward center of gravity. It accounts for inaccuracies in the estimation of the tank geometry and center of gravity of the fuel mass.
- **Calibration of the main landing gear tip-back angle:** for a tricycle landing gear, the tip-back angle can be defined as the maximum aircraft nose-up attitude, with the aircraft tail touching the ground while the gear strut is fully extended. The angle on the vertical, between the most aft center of gravity position of the aircraft and the main gear, has to be bigger than this tip-back. This will prevent the aircraft from tipping back on its tail [90]. Literature suggests a value for the tip-back angle of around 15° [90], which is also taken as default by OpenAD. The landing gear position will be calibrated through a factor on the tip-back angle.

OpenAD contains all methods used for aircraft design, geometry definition, and center of gravity estimation. The factors were applied to an OpenAD input file. An iterative process was followed, adjusting the factors until obtaining an output that matched the available data from the reference aircraft. A calibration workflow was used to automate the task. For the converged design, the following factor combination was found:

- Factor on the longitudinal position of the passenger mass center of gravity: the center of gravity is located at 53 % of the cabin length. This results in a factor of 1.06.
- Factor on the longitudinal position of the operating empty mass center of gravity: 0.9875.
- Factor on the longitudinal position of the fuel mass center of gravity: 0.94.
- Factor on the tip-back angle: 1.07, so a 16º tip-back angle is assumed.

In the aircraft sizing workflow, these factors were applied to the main long family member, i.e. the D239 reference, as well as to the shorter family versions derived.

3.3.2. Baseline aircraft: D250

The D250 kerosene aircraft concept consists on a short-medium range (SMR) turbofan powered aircraft developed as the baseline model for the EXACT LH2 concepts [11] [89] . The TLARs are shown in Table 3.2.

Table 3.2: D250 baseline aircraft concept TLARs [11]

TLAR	Value	Units
Design Range	1500	[NM]
Design PAX (single class)	250	[-]
Design Payload	23750	[kg]
Max. Payload	25000	[kg]
Approach speed	< 140	[kt]
TOFL (ISA +0K SL)	1900	[m]
Wing span limit	≤ 42	[m]

Note that the TLARs have been primarily derived from the reference, with some adjustments made for the assumed EIS in 2040, as detailed below. A summary of the key technological factors considered is presented in Table 3.3.

- **Change in the payload and range:** higher passenger demand is expected in the coming years [89]. The aircraft capacity has been increased from 239 to 250 passengers in a maximum-density layout. Regarding the range, it has been decreased to 1500 NM for the design mission [89]. This payload and range combination was found to be a "sweet-spot" for the design of an LH2 SMR aircraft, as showcased by the results from the EXACT project [89]. Thus, the kerosene baseline aircraft is designed assuming the same TLARs for comparison.

- **Change in the aircraft operating empty mass:** new technology factors are assumed for the structural weight of the wing and aircraft fuselage. A lighter aircraft results.

- **Change in the aircraft geometry:** the fuselage increases around 2.3 meters, due to the 11 extra passengers. Regarding the wing design, the wingspan is increased up to 42 meters (including folding wing tips for airport gate compatibility). The higher aspect ratio wing also results in a shorter mean aerodynamic chord (MAC), when compared to the reference.

- **Change in the overall aircraft weight:** the resulting baseline is around 13 tones lighter than the A321neo. This is due to the lower structural weight, coupled with the lower range, thus lower mission fuel mass.

- **Cruise mach number**: the value for the cruise Mach number was set as a variable that needed optimization [89].

Table 3.3: D250 baseline technology factors compared to the D239 reference [11]

Component	Technology factor
Gas Turbine	+ 5 % efficiency and no thrust reverse
Fuselage	- 5 % mass vs state of the art aluminum fuselage
Wing	CFRP wing with foldable wingtips.
Empennage	- 8 % mass

The re-calibration factors applied for the reference were also translated into the baseline aircraft.

3.4. Liquid Hydrogen Aircraft Concepts Definition

This section describes the hydrogen aircraft concepts that will be used to carry out the multiple design studies of the thesis.

3.4.1. D250-LH2 concept

The D250-LH2 concept is part of the results from the EXACT project. This aircraft is developed from the the D250 baseline (see Section 3.3.2), and represents a SMR aircraft with two turbofan engines powered by direct combustion of liquid hydrogen (LH2) [13]. The TLARs of this concept are shown in Table 3.4.

Table 3.4: D250-LH2 aircraft concept TLARs [11] [89]

TLAR	Value	Units
Design Range	1500	[NM]
Design PAX (single class)	250	[-]
Design Payload	23750	[kg]
Max. Payload	25000	[kg]
Approach speed	< 140	[kt]
TOFL (ISA +0K SL)	1900	[m]
Wing span limit	≤ 42	[m]

The concept incorporates two cryogenic non-integral hydrogen tanks for redundancy, which are located behind the cabin at the unpressurized rear of the fuselage [13]. The material chosen for the tank is aluminum, and it is insulated using multi-layer insulation (MLI) [13]. Note that the concept presented in [13] features a conventional horizontal tail configuration, as also does the kerosene D250 baseline. However, in more recent unpublished updates of the concept, this configuration has evolved into a T-tail design. The T-tail configuration was selected primarily due to the placement of the cryogenic tanks, which limits the space available for a conventional tail configuration. Besides this, a smaller HTP results, which is specially beneficial for a concept of these characteristics.

The same changes as for the baseline regarding the calibration factors have been applied to the derived LH2 concept. Nevertheless, three design changes have to be considered that do not allow to use exactly the same values for calibration:

- In Section 3.3.1, a calibration factor for the longitudinal position of the center of gravity of the aircraft OEM was estimated. The value obtained was 0.9875. This factor accounted for the uncertainties in the methodology for the estimation of the center of gravity position of the different aircraft components. However, the same factor cannot be used for an LH2 aircraft that features additional tanks and LH2 systems. These masses are not included in the reference or baseline aircraft. Thus, the calibration factor is recalculated, obtaining a value that achieves the same effect as shifting the OEM center of gravity by 0.9875 without considering the LH2 systems. Based on the D250-LH2 results, the new factor is 0.99.

- The factor for the fuel mass center of gravity is not applied. The location and tank geometry of the LH2 concept differ significantly from those of the baseline and reference aircraft.

- Lastly, the tip-back angle calibrated for the reference might be changed. Due to the aft tanks, if the same value as for the kerosene aircraft is used, the landing gear will be positioned too far aft. This will result in a huge HTP and fuselage-integrated landing gear. Some studies have already identified the need to reduce the tip-back to improve the efficiency of the design, bringing the gear forward. However, this design decision has an impact on the stability of the aircraft during ground operations [7]. This trade-off is further discussed in Chapter 5, where a value for the tip-back will be chosen based on finding the best compromise.

3.4.2. Design space exploration for LH2 aircraft family concepts

The last part of the thesis is dedicated to the design space exploration of LH2 aircraft family concepts. The different tank positioning than in a kerosene aircraft allows for unexplored family strategies with different levels of commonality. Three components have been selected for the study, that are influenced by the changes in the design of an LH2 aircraft when compared to a conventional kerosene design.

- **Vertical and Horizontal stabilizers**: for a kerosene aircraft family, these components are shared. The performance penalties because of having an oversized empennage in some of the family members, are overcome by the commonality benefits. For LH2 aircraft concepts, literature shows that especially the HTP size becomes a critical point in the design. The commonality benefits in the case of an LH2 aircraft family are still to be explored.

- **Cryogenic hydrogen tanks:** for a kerosene aircraft family, the fuel requirements are usually defined for the stretched family version [8]. The tanks are positioned at the wings and the gravimetric index is one. Since the wings are shared among all members, it does not represent any major penalty for the shorter members. These can even use the leftover tank space for payload-range flexibility [8], achieving a higher range. For a hydrogen aircraft, the tank is also sized for the stretched version. However, sharing the tank is not that trivial. The tank is commonly sized for the design mission [7] [70]. In contrast to a kerosene aircraft family, no extra space is allocated in the tank for the payload-range flexibility of the stretched version, which simultaneously restricts the payload-range flexibility of the shorter variants if the same tank is utilized. Oversizing it for the design mission is usually not considered, as it results in a big weight and thus fuel penalty [10].

  Cryogenic tank design appears to be one of the main challenges for this new technology. Thus, it is important to study to which extent is it still feasible for an LH2 aircraft family to share this component. Being able to have a common tank, while achieving the desired range for every member, will definitely reduce the design and manufacturing costs.

- **Fuselage length:** if a trade-off between payload and range is done for a kerosene aircraft family, the fuselage length is never shared. A change in the passenger number always implies a change in the fuselage length, to fit a different size cabin. However, this is not necessarily the case for an LH2 family. The design published by Huete et.al. [73], showcases the possibility of using the same fuselage length. The LH2 tank changes in size to modify the range, shrinking or stretching the cabin length for a constant fuselage length.

  Nevertheless, the benefits of sharing the same fuselage length are still to be investigated. Although currently the fuselage length is not shared among kerosene aircraft members, the change in length is just obtained by adding or removing fuselage sections from the cabin (see Figure 3.3). These are the so-called family sections.

  In the case of an LH2 aircraft family, although the fuselage length can be kept constant [73], the pressure bulkheads for the cabin would have to be positioned differently, together with the windows or tank crash structure. This in the end results also in the use of different fuselage sections for each member. Consequently, what could be shared among LH2 family members is the outer skin, together with the structural elements [91]. Some benefits from this could be the standardization of the different parts of the fundamental structure of the fuselage. Besides this, the manufacturing infrastructures will only have to adapt to a single fuselage length, reducing the modifications needed in the production chain for all members.

Based on the components above, the commonality of the tank, the HTP, and the VTP will be studied for different LH2 aircraft families. On the other hand, the fuselage length commonality is not considered. The benefits from the commonality of this last component are simple hypotheses. A more detailed study is required. The same engine, wing, and landing gear attachment is assumed for every member.

The three different family strategies explained in Section 2.2.2.1 for kerosene aircraft will be studied using as the main family member the D250-LH2 concept [13]. The various family versions will be

derived from it. In order to carry out this study, a simplified version of the Set-Based-Design approach for family design is used (see Riaz et al. in [33]). The purpose of this thesis leans more towards the evaluation of the performance penalties that come from the commonality of certain components. Thus, the main member of the aircraft family is an input in this case and will not be optimized. The simplified SBD approach involves varying the degree of commonality for the tank, VTP, HTP, along with the definition of different payload and range requirements for the family versions.

The first strategy explores the **payload variation among family members. The same fuel capacity is used among all members.** The main idea behind this strategy is a payload-range trade-off [41]. Reducing the payload, and thus the fuselage length, increases the range for a given family member and vice-versa, given a constant family fuel capacity [33]. This is for example the case in the A320ceo family [44]. The following points aim to be addressed:

- Quantify the payload-range flexibility in the case of an LH2 aircraft family with shared tanks.
- Assess the impact of varying the payload value on the fuselage length, empennage size and commonality, and the resulting family range for a given fixed tank size.

A representation of this first family strategy for LH2 aircraft is shown in Figure 3.10. The main family member (D250-LH2) is sketched on top.

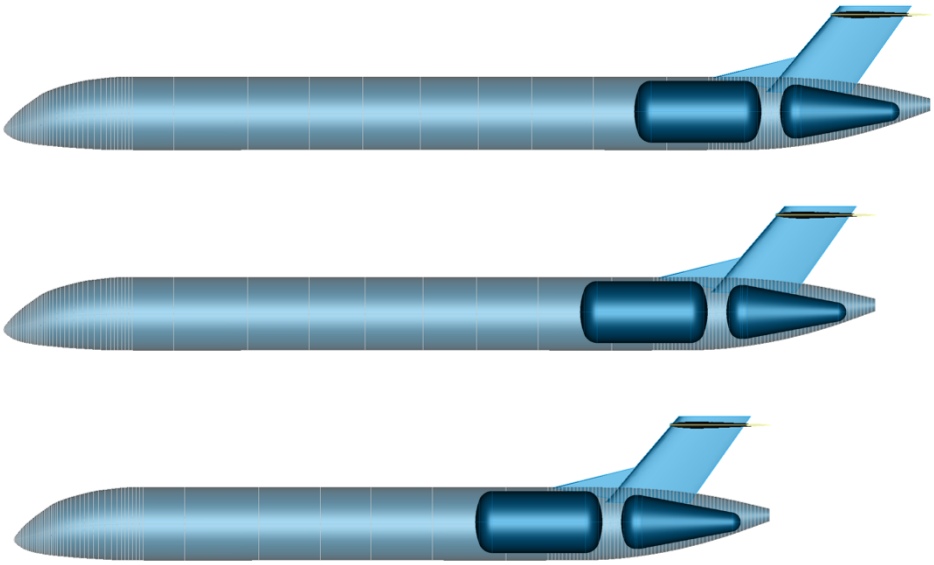

Figure 3.10: LH2 family concept with constant fuel capacity and varying payload

The second strategy considers **constant payload and increased fuel capacity**. This strategy is seen in industry with the -ER (extended range) versions from the Boeing 777 family. In the case of a kerosene aircraft family, fuel capacity can be easily increased by adding center tanks in the wing box dry bay areas [33]. A representation of this second family strategy for LH2 aircraft is shown in Figure 3.11. The main family member (D250-LH2) is sketched on top. This second study aims to address the following points:

- Quantify the impact of increasing the tank size on the aircraft performance. For this case, a typical evaluation mission for a SMR aircraft will be analyzed for both the base and -ER versions to assess the impact of the larger tank on the performance of the -ER version.
  Different ranges will be defined for the same payload to analyze the trend in fuel consumption for the evaluation mission.
- Quantify the impact that different tank sizes have on the HTP size and its commonality among family members.
- Identify whether the aircraft with the shorter fuselage or the one with the heavier tank is the sizing member for the horizontal tailplane.

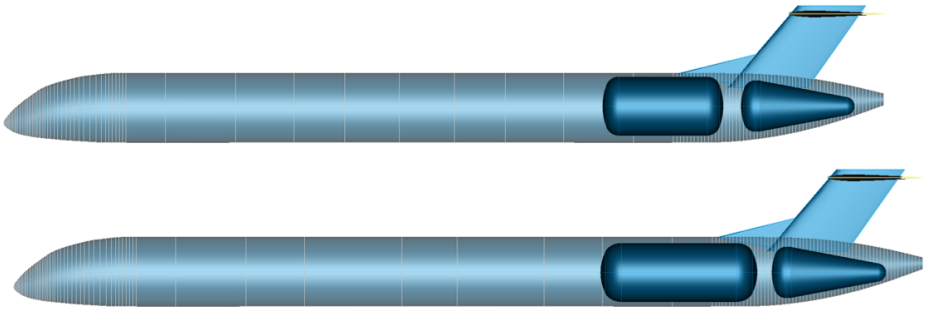

Figure 3.11: LH2 family concept with constant payload and varying fuel capacity

The last strategy considers a **variation of both payload and range among family members**. In this case, the payload will be reduced compared to the main family member, while the tank capacity will be increased. This strategy is atypical for kerosene aircraft, where payload and range are usually increased simultaneously. However, due to the limited payload-range flexibility of LH2 aircraft [8], it is valuable to study this approach. The following points will be addressed:

- Calculate how reducing the fuselage length due to payload reduction while increasing the tank size affect tailplane commonality.
- Compare the results obtained with the ones from the previous strategy, where also different tanks where used but the payload was kept constant.
- Draw conclusions regarding the commonality of the tailplane in a scenario in which both fuel capacity and payload were increased, as done conventionally for kerosene families.

A representation of the final family strategy is shown in Figure 3.12. The main family member (D250-LH2) is sketched on top.

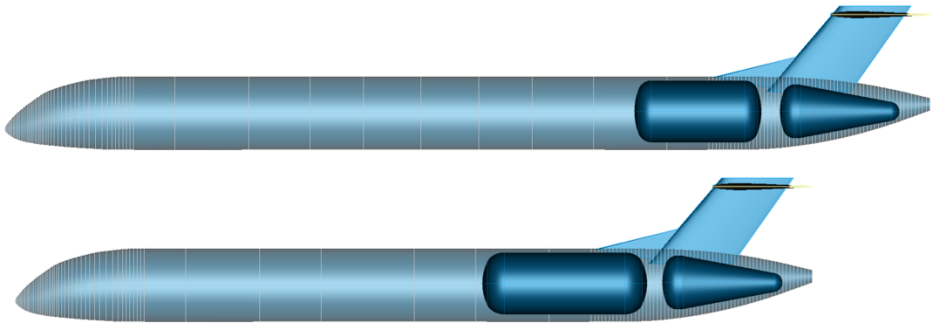

Figure 3.12: LH2 family concept with varying fuel capacity and payload

Note that for the two last family strategies, another modification had to be done to the workflow in Figure 3.1. Since a different tank is sized for each family member, the corresponding branch for the LH2 sub-workflow was integrated as well in the aircraft design loops for the family versions, as done for the main family member.

4

Validation and Verification

The fourth chapter of the thesis presents the verification and validation results for the methodology outlined in Chapter 3. Section 4.1 establishes the general assumptions, workflow settings, and limitations of the study. Section 4.2 details the verification and validation processes, using the D239 aircraft as a the reference aircraft. The results for the D239 aircraft family not only confirm the validity of the workflow but also address the first research question of the study.

4.1. Methodological Framework and Limitations

Before getting into the results, it is important to establish some assumptions taken for the design study carried out in this thesis, together with its limitations. This section justifies the convergence criteria used for the aircraft sizing loops, the analysis settings chosen for the different tools, and its limitations.

4.1.1. Convergence criteria chosen for the design study

As described in Section 3.1.2, the workflow converges all disciplinary analysis tools in parallel. After every iteration, the values for OEM and MTOM are checked. The criteria chosen to determine when the design has converged is justified in this section.

For the outer convergence loop, a criterion has to be chosen to determine when both VTP and HTP sizes are converged. For this study, a difference between consecutive iterations of less than 0.5 m^2 is considered for both lifting surfaces. Based on the reference aircraft family, the A320neo family, and the corresponding HTP and VTP sizes of approximately 31 m^2 and 20.4 m^2 respectively [48], this translates into an error of around 2 %.

The convergence criteria for each of the aircraft sizing loops is chosen based on the tolerance set for the HTP and VTP. For the main aircraft sizing loop, a weight convergence criteria of less than 20 kg difference for both MTOM and OEM is established between three consecutive iterations. After every iteration, the aircraft weight changes due to the recalculated fuselage mass, wing mass, fuel mass, and HTP and VTP masses, that come from the Level-1 fidelity tools. A sensitivity analysis was performed, that identified that a change in the vertical or horizontal tail size of 0.5 m^2 equaled to a 10 kg change in the aircraft OEM. Since all mass values are converged at the same time, a change in 20 kg was considered small enough for the design to be converged. A bigger difference will still detect changes in the VTP and HTP sizes bigger than 0.5 m^2.

On the other hand, if the LH2 tank sub-workflow is also active in the main design loop, the weight convergence criterion is raised to 30 kg. In this case, the weight of the cryogenic tank and other LH2

systems, as well as the fuselage length, is converged in parallel with the other aforementioned values. For the family versions design loops, a weight convergence criteria of less than 15 kg difference for both MTOM and OEM is established between three consecutive iterations. In this case, only the fuel and the empennage masses are converged. Thus a smaller tolerance is taken.

The minimum step for wing positioning in the HTP sizing algorithm was also calibrated based on the reference aircraft and the assumed error of 0.5 m^2. A study was carried out to see how sensitive the HTP size was to a shift in the wing position. A change in the HTP surface area of 0.5 m^2 was approximately equivalent to shifting the wing by ±0.03 m. Therefore, this value was set as the minimum step for the wing position algorithm.

4.1.2. Horizontal tailplane sizing tool settings and assumptions

The validation of the tool as an analysis instrument is shown in Appendix A. The tool was run for different aircraft families. The assumptions taken for some of the parameters and its justification are showcased in Appendix A. The same settings were taken for this study, depicted in Table 4.1.

Table 4.1: Horizontal tailplane sizing tool assumptions

TLAR	Value	Units
DPR cruise (conventional/T-tail)	0.875/1	[-]
DPR take-off flap settings (conventional/T-tail)	0.825/1	[-]
DPR landing flap settings (conventional/T-tail)	0.75/1	[-]
DPR rolling (conventional/T-tail)	1/1	[-]
SM ($\%MAC$**)**	10 %	[-]
$i_{h_{max}}$	-10	[°]
$\delta_{e_{max}}$	-30	[°]
V_R/V_S	1.05	[-]
$c_{m_{ac}}$	-0.01	[-]

4.1.3. Limitations

It is crucial to establish certain limitations of the methodology outlined in Chapter 3, as these will help with the interpretation of the study's outcome. Most of them are related to the usual uncertainties that characterize the early stages of an aircraft design.

Firstly, it is important to recognize that it is not feasible to perfectly match all reference aircraft parameters using the available methods. A calibration process is always required, during which specific calibration factors are established. These factors are applied to the results generated by the methodology, ensuring alignment with publicly available data across the various disciplines of the reference aircraft.

The horizontal tailplane sizing tool has also some parameters that have to be guessed. Its values are really difficult to estimate at the early stages of the aircraft design process. Specially, 2 parameters have been set as a fixed value inside the tool. These are the dynamic pressure ratio (DPR) at the tail and the horizontal stabilizer maximum incidence angle. The justification behind these assumptions, together with the validation process using different aircraft families, is shown in the internship report extract from Appendix A.

The HTP sizing tool is based on some semi-empirical methods developed from wind tunnel experiments during the 50s and 60s [17]. The aircraft geometries that were tested 70 years ago were slightly different to the ones from today. However, the aircraft configurations studied in this thesis are still in line with the tube & wing design philosophy. Consequently, these methods have been considered enough for this study to model the aircraft behaviour. Nevertheless, it has to be taken into account that in some situations, the methods from DATCOM do not contain sufficient information. This has been observed especially for high aspect ratio wings. The DATCOM plots only show data up

to AR = 10 [17]. In the case of an AR > 10, the value for an aspect ratio equal to 10 is taken as an approximation of the actual value for the higher AR wing. Extrapolation has not been considered an option.

When comparing a point and a family design, some considerations have to be taken into account. As explained in Section 3.1.2, only the re-sizing of the HTP and VTP is considered among family members. Thus, a point vs family design comparison for the long member is the only one that actually makes sense. All shared components are usually sized for the stretched version except for the empennage. In order to have a fair comparison for the remaining family members, the resizing of other components, such as the engine, should also be also accounted for.

In these comparisons, the mission fuel mass (MFM) or block fuel mass (BF) are typically selected as the performance metric. It is important to note that the aircraft fuel mission calculator tool does not account for trim drag. Although trim drag may vary significantly between LH2 and kerosene aircraft due to differences in center of gravity range, this variation is not critical, as only comparisons between the same type of aircraft are being made, with no direct kerosene-to-hydrogen performance comparisons. Consequently, the effect of trim drag is not expected to impact the final results.

The enhanced workflow considers the change in both VTP and HTP size among family members. The methodology used for the HTP has a much higher level of fidelity than for the VTP. In this latter case, a really simple empirical formula is used (see Section 3.1.2). This expression is purely based on the aircraft geometry. Thus, it captures the difference in the VTP size due to the change in the lever arm, identifying the short member as the sizing case. However, in an aircraft family, not only the change in geometry between members influences the VTP size. Although the engine is shared, the thrust value is artificially down-rated for the shorter members [47]. The empirical expression used to size the VTP in this study does not consider this thrust down-rating. For a conventional transport aircraft design, the vertical tailplane (VTP) is typically sized for the one-engine inoperative (OEI) condition [5] [23]. Considering the variations in thrust among different family members—especially with the stretched variant having the highest thrust—could reduce the differences in VTP size between members.

One last point is made on the methodology used for the design of an LH2 aircraft family with common tanks. For this case, the tanks are sized for the long family member based on the range set as a TLAR. The same tank is then used for the design of the short family members. The ranges of these aircraft are a result of the reduction in aircraft payload and the fuel mass defined for the long member. The aircraft mission calculator tool calculates the ranges in an interative process from the fixed fuel value. It should be noted that LH2 boil-off is neglected in the calculations, as no thermodynamic analysis of the mission is conducted within this tool. The impact of boil-off on the final range result is neglected. This assumption is based on the excellent insulation properties of MLI tanks, along with the small increase in flight time for the shorter members compared to the long family variant.

4.2. Verification and Validation Results

This section showcases the verification and validation procedures followed for the aircraft family design workflow. The goal is to verify and validate the integration of the horizontal tailplane sizing tool as part of the EXACT workflow. The D239 reference aircraft will be used as the validation case, comparing the obtained results to the publicly available data of the Airbus A320neo family [49] [48] [50].

4.2.1. Verification procedures

The following means of verification were used to ensure that the design process was internally being carried out correctly:

- **HTP sizing tool:** as explained in Section 3.2 and Appendix A, the tool includes several semi-empirical formulas for calculating various required parameters, such as $C_{L_{max}}$ or $C_{m_{ac_{wf}}}$. A separate Python script was used for each of these calculations. This approach facilitated debugging and ensured that each parameter was computed correctly, ultimately leading to reliable results for each tail sizing requirement.

- **Modified workflow:** for every run, RCE generates a workflow data browser module. Every time a workflow component runs, the input and output files are stored here. This makes it easy to check at every point if the implemented modifications are influencing the design as expected.
  At the end of each iteration of the aircraft design loops, the values of some key parameters were stored in a vector. These were the HTP and VTP sizes, wing position, block and mission fuel mass, fuselage length (for LH2 aircraft), OEM, and MTOM. These vectors were used as a quick check to see if the design was converging correctly and to spot any irregularities in the process.

4.2.2. Validation process

The reference aircraft for the study is the D239 aircraft concept, the DLR interpretation of the A321neo [11]. The TLARs are specified in Table 3.1. This aircraft will be sized as the main family member, with two shorter versions derived from it. These will be similar to the A320neo and A319neo aircraft, and named for this study D239-mid and D239-short respectively. The three aircraft collectively constitute the D239 family. The definition of the two shorter family versions is done based on a series of parameters as explained in Section 3.1.2 of the document. Their values are shown in Table 4.2. The definition of the design mission ranges and payloads of the shorter family members is done based on the available information for the A320 family [24]. A similar proportional change is applied, considering the values of 2500 NM and 239 PAX used during the EXACT project for the D239 reference [11].

Table 4.2: Family versions definition for the D239 family concept

TLAR	D239-mid	D239-short	Units
Design Range	2900	3300	[NM]
Design PAX (single class)	185	156	[-]
Design Payload	17000	16400	[kg]
Max. Payload	19200	19000	[kg]
Δl_f	-6.93	-10.67	[m]
Δl_{VTP}	-2.70	-4.70	[m]
dm_f/dl_f	275	275	[kg/m]
Δm_w	-1400	-1400	[kg]

The goal of the workflow is to size the D239 reference aircraft taking into account potential family members in the design loop. The D239 is sized as the main family member, sizing in parallel the other two shorter family members. These two aircraft will help mainly to define the empennage size for the family. The process followed can be divided into two steps as explained in Section 3.1.2: the point design and the family design. The results for both and its comparison are presented in the sections below.

4.2.2.1. Point design results for the D239 aircraft family

The differences between family members in the first iteration of the design loop are depicted in Table 4.3. The $x_{root,LE}$ parameter from OpenAD is taken as the indicator for the wing position. It represents the position of the leading edge of the root chord of the wing measured in meters from the aircraft nose.

Table 4.3: Point design results for the D239 reference aircraft family

	D239	D239-mid	D239-short	Units
$x_{root,LE}$	16.68	12.68	10.85	[m]
S_v	18.07	19.19	20.50	$[m^2]$
S_h	26.20	29.28	31.81	$[m^2]$

The short family member is the sizing aircraft for both the HTP and VTP. This was expected, as it is **the one with the shortest tail lever arm**. The scissors plots corresponding to the results in the third

row of Table 4.3 are shown in Figures 4.1 and 4.2, for the D239 and D239-short variants, respectively. The scissors plot for the D239-mid is not shown, as it follows the same trend as the figures below, with the center of gravity range positioned neatly between the take-off rotation and stability boundaries. Note that the green line corresponding to the take-off rotation requirement at sea level (SL) in Figure 4.2 is hidden behind the take-off rotation requirement at airport conditions (AP).

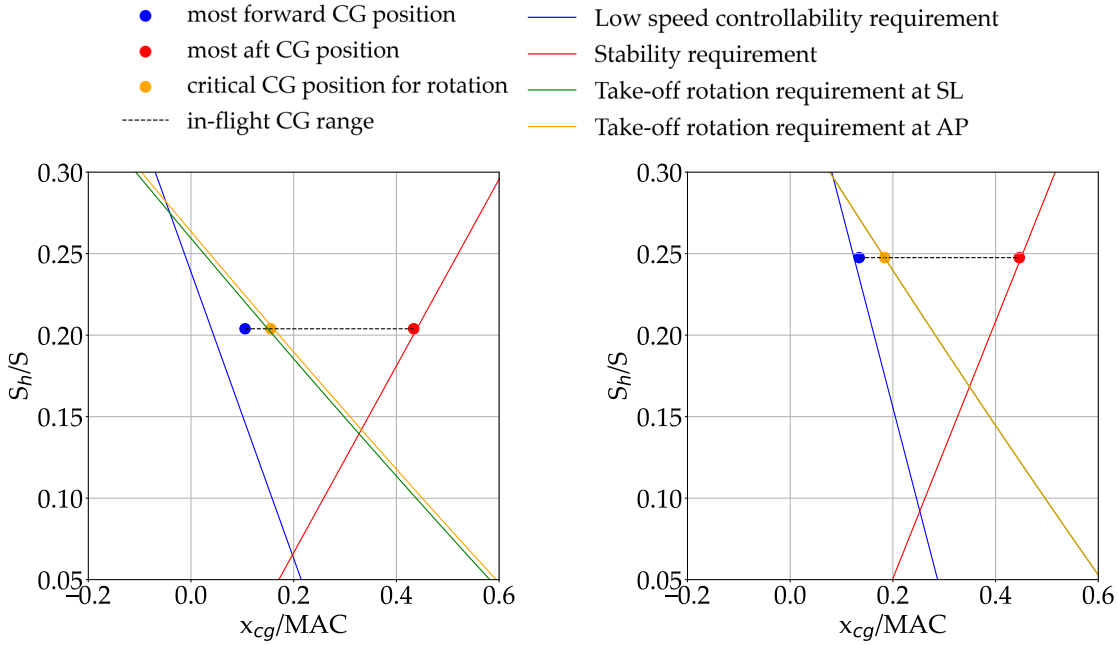

Figure 4.1: Scissors plot for the D239 concept (point design). Wing surface area S = 128.45 m^2

Figure 4.2: Scissors plot for the D239-short concept (point design). Wing surface area S = 128.45 m^2

For all D239 family members the wing position is adjusted individually until obtaining the minimum HTP size for each family member. As can be observed in the X-plots, the center of gravity range lies perfectly between the take-off rotation and the stability requirements. The tail is oversized for control. However, shifting the wing further aft would increase the HTP size required for rotation by reducing the tail arm with respect to the main landing gear position.

As explained in Section 3.1.2, for wing-box commonality, the landing gear aims to be integrated for all members at the same relative position along the wing chord. In this case, the common position is taken from the result of the main family member design, and is fixed for the shorter versions. In the case of a kerosene aircraft family, it is observed that for the point design all aircraft have a similar center of gravity range, with the most aft center of gravity positioned in a comparable MAC percentage (see scissors plots above). Only small adjustments in the tip-back angle of the short family versions are required to achieve the desired position for the main gear integration. However, these assumptions do not hold anymore for LH2 families, as will be further discussed in Chapter 5.

4.2.2.2. Family design results for the D239 aircraft family

For the point designs, the D239-short concept resulted as the sizing family member for both VTP and HTP. In the second iteration of the workflow, the D239 main family member is resized using fixed reference areas for both the VTP and HTP, based on the values determined by the sizing member.

The wing position for the main family member is calculated as well based on the results from the D239-short. The value for the $x_{root,LE}$ parameter is reversed engineered from the wing position of the short family member (see Table 4.3), and the change in fuselage length (see Table 4.2). For these later values, the data from the A320 family in Figure 3.3 has been used as reference. Equation (4.1) is used for the calculation of the wing position of the long family member. The value for the D239-mid is calculated based on this result, see equation (4.2).

$$x_{root,LE_{long}} = x_{root,LE_{short}} - \Delta l_{f,short} + \Delta l_{VTP,short} = 10.85 + 10.67 - 4.7 = 16.82\ m \tag{4.1}$$

$$x_{root,LE_{mid}} = x_{root,LE_{long}} + \Delta l_{f,mid} - \Delta l_{VTP,mid} = 16.82 - 6.93 + 2.7 = 12.59\ m \tag{4.2}$$

The family design phase continues until equal VTP and HTP sizes are obtained between consecutive iterations, as explained in Section 3.1.2. The D239 family design took 3 more iterations to converge. The final scissors plots are shown in Figures 4.3 and 4.4, for the D239 and D239-short respectively. The D239-mid is again not shown as it does not provide any additional information.

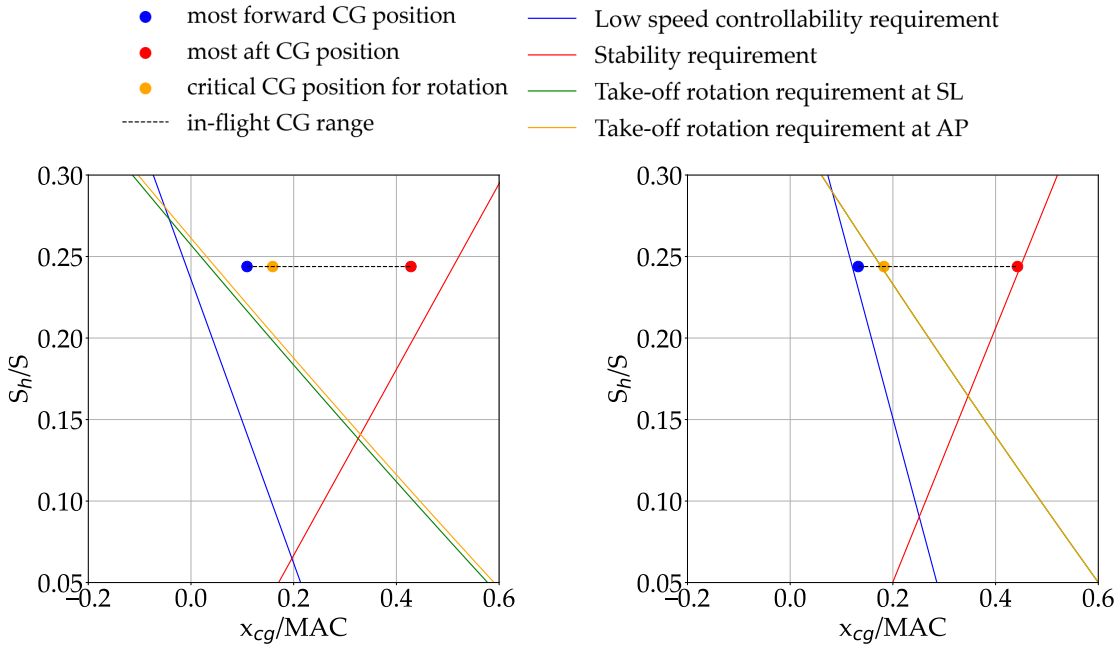

Figure 4.3: Scissors plot for the D239 concept (family design). Wing surface area S = 128.96 m^2

Figure 4.4: Scissors plot for the D239-short concept (family design). Wing surface area S = 128.96 m^2

In Table 4.4, the results for the point designs and family designs for all aircraft members are compared alongside actual data from the Airbus A320neo family [48] [49] [50].

Table 4.4: Final results for the D239 reference aircraft family

	Units	**Point design**			**Family design**			**A320neo family**		
		D239	**D239 mid**	**D239 short**	**D239**	**D239 mid**	**D239 short**	**A321**	**A320**	**A319**
$x_{root,LE}$	$[m]$	16.68	12.68	10.85	16.77	12.54	10.85	16.80	12.71	10.86
S_v	$[m^2]$	18.07	19.19	20.50	19.92	19.92	20.06	20.40	20.40	20.40
S_h	$[m^2]$	26.20	29.28	31.81	31.45	31.45	31.19	31.0	31.0	31.0

As depicted in Figure 4.3 and the results in Table 4.4, the tail is oversized for both the D239 and D239-mid variants. In the case of the D239-short, the tail size is minimized, and the wing is positioned accordingly. Note that the values for both the tailplane size and $x_{root,LE}$ differ slightly from the first iteration results of the D239-short. This discrepancy arises from the changes made to the D239 main family member, which also affect the design of the -short version as highlighted in Section 3.1.2.

The final wing position of the non-critical family members changes also with respect to the optimum found during the point design. The family fuselage sections are the ones that define this final position. The definition of the length of these sections is also part of the family design process. For the reference the values were already defined (see Table 4.2), which were taken from the available data in Figure 3.3.

A study on how to define the family sections length and its impact on the family design is done for both the D250 and D250-LH2 aircraft families in Chapter 5.

A small difference is given between the VTP and HTP sizes for the D239-short and the ones for the D239 and D239-mid. Note that this difference is below the 0.5 m^2 threshold established for the study. Thus, the family design is converged. This difference could be further reduced with additional iterations; however, this would only increase computational costs without providing any new insights.

The final results for the D239 aircraft family design closely align with the data available from the Airbus Airport Planning manuals for the A320neo family [48] [49] [50]. This validation process confirms the effectiveness of the new methodology for sizing an aircraft tailplane while considering potential family members within the design loop. This approach successfully aligns with the available data from the A320neo family, accurately matching key parameters relevant to the study, including the tail size and wing position across all family members. It should be noted that the measurements for the tail areas and wing positions in Table 4.4 were taken directly from CAD sketches, as no explicit values were provided in the manuals. This together with the uncertainties associated to the methodology, explains the small difference between the obtained results and the actual aircraft data.

A final verification check is conducted to ensure that the modifications made to the workflow continue to produce a consistent reference aircraft for the study. The reference was initially calibrated for various studies under the EXACT project, see for instance [11]. Therefore, the development of the reference model from scratch was not the primary objective of this thesis. Instead, only straightforward calibration factors were applied to the existing reference model to align with the specific parameters of interest, particularly due to the incorporation of higher fidelity models for HTP sizing. Table 4.5 compares different weight values of the D239 reference against the public data provided in the A321neo Airport Planning Manual for the WV053 weight variant [50]. The weight values are still close to the actual data. Figure 4.5 shows the payload-range diagram. The short substitution segment until reaching maximum fuel capacity in the diagram is characteristic from a stretched family version like the D239. In these designs, there is a small gap between the mission fuel mass and the maximum fuel capacity.

Table 4.5: Mass comparison between the D239 concept (family design (F)) and the A321neo WV053 data [50]

	D239 (F)	A321neo (WV053)	Units
MTOM	93350	93500	[kg]
MLM	78988	79200	[kg]
MZFM	75378	75600	[kg]
OEM	50378	50600	[kg]

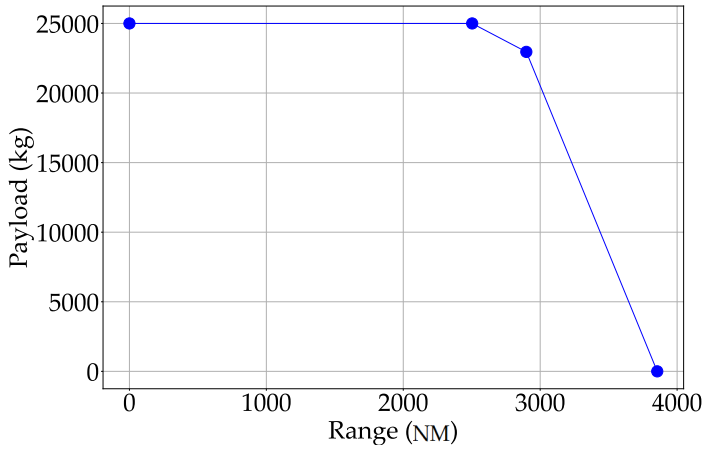

Figure 4.5: D239 main family member payload-range diagram

Following this section, **it can be concluded that the first research question of the study has been addressed**. The developed methodology effectively sizes an aircraft, in this case the D239 reference, while considering potential family members in the design loop. Both the HTP and VTP are sized according to the most critical member, and the wing is positioned to achieve the minimum HTP size for the family. The methodology has also been validated. The obtained results show a small error when compared to publicly available data from the A320neo family [48] [49] [50] as depicted in Table 4.4. The three-view representation for the D239 and D239-short concepts are shown in Appendix B. In addition, the center of gravity range for the final D239 design, as shown in Figure 4.3, aligns with the target values established in Section 3.3.1, based on the data from [50] and [88].

4.2.2.3. Comparison of point design and family design

In this section, the the MTOM-breakdown for the long member of the D239 aircraft family is analyzed. The point design (D239 (P)) mass values are compared to the ones from the family design (D239 (F)). As explained in Section 4.1.3, the D239 stretched version is the only family member for which this comparison makes sense. The MTOM-breakdown comparison is depicted in Figure 4.6. The first expected change is the increase in the aircraft operating empty mass. **The family design is 0.7 % heavier than the point design**. This results in a difference of 350 kg, which can be broken-down into the different aircraft components:

- **VTP and HTP:** the short family member is the sizing case for both lifting surfaces. Fitting a bigger empennage than for the point design into the D239 concept, increases the OEM value.
- **Engines:** the engines must be resized to meet the established TLARs due to the increased weight of the design. This resizing will result in larger and heavier propulsion systems.
- **Wing:** the wing mass increases slightly due to the heavier engines.
- **Fuselage:** the fuselage mass increases slightly to provide structural support for the heavier wing and tailplane surfaces.

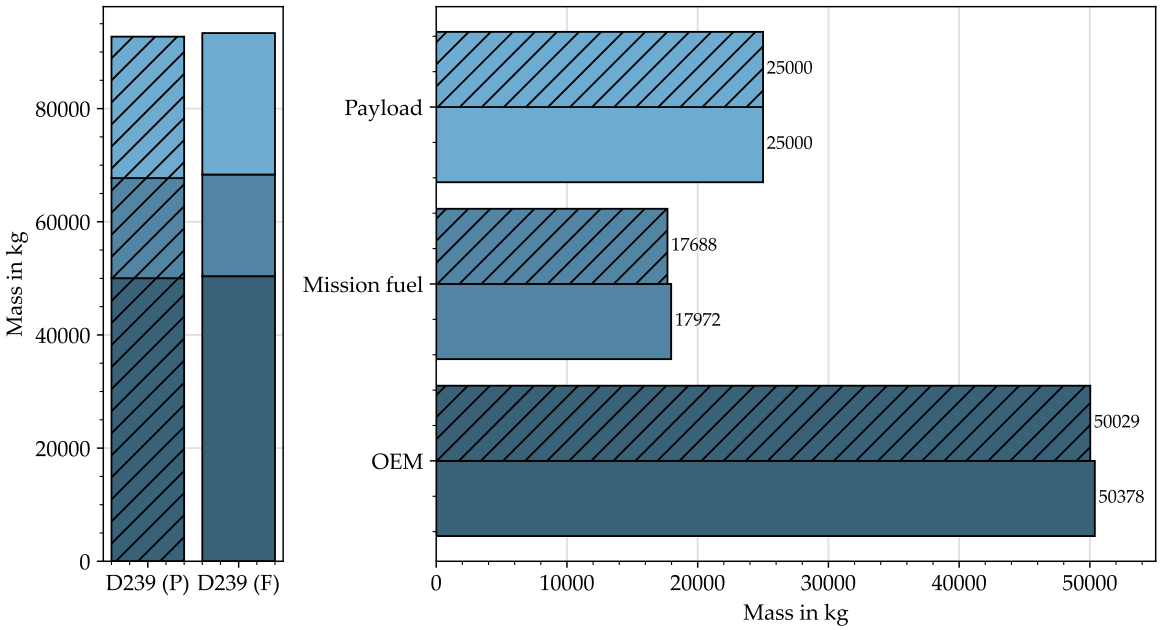

Figure 4.6: D239 concept MTOM-breakdown comparison of point design (P) vs family design (F)

To evaluate the impact of the increased OEM on aircraft performance, a mission analysis was performed to calculate the required mission fuel mass (MFM) for each design. The results, shown in Figure 4.6, indicate that the higher OEM in the family design leads to an additional 238 kg of fuel for the same mission compared to the point design. **This makes the family design 1.65 % less efficient overall**. In practice, all members of the A320neo family use the same vertical and horizontal tailplanes [48] [49] [50]. Consequently, **the performance penalty given of 1.65 % is justifiable given the commonality benefits of this real case industry example**.

5

Results and Discussion

This chapter puts together the results obtained for the different aircraft family conceptual designs. It includes both kerosene as well as LH2 aircraft. All concepts have been produced using the methodology outlined in Chapter 3 and validated in Chapter 4.

The thesis work builds upon the methodology and results from the EXACT project [12]. The D250 [11] [89] and D250-LH2 [13] concepts are utilized in this chapter to conduct various family design studies. Firstly, both concepts have been redesigned using the updated aircraft sizing workflow. This new workflow incorporates a higher-fidelity tool for sizing the HTP, and includes potential family members in the design loop that influence the main aircraft design. These considerations have led to trade-off studies that were not possible during the initial sizing of these concepts.

Section 5.1 presents the redesign of the D250 kerosene baseline aircraft, along with the results of the D250 aircraft family. The family strategy used is the same as for the D239, in which payload is traded for range, for a fixed fuel capacity. Two shorter family members are derived from the D250 baseline. The section introduces the design trade-offs that will be carried out for the LH2 configurations, and establishes a baseline for comparing the results obtained.

Section 5.2, presents the redesign of the D250-LH2 aircraft concept and the D250-LH2 family. The same family design strategy is used as for the D239 and D250 for comparison. Several design studies are conducted in this section to come up with the final family design:

- Landing gear integration trade-off study
- Landing gear positioning trade-off study
- Study of the benefits of HTP leading edge high-lift devices
- Study of the optimum length definition for the fuselage family sections

A final comparison is conducted between the D250 and D250-LH2 aircraft families to identify general trends in the horizontal tailplane sizing process and its commonality specific to LH2 aircraft families.

In the final section of this chapter, Section 5.3, the sensitivities of the D250-LH2 family design introduced in Section 5.2 are further examined. A design space exploration is carried out by varying the payload and range requirements for the different family members, together with the degree of commonality of the cryogenic hydrogen tank. The goal is to identify general trends regarding how various family design strategies, in addition to the one discussed in Section 5.2, affect tailplane commonality and how these impacts compare to conventional kerosene family designs.

5.1. Baseline Aircraft Family: the D250 Family

The D250 kerosene concept (see Section 3.3.2) served as the baseline aircraft for the EXACT project SMR LH2 concepts. The same concept is also used as the baseline aircraft model for this thesis study. Several modifications were introduced into the aircraft sizing routine, as explained in the previous chapters. These modifications can be summarized in three key points:

- A re-calibration process was conducted for the D239 reference aircraft. These calibration factors were also applied to the baseline.
- A higher level of fidelity has been included for sizing the HTP, with an algorithm that influences the final position of the wing to achieve the minimum HTP size.
- Potential family members are considered in the design loop, influencing the tailplane sizing process of the main aircraft.

These modifications have led to new trade-off studies and design decisions that were initially not possible during the design of the D250 concept. Section 5.1 of the document presents the results for the re-design of the baseline using the enhanced EXACT workflow.

The D250 aircraft will serve as the main family member for the D250 aircraft family. Two shorter family members, the D250-mid and D250-short, are designed in parallel. The TLARs for the main family member are provided in Tables 3.2 and 3.3. Table 5.1 summarizes the parameters used to define the shorter family versions.

Table 5.1: Family versions definition for the D250 family concept

TLAR	D250-mid	D250-short	Units
Design Range	1700	2000	[NM]
Design PAX (single class)	220	190	[-]
Design Payload	20900	18050	[kg]
Max. Payload	22000	19000	[kg]
Δl_f	-3.7	-7.4	[m]
dm_f/dl_f	305	305	[kg/m]
Δm_w	0	0	[kg]

The change in range for the shorter members has been defined based on the value of the D250 main family member, using a similar proportional adjustment as applied to the D239 reference aircraft family. The passenger number for the shorter members is defined using a similar passenger ratio as for the reference aircraft family. Note as well that the value for Δl_{VTP} is not included in Table 5.1. Its value is defined in Section 5.1.2, which examines the number of fuselage sections to be positioned behind the wing, along with the definition of their length. The goal is to determine the best relation for the wing position among family members that minimizes the horizontal tail size.

5.1.1. Landing gear integration trade-off study

The D250 aircraft family design serves as a first case study of the observed relationship between landing gear integration and horizontal tailplane sizing. This relationship is accentuated due to the high aspect ratio wing of the D250 design.

The shorter wing inner chord results in a trade-off that was not given for the D239. To minimize the horizontal tailplane size of the D250 family, the resulting wing position does not allow the integration of the landing gear into the wing. During the algorithm for HTP sizing, shifting the wing forward results in a backward movement of the aircraft´s CG range relative to the wing chord. This adjustment also shifts back the landing gear position. Consequently, there will be a point where the wing is positioned too far forward to allow for the integration of the landing gear mechanism into the wing.

As a result, the D250 design requires a trade-off between fuselage-mounted and wing-mounted landing gear, which will affect its final wing position and HTP size. The following section presents a detailed trade-off study between these two integration solutions for the D250 aircraft family. The identified benefits and drawbacks of each approach are discussed, along with the assumptions made in the methodology used to model each solution.

Wing-mounted landing Gear

Advantages:
- More efficient fuselage shape
- Better stability for turning manoeuvres
- Easier access for maintenance
- Better optimization of the revenue space

Disadvantages:
- Heavier empennage
- Sub-optimal wing position
- Higher trim drag

Design Assumptions:
In order to determine if the main landing gear can be integrated into the wing-box, the xsi_{mg} parameter is checked. Its value represents the dimensionless position of the main landing gear along the wing chord. For the D239 design, the main landing gear is positioned at 82 % of the wing chord ($xsi_{mg} = 0.82$).

Based on previous Airbus aircraft designs, the attachment point in the wing-box is typically positioned between 70 % and 80 % of the wing chord. The remaining 20 % of space is typically allocated for accommodating the flaps and actuator mechanisms. A tilted strut can be assumed on top, which will slightly shift the gear position aft, and thus the final xsi_{mg} value. Aircraft such as the 737-MAX employ this solution, as shown in Figure 5.1. In this case, the strut is tilted approximately 10°.

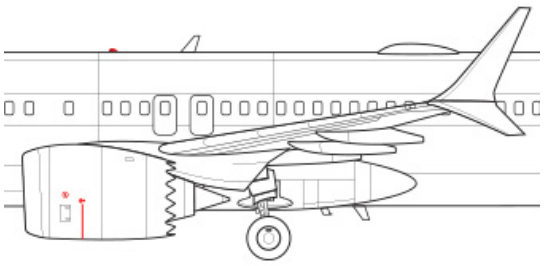

Figure 5.1: Representation of the tilted landing gear strut for the Boeing 737-800MAX [92]

For the design of the D250 family, a 7° tilted strut is assumed. A more conservative solution is adopted, accounting for the longer landing gear that is given for the D250 family compared to the one from Figure 5.1.

In the case of the D250 wing shape, the landing gear is located at a span-wise position corresponding to a wing chord of 4.76 meters. This position is based on a landing gear width of 8 meters, similar to that of the A321 [50]. The resulting height of the landing gear strut from OpenAD, that ensures enough ground clearance, is 2.99 meters. Assuming the wing's landing gear attachment is located at 80 % of the chord length, the combination of the strut height and a tilt angle of 7 degrees places the actual gear position at approximately 87.5 % of the chord length, $xsi_{mg} = 0.875$. This value will be assumed as the limiting case. The wing will be shifted forward, reducing the HTP size, until matching this relative gear position to the wing chord.

Another limitation to consider is that the methodology does not include trim drag calculations when estimating the mission fuel mass. Neglecting the trim drag leads to a slight overestimation of the performance of the wing-mounted gear design. The aft position of the wing increases the static margin, resulting in higher trim drag during cruise.

Fuselage-mounted landing Gear

Advantages:
- Lighter empennage
- Optimum wing position
- Lower trim drag

Disadvantages:
- Less efficient fuselage shape
- Less stable for turning manoeuvres
- Complex big belly fairing design
- Less revenue space available for cargo

Design Assumptions:
As explained in Section 3.1.1, a Level-1 fidelity tool is utilized to estimate the fuselage mass. However, the methods employed do not account for variations in fuselage mass arising from different landing gear integration solutions. The preliminary estimation of the mass, size, and shape of belly fairing is done solely using OpenAD [76]. The methods used primarily consist on simple empirical formulas based on previous DLR project results. To obtain an initial estimate, several assumptions are made:

- The fuselage mass is assumed to increase 3 % compared to the fuselage mass of the wing-mounted gear concept. This factor accounts for the additional weight of the belly fairing and the necessary structural reinforcement of the fuselage.
- The length of the fairing is set to be 2.8 times the length of the wing root chord.
- The width is set to be 1.1 times the landing gear width.
- The fuselage form factor is corrected with an empirical expression that accounts for the increased cross-section area due to the belly fairing. However, no interference drag is considered in the calculations.

The landing gear width is critical for the performance of this configuration. The belly fairing width is defined based on this parameter, which directly influences the fuselage final pressure drag. Figure 5.2 depicts the loading diagram for the D250 concept with fuselage-mounted landing gear.

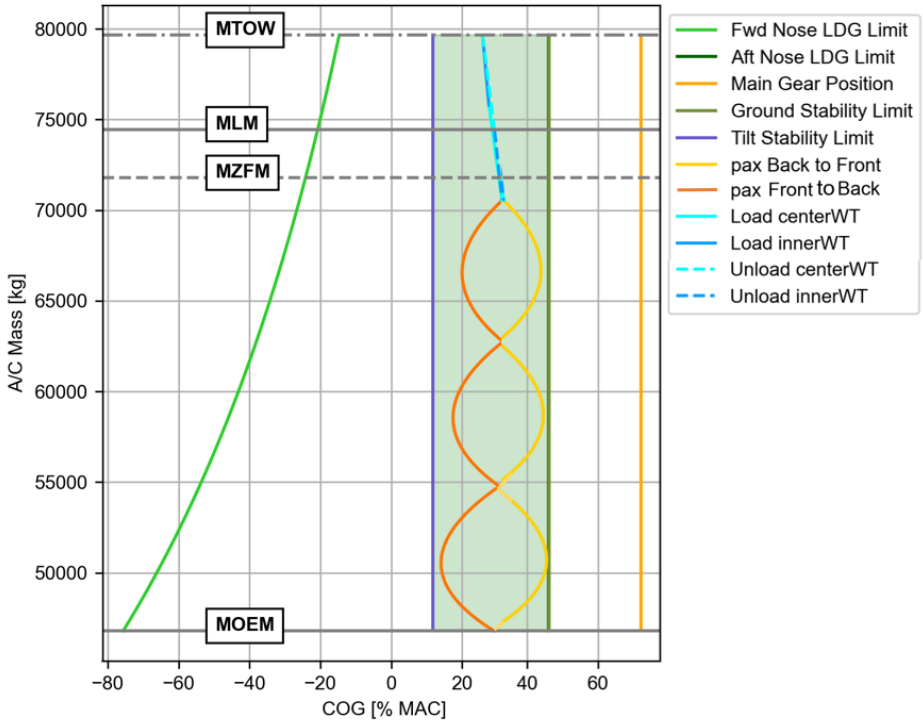

Figure 5.2: Loading diagram for the D250 concept with fuselage-integrated landing gear

The width of the landing gear has been reduced so that the center of gravity shift falls within the tilt and ground stability limits. Consequently, the resulting gear width is approximately 3 meters narrower

compared to the wing-mounted design. Further reduction in width would minimize the size of the fairing, thereby enhancing the aircraft's performance. However, this would compromise stability during ground turns due to an excessively narrow gear track. The overturn angle considered is 63°, which is the maximum value specified in the literature [90]. The higher the overturn angle the narrower the gear track [90]. The same landing gear track is used for the D250-mid and D250-short family versions.

Finally, for the design of the D250 concept with fuselage-mounted landing gear, the inner flap span is reduced. The larger belly fairing causes the inner flap to start at a more outward position compared to the wing-mounted configuration. This reduction in flap span will affect the maximum lift coefficient of the wing, and consequently, the wing reference area.

After establishing the assumptions for both conceptual designs, the results of the trade-off study are presented below. Two aircraft families are designed to determine which one offers the best compromise. A comparison is made between the point designs of each family member. The geometric changes between both integration solutions are summarized in Table 5.2.

Table 5.2: Impact of the landing gear integration on the geometry of the D250 point design family members

	Units	**Wing-mounted**			**Fuselage-mounted**		
		D250	**D250-mid**	**D250-short**	**D250**	**D250-mid**	**D250-short**
S_h	$[m^2]$	24.72	28.05	30.50	25.05	26.79	29.1
$x_{root,LE}$	$[m]$	16.54	14.64	12.80	16.05	14.03	12.18
xsi_{mg}	[-]	0.875	0.875	0.875	0.96	0.96	0.96

Figure 5.3 presents the plan view of both D250 point designs. Above the symmetry line, the fuselage-mounted solution is shown, featuring its prominent belly fairing. Below the symmetry line, the wing-integrated concept is depicted, displaying a slightly aft wing position. Note that the main landing gear is visible behind the wing's trailing edge only in the fuselage-mounted configuration. The plan views for the point designs of the shorter family versions are not included, as they follow the same pattern as the D250 main family member (see Table 5.2).

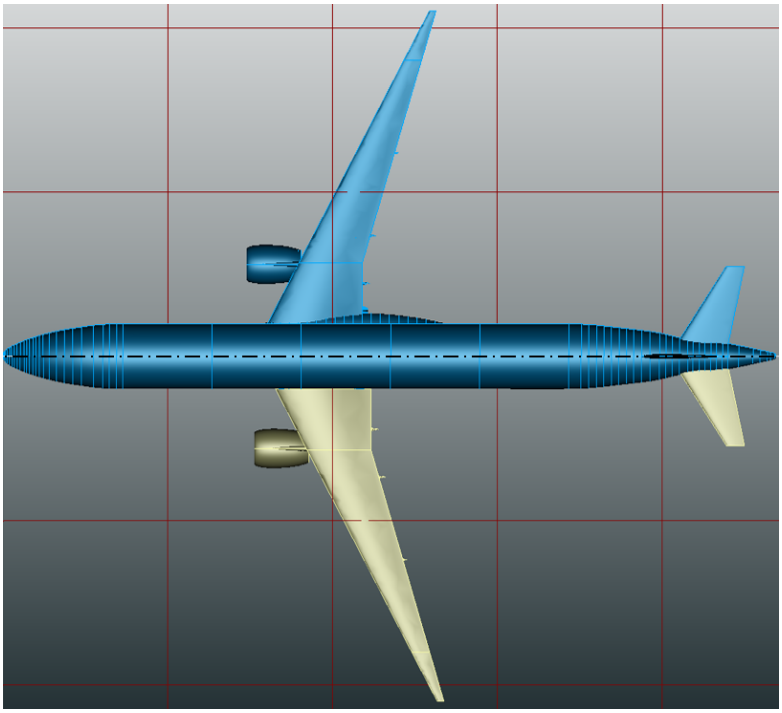

Figure 5.3: Plan view of the D250 concept (point design) with fuselage-mounted (top) and wing-mounted landing gear (bottom)

As discussed above, for the wing-integrated solution, the wing is positioned such that the most aft center of gravity places the gear at 87.5 % of the chord, allowing it to be integrated into the wing. The attachment point is located at 80 % of the chord, resulting in a final xsi_{mg} value of 0.875. The calculation accounts for both the assumed attachment point and the additional distance caused by the gear strut's tilt of 7 degrees. This translates into an extra constraint in the scissors plot that limits the position of the most aft CG, as shown in Figure 5.5 for the D250 main family member. The plot shows a gap between the most aft CG and the stability boundary, indicating a slightly more aft wing position and a design with a higher static margin. On the other hand, the fuselage-integrated design shown in Figure 5.4, depicts a CG range that lies perfectly between the boundaries of the scissors plot, indicating an optimum HTP size and wing position. However, the landing is located at 96 % of the chord, which can no longer be integrated into the aircraft wing. The plots for the shorter versions follow the same trend.

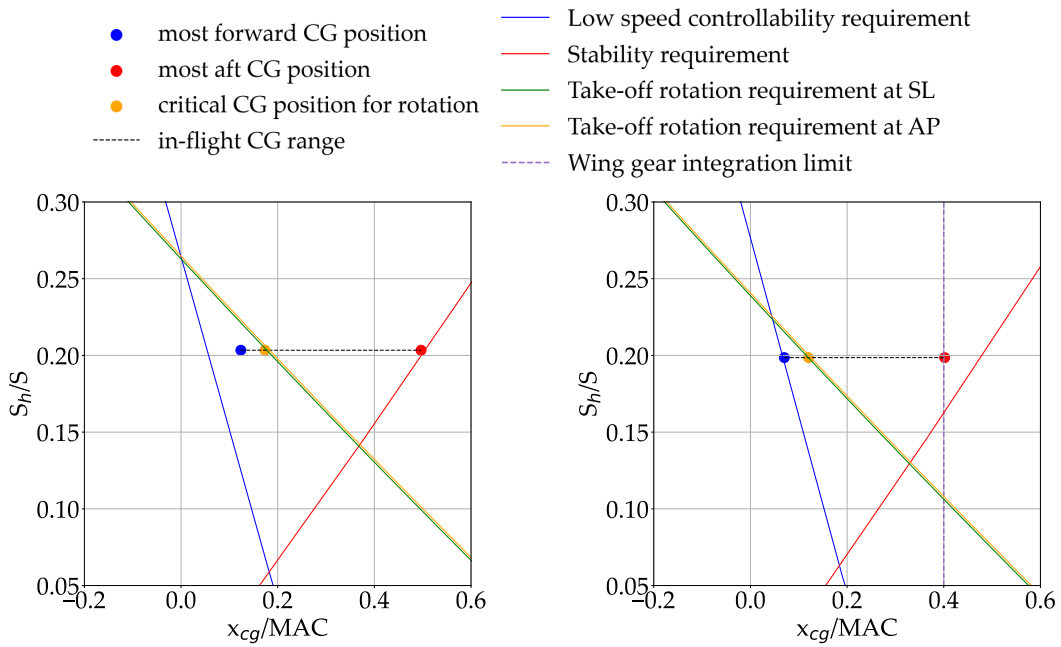

Figure 5.4: Scissors plot for the D250 concept (point design) with fuselage-integrated landing gear

Figure 5.5: Scissors plot for the D250 concept (point design) with wing-integrated landing gear

Note that the HTP size for both long family members is quite similar, which may seem counter-intuitive given previous statements. However, this is merely a coincidence caused by the differing mass distributions of the designs. Due to variations in the center of gravity ranges, the wing-mounted concept actually requires a slightly smaller HTP. Nevertheless, when considering all family members, the general trend aligns with the initial hypothesis as shown in the results in Table 5.2. The horizontal tailplane size of the aircraft concept with fuselage-integrated landing gear is generally smaller across the family.

To determine which concept performs better, the mission fuel masses are compared. Table 5.3 shows the changes in aircraft and mission fuel masses for the point design of all family members.

Table 5.3: Impact of the landing gear integration on the aircraft and fuel mass of the D250 point design family members

	Units	**Wing-mounted**			**Fuselage-mounted**		
		D250	**D250-mid**	**D250-short**	**D250**	**D250-mid**	**D250-short**
MFM	$[kg]$	9123	9376	9867	9207	9425	9898
OEM	$[kg]$	47199	44778	42232	46788	44345	41808
MTOM	$[kg]$	80073	74976	70075	79745	74586	69672

As shown in Table 5.3, the fuselage-integrated gear solution results in a lighter design across all family members. The OEM breakdown for the point design of the main D250 family member is

illustrated in Figure 5.6, highlighting where the weight differences originate. This same trend has been observed for both the D250-mid and D250-short versions.

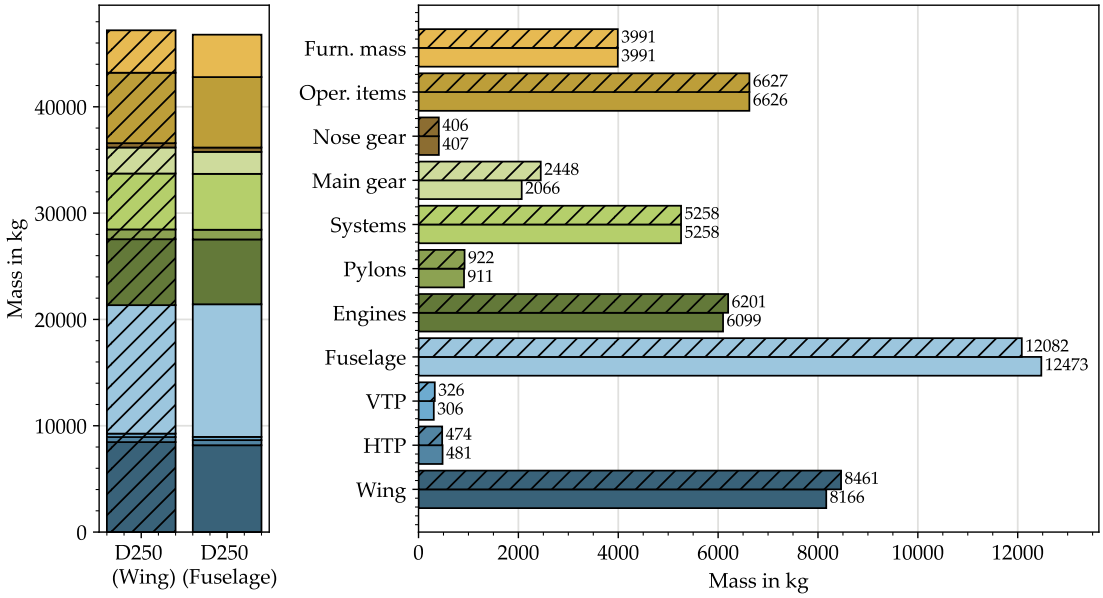

Figure 5.6: D250 concept (point design) OEM-breakdown comparison of fuselage-integrated vs wing-integrated gear design

Although the fuselage itself becomes heavier, the rest of the components are lighter. The wing is lighter because it no longer houses the landing gear, and does not require for structural reinforcement. The landing gear is shorter and therefore lighter. The engines are also lighter as a result of the overall lighter aircraft. Although not depicted in Figure 5.6, for the shorter family members the change in VTP and HTP masses is also noticeable.

However, despite all family members being almost 0.6 % lighter in MTOM and almost 1 % in OEM, the mission fuel mass is slightly higher for all of them. This is primarily due to increased fuselage drag. A drag-breakdown is shown in Figure 5.7. The zero-lift drag for every aircraft component is plotted, together with the total wave and induced drag. The results are expressed in drag counts.

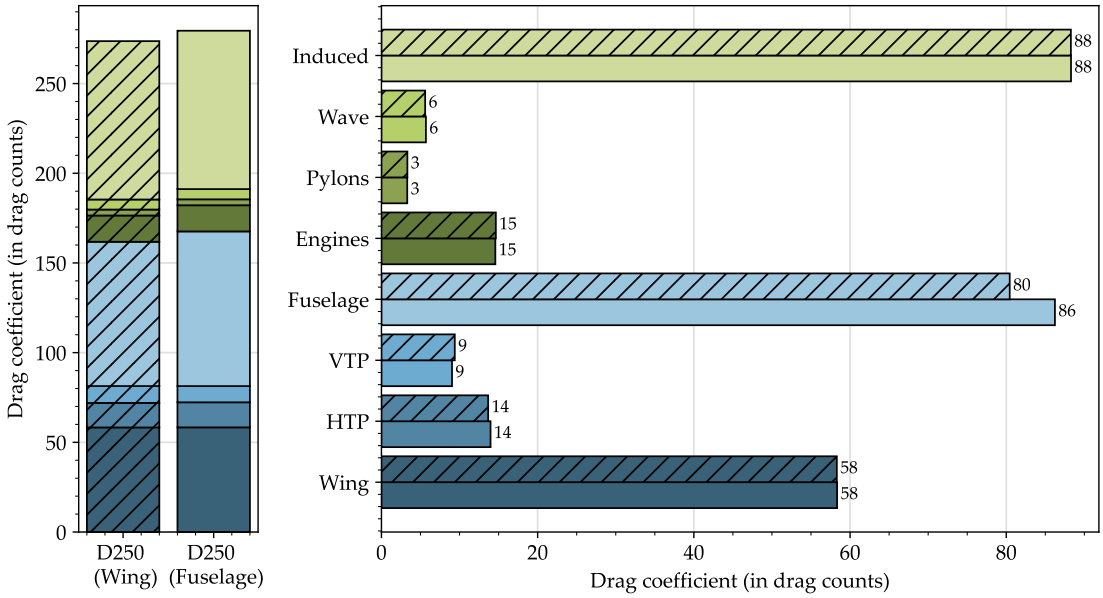

Figure 5.7: D250 concept (point design) drag-breakdown comparison of fuselage-integrated vs wing-integrated gear design

It can be observed that the only noticeable drag change between both concepts comes from the fuselage component, which is higher in the case of the fuselage-mounted gear concept due to the increased cross-sectional area.

After comparing the performance of both concepts, and before making a final decision, a few final considerations need to be taken into account. As depicted in Figure 5.5, the HTP for the wing-mounted concept is slightly oversized for stability. The resulting static margin is bigger than the 10 % value that is assumed for the design of the concepts in the thesis (see Table 4.1). The impact on the performance of the increased static margin is not accounted for in the methodology. This leads to higher trim drag during cruise which is not reflected in the calculations.

On the other hand, interference drag for the fuselage fairing is not modeled. Additionally, the mass and shape of the fairing are roughly approximated using empirical formulas. This approximation introduces uncertainties into the performance evaluation of the fuselage-mounted concept.

All in all, the uncertainties in the performance estimation for both configurations prevent a clear determination of which one is superior. Based on the current assumptions, both designs exhibit similar performance. Increasing the fidelity of drag calculations could potentially demonstrate the fuselage-mounted design's superiority over the wing-mounted design. On the other hand, a more accurate aerodynamic model of the belly fairing might further highlight the advantages of the wing-mounted concept.

In summary, the implemented method is sufficiently accurate to provide an initial understanding of the landing gear integration trade-off for the D250 concept. Both concepts perform similarly, indicating that the decision cannot be based solely on the differences in mission fuel mass. Other factors have played a role in **the selected final configuration, which is the one with wing-mounted landing gear**. Wing-mounted gear offers better maintenance access, superior stability qualities, and it also allows for a better optimization of the cargo bay, resulting into a larger revenue space. These benefits, combined with similar performance metrics, support the decision. The choice made is consistent with common industry practices for transport aircraft design, where wing-mounted landing gear is typically favored for low-wing configurations. Fuselage-mounted landing gear solutions are generally considered only when they offer significant performance advantages, which could be the case for hydrogen-powered aircraft, as will be discussed in Section 5.2.1.

5.1.2. Family fuselage sections length definition

The D250 family concept with wing-mounted gear has been selected as the preferred option. In the first iteration of the workflow, i.e. point design, the wing for each family member is moved independently to match the required gear position at 87.5 % of the chord. However, for the final family design, the wing positions for all family members have to be related through the Δl_f and Δl_{VTP} values.

Δl_f results from the change in passenger number defined for each family member (see Table 5.1), and is a fixed input. A seat pitch of 74 cm is assumed [93]. On the other hand, the value for Δl_{VTP} is defined during the family design process. Since the short member is sizing for the HTP, the following expressions are used to calculate the wing positions for both D250 and D250-mid in the second iteration.

$$x_{root,LE_{long}} = x_{root,LE_{short}} - \Delta l_{f,short} + \Delta l_{VTP,short} = x_{root,LE_{short}} + 7.4 + \Delta l_{VTP,long} \tag{5.1}$$

$$x_{root,LE_{mid}} = x_{root,LE_{long}} + \Delta l_{f,mid} - \Delta l_{VTP,mid} = x_{root,LE_{long}} - 3.7 - \Delta l_{VTP,mid} \tag{5.2}$$

Expression (5.1) positions the wing of the long family member based on the wing position of the short (sizing) family member. Then, the D250-mid wing position is obtained from the long member with equation (5.2). The goal is to determine a value for Δl_{VTP} that positions the wing for both D250 and D250-mid in such a way that the resulting center of gravity (CG) range allows the landing gear to be positioned at 87.5 %. Fitting larger horizontal and vertical tailplanes for these family members shifts the aircraft's

center of gravity range aft. As a result, the wing must also be moved further aft compared to the first iteration. This adjustment shifts the relative CG range forward, ultimately achieving the desired xsi_{mg} value.

The chosen value for Δl_{VTP} is constrained by the need to maintain a constant length for the fuselage family sections ($l_{section}$) for commonality. Based on Figure 3.3, this length must fall roughly between 0.45-0.65 meters. For example, selecting a Δl_{VTP} = 3.6 m would position the wing of the long member at 16.6 meters. This satisfies the first condition for the wing position being slightly aft the result of the first iteration, which was 16.54 meters. However, this choice results in a value of $\Delta l_f - \Delta l_{VTP}$ = 3.8 m, which causes unequal lengths in the fuselage sections ahead of and behind the wing. The value closest to achieving equality is Δl_{VTP} = 3.7 m. The final results are shown in Table 5.4.

Table 5.4: Fuselage family sections definition for the D250 aircraft family concept

	D250-short	D250-mid	D250	Units
Δl_f	-	3.7	7.4	[m]
Δl_{VTP}	-	1.85	3.7	[m]
$l_{section}$	0.62	0.62	0.62	[m]
$n_{sections,ahead}/n_{sections,behind}$	-/-	3/3	6/6	[-]
$x_{root,LE}$	12.81	14.66	16.51	[m]
xsi_{mg}	0.875	0.875	0.875	[-]
tip-back angle	16	16	14	[°]

Note that the Δl_f and Δl_{VTP} values are expressed in this case with respect to the short family member. That is why the defined values are positive, in contrast to the ones shown in Table 5.1 which are defined with respect to the long family member. The fuselage family sections length has been chosen with a similar value to the one from Figure 3.3 and it is conditioned by the value of Δl_{VTP} from the D250-mid. The tip-back angle for the D250 is slightly smaller than that of the -short and -mid versions. In this case, it was not possible to position the wing slightly aft of the point design result due to the limitation of constant-length sections; therefore, the wing is positioned slightly forward. If a 16° tip-back angle had been used, the resulting xsi_{mg} would have been 0.89. As a result, the tip-back angle was reduced to achieve an xsi_{mg} of 0.875. The loading diagram was reviewed to ensure that this minor reduction in the tip-back angle does not compromise the aircraft's ground stability.

5.1.3. Family design results for the D250 aircraft family

The D250 family concept final results are shown in this section. The final concept has wing-mounted landing gear. The fuselage family sections characteristics have been defined in Table 5.4. The three-view of the final concept of the main member is presented in Appendix B. Table 5.5 compares the final results for the D250 family to the point design. It took 3 more iterations of the outer loop to converge.

Table 5.5: Final results for the D250 baseline aircraft family

	Units	Point design			Family design		
		D250	D250-mid	D250-short	D250	D250-mid	D250-short
$x_{root_{LE}}$	$[m]$	16.54	14.64	12.80	16.51	14.66	12.81
S_v	$[m^2]$	17.38	20.61	21.97	21.12	21.12	21.08
S_h	$[m^2]$	24.72	28.05	30.50	29.90	29.90	30.05

Similar to the D239 family design, the final tailplane is oversized for both the D250 and D250-mid. **The short family member is again the sizing version for both the VTP and the HTP**. In this case, the only active constraint in the scissors plot is the controllability requirement, which limits the most forward CG position. Both the take-off rotation and stability boundaries lie significantly ahead of and behind the most forward and aft CGs, respectively. As a result, the final plot for the D250-short follows the same trend as the one shown for the D250 main family member in Figure 5.5.

The point (P) and family (F) designs for the D250 main family member (stretched version) are compared by examining the MFM, OEM, and MTOM values, summarized in Table 5.6. Note that the payload mass is the same in both cases.

Table 5.6: Mass comparison for the point (P) and family (F) designs of the D250 aircraft concept

	D250 (P)	D250 (F)	Units
MFM	9123	9310 (+ 2.04 %)	[kg]
OEM	47199	47561 (+ 0.77 %)	[kg]
MTOM	80073	80621 (+ 0.68 %)	[kg]

To further understand the effect of fitting a larger empennage on the overall aircraft weight, Figure 5.8 provides the OEM breakdown for the main aircraft components of the D250 concept, comparing again the point (P) and family (F) designs.

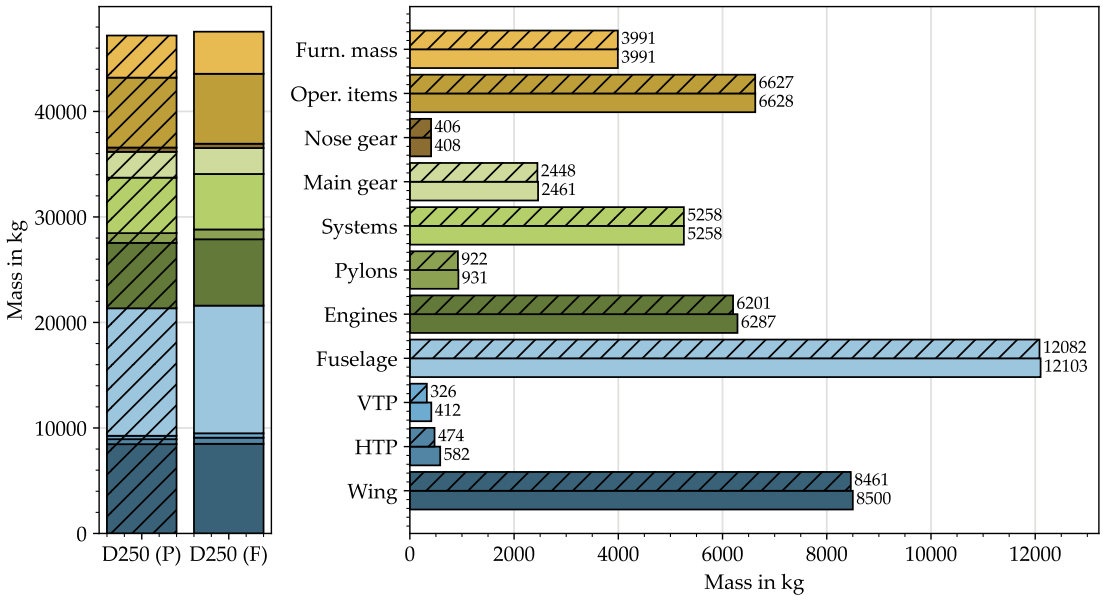

Figure 5.8: D250 concept OEM-breakdown comparison of point design (P) vs family design (F)

Several conclusions can be drawn comparing the results to the reference aircraft in Section 4.2:

- **The same trend is observed for both D250 and D239 families. The short family member sizes both vertical and horizontal tailplanes**. A slightly smaller VTP and HTP are given for the point and family designs of the D250 family, when compared to the D239 family values. The aircraft family is lighter and has a longer fuselage, thus longer lever arm, which explains the slightly smaller family empennage.
- The OEM breakdown in Figure 5.8 follows a trend similar to that of the D239 reference discussed in Chapter 4. When a larger empennage size is fitted into the long family member, not only the VTP and HTP masses increase. The fuselage, wing, and engine masses are directly influenced by this change, increasing with respect to the point design values. **A similar increase of around 0.8% in OEM is given.**
- **For the D250 long family design, sharing the tailplane leads to a 2 % increase in the mission fuel mass**. **The performance penalty is similar to the one that resulted for the D239 reference, suggesting that it is similarly advantageous for the D250 family to share both the horizontal and vertical tailplanes.** For the LH2 families discussed in the following sections, the result of a 2 % fuel penalty will serve as a guideline for determining whether the benefits of empennage commonality justify the increase in fuel consumption.

5.2. Hydrogen Aircraft Family: the D250-LH2 Family

The redesign of the D250-LH2 aircraft concept from the EXACT project, see Section 3.4.1, is presented in this section. The D250-LH2 TLARs for the main family member, i.e the stretched version, are shown in Table 3.4. Besides this, two shorter family members are defined, the D250-LH2-mid and D250-LH2-short concepts. The same family design strategy as for the D239 and D250 families is followed. Their characteristics are defined in Table 5.7. All of them compose the D250-LH2 aircraft family.

Table 5.7: Family versions definition for the D250-LH2 family concept

TLAR	D250-LH2-mid	D250-LH2-short	Units
Design PAX (single class)	220	190	[-]
Design Payload	20900	18050	[kg]
Max. Payload	22000	19000	[kg]
Δl_f	-3.7	-7.4	[m]
dm_f/dl_f	305	305	[kg/m]
Δm_w	0	0	[kg]

The definition of the family versions follows that of the D250 kerosene baseline for comparison. Note that the range is not specified as a TLAR in this case. For the D250-LH2-mid and -short family variants, this parameter is no longer an input but a result determined by the tank size and fuel capacity of the long family member. This component will be shared among all family members as done for the D250 kerosene baseline family. The tank will be sized for the design mission of the D250-LH2 (see Table 3.4). The same fuel capacity will be used for the shorter members. The amount of fuel, together with the reduction in payload, will determine the design mission range for each of the shorter variants. The scenario with maximum fuel capacity in the tanks for the short family members represents the most extreme case for HTP sizing, as it achieves the largest longitudinal CG shift.

The resulting ranges for both the D250-LH2-mid and D250-LH2-short will serve as a starting point for the design space exploration in Section 5.3 of this chapter. In this section, the D250-LH2 aircraft family will be designed considering different family strategies, using different payload and range values for the definition of the short variants. The sensitivity of variations in the family TLARs on the commonality of the empennage will be analyzed.

Three trade-off studies are carried out in this section for the D250-LH2 family. The first two of them focus more on the aircraft level, and the aforementioned relationship between landing gear integration and horizontal tailplane sizing. The same trade-off analysis as conducted for the D250 kerosene baseline is performed for the D250-LH2, focusing on the landing gear integration in either the wing or the fuselage. The goal is to see the effect of this trade-off for an LH2 aircraft design. Additionally, a parallel trade-off is conducted exploring different values for the tip-back angle, used for lading gear positioning. This parameter has been observed to be critical when comes to the design of LH2 aircraft concepts with rear-fuselage tanks. The results for this double trade-off are shown in Section 5.2.1.

The third study is focused more on a family level. The goal of this final trade-off is to find the optimum length of the fuselage family sections, together with the number of those to be positioned ahead of and behind the wing. The results of this last trade-off are shown in Section 5.2.2.

The final results for the D250-LH2 family are presented in Section 5.2.3, featuring an optimized fuselage family section definition, tip-back angle, and landing gear integration solution. The resulting family will be compared to the D250 family outlined in Section 5.1.3. The main differences in the tailplane sizing processes and commonality penalties between the kerosene and LH2 family designs will be discussed.

5.2.1. Landing gear integration and position trade-off study

The trade-off study carried out for the D250 kerosene baseline in Section 5.1.1 is even more relevant for a hydrogen aircraft with rear-mounted tanks, as is the case for the D250-LH2 concept. The most aft center of gravity position for an LH2 concept of this characteristics is positioned much farther back compared to a kerosene-powered aircraft. This will position the landing gear even more aft to ensure a stable design during ground operations. In the case of a wing-mounted gear concept, this new landing gear position might lead to a significantly rearward wing position, resulting in an HTP size that is far from optimal.

Another design factor to consider with hydrogen-powered concepts, adding to the previously mentioned integration trade-off, is the positioning of the landing gear. Throughout the numerous tests conducted during the thesis, it was observed that the take-off rotation requirement predominantly influences the HTP sizing process for an LH2 concept. From a flight mechanics perspective, this requirement is highly sensitive to the landing gear position. The aft landing gear placement in these designs results in a notably shorter HTP lever arm. To minimize the size of the HTP, the landing gear can be moved forward by reducing the tip-back angle. A significantly lower value than those typically recommended in the literature for conventional kerosene aircraft designs can be selected. Reducing the tip-back angle indeed helps to reduce the tail size, while also allows for an easier integration of the landing gear under the wings. However, a trade-off is being made in this case between the efficiency of the design and the stability during ground operations. Positioning the landing gear too close to the most aft center of gravity can compromise the aircraft on-ground stability.

To sum up, two trade-off studies are conducted in parallel for the D250-LH2 family design. The first study compares fuselage-mounted versus wing-mounted landing gear. The second study examines the trade-off between the HTP size and the limitations on ground operations by reducing the tip-back angle. The same assumptions used for the kerosene baseline described in Section 5.1.1 are applied here.

5.2.1.1. Tip-back angle definition

To define the tip-back angle values for the study, the D250-LH2 main family member was designed with various tip-back configurations. Based on the results, two extreme cases were selected to represent the limits for the trade-off study, with angles of 7.5° and 17.5° . The corresponding loading diagrams, showing passengers boarding from back to front, are illustrated in Figure 5.9.

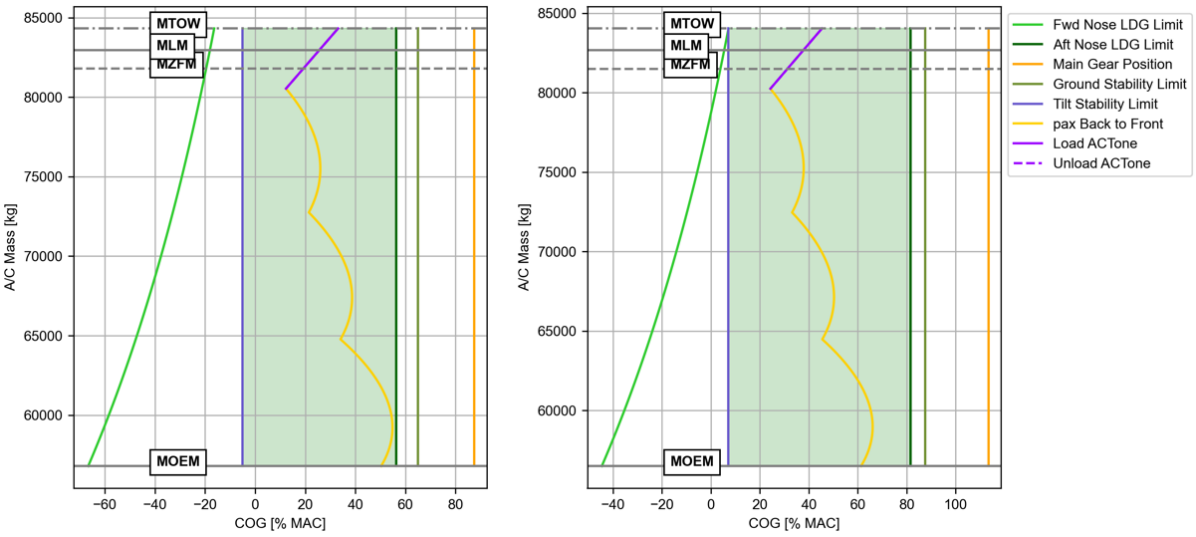

Figure 5.9: Loading diagrams for the D250-LH2 concept (point design) with passengers loaded back-to-front and tip-back angles of 7.5° (left) and 17.5° (right). The landing gear is integrated into the fuselage

Note that only the loading diagrams for the D250-LH2 with fuselage-mounted gear are presented here. The diagrams for the wing-mounted gear concept are virtually identical. The only difference lies

in the tilt stability limit, which will shift to the left due to a wider gear track, resulting in a larger green shaded area. However, the points of interest in the loading diagrams are the ground stability and aft nose landing gear limits, which remain unchanged regardless of the gear integration. To ensure safe ground operations, the center of gravity must always remain ahead of these limits. Consequently, only the back-to-front loading scenario is depicted, as it represents the most critical case.

The diagram on the left in Figure 5.9 shows the loading diagram for a tip-back of 7.5°. In this design, the passengers can be loaded and after them the fuel, without surpassing any of the limits. A lower tip-back than 7.5° will result in the yellow line surpassing at some point the aft nose landing gear limit. However, in ferry flight operations—where only fuel is loaded—the aft nose landing gear limit is exceeded, along with the ground stability limit. A similar issue arises when the aircraft is loaded with a low payload mass and maximum fuel mass. In cases where maximum fuel mass is loaded, the aircraft can only operate with at least 50 % of its passenger capacity, i.e., when the OEM and payload exceed 70,000 kg.

While the unfeasible combinations of payload and fuel mass are not typical of normal operating conditions of the aircraft, they still limit the design's operational flexibility. Some solutions can be adopted to solve this problem:

- Tail stand: this element is used to support the aft fuselage part of the aircraft during the loading and unloading phases. It increases stability and avoids the aircraft from tipping back [94]. An example of this solution is shown in Figure 5.10.

Figure 5.10: Example of an aircraft being loaded on ground with a tail support [95]

  Nevertheless, the tail support only partially addresses the issue. While it allows the aircraft to be loaded with a significantly aft center of gravity, the aircraft remains unstable during ground maneuvering, once the stand is removed.
- Cargo ballast: placing a cargo mass in the front compartment can shift the overall center of gravity forward, improving stability during loading and ground maneuvering. However, this approach introduces a mass penalty and reduces operational flexibility, as the aircraft must always carry a front ballast to maintain stability for specific payload and range configurations.

A design with a tip-back of 17.5° represents the second limiting case chosen for the trade-off study. As shown on the right diagram in Figure 5.9, increasing the tip-back up to 17.5 ° allows the aircraft to be loaded and maneuver on ground for almost every payload and range combination. This includes ferry flight capability and standard loading procedures without using a tail stand. Although this design will have a larger HTP, it offers significantly greater operational flexibility at airports compared to the previous design.

Note that a tail stand might still be required if fuel and passengers are loaded at the same time, in cases where the passenger capacity is still below 20 %. Additionally there are still payload and range combinations, i.e. full tanks and payload under 20 %, that are still unfeasible. However, these are really off-design conditions. Oversizing the tailplane for these cases will result in a big performance penalty without significant benefits. Instead, cargo ballast can be used in this punctual scenarios to tackle the stability problem of the design.

The D250-LH2 family is designed using both tip-back angles, integrating the landing gear either in the wing or in the fuselage. This results in 4 different aircraft families. All point designs resulting from the first iteration of the workflow for all family members are compared. The goal is to get to the design which results in the best compromise for the landing gear integration and positioning. The results are presented below.

5.2.1.2. Point design results

The performance of the four resulting D250-LH2 concepts is compared in Figure 5.11, with the mission fuel mass (MFM) serving as the primary performance metric. The horizontal tailplane size is plotted on the y-axis, as it represents the main design change influenced by variations in landing gear integration and tip-back angle. Note that the results shown are taken from the first iteration of the methodology, i.e the point design. These results provide an initial indication of which design performs better. Running the entire design loop multiple times to achieve a fully converged family design is computationally expensive and does not offer further insights into the trade-off study. The results for the performance of the shorter family members are not presented, as they follow the same trends.

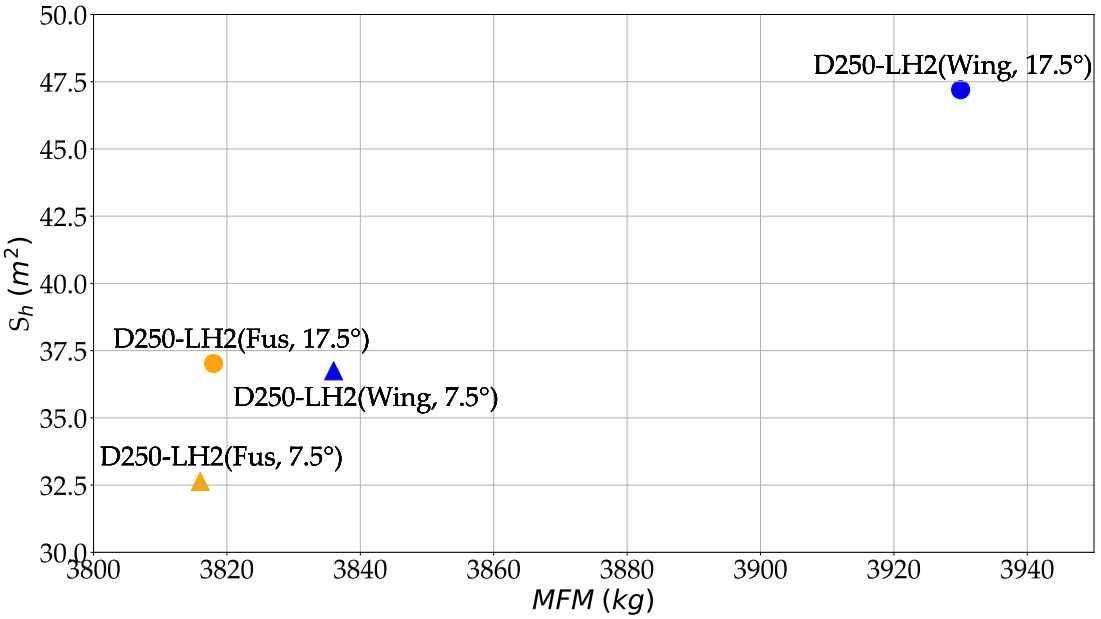

Figure 5.11: D250-LH2 concept (point design) performance comparison for different landing gear integration solutions (wing-mounted (Wing) and fuselage-mounted (Fus)) and different tip-back angle values (7.5° and 17.5°)

The impact on aircraft weight and performance of the different landing gear integration solutions for a tip-back angle of 7.5 ° follows a similar trend as observed for the D250 kerosene design in Section 5.1.1. The MTOM breakdown is shown in Figure 5.12 for the D250-LH2 main family member, with (Wing) indicating wing-integrated gear and (Fuselage) indicating fuselage-integrated gear. The weight variations for the shorter family versions follow the same trend and are therefore not displayed.

As for the D250 baseline, the wing-mounted D250-LH2 design results in a heavier aircraft. In terms of mission fuel, both aircraft with a tip-back angle of 7.5 ° perform similarly, as shown in Figures 5.11 and 5.12. However, in this case it is the wing-mounted design the one that showcases a slightly worse performance. The optimal position for the landing gear is now at xsi_{mg} = 1.05 due to the more aft CG location, which is is significantly further aft than the previous optimal position for the kerosene baseline at xsi_{mg} = 0.96 (see Table 5.2). Consequently, the forward shift of the wing is more limited for the LH2 design, resulting in a more pronounced difference between the HTP size of the two gear integration solutions as depicted in Figure 5.11. Nonetheless, the penalty is minimal, with less than a 1 % difference in mission fuel mass. This slight drawback is more than acceptable given the multiple design advantages that a wing-integrated landing gear offers over a fuselage-integrated configuration.

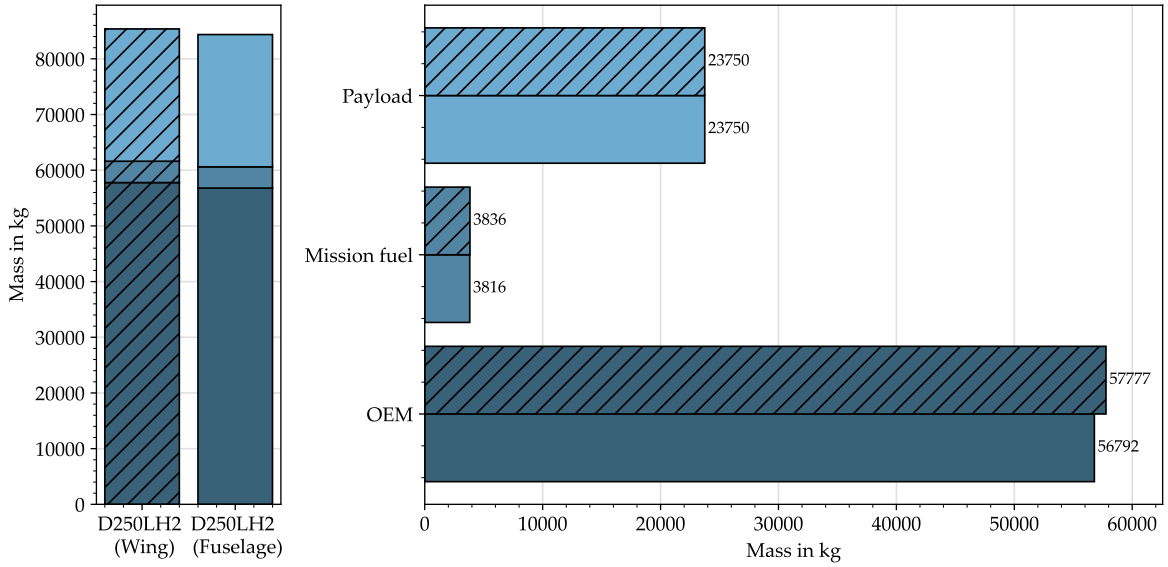

Figure 5.12: D250-LH2 concept (point design) MTOM-breakdown comparison of fuselage-integrated vs wing-integrated landing gear design (tip-back of 7.5°)

However, the tip-back angle also plays a critical role in selecting the final landing gear configuration. Increasing the tip-back angle to the typical range of values used in kerosene aircraft leads to a significantly different trend. The impact of the increase becomes more evident in the case of the wing-mounted landing gear design. The HTP size of the wing-mounted concept is observed to become really sensitive to changes in this parameter. The optimal xsi_{mg} for a tip-back of 17.5 ° equals 1.23, which is even more aft the required xsi_{mg} of 0.875 for wing integration. Consequently, the forward wing shift is really limited. For the D250 baseline, the difference in wing position between the two landing gear integration solutions was approximately 0.5 meters (see Table 5.2). For the D250-LH2 this difference has now expanded almost to 3 meters, meaning that the wing is almost 3 meters behind its optimum position. Consequently, it can be concluded that a wing-mounted gear configuration, when designed with a tip-back angle that ensures aircraft stability on ground during all operations, leads to an unfeasible design. The unfavourable wing position leads to an impractically large HTP size. The aircraft fuel mass for the mission increases up to 3 % compared to the fuselage-mounted designs. Additionally, the significantly bigger static margin of the design, which impacts trim drag but is not considered in the current results, further justifies the decision to discard this design.

The impact on the performance of the same trade-off in the case of a fuselage-mounted configuration is much lower as can be observed when comparing the mission fuel mass values in Figure 5.11. The HTP size increases due to the more aft gear position. Nonetheless, the mass breakdown plot indicated that the fuselage mass was actually lighter for the larger tip-back design. In the end, the impact of the tip-back on the performance is negligible for the fuselage-mounted design. Considering the level of fidelity used in the workflow, it appears to be true that the fuselage mass is slightly smaller for a larger tip-back angle value. However, this difference is minimal and should not be generalized as a basis for determining which design is superior. The observed variation could also be attributed to the combination of uncertainty bands of the low-to mid fidelity tools employed in the workflow. Nevertheless, what can be captured based on the methodology used is that **the tip-back angle sensitivity for the wing-mounted design is much higher. Consequently, for the D250-LH2 design, a fuselage mounted gear is chosen. The better performance, together with the possibility of increasing the tip-back angle without a major penalty, are the deciding factors against the wing-mounted**. A tip-back of 17.5° is then selected to conduct the remaining family studies.

Lastly, it is important to note that the horizontal tailplane size values shown in Figure 5.11 for the D250-LH2 point design are significantly larger compared to the kerosene baseline point design results discussed in Section 5.1.1. Regardless of the tip-back angle, the HTP size is 40 % to 50 % greater.

5.2.1.3. Impact of leading-edge high-lift devices on HTP size reduction

In the previous section, it was concluded that an LH2 aircraft with wing-integrated landing gear and a tip-back angle with a similar value than a kerosene aircraft was unfeasible. The resulting design was inefficient, particularly due to the excessively large size of the horizontal tailplane required.

The wing-integrated landing gear is the most common solution within the industry. It was also demonstrated to be the preferred option for the kerosene D250 baseline aircraft in Section 5.1.1. Nonetheless, to continue with this trend in the case of LH2 aircraft designs the HTP size has to be significantly reduced. This section explores the effect of leading edge high-lift devices on the size of the HTP. A droop nose-type of device has been selected to increase the capability of the stabilizer to produce downforce. This will specially help during take-off rotation, which has been observed to be a critical maneuver in the case of LH2 aircraft. The use of leading edge high-lift devices for the tailplane is not a standard practice in aircraft design. However, a few experimental studies have been done on this topic, aiming to either reduce the horizontal tailplane size [96] or increase the CG range [97].

The enhanced methodology for preliminary horizontal tailplane sizing is applied to assess the impact of a droop-nose on the aircraft design. To model the effect of the high-lift device, a Δcl for the 2D lift coefficient of the airfoil is added on top of the value of the maximum tail lift coefficient calculated by the tool (see method in Appendix A). The effect of varying the Δcl value on the HTP size and the associated reduction in mission fuel is illustrated in Figure 5.13. The range studied for Δcl has been selected based on a combination of multiple results and empirical data from various aircraft design references [98] and journal articles [99]. It is important to note that all values are compared against the D250-LH2 point design. This reference design features wing-integrated landing gear and a tip-back angle of 17.5°. It has a mission fuel mass of 3930 kg and a HTP size of 47.2 m^2 (see Figure 5.11). When compared to the fuselage-integrated solution, the performance is 3 % worse.

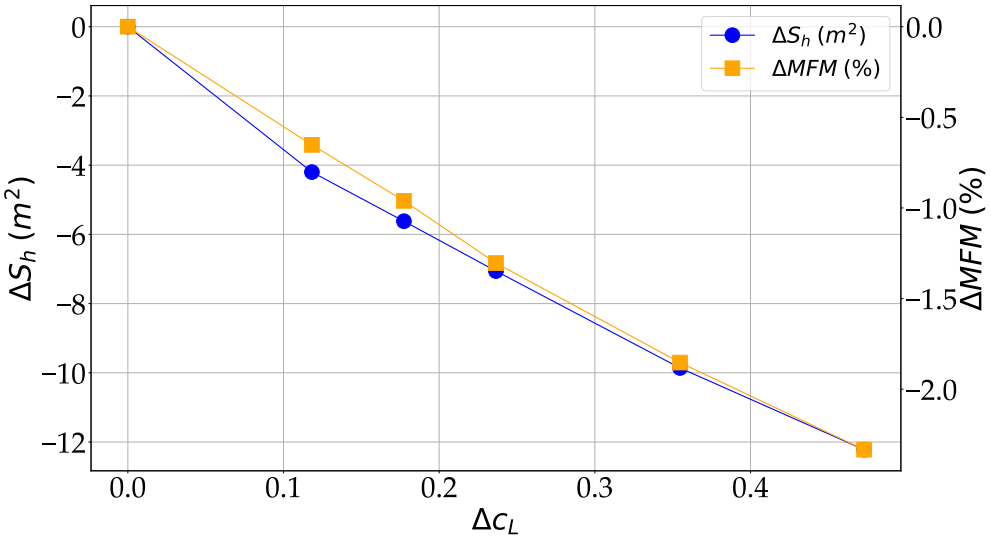

Figure 5.13: Impact of leading edge high-lift devices on HTP size and performance of the D250-LH2 aircraft concept (point design) with wing-mounted landing gear and tip-back angle of 17.5°

The reduction in fuel consumption for optimistic values of Δcl is clearly noticeable, with the performance of both aircraft configurations (wing-integrated and fuselage-integrated gear) becoming very similar when compared. The tailplane size reduces from 47 m^2 to 34 m^2, achieving a reduction in mission fuel mass of around 2.5%. In a more conservative scenario, with $\Delta cl = 0.2$, the impact on performance remains significant. The performance of both designs differs by approximately 1.7 %.

For both cases, it can be argued that the advantages of wing-integrated gear may compensate the marginally better performance of the fuselage-integrated design. Without high-lift devices, there is no

doubt that integration inside the fuselage is the preferred option. All in all, although the potential exists, the study will continue to focus on the fuselage-integrated landing gear for the remainder of the designs. The uncertainties associated with this new technology, along with the lack of consideration for trim drag in the calculations—especially with such an unfavorable wing position—require a higher-fidelity analysis to accurately determine the real benefits of the droop-nose concept.

5.2.1.4. Horizontal tailplane sizing trends in an LH2 aircraft family

Four families have been designed to identify the optimal landing gear integration and positioning solution for the D250-LH2 family. The previous sections focused exclusively on the performance and weight results for the D250-LH2 main member, as similar trends were observed for the -mid and -short versions. A final configuration was chosen, with a fuselage-mounted gear and a tip-back angle of 17.5°. In this section, the results of all families are compared concerning the required HTP size for the point design of each member. Figure 5.14 depicts the relationship between the change in HTP size and the reduction in fuselage length. This relationship is shown for both the final D250 design and the four proposed D250-LH2 concepts. For every case, the base (main or long) family member serves as a reference for the variations in fuselage length and HTP size.

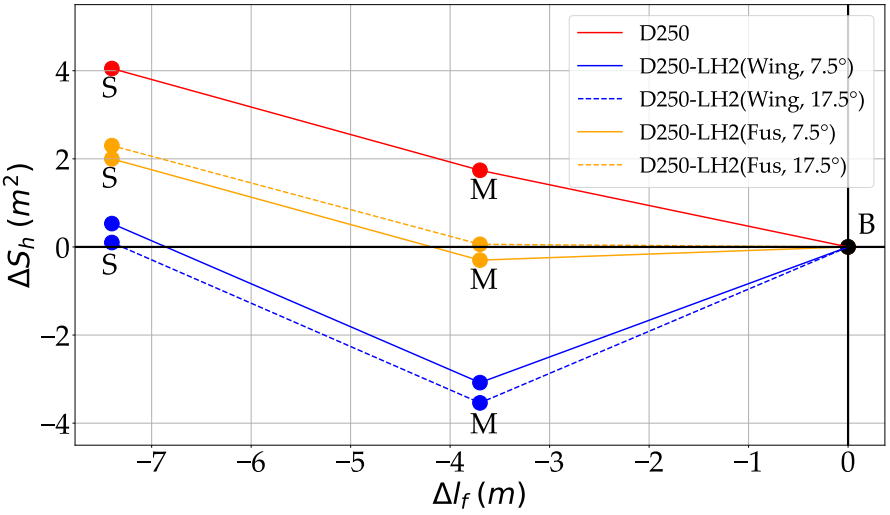

Figure 5.14: Point design results for the required HTP size as a function of the change in fuselage length for both D250 and D250-LH2 family concepts. Results are shown for all base (or long) (B) mid (M) and short (S) family variants

The findings from the D239 and D250 aircraft families have confirmed the established trends in HTP sizing for kerosene aircraft families. A reduction in fuselage length results in a shorter tail lever arm, which is reflected in the scissor plot by the convergence of the boundaries of the different sizing requirements. As a result, for a given CG range, the required tailplane size increases as the fuselage length decreases. Typically, the short family member serves as the sizing case for the HTP. This trend is illustrated for the D250 family in Figure 5.14.

However, as depicted in Figure 5.14, this ascending trend is not given for the D250-LH2 family designs. The reason behind relies on the variation of CG range with fuselage length that is given for an LH2 aircraft family. For an LH2 concept, the tank position relative to the wing increases with fuselage length. When the fuselage is stretched, the tank is shifted backwards a distance equal to Δl_f , whereas the wing is only shifted backwards a distance equal $\Delta l_f - \Delta l_{VTP}$. This results in a larger longitudinal CG travel for the stretched member. This effect is not given for a kerosene aircraft family, where the fuel mass is positioned in the wing, resulting in similar longitudinal CG ranges among all members (see scissor plots for the D239 and D250 families in Sections 4.2.2.1 and 5.1.1 respectively).

For the wing-mounted landing gear concepts in Figure 5.14, the variation in horizontal tailplane size between the long and short family members is minimal. The -mid version has the smallest HTP overall. Figures 5.15 and 5.16 present a comparison of the scissors plots for the main (long) and short members.

Note that no specific airport conditions were defined for the family. Thus, the green line corresponding to the take-off rotation requirement at sea level (SL) coincides in both figures with the take-off rotation requirement at airport conditions (AP).

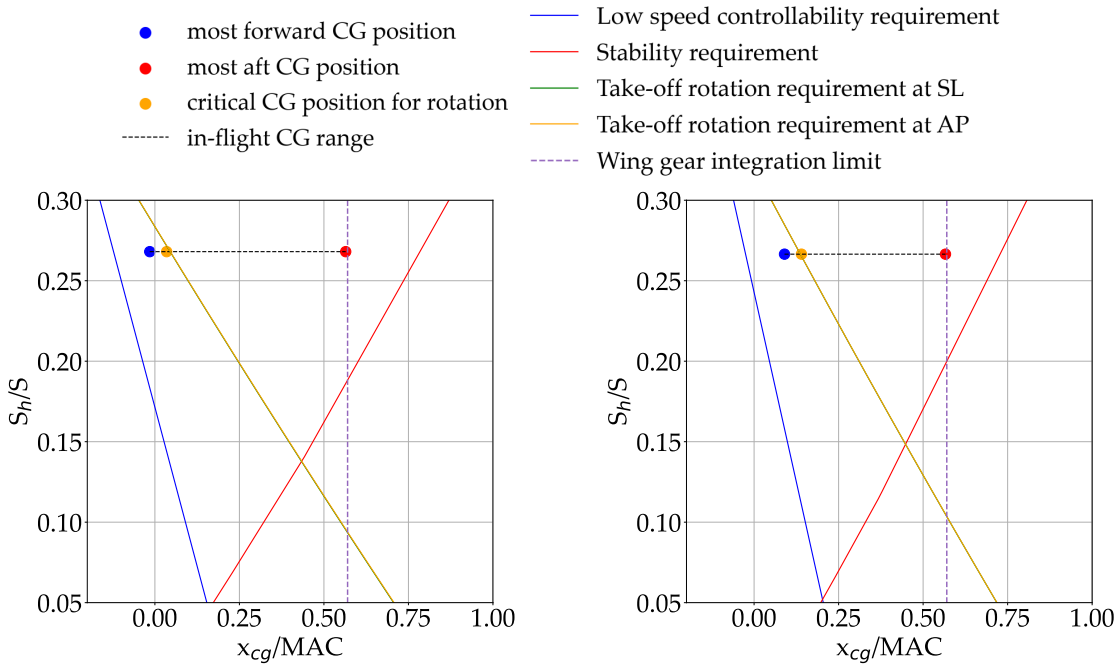

Figure 5.15: Scissors plot for the D250-LH2 concept (point design) with wing-mounted landing gear (tip-back angle of 7.5°)

Figure 5.16: Scissors plot for the D250-LH2-short concept (point design) with wing-mounted landing gear (tip-back angle of 7.5°)

Two effects are then given for the shortest member, when compared to the long family member. On the one hand, the shorter fuselage results in a smaller lever arm. The shorter lever arm decreases the amplitude between the bounds of the scissors plot, limiting the allowable center of gravity travel for a given horizontal tailplane size. This effect mirrors the behavior observed in the kerosene-powered aircraft family. On the other hand, the CG range is also shorter for the short family member. This effect is only given for LH2 aircraft due to its tank position. In the end, the shorter CG range compensates the aforementioned lever arm effect, resulting into a similar HTP size between both long and short family members. The same trend is observed for the D250-LH2-mid, which also has a shorter lever arm and a shorter center of gravity range than the long family member. The reduction in lever arm is not as big as for the short member, resulting in an HTP size that is actually the smallest.

The same trends as for the wing-mounted designs are given for the fuselage-mounted solution. The D250-LH2-short still has the shortest CG range, that compensates for the more constrained boundaries of the scissors. However, based on the results in Figure 5.14, the difference in HTP size between the short and the long family members of the fuselage-mounted solution remains noticeable, despite it being almost half of the difference observed for the D250 kerosene family. A third effect must be considered.

For the wing-mounted landing gear configuration, the wing was positioned to achieve a fixed landing gear position relative to the wing chord, with xsi_{mg} set equal to 0.875 for all family members. The most aft CG for all members is set at 57 % of the MAC, as shown in Figures 5.15 and 5.16 indicated by the dashed purple limit. This value is far from the ideal landing gear position for minimum HTP size.

In contrast, fuselage-integrated landing gear does not impose a constraint on the most aft CG position. Consequently, each aircraft member exhibits a different xsi_{mg} due to variations in the aft CG location. The results for the fuselage-integrated solution and tip-back of 7.5° are shown in Figures 5.17 and 5.18 for the D250-LH2 and D250-LH2-short respectively. Note that again both take-off rotation requirements at sea level (SL) and airport conditions (AP) coincide in both figures.

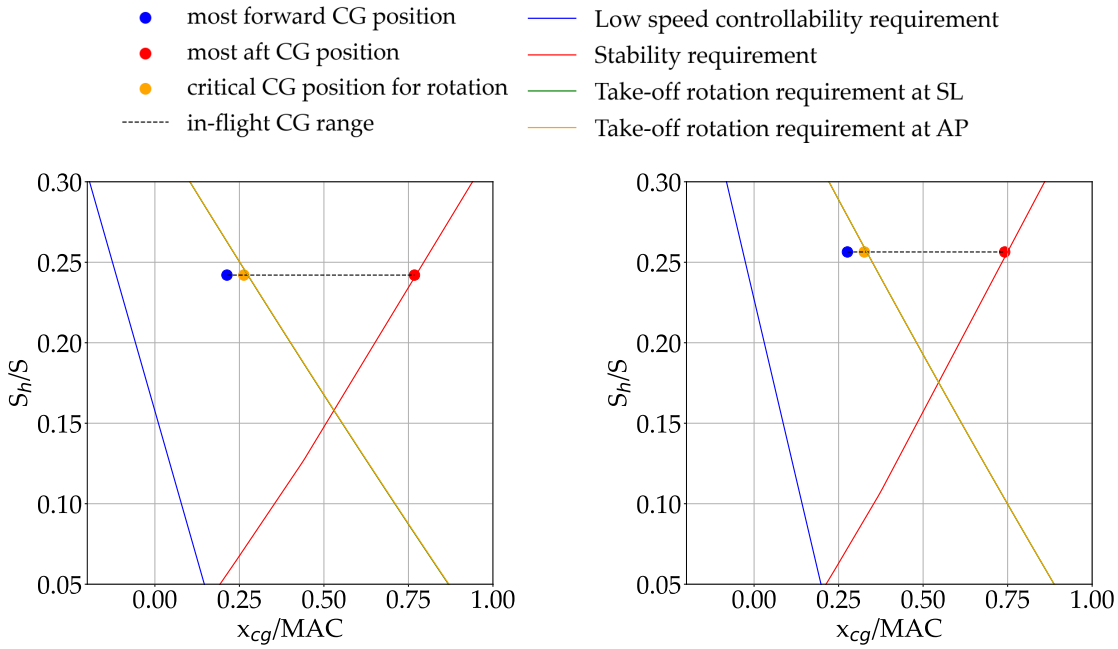

Figure 5.17: Scissors plot for the D250-LH2 concept (point design) with fuselage-mounted gear (tip-back angle of 7.5°)

Figure 5.18: Scissors plot for the D250-LH2-short concept (point design) with fuselage-mounted gear (tip-back angle of 7.5°)

When comparing both Figures 5.17 and 5.18, it can be noted that the most aft CG is slightly more aft along the wing chord for the long family member. For a given tip-back angle, the main landing gear of the short family member would be positioned more forward relative to the wing, compared to the long family member, thereby increasing the tail lever arm. In this scenario, the same trend observed for the wing-mounted configuration would emerge. This outcome would occur if a different value for the relative position of the landing gear attachment to the wing (xsi_{mg}) were assumed for each family member. However, to maintain design commonality, it is assumed that the central fuselage section, where both wing and main gear are attached, is formed by one single piece and is shared among all members. Thus, the gear has to be attached at the same relative position to the wing for all members. The same xsi_{mg} value is used across all family members. Consequently, the gear attachment for the short member is shifted slightly aft from its optimum position.

The change in the optimum gear position for the short family member shifts the take-off rotation line to the right in the scissors plot in Figure 5.18. The shorter CG range cannot compensate this time for the reduction in lever arm, caused by the shorter fuselage plus the sub-optimal gear position. In the end, it results in a larger HTP size than for the long family member. A similar effect is observed for the -mid version, which ultimately results in the same horizontal tailplane size as the long family member.

To sum up, the difference in the horizontal tailplane size among family members is smaller in an LH2 aircraft family, regardless of the landing gear integration. This outcome is driven by the difference in the center of gravity range between the family members, and it already suggests a lower commonality performance penalty than the one that is given for kerosene families.

5.2.2. Family fuselage sections length definition

The same study as for the D250 kerosene baseline is carried out in this section. The number of fuselage sections to be positioned in front and behind the wing for each family member are calculated, together with its length. The goal is to get to the most efficient family design with minimum HTP size. The short family member is also sizing for the HTP in the case of the D250-LH2 family concept. Expressions (5.1) and (5.2) are used to position the wing for the other family members.

A study was carried out using different values for the Δl_{VTP} to decide which one to use for the family design. Note that not every Δl_{VTP} value is eligible, as explained in Section 5.1.2. Table 5.8 presents a summary of the results obtained. The values for the resulting wing position ($x_{root_{LE}}$) and landing gear relative position to the wing chord (xsi_{mg}), are shown for the first (subscript 1) and second (subscript 2) iterations of the method for the design of the D250-LH2 long family member.

Table 5.8: Influence of the change in Δl_{VTP} on the geometry of the D250-LH2 concept for the first two design iterations

Δl_{VTP} [m]	$n_{sections}$ [-]	$l_{section}$ [m]	$x_{root_{LE_1}}$ [m]	$x_{root_{LE_2}}$ [m]	xsi_{mg_1} [-]	xsi_{mg_2} [-]
3.7	7	0.53	19.50	18.75	1.23	1.3
2.78	6	0.46	19.50	19.63	1.23	1.21
2.64	5	0.53	19.50	19.82	1.23	1.19
2.47	5	0.62	19.50	19.99	1.23	1.17

A trend is observed in the table above which is characteristic from the LH2 aircraft family design process. The first row, for Δl_{VTP} = 3.7 m, shows an unstable family design. For the second iteration, the wing for the D250-LH2 is positioned more forward than the result of the point design, shifting the center of gravity range aft with respect to the wing chord. As has been observed for the kerosene designs, increasing the empennage size of the main family member increases also the overall aircraft weight, and thus the fuel consumption. In the case of an LH2 aircraft where the tank is sized for the design mission, the tank has to be resized to account for the extra fuel mass due to the family design. The combination of a heavier empennage, a larger fuel tank, and an increase in mission fuel mass shifts the aircraft's center of gravity further aft, necessitating a corresponding shift in the position of the landing gear.

Based on Table 5.8, the new xsi_{mg} equals 1.3, which is behind the 1.23 result from the first iteration. The new value is then used to position the landing gear for the short family member. A bigger HTP results than for the first iteration. Consequently, the family design will never converge. After every iteration, a bigger HTP will be fitted into the main family member. The bigger tail will resize the tank accordingly, and shift the gear further aft. This new gear position will then be used to recalculate the HTP size required for the short member, which will always increase.

Any Δl_{VTP} that positions the wing in front of the point design position, results in an unstable LH2 family design. Therefore, the goal when designing an aircraft family should be to select a Δl_{VTP} that positions the wing further aft of the point design result. This would reduce the xsi_{mg} value for the entire family, bringing it closer to the optimal value for the shortest member. However, choosing a value that positions the wing too far behind the point design result, can also lead to a sub-optimal family design. This was the case observed for a Δl_{VTP} = 2.46 m in the forth row of Table 5.8. In this scenario, the opposite as before happens. As the wing shifts aft, the landing gear position relative to the wing moves forward. This adjustment prevents the family design from diverging. However, the horizontal tailplane size converges to a larger value than the one obtained in the point design phase. The D250-LH2 main family member became the sizing case for the HTP due to the sub-optimal wing position, causing the controllability requirement to increase the required area.

To sum up, the value for Δl_{VTP} has to be selected carefully, and always a preliminary study is required. For the D250-LH2 family design, a compromise was found for both a Δl_{VTP} = 2.64 m and a Δl_{VTP} = 2.78 m. Both values position the wing slightly aft the 19.51 m from the point design, without compromising the controlabillity of the design of the long member. Between these two values, a Δl_{VTP} = 2.64 m was finally chosen. It results in a lower value for the xsi_{mg}, closer to the optimal for the -short member.

In conclusion, the final HTP size for the family was reduced compared to the point design result by conducting a detailed study on the definition of the fuselage family sections. A value for the Δl_{VTP} equal to 2.64 m shifts the gear position of the main family member from xsi_{mg} = 1.23 to xsi_{mg} = 1.19. The same reasoning has been applied for the definition of the Δl_{VTP} for the D250-LH2-mid. The final results are shown in Table 5.9.

Table 5.9: Fuselage family sections definition for the D250-LH2 aircraft family concept

	D250-LH2	D250-LH2-mid	D250-LH2-short	Units
Δl_f	-	-3.7	-7.4	[m]
Δl_{VTP}	-	-1.06	-2.64	[m]
$l_{section}$	0.53	0.53	0.53	[m]
$n_{sections,ahead}/n_{sections,behind}$	-	5/2	9/5	[-]
$x_{root_{LE}}$	19.94	17.29	15.18	[m]
xsi_{mg} (optimum xsi_{mg})	1.19 (1.19)	1.19 (1.18)	1.19 (1.17)	[-]
tip-back angle	17.5	17.5	17.5	[°]

5.2.3. Family design results for the D250-LH2 aircraft family

The final D250-LH2 family results are shown in this section. Appendix B showcases the three-view for the final concept. Table 5.10 shows the comparison between the point and family designs.

Table 5.10: Final results for the D250-LH2 aircraft family (fuselage-integrated gear and tip-back angle of 17.5 °)

Units		Point Design			Family Design		
		D250-LH2	D250-LH2-mid	D250-LH2-short	D250-LH2	D250-LH2-mid	D250-LH2-short
$x_{root_{LE}}$	$[m]$	19.50	17.01	15.06	19.94	17.29	15.18
S_h	$[m^2]$	37.02	37.08	39.50	38.50	38.50	38.50
S_v	$[m^2]$	20.39	20.48	21.34	21.41	21.41	21.46
xsi_{mg}	$[-]$	1.23	1.23	1.23	1.19	1.19	1.19

The shortest family member is sizing for the horizontal tailplane. As discussed before, the gap in HTP size between the family designs and the point designs is reduced when compared to the results for the kerosene baseline family (compare results from Table 5.5 to the ones from 5.10). This is mainly because of two reasons based on the trends observed in Sections 5.2.1 and 5.2.2:

- For the D250 baseline, the difference in lever arm (Δl_{HT}) between the short and main family members is 3.7 m. In contrast, the Δl_{HT} value for the D250-LH2 family is 3.1 m. Although there is a slight variation in this value due to differences in landing gear integration, the figures remain close because the same Δl_f is used for the shorter versions in both cases.
  However, the impact of the lever arm reduction on the tail size difference between the short and long members, and thus on the final family HTP size, is much bigger in the case of the D250 baseline as depicted in Table 5.5. The reduction in the CG range for the D250-LH2 short variants compensates for the shorter lever arms, resulting in a smaller gap for the LH2 family.
- The study conducted on the Δl_{VTP} value allows the main landing gear to be positioned closer to the optimal location for the short family member. As a result, the final HTP size for the converged family design is smaller than the 39.5 m^2 that was obtained in the point design phase for the -short member. This latter effect is shown in the last row of Table 5.10.

Conversely to the D250 baseline, this time the gear is integrated into the fuselage. The HTP size is minimized and the CG range lies perfectly between the boundaries of the scissors. The final scissors plot for the -short member looks similar to the one in Figure 5.18, but with a more aft CG range due to the higher tip-back angle value used for the final D250-LH2 family concept.

The mass-breakdown comparison for the point (P) and family (F) designs of the D250-LH2 long member yields the same trends as observed for the D239 and D250. The OEM increases, due to a heavier empennage, fuselage, and wing structure. The family design becomes less efficient as a result. Table 5.11 summarizes the main changes in MFM, OEM and MTOM. The payload is the same in both cases.

Table 5.11: Mass comparison for the point (P) and family (F) design of the D250-LH2 aircraft concept

	D250-LH2 (P)	D250-LH2 (F)	Units
MFM	3818	3856 (+ 1.0 %)	[kg]
OEM	56497	56890 (+ 0.73 %)	[kg]
MTOM	84038	84464 (+ 0.54 %)	[kg]

Note that, although the variation in empennage size for the D250-LH2 family is smaller compared to the kerosene baseline family, the relative change in operating empty mass between the two configurations remains closely comparable (recall the 0.77 % increment for the D250 family design in Table 5.6). Figure 5.19 shows the breakdown of the operating empty mass increase by component, expressed as a percentage of the total increase. This comparison is conducted for both the D250 and D250-LH2 main family designs, which exhibit comparable mass increases of 362 kg and 393 kg, respectively.

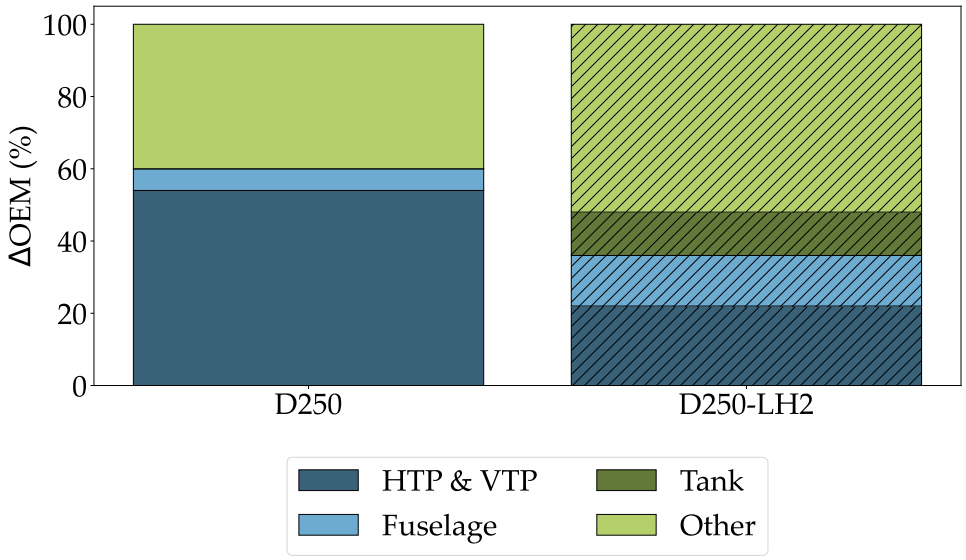

Figure 5.19: OEM-breakdown by component increment due to tailplane commonality for the D250 and D250-LH2 concepts

As depicted in Figure 5.19, for the LH2 design the change in OEM due to the empennage size is indeed smaller. However, there are mass changes that are given for an LH2 aircraft family design that are not given in the case of the kerosene family. As explained before, the D250-LH2 tank is sized for the design mission. Thus, fitting a bigger empennage will result into a bigger tank and longer fuselage to still fulfil the range for the design mission. This corresponds to almost 25 % of the total increase in OEM, which compensates the reduced impact of the empennage size increase, and ultimately leads to similar OEM variation between point and family designs.

However, although the changes in OEM are comparable between both LH2 and kerosene families, the impact that the weight increment has on the performance is much lower for the LH2 design. An oversized HTP has a more pronounced impact on the fuel consumption of the aircraft, than heavier fuselage and tanks. As a result, **the fuel penalty for the same family design strategy is halved for the LH2 design. Tailplane commonality is feasible for an LH2 aircraft family, which answers the second research question of the study.**

To conclude the section, a comparison is made between the final D250 and D250-LH2 aircraft concepts, as shown in Figure 5.20. The Figure illustrates the key differences in horizontal tailplane size, fuselage length, and landing gear integration between the two concepts.

As showcased in previous studies (see Section 2.3), the HTP size for a hydrogen aircraft with rear tanks is substantially larger than for a kerosene aircraft. The larger CG travel due to the rear-integrated

tanks leads to a much more aft CG position than in a conventional kerosene aircraft, which influences the main landing gear position and ultimately the required horizontal tailplane size. As anticipated based on the scissor plots in Section 5.2.1.4, **the take-off rotation requirement mainly drives the HTP sizing process, being it significantly more restrictive than the controllability requirement**. The aft landing gear position characteristic of LH2 concepts with rear tanks results in a short tail lever arm, which significantly increases the required HTP size.

Even for this case, in which the HTP for the kerosene baseline was not minimized due to landing gear integration issues, and also the LH2 has a T-tail which reduces the size, **the volume coefficient is more than 40 % larger.** The HTP size and volume coefficient for all main family members designed in this study are compared in Table 5.12, outlining the difference between the LH2 and the kerosene designs.

Table 5.12: Comparison of the HTP size and volume coefficient for the kerosene and LH2 main family members

	D239	D250	D250-LH2	Units
S_h	26.20	25.05	37.02 (+ 47.8 %)	$[m^2]$
c_{HT}	1.0	1.2	1.71 (+ 42.5 %)	[-]

Note that the values presented in the table above are those for the point design, without considering potential family members in the tailplane design. This approach allows for a more accurate comparison between the LH2 and kerosene designs, focusing purely on the different aircraft mass distribution and its impact on tailplane size from a flight mechanics perspective.

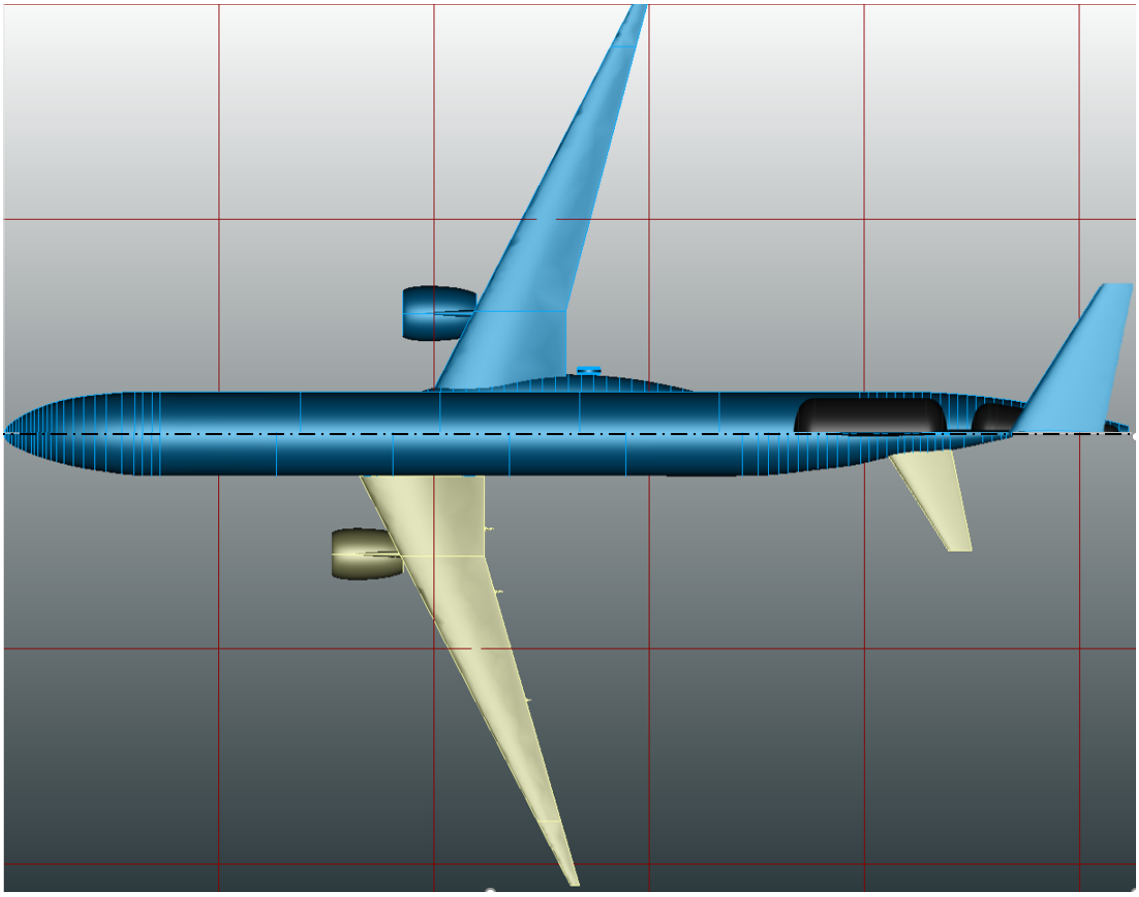

Figure 5.20: Plan view comparison of the final point design results for the D250 (bottom) and D250-LH2 (top) aircraft concepts

5.3. Hydrogen Aircraft Family Design Space Exploration

The D250-LH2 family designed in Section 5.2.3 is further studied in this section. The goal is to draw trends for the commonality of the empennage among family members by comparing the different design strategies existing for kerosene aircraft families (see Section 2.2.2.1).

5.3.1. First family strategy: varying payload and constant fuel capacity

As explained in 2.2.2.1 and 3.4.2, this first strategy represents a trade-off between payload and range. This is the case for both D239 and D250 families. In Table 5.13, the payload-to-range trade-offs for the design mission, as well as the block fuel (BF), mission fuel (MFM), and maximum fuel masses ($m_{fuel,max}$), are presented for all members of both families.

Table 5.13: Range and payload inputs and fuel mass results for the D239 and D250 aircraft family concepts

	D239 family			D250 family		
	D239	**D239-mid**	**D239-short**	**D250**	**D250-mid**	**D250-short**
Range [NM/km]	2500/4630	2900/5371	3300/6112	1500/2778	1700/3148	2000/3704
Payload [kg]	25000	19000	16400	23750	20900	18050
BF [kg]	14765	14196	14931	6946	7184	7763
MFM [kg]	17972	16998	17613	9310	9449	9895
$m_{fuel,max}$ **[kg]**	20030	20030	20030	17325	17325	17325

As depicted in Table 5.13, for a kerosene aircraft family the maximum fuel capacity does not limit the range of the design mission. There is enough left over space in the wings to put more fuel. For the LH2 aircraft family designed in Section 5.2.3, the fuel capacity is also shared among family members. A trade-off is also given between payload and range. The results are shown in Table 5.14.

Table 5.14: Range and payload inputs and fuel mass results for the D250-LH2 aircraft family concept (range is also an output in the case of the -mid and -short family variants)

	D250-LH2	**D250-LH2-mid**	**D250-LH2-short**
Range [NM/km]	1500/2778	1643/3043	1840/3405
Payload [kg]	23750	20900	18050
BF [kg]	2863	2904	2962
MFM [kg]	3856	3856	3856
$m_{fuel,max}$ **[kg]**	3856	3856	3856

In this case, the tanks are sized for the design mission of the long member. Due to the constrained size, the resulting range for the -mid and -short versions is limited. The payload-range diagram in Figure 5.21 illustrates this effect. It compares the base (long) family members with the shorter variants across the D239, D250, and D250-LH2 families. A notable difference can be observed in the length of the substitution segment (payload for range) when comparing kerosene to hydrogen aircraft families. The segment is significantly longer for the kerosene -short variants. In the case of the LH2 family, both segments for the long and short members have roughly the same length. This translates into a bigger spectrum of ranges covered by the members of the kerosene family designs. For LH2 families the tank is sized for the design mission of the main (long) family member. Using the same tank for the short version significantly reduces the length of the substitution segment, limiting the payload-range flexibility of the variant. **Consequently, the LH2 aircraft family might result less attractive at first from an airline's point of view. It shows a lower payload-range flexibility, not being able to cover the same amount of routes as its kerosene analogous.** Over-dimensioning the tank for the design mission of the D250-LH2 main family member to achieve a similar a payload-range flexibility as the kerosene designs is unfeasible due to the mass penalties it implies.

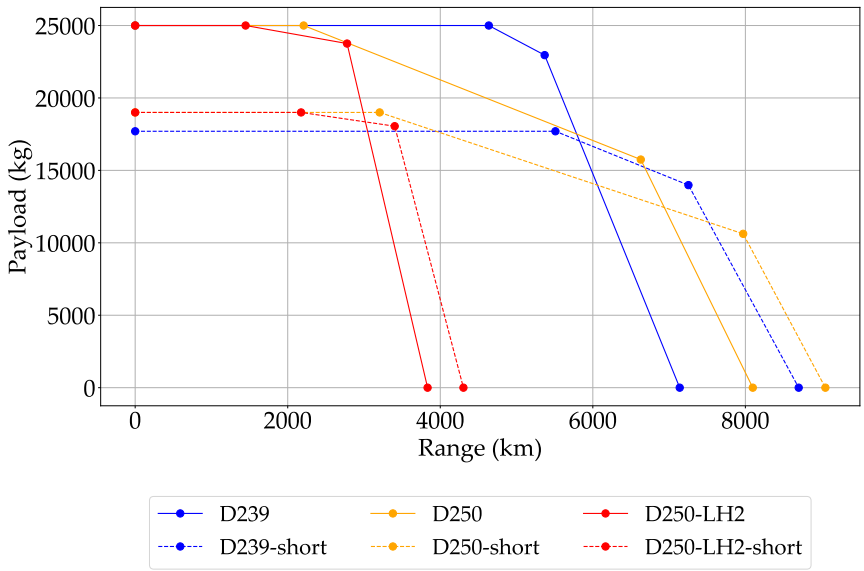

Figure 5.21: Payload-range diagram comparison for the -long and -short members from the D239, D250, and D250-LH2 families

To further understand the sensitivities of this family strategy to changes in the fuselage length, a study was conducted on an LH2 family configuration similar to that illustrated in Figure 5.22. The starting point in every case was the final D250-LH2 design from Section 5.2.3, shown on top of the figure. Different passenger capacities were defined for both the -mid and -short versions. The objective was to evaluate how the results for the design mission range and the performance penalty due to tailplane commonality compare to the D250 kerosene family design.

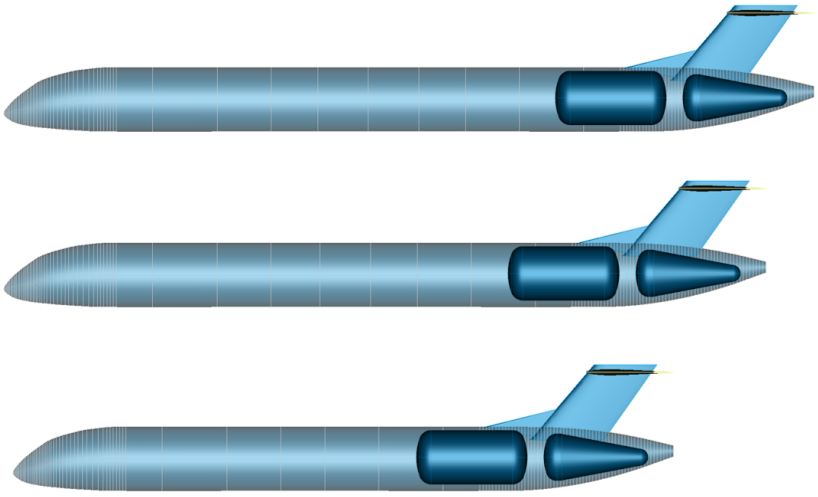

Figure 5.22: LH2 family with constant fuel capacity and varying payload. D250-LH2 base is shown on top. The D250-LH2-mid and D250-LH2-short variants are shown below

The results for the D250-LH2-mid and D250-LH2-short, with a reduction of 12, 24 and 36 passengers with respect to the designs in Table 5.14, are shown in Table 5.15. The same seat pitch is assumed. Note that the results are already the ones for the family design. The family sections length definition has been done as explained for the original D250-LH2 family in Section 5.2.2. As expected, reducing the passenger capacity of the shorter variant makes it even more critical for the final family HTP size.

The reduction in passenger number results in an increase in range. However, the payload has to be significantly reduced, approximately 3400 kg, to match the range set as a TLAR for the D250-short kerosene aircraft. It reaffirms the previous statement of **LH2 aircraft families with common tanks being less flexible to payload-to-range trade-offs.**

Table 5.15: Influence of passenger capacity on the range and tailplane size for the D250-LH2 -mid and -short family members. Δ values are expressed with respect to the original D250-LH2-mid and D250-LH2-short designs from Section 5.2.3

	-short	-mid	-short	-mid	-short	-mid
ΔPAX [-]	-12		-24		-36	
ΔPayload [kg]	-1140		-2280		-3420	
ΔRange [km]	115	137	266	285	400	402
Δl_f	-1.48		-2.96		-4.44	
S_h $[m^2]$	40.15		41.21		43.18	
S_v $[m^2]$	21.71		22.11		22.40	

The influence on the design of the different fuselage length reductions outlined in Table 5.15, has been calculated also for the D250 kerosene family from Section 5.1.3. As expected, the D250-short is the sizing member of the empennage in every case. Figure 5.23 compares the impact that empennage commonality would have in the performance of the long family member for both the D250 and D250-LH2 family concepts. The x-axis shows the Δl_f of the short family member and its corresponding reduction in passenger capacity. The y-axis represents the fuel penalty for the long family member as a result of tailplane commonality. The values are expressed as a percentage relative to the mission fuel mass of the point design for both the D250 (Table 5.6) and D250-LH2 (Table 5.11) concepts.

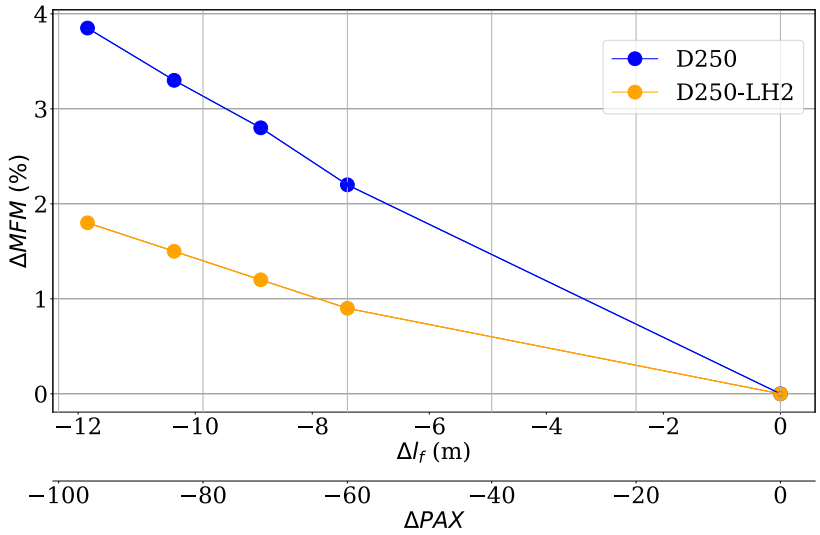

Figure 5.23: Effect of fuselage length reduction on the performance penalty due to empennage commonality

It can be concluded that **the potential fuselage length reduction in the case of an LH2 family, assuming empennage commonality, is considerably bigger than for a kerosene family.** Note that for both families, the -short member is the sizing case for the tailplane. Based on the results, the fuselage of this member can be shrinked between almost two and three times more, for the same fuel penalty.

5.3.2. Second family strategy: varying fuel capacity and constant payload

In kerosene-powered aircraft fuel capacity can be easily increased, which is often done by adding a center tank. This approach enables different aircraft within the same family to maintain the same payload while offering varying design ranges. This strategy is implemented in aircraft such as the -ER (extended range) versions of the Boeing 777 family [33]. This strategy is also applicable to LH2 aircraft. In this section, different D250-LH2-ER versions are also derived from the D250-LH2 concept. Different design ranges are explored for the -ER version, to see the impact on the family design. The focus is put into two specific trends that are expected for an LH2 design:

- In the case of kerosene-powered aircraft, fuel capacity can be increased without significant penalties by converting empty space within the wing-box, or the cargo compartments, into additional

fuel tanks. On the other hand, for an LH2-powered aircraft, increasing the size of the fuel tank introduces certain drawbacks. As the tank grows in size, it necessitates a longer fuselage to house it. This extension of the fuselage length, together with a heavier tank, reduces the aircraft´s performance. This is shown in the example from Figure 5.24.

- Having a larger tank increases the CG travel of the -ER family version. The lading gear position will be affected, thus influencing the HTP size of the family and its commonality.
  Conversely, this effect does not apply to the kerosene case. The center tanks have minimal impact on the aircraft's mass distribution. They can be positioned freely along the cargo bay to compensate for the center of gravity shift while maintaining an acceptable range. Consequently, for kerosene families, the HTP size will be approximately the same for both the base and -ER designs.

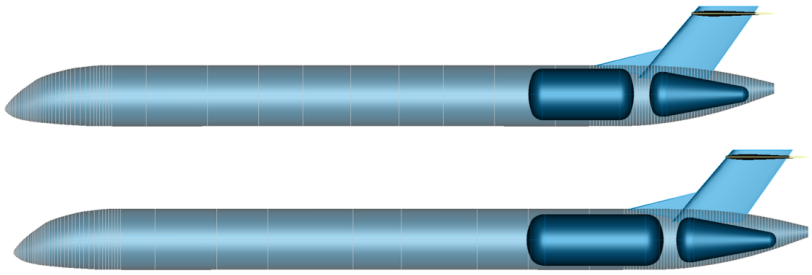

Figure 5.24: LH2 family with varying fuel capacity and constant payload. D250-LH2 (top) and D250-LH2-ER (bottom)

In Figure 5.25 the results from the different -ER versions are plotted. The change in the design range with respect to the D250-LH2 base is plotted in the x-axis. The increase in MFM for the evaluation mission for every -ER concept is plotted in the y-axis. The results are shown as a percentage with respect to the mission fuel mass of the D250-LH2, with a value for the evaluation mission of 2626 kg. The evaluation mission chosen is of 1482 km (800 NM) which is a typical value for a SMR aircraft design.

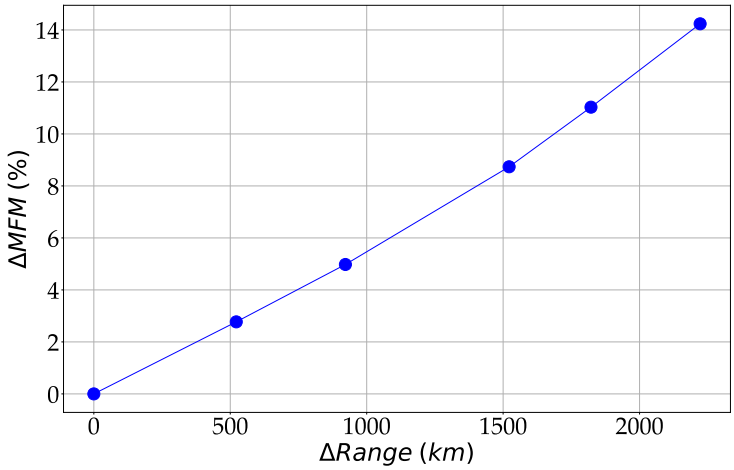

Figure 5.25: Evaluation mission performance comparison of different -ER family versions to the original D250-LH2 design

As expected, there is an increase in the fuel consumption for the evaluation mission. The longer the design range for the -ER version, the heavier the tanks and the fuselage. Consequently, for the same mission of 800 NM, the fuel mass increases, following an approximate exponential trend. However, this should not be considered a definitive conclusion. It is important to note that designs with a ΔRange > 500 km, as shown in Table 5.16, are pushing the original D250-LH2 design to its limits. The fuselage length exceeds 54 meters, surpassing the longest single-aisle aircraft fuselage ever produced, as set by the Boeing 757-300 [100]. Additionally, the aft positioning of the landing gear results in a large belly fairing. The penalties associated with these design features may not be fully captured by the current methodology, which primarily relies on statistical data from previously manufactured aircraft to estimate the fuselage structural mass and the size and performance impact of the belly fairing.

The goal of this small study was also to see the effect of different tank sizes on the tailplane commonality, in the case of an aircraft family with an -ER version. In Table 5.16 the results for the first iteration of the point design are shown. The D250-LH2 results are shown once again for reference in the first column. The rest of the columns show the values for the different -ER versions studied. In total, there are six different aircraft families, consisting of the D250-LH2 base and each of the six -ER versions, as the example shown in Figure 5.24.

Table 5.16: Impact of the design range on the tailplane size and fuselage length of the D250-LH2-ER family versions

	D250-LH2	ER_1	ER_2	ER_3	ER_4	ER_5	ER_6
Range [km]	2778	3300	3700	4000	4300	4600	5000
l_f **[m]**	52.2	53.6	54.7	55.6	56.6	57.6	59.0
Δl_f **[m]**	-	1.39	2.52	3.41	4.36	5.37	6.8
S_h $[m^2]$	37.1	40.2	42.6	44.4	46.4	48.4	51.6
ΔS_h $[m^2]$	-	3.1	5.5	7.26	9.3	11.3	14.5
$m_{LH2,sys}$ **[kg]**	5900	6469	6961	7353	7755	8181	8813
xsi_{mg} **[-]**	1.23	1.28	1.31	1.35	1.38	1.41	1.45

Despite the increased fuselage length and, consequently, a longer lever arm, the change in tank size—indicated by the LH2 system's mass parameter ($m_{LH2,sys}$)—primarily drives the horizontal tailplane sizing process. The landing gear is re-positioned with respect to the wing due to the aft shift of the CG range. This is shown in the last row of Table 5.16, where the optimum xsi_{mg} value is shown for each design. The -ER version drives the horizontal tailplane size in each case. Once again, **the HTP size exhibits a bigger sensitivity to the increased CG range, which offsets the benefits of the increased lever arm of the -ER design.**

Note that the values shown above are for the point design. If the same landing gear position is used for both members (D250-LH2 and D250-LH2-ER) as has been assumed for the studies in this thesis, the D250-LH2 design will have its gear further aft. The aft shift of the xsi_{mg} value, together with a shorter fuselage than the -ER version, can change the sizing member for the HTP. The second iteration of the workflow indeed shows an increased HTP size with respect to the 37.1 m^2 value in Table 5.16. However, for all cases, the values obtained for the second iteration of the D250-LH2 are still below the ones for the D250-LH2-ER version also shown in Table 5.16. Once again, the same effect is observed. For the same gear position, the reduction in lever arm is less critical than the increase in the CG range.

5.3.3. Third family strategy: varying fuel capacity and payload

As explained in Section 5.3.1, the payload-range trade-off is limited for an LH2 aircraft family if the tank is shared. This analysis focuses on a scenario where the market demands a family of aircraft with range requirements for the shorter versions that exceed what can be achieved with shared tanks. The payload reduces, while the fuel capacity increases to achieve the required range, as depicted in the example from Figure 5.26.

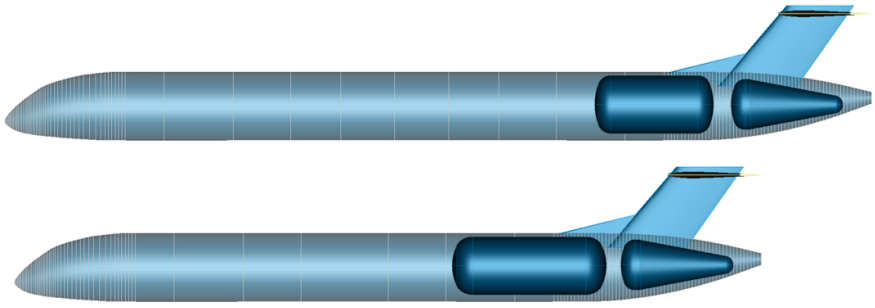

Figure 5.26: LH2 family with increasing fuel capacity and decreasing payload. D250-LH2 (top) and D250-LH2-ER-short (bottom)

This strategy is not typically employed in kerosene-powered aircraft, as shorter-range variants generally do not face range limitations when payload is reduced. Instead, the approach for different

variants within a family often involves increasing both fuel capacity and payload. Doing this for the D250-LH2 concept is not feasible, as the methodology is limited by the maximum length of a single aisle fuselage. Therefore, the strategy of reducing payload and increasing range is studied. Based on the results from the analysis a final conclusions can be drawn for the strategy in which both are increased.

Four families are derived from the D250-LH2 as the main member. In contrast to the original D250-LH2 family, for this study only one shorter version is derived, with the same passenger capacity as the original D250-LH2-short of 190 PAX. A specific range is defined as a TLAR for each of the new **-ER-short versions**, with the tank sized accordingly. Each family will then have two family members: the D250-LH2 and the D250-LH2-ER-short$_x$, where the x represents each of the ranges studied. The impact of the new tank size on the D250-LH2-ER-short$_x$ geometry, and the final empennage size for the family is shown in Table 5.17. The values for the original D250-LH2-short are shown for comparison, referred in the table as $short_0$. As discussed in 5.2.3, the $short_0$ was originally sizing for the HTP.

Table 5.17: Impact of the design range on the tailplane size and fuselage length of the D250-LH2-short$_x$ family versions

	$short_0$	$ER-short_1$	$ER-short_2$	$ER-short_3$	$ER-short_4$
Range [km]	3405	3750	4200	4600	5000
l_f **[m]**	44.85	45.59	46.55	47.41	48.34
Δl_f **[m]**	-	0.7	1.65	2.56	3.49
S_h **[m^2]**	38.5	39.3	40.2	41.3	42.1
ΔS_h **[m^2]**	-	0.8	1.7	2.8	3.6
$m_{LH2,sys}$ **[kg]**	5900	6191	6606	6970	7372
xsi_{mg} **[-]**	1.18	1.21	1.23	1.26	1.29

When the range for the shorter family member is increased, tank commonality is no longer possible. The bigger tank has an impact on the whole aircraft geometry, increasing the fuselage length and the HTP size as explained in 5.3.2. For all four new families, the short family member is still sizing. The heavier the tank, the bigger the HTP change with respect to the original design. The same effect as for the previous family strategy in Table 5.16 occurs. The longer fuselage not only increases the lever arm, but also the relative distance of the wing to the tank. This, along with the heavier tank, further increases the CG range, compensating for the increase in lever arm, and ultimately leading to a larger HTP.

A final comparison can be drawn between the values in Tables 5.16 and 5.17. Both tables illustrate the impact of fitting a larger tank on an aircraft design. The only difference relies on the passenger capacity of the family version that is created. In Table 5.16, a family version is derived from the D250-LH2 that has the same passenger capacity and increased range. On the other hand, in Table 5.17, the family version derived has increased range as well as reduced passenger capacity. The impact of the change in $m_{LH2,sys}$ (which reflects the increase in tank size) on both fuselage length and HTP size (directly linked to the fuel penalty due to commonality) is shown in Figures 5.27 and 5.28, respectively. Both Δl_f and ΔS_h are referenced to the original D250-LH2 values for fuselage length and HTP size, which are 52.2 m and 37.1 m^2, respectively.

For a given increase in tank size, Figure 5.27 shows that both family versions follow a similar increase in fuselage length, maintaining an approximately constant difference of -7.4 m. This difference is due to the 60 PAX variation in payload between the two aircraft. However, as shown in Figure 5.28, the impact of the same increase in the tank size on the HTP is significantly more pronounced in the case of the -ER versions. It might seem counter-intuitive, but when a bigger tank is fitted into a base design, decreasing the payload, and thus the tail lever arm, has a lower impact on HTP commonality than keeping the same payload. Increasing the tank size while keeping the payload fixed, as done in Table 5.16, automatically increases the CG range, and shifts the landing gear position aft. Increasing the tank size and simultaneously reducing the fuselage length as done in in Table 5.17, does not have such an impact on tail commonality. The shorter lever arm and heavier tank are offset by the reduced fuselage length, which decreases the relative distance between the wing and the tank. This, in turn, narrows the overall center of gravity range of the design.

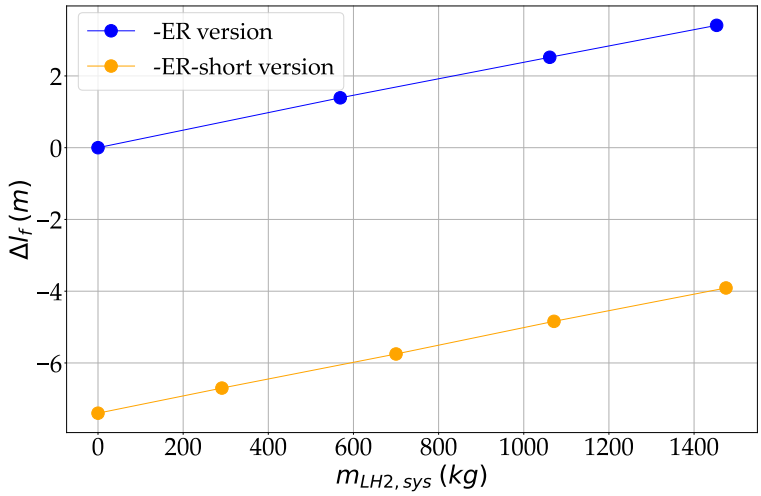

Figure 5.27: Impact of the increase in tank mask on the fuselage length for both D250-LH2-ER$_x$ versions from Table 5.16 and D250-LH2-ER-short$_x$ versions from Table 5.17

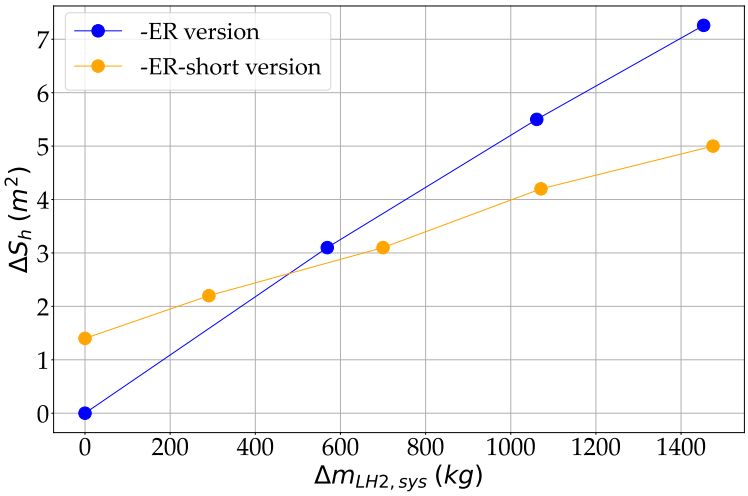

Figure 5.28: Impact of the increase in tank mask on the HTP size for both D250-LH2-ER$_x$ versions in Table 5.16 and D250-LH2-ER-short$_x$ versions from Table 5.17

Note that for the first tank mass values in Figure 5.28, the -ER-short version is above. This is because the main gear is not located in its optimum position, but it is still sized by the long family member as explained in Section 5.3.1. Once the -ER-short version dictates the position for the landing gear of the family, with the xsi_{mg} value exceeding 1.23, the behavior follows the explanation provided above.

For the thesis work, the strategy of increasing both payload and fuel capacity has not been considered. The D250-LH2 design is almost at its limit concerning the fuselage length for a single-aisle aircraft. Further increasing the passenger capacity will require for a twin-aisle configuration, thus the re-design of the whole concept. However, based on the results above, it can be concluded that **the family strategy of increasing both payload and range would be the most critical out of all studied for an LH2 family, concerning tailplane commonality. An even longer fuselage, combined with a heavier tank, will further increase the center of gravity travel, and will shift the landing gear position further aft.** This is completely the opposite of what would be expected with a kerosene design. In this case the increase in fuselage length only contributes to reducing the HTP lever arm and thus its size.

6

Conclusions

Most conceptual aircraft design studies focus on the point design approach, where all components are sized to meet the requirements of a specific aircraft. However, this approach does not align with industry practices, where big aircraft manufacturers like Airbus develop programs that result in multiple aircraft designs with a high degree of commonality, grouping them into the same aircraft family. The first goal of this thesis has been to adapt this industry approach of family conceptual design to the methodologies used at DLR-SL for its research on future aircraft designs. A special focus has been given to the sizing process of the horizontal tailplane. This component has been identified as one of the most critical in family design, due to the change in lever arm among family members. Understanding the behaviour of the sizing process of this component within an aircraft family, comes with special relevance for future aircraft concepts with rear fuselage LH2 tanks. The required size for the HTP in these designs is known to be considerably bigger than the actual values for a kerosene aircraft. However, there are no studies in the literature that address its commonality or potential performance penalties.

The developed methodology has an increased level of fidelity for sizing the horizontal tailplane. It is based on the scissor-plot methodology and incorporates an algorithm that positions the wing to obtain the minimum size. The long member is considered as the main aircraft design of the family. Two shorter family versions are designed in parallel, that influence the main design, resizing the HTP and VTP until a common size is achieved across all members.

The methodology has been validated using publicly available data for the A320neo family. The D239 reference aircraft, a DLR interpretation of the A321neo, has been sized taking potential family members into account. As expected, due to the shorter lever arm, the short family member was sizing for both the VTP and HTP. The performance difference between the point design and the family design of the D239 concept leads to an approximate 2% increase in mission fuel mass. In practice, the A320neo family also shares the same tailplane across its members. Consequently, a 2% performance penalty is considered assumable and is outweighed by the commonality benefits that come from using a shared tailplane within the aircraft family.

With the validation of the methodology, the **first research question** of the study was answered. The workflow was able to size an aircraft, in this case the D239, accurately predicting its tail size and wing position. The sizing of both VTP and HTP was done taking potential family members into account in the design loop. The results obtained shown in Section 4.2.2.2, match quite well the available data for the reference aircraft family.

Once validated, the methodology has been applied for the redesign of some DLR aircraft concepts. These are the D250 and D250-LH2 concepts developed during the DLR EXACT project [12]. The new level of fidelity for HTP sizing, together with the consideration of potential family members in the design loop, resulted in trade-off studies that were not possible during the initial sizing of these concepts. The results obtained can be generalized to draw **trends regarding the conceptual design of LH2 aircraft families with rear-fuselage tanks, with a special focus on the horizontal tailplane sizing process and its commonality**

- A first conclusion that can be extracted is that **HTP sizing is closely related to landing gear integration.** A **trade-off study** was conducted for both kerosene and hydrogen designs, between **wing-mounted and fuselage-mounted gear**.
  - For the D250 **kerosene** design, the high aspect ratio wing does not allow to integrate the gear in the wing for minimum HTP size. Consequently, a bigger HTP results than for the fuselage-mounted concept. However, the performance penalties due to the oversized HTP are damped by the reduced belly fairing in the **wing-mounted design**. This latter resulted in the end as the **better option**, due to the similar performance together with the better design characteristics.
  - In the case of a **hydrogen** aircraft, this trade is even more critical. Due to the aft tanks, the main landing gear is positioned too far aft. If the landing gear is intended to be integrated into the wing, the wing would need to be positioned too far aft, moving it away from its optimal position, and heavily influencing the size oft the HTP and trim drag.

    The **tip-back angle** value chosen also plays a role in **LH2 aircraft design**. The traditional aircraft design methods for landing gear positioning used for the D239 and D250, do no longer work for hydrogen aircraft. Using these values result in a huge HTP size. On the other hand, reducing the tip-back comes with a reduced payload-range flexibility due to constrained ground operations. The penalties of using the traditional tip-back angles have been observed to be much more critical for a wing-mounted design, where the resulting HTP size is unfeasible. Consequently, for the D250-LH2 design, a **fuselage-mounted gear** is shown as the **preferred option**. The performance is similar to the wing-mounted design, while still allows to use higher values of the tip-back angle without significant penalties, improving the ground stability. The wing-mounted design only demonstrates a similar performance if leading-edge high-lift devices on the horizontal tailplane are considered.
- Another trend that was observed is that **the take-off rotation requirement drives the tail size for LH2 concepts**. For a kerosene design, both controllability and take-off rotation requirement boundaries were close in the scissors plot. However, for the LH2 concepts there is a clear dominance of the take-off rotation requirement. The HTP size is really sensitive to the main gear position, which is specially aft for an LH2 aircraft, reducing the horizontal tail lever arm.

  Even in this study, where the HTP for the kerosene baseline was not minimized and the LH2 concept incorporates a T-tail, the volume coefficient remains still 40% larger for the hydrogen aircraft. **As anticipated in the literature, the LH2 aircraft horizontal tail is significantly larger** than that of a kerosene aircraft. Using statistical volume coefficient values, as outlined in Section 2.1.2.2, with values around 0.9–1.1, indeed results in an underestimated HTP size for an LH2 design.

- Regarding the **HTP and VTP commonality**, the thesis results present some first **guidelines on how to design LH2 aircraft families with rear-fuselage tanks, concerning the commonality of these components**. A first estimate of the performance penalty across family members is provided, comparing it to conventional kerosene-powered aircraft families.

  The methodology used behaves as expected for **kerosene aircraft families**. For both D239 and D250 families, the **same trend is followed**. In both cases, the aircraft family is derived from the longer family member by reducing the payload while maintaining the same fuel capacity.

As expected, the reduction in lever arm negatively impacts the size of both the VTP and HTP, leading to an increase in its size. The short variants, the D239-short and D250-short, are the sizing member both lifting surfaces. Using a common empennage results in a heavier design for the main family members, with increased weights for the empennage, fuselage, wing, and consequently the engines. However, the performance penalty is still considered manageable, falling around 2% for both designs. This penalty is deemed acceptable, as observed in the real-life A320neo family.

Nevertheless, **these trends** that are given for a kerosene aircraft family with reduced payload and constant fuel capacity among family members **change when introducing LH2 cryogenic tanks integrated in the rear fuselage**. For an **LH2 aircraft family of these characteristics, the difference in the HTP size among the point designs is smaller**. Despite the extra penalties that are given in an LH2 family when a bigger empennage is fitted into the long member (such as the increase in both tank size and fuselage length to maintain the design range with the new tailplane size), the **commonality penalties are actually lower than for a kerosene family**.

The primary reason for this effect is the variation in the CG range across family members, which is a characteristic of LH2 aircraft families with rear tanks. The **relative tank position to the wing increases with the fuselage length.** This results in a a longer CG range for the long member. The shorter family member will have a shorter CG range, which will compensate for the shorter lever arm. In the end, this closes the gap between the optimum HTP values for each member. This effect is bigger in the case of **wing-mounted gear** designs, where the landing gear is integrated for all members in a non-optimum position. As a result, it has been observed that the long family member can become the sizing case for the HTP in some scenarios.

On the other hand, for **fuselage-mounted gear**, the short member is still generally sizing for the HTP. This is driven by commonality requirements, as the relative position of the main landing gear to the wing must remain consistent across all family members. The longest center of gravity range, i.e. the long version, determines this value, with the optimal position for the short version being located ahead of it. Note that during the family design the main gear position can be optimized by selecting the correct value for the section length and Δl_{VTP}. The correct definition of these parameters can shift the position of the main gear from the long family member closer to the optimum gear position of the short member. The empennage commonality penalties can be reduced as a result.

In the end, and regardless of the gear integration, in an aircraft family where payload is traded for range for a given fuel capacity, **the empennage commonality penalties are reduced for an LH2 family when compared to a kerosene family**. **This statement answers the second research question of the study**. For an LH2 family of these characteristics the fuselage can be shrinked more, covering a much wider spectrum of payloads without sacrificing empennage commonality. This compensates the lower payload-range flexibility that is given for the shorter LH2 family variants due to tank commonality.

Lastly, to address the **last research question**, a design space exploration was conducted to assess the influence of **alternative family design strategies on the commonality of the tailplane, such as increasing fuel or passenger capacity**. In the case of kerosene-powered aircraft, neither of these factors adversely impacts the lever arm or CG range, and thus, they do not present significant challenges for tailplane commonality. The following observations were made for LH2 aircraft families with rear tanks which only confirmed the trend observed above:

- In the case of an **extended range family strategy**, increasing the tank size has a bigger effect on tailplane commonality if the payload is kept constant, rather than reduced, with respect to the base family member.
- An **LH2 aircraft family in which both range and payload are increased** represents the most critical scenario for empennage commonality, conversely to what is observed for conventional family designs.

To sum up, the lever arm effect on the sizing member of an LH2 aircraft family slightly changes what is given for kerosene aircraft. A shorter lever arm does not longer necessarily result into a larger horizontal tail. A shorter fuselage brings closer the wing and the tank, reducing the CG range, which compensates the reduction in lever arm. Thus, when the fuselage length is reduced with respect to the main family member, the commonality penalties are lower than for a kerosene family. On the other hand, increasing the fuselage length turns out to be now the critical strategy for tailplane commonality in an LH2 aircraft family design. Increasing payload, fuel capacity, or both, results in an increased fuselage length, and thus CG range. Note that all this conclusions are applicable only for LH2 designs with rear-fuselage tanks.

To conclude the thesis some **recommendations for future work** on the topic are listed below:

- The next logical step would be to further develop the workflow to be used for sizing any aircraft as the base family member. The current methodology is applicable only if the long member is sized as the base family member. The workflow begins by designing this aircraft, from which family variants are derived by shortening the fuselage and adjusting some of the TLARs. In the outer loop, only the resizing of the empennage is taken into account; other components, such as engines, landing gear, and wings, are not considered, taking the results directly from the base design.

- Currently, the same engine is used for all family members. This is actually done in a family. However, the thrust is artificially down-rated for the shorter versions due to the lower thrust requirements. Implementing a method to down-rate the engine for the shorter family variants would significantly improve the accuracy of estimating the HTP size, and particularly the VTP size, for the entire family. Currently, the latter is estimated based on an empirical formula that does not account for engine down-rating.

- As depicted in the the results and conclusions, fuselage-integrated gear appears as the best solution for an LH2 aircraft. Considering the influence of trim drag would further increase the quality of the results, and potentially the confidence for choosing a fuselage-mounted landing gear solution due to the lower static margin value.
  Besides this, a study could be performed to see the impact of a wing-mounted gear with a faring, as done in some aircraft designs like the Tupolev TU-154 aircraft. The fairing would allow for shifting the landing gear further aft while still maintaining a wing-integrated gear configuration.

- The conclusions from this study are only applicable to the family design of LH2 aircraft with rear-fuselage tanks. The design space could be further explored, by analyzing the impact of different tank configurations (front and back tanks), or cabin layouts (double-aisle), on the family design and tailplane commonality.

- The development of a comprehensive model to calculate the manufacturing, design, and maintenance costs associated with common components, such as the tailplane and tanks for an LH2 aircraft family, would significantly enhance the conclusions of this work. This model would provide a more accurate representation of the performance versus commonality trade-offs, enabling a better understanding of the economic implications of design decisions within the family.

References

[1] S. Tiwari, M. J. Pekris, and J. J. Doherty, "A review of liquid hydrogen aircraft and propulsion technologies," *International Journal of Hydrogen Energy*, vol. 57, pp. 1174–1196, Feb. 2024. DOI: 10.1016/j.ijhydene.2023.12.263. [Online]. Available: https://www.scopus.com/inward/record.uri?eid=2-s2.0-85182594835&doi=10.1016%2fj.ijhydene.2023.12.263&partnerID=40&md5=4f7b084ae975899ce9d16120f3966d64.

[2] Airbus. "Global Market Forecast 2023-2042." (2024), [Online]. Available: https://www.airbus.com/en/products-services/commercial-aircraft/market/global-market-forecast (visited on 03/10/2024).

[3] E. J. Adler and J. R. Martins, "Hydrogen-powered aircraft: Fundamental concepts, key technologies, and environmental impacts," *Progress in Aerospace Sciences*, vol. 141, no. 100922, Aug. 2023. DOI: 10.1016/j.paerosci.2023.100922. [Online]. Available: https://www.scopus.com/inward/record.uri?eid=2-s2.0-85160937428&doi=10.1016%2fj.paerosci.2023.100922&partnerID=40&md5=65867d14eb09595b6b5617a027c1abf3.

[4] Airbus. "Zeroe: Airbus' hydrogen-powered future." (2024), [Online]. Available: https://www.airbus.com/en/innovation/low-carbon-aviation/hydrogen/zeroe (visited on 02/27/2024).

[5] E. Torenbeek, *Synthesis of Subsonic Airplane Design*, 1st ed. Dordrecht, The Netherlands: Kluwer Academic Publishers, 1982.

[6] D. Verstraete, P. Hendrick, P. Pilidis, and K. Ramsden, "Hydrogen fuel tanks for subsonic transport aircraft," *International Journal of Hydrogen Energy*, vol. 35, Issue 20, pp. 11 085–11 098, Oct. 2010. DOI: 10.1016/j.ijhydene.2010.06.060. [Online]. Available: https://www.scopus.com/inward/record.uri?eid=2-s2.0-77957372091&doi=10.1016%2fj.ijhydene.2010.06.060&partnerID=40&md5=df4ec094672b6b86588f465ed76d4bbf.

[7] S. Wöhler, T. Burschyk, J. Häßy, and M. Iwanizki, "Design and assessment of long range aircraft concepts with focus on fossil kerosene, sustainable aviation fuel and liquid hydrogen as energy carriers," in *AIAA Aviation Forum*, San Diego, California, USA, 2023. DOI: 10.2514/6.2023-3229. [Online]. Available: https://www.researchgate.net/publication/371438420_Design_and_Assessment_of_Long_Range_Aircraft_Concepts_with_focus_on_Fossil_Kerosene_Sustainable_Aviation_Fuel_and_Liquid_Hydrogen_as_Energy_Carriers.

[8] A. Westenberger, "LH2 as Alternative Fuel for Aeronautics – Study on Aircraft Concepts," Airbus Deutschland GmbH, Final Report Cryoplane Project, 2008. [Online]. Available: https://www.semanticscholar.org/paper/LH2-as-Alternative-Fuel-for-Aeronautics-Study-on-Westenberger-Deutschland/bbda93f6df116ae82d32ada43dacb41786e7ba59.

[9] A. Gomez and H. Smith, "Liquid hydrogen fuel tanks for commercial aviation: Structural sizing and stress analysis," *Aerospace Science and Technology*, vol. 95, no. 105438, Dec. 2019. DOI: 10.1016/j.ast.2019.105438. [Online]. Available: https://www.scopus.com/inward/record.uri?eid=2-s2.0-85072851385&doi=10.1016%2fj.ast.2019.105438&partnerID=40&md5=f48693019ce3c5e64a737a3c61f6d847.

[10] G. Onorato, "Fuel tank integration for hydrogen airliners," Master's Thesis, Aerospace Engineering Department, Delft University of Technology, Delft, NL, 2021. [Online]. Available: https://repository.tudelft.nl/islandora/object/uuid%3A5700b748-82c6-49c9-b94a-ad97c798e119?collection=education.

[11] G. Atanasov, J. Wehrspohn, M. Kühlen, *et al.*, "Short-medium-range turboprop-powered aircraft as a cost-efficient enabler for low climate impact," in *AIAA Aviation Forum*, San Diego, CA, USA, 2023. DOI: 10.2514/6.2023-3368. [Online]. Available: https://arc.aiaa.org/doi/10.2514/6.2023-3368.

[12] DLR. "DLR EXACT: Project Overview." (2024), [Online]. Available: https://exact-dlr.de/project-overview/ (visited on 09/14/2024).

[13] J. Ramm, A. A. Pohya, K. Wicke, and G. Wende, "Uncertainty quantification in hydrogen tank exchange: Estimating maintenance costs for new aircraft concepts," *International Journal of Hydrogen Energy*, vol. 68, pp. 159–169, Apr. 2024. DOI: 10.1016/j.ijhydene.2024.04.157. [Online]. Available: https://elib.dlr.de/204152/.

[14] D. P. Raymer, *Aircraft Design: A conceptual Approach*, 5^{th} ed. Reston, Virginia, USA: American Institute of Aeronautics and Astronautics, 2012.

[15] T. Druot, S. Alestra, C. Brand, and S. Morozov, "Multi-objective optimization of aircrafts family at conceptual design stage," in *Inverse Problems, Design and Optimization Symposium*, Albi, France, 2013. [Online]. Available: https://www.pseven.io/company/publications/multi-objective-optimization-of-aircrafts-family-at-conceptual-design-stage.html.

[16] J. Roskam, *Airplane Design, Parts I-VIII*. Lawrence, Kansas, USA: Roskam Aviation and Engineering Corporation, 1985-2000.

[17] "U.S. Air Force Stability and Control Digital DATCOM," Air Force FDL, Wright-Patterson AFB, Ohio, USA, Tech. Rep. AFWAL-TR-83-3048, 1978.

[18] D. Ciliberti, P. Della Vecchia, F. Nicolosi, and A. De Marco, "Aircraft directional stability and vertical tail design: A review of semi-empirical methods," *Progress in Aerospace Sciences*, vol. 95, pp. 140–172, Nov. 2017. DOI: 10.1016/j.paerosci.2017.11.001. [Online]. Available: https://www.sciencedirect.com/science/article/pii/S0376042117301598.

[19] Y. Eraslan, "A training sailplane design," Master's Thesis, University of Gaziantep, Gaziantep, TR, 2018. [Online]. Available: https://www.researchgate.net/publication/348150678_A_Training_Sailplane_Design/link/5ff046a692851c13fedf40e1/download?_tp=eyJjb250ZXh0Ijp7InBhZ2UiOiJwdWJsaWNhdGlvbiIsInByZXZpb3VzUGFnZSI6Il9kaXJlY3QifX0.

[20] *Certification Specifications and Acceptable Means of Compliance for Large Aeroplanes (CS-25)*, European Union Aviation Safety Agency (EASA), 2007. [Online]. Available: https://www.easa.europa.eu/sites/default/files/dfu/CS-25_Amdt%203_19.09.07_Consolidated%20version.pdf.

[21] *Certification Specifications for Normal, Utility, Aerobatic, and Commuter Category Aeroplanes (CS-23)*, European Union Aviation Safety Agency (EASA), 2015. [Online]. Available: https://www.easa.europa.eu/sites/default/files/dfu/CS-23%20Amendment%204.pdf.

[22] D. Scholz, "Empennage sizing with the tail volume complemented with a method for dorsal fin layout," *INCAS Bulletin*, vol. 13, Issue 3, pp. 149–164, Aug. 2021. DOI: 10.48441/4427.245. [Online]. Available: https://www.fzt.haw-hamburg.de/pers/Scholz/Aero/AERO_PUB_INCAS_TailVolume_Vol13No3_2021.pdf.

[23] D. Scholz, *Aircraft design: Empennage sizing*, PDF, Aircraft Design. Lecture Notes by Prof. Dr. D. Scholz.. Hamburg University of Applied Sciences. Available from: http://LectureNotes.AircraftDesign.org, 2015.

[24] F. Oliviero, *Requirement analysis and design principles for a/c stability & control*, PDF, AE3211-I - Systems Engineering and Aerospace Design. Lecture Notes by Dr. F. Oliviero. Delft University of Technology, 2022.

[25] M. H. Sadraey, *Aircraft Design: A Systems Engineering Approach*, 1^{st} ed. Hoboken, New Jersey, USA: John Wiley & Sons, 2012.

[26] J. Kay, W. H. Mason, W. Durham, F. Lutze, and A. Benoliel, "Control authority issues in aircraft conceptual design," Virginia Polytechnic Institute and State University, Blacksburg, Virginia, USA, Tech. Rep. VPI-Aero 200, 1993. [Online]. Available: https://archive.aoe.vt.edu/mason/Mason_f/VPI-Aero-200.pdf.

[27] R. Slingerland, "Minimum unstick speed impact on horizontal tail sizing for jet transports," in *AIAA Aviation Forum*, Reno, Nevada, USA, 2005, pp. 8733–8744. DOI: 10.2514/6.2005-815. [Online]. Available: https://www.scopus.com/inward/record.uri?eid=2-s2.0-30744458592&doi=10.2514%2f6.2005-815&partnerID=40&md5=e88efc2d0e1d8bb9c3d0aa99602d2f07.

[28] Airbus. "Flight Operations Briefing Notes: Takeoff and Departure Operations – Understanding Takeoff Speeds." (), [Online]. Available: https://skybrary.aero/sites/default/files/bookshelf/493.pdf (visited on 03/07/2024).

[29] D. Scholz, *Aircraft design: Empennage general design*, PDF, Aircraft Design. Lecture Notes by Prof. Dr. D. Scholz.. Hamburg University of Applied Sciences. Available from: http://LectureNotes.AircraftDesign.org, 2015.

[30] R. Karunanidhi, D. Scholz, J. Majak, and M. Eerme, "Empennage sizing using tail volume," *AIP Conference Procedings*, vol. 2425, Issue 1, no. 380007, Apr. 2022. DOI: 10.1063/5.0082095. [Online]. Available: https://pubs.aip.org/aip/acp/article/2425/1/380007/2824375/Empennage-sizing-using-tail-volume.

[31] C. Cuerno-Rejado and A. Sanchez-Carmona, "Preliminary sizing correlations for the rear-end of transport aircraft," *Aircraft Engineering and Aerospace Technology*, vol. 88, Issue 1, pp. 24–32, Jan. 2016. DOI: 10.1108/AEAT-04-2014-0051. [Online]. Available: https://www.emerald.com/insight/content/doi/10.1108/AEAT-04-2014-0051/full/html.

[32] L. A. McCullers, *Flight optimization system, user's guide*, NASA Langley Research Center, Hampton, Virginia, USA, 2011.

[33] A. Riaz, M. D. Guenov, and A. Molina-Cristobal, "Set-based approach to passenger aircraft family design," *Journal of Aircraft*, vol. 54, Issue 1, pp. 310–326, 2017. DOI: 10.2514/1.C033747. [Online]. Available: https://www.scopus.com/inward/record.uri?eid=2-s2.0-85013657707&doi=10.2514%2f1.C033747&partnerID=40&md5=55810262fbe51aed2c19a3f6121e7428.

[34] F. Nicolosi, P. Della Vecchia, and S. Corcione, "Design and aerodynamic analysis of a twin-engine commuter aircraft," *Aerospace Science and Technology*, vol. 40, pp. 1–16, Jan. 2015. DOI: 10.1016/j.ast.2014.10.008. [Online]. Available: https://www.sciencedirect.com/science/article/pii/S1270963814002065.

[35] T. E. Boogaart, M. F. M. Hoogreef, and A. Gangoli Rao, "Installation penalty of aero-engines on narrow body aircraft," in *33rd Congress of the International Council of the Aeronautical Sciences (ICAS)*, Stockholm, Sweden, 2022. [Online]. Available: https://repository.tudelft.nl/record/uuid:4fe8f425-3b2c-41c3-a48f-b199eeea1279.

[36] J. Bussemaker, P. Ciampa, J. Singh, *et al.*, "Collaborative Design of a Business Jet Family Using the AGILE 4.0 MBSE Environment," in *AIAA Aviation Forum*, Chicago, Illinois, USA, 2022. DOI: 10.2514/6.2022-3934. [Online]. Available: https://www.scopus.com/inward/record.uri?eid=2-s2.0-85135002509&doi=10.2514%2f6.2022-3934&partnerID=40&md5=46e6badf2aca80a6c4beb41cd7ed6376.

[37] "Contribution of fin to sideforce, yawing moment and rolling moment derivatives due to sideslip, (Yv) F, (Nv) F, (Lv) F, in the presence of body, wing and tailplane," ESDU, London, United Kingdom, Tech. Rep. ESDU 82010, 1982.

[38] F. Nicolosi and G. Paduano, "Development of a software for aircraft preliminary design and analysis," in *Proceedings of the 3rd CEAS (Council of European Aerospace Societies) Congress*, Venice, Italy, 2011.

[39] R. Perez, H. Liu, and K. Behdinan, "Multidisciplinary optimization framework for control-configuration integration in aircraft conceptual design," *Journal of Aircraft*, vol. 43, pp. 1937–1948, Nov. 2006. DOI: 10.2514/1.22263. [Online]. Available: https://www.researchgate.net/publication/245430724_Multidisciplinary_Optimization_Framework_for_Control-Configuration_Integration_in_Aircraft_Conceptual_Design.

[40] G. Onorato, P. Proesmans, and M. F. M. Hoogreef, "Assessment of hydrogen transport aircraft: Effects of fuel tank integration," *CEAS Aeronautical Journal*, vol. 13, Issue 4, pp. 813–845, Sep. 2022. DOI: 10.1007/s13272-022-00601-6. [Online]. Available: https://pubmed.ncbi.nlm.nih.gov/36157265/.

[41] Z. Yongjie, Z. Yongqi, C. Kang, D. Wenjun, and D. Dayong, "A review of the development of civil aircraft family," *Journal of Physics: Conference Series*, vol. 1877, Apr. 2021. DOI: 10.1088/1742-6596/1877/1/012024. [Online]. Available: https://iopscience.iop.org/article/10.1088/1742-6596/1877/1/012024.

[42] Z. Yongjie, Z. Yongqi, C. Kang, Y. Zheng, D. Wenjun, and D. Dayong, "A review of commonality design for civil aircraft," in *12th International Conference on Mechanical and Aerospace Engineering (ICMAE)*, Athens, Greece, 2021. DOI: 10.1109/ICMAE52228.2021.9522472. [Online]. Available: https://www.scopus.com/inward/record.uri?eid=2-s2.0-85115380238&doi=10.1109%2fICMAE52228.2021.9522472&partnerID=40&md5=8f88fe9e0e02378cc7f4000aec300cc4.

[43] P. Zhuravlev and V. Zhuravlev, "Significance of modifications for development of passenger airplanes," *Aircraft Engineering and Aerospace Technology*, vol. 84, Issue 3, pp. 172–180, May 2012. DOI: 10.1108/00022661211222021. [Online]. Available: https://www.scopus.com/inward/record.uri?eid=2-s2.0-84861356179&doi=10.1108%2f00022661211222021&partnerID=40&md5=d9827cbb9414a7f5c6a4418396070b68.

[44] Airbus. "A320 Family." (2024), [Online]. Available: https://www.airbus.com/en/products-services/commercial-aircraft/passenger-aircraft/a320-family (visited on 07/14/2024).

[45] Wikipedia. "Boeing 777." (2024), [Online]. Available: https://de.wikipedia.org/wiki/Boeing_777 (visited on 03/11/2024).

[46] Wikipedia. "Airbus A320 family." (2021), [Online]. Available: https://en.wikipedia.org/wiki/Airbus_A320_family (visited on 02/27/2024).

[47] "CFM56-5A & 5B Specifications," Aircraft Commerce, Tech. Rep. Issue 50, 2006. [Online]. Available: https://www.aircraft-commerce.com/wp-content/uploads/aircraft-commerce-docs1/Aircraft%20guides/CFM56-5A-5B/ISSUE%2050-CFM56-5A-5B%20SPECS.pdf.

[48] Airbus, *Airport Planning Manual: Airbus A320*, Online, Nov. 2021. [Online]. Available: https://www.airbus.com/sites/g/files/jlcbta136/files/2021-11/Airbus-Commercial-Aircraft-AC-A320.pdf (visited on 04/04/2024).

[49] Airbus, *Airport Planning Manual: Airbus A319*, Online, Nov. 2021. [Online]. Available: https://www.airbus.com/sites/g/files/jlcbta136/files/2021-11/Airbus-Commercial-Aircraft-AC-A319.pdf (visited on 04/04/2024).

[50] Airbus, *Airport Planning Manual: Airbus A321*, Online, Nov. 2021. [Online]. Available: https://www.airbus.com/sites/g/files/jlcbta136/files/2021-11/Airbus-Commercial-Aircraft-AC-A321.pdf (visited on 04/04/2024).

[51] Airbus, *Airport Planning Manual: Airbus A350*, Online, Nov. 2021. [Online]. Available: https://www.airbus.com/sites/g/files/jlcbta136/files/2021-11/Airbus-Commercial-Aircraft-AC-A350-900-1000.pdf (visited on 01/15/2024).

[52] K. Willcox and S. Wakayama, "Simultaneous optimization of a multiple-aircraft family," *Journal of Aircraft*, vol. 40, Issue 4, pp. 616–622, Jul. 2003. DOI: 10.2514/2.3156. [Online]. Available: https://arc.aiaa.org/doi/epdf/10.2514/2.3156.

[53] K. Fujita, S. Akagi, T. Yoneda, and M. Ishikawa, "Simultaneous optimization of product family sharing system structure and configuration," in *International Design Engineering Technical Conferences and Computers and Information in Engineering Conference*, Atlanta, Georgia, USA, 1998. DOI: 10.1115/DETC98/DFM-5722. [Online]. Available: https://asmedigitalcollection.asme.org/IDETC-CIE/proceedings-abstract/DETC98/80340/V004T04A011/1098596.

[54] Wikipedia. "Airbus A350." (2021), [Online]. Available: https://en.wikipedia.org/wiki/Airbus_A350 (visited on 02/27/2024).

[55] H. Takami and S. Obayashi, "A formulation of the industrial conceptual design optimization problem for commercial transport airplanes," *Aerospace*, vol. 9, Issue 9, Sep. 2022. DOI: 10.3390/aerospace9090487. [Online]. Available: https://www.scopus.com/inward/record.uri?eid=2-s2.0-85138564398&doi=10.3390%2faerospace9090487&partnerID=40&md5=7f5703e59399e298847461139d3a0a14.

[56] S. Ding, Q. Gu, R. Ge, and X. Wang, "The study of wide-body aircraft family using nsgaii," in *8th International Conference on Electronics, Computers and Artificial Intelligence (ECAI)*, Ploiesti, Romania, 2017. DOI: 10.1109/ECAI.2016.7861158. [Online]. Available: https://www.scopus.com/inward/record.uri?eid=2-s2.0-85016212585&doi=10.1109%2fECAI.2016.7861158&partnerID=40&md5=4f34e6b6d8ce89fbe2cbd3f0070b4d86.

[57] J. Allison, B. Roth, M. Kokkolaras, I. Kroo, and P. Y. Papalambros, "Aircraft family design using decomposition-based methods," in *11th AIAA/ISSMO Multidisciplinary Analysis and Optimization Conference*, Portsmouth, Virginia, USA, 2006, pp. 606–617. DOI: 10.2514/6.2006-6950. [Online]. Available: https://www.scopus.com/inward/record.uri?eid=2-s2.0-33846522459&doi=10.2514%2f6.2006-6950&partnerID=40&md5=a9f2aa4fb71ae46565b0603d930620b6.

[58] Agile. "Agile project - advanced design for efficient and lightweight applications." (2024), [Online]. Available: https://www.agile-project.eu/ (visited on 03/11/2024).

[59] Agile4. "Agile4 - agile manufacturing for the future." (2024), [Online]. Available: https://www.agile4.eu/ (visited on 03/11/2024).

[60] C. Cabaleiro, J. Bussemaker, M. Fioriti, L. Boggero, P. D. Ciampa, and B. Nagel, "Environmental and flight control system architecture optimization from a family concept design perspective," in *AIAA Aviation Forum*, Orlando, Florida, USA, 2020. DOI: 10.2514/6.2020-3113. [Online]. Available: https://arc.aiaa.org/doi/abs/10.2514/6.2020-3113.

[61] I. Kroo, "An interactive system for aircraft design and optimization," in *AIAA Aerospace Design Conference*, Irvine, California , USA, 1992. DOI: 10.2514/6.1992-1190. [Online]. Available: https://arc.aiaa.org/doi/10.2514/6.1992-1190.

[62] D. Verstraete, "The potential of liquid hydrogen for long range aircraft propulsion," Ph.D. dissertation, School of Engineering, Cranfield University, Bedford, UK, 2009. [Online]. Available: https://dspace.lib.cranfield.ac.uk/handle/1826/4089.

[63] A. Silverstein and E. W. Hall, "Liquid hydrogen as a jet fuel for high-altitude aircraft," NASA, Washington, D.C., USA, Tech. Rep. NACA-RM-E55C28a, 1955. [Online]. Available: https://ntrs.nasa.gov/citations/19930088689.

[64] P. Rompokos, A. Rolt, T. Sibilli, and C. Benson, "Cryogenic fuel storage modelling and optimisation for aircraft applications," in *ASME Turbo Expo: Turbomachinery Technical Conference and Exposition*, 2021. DOI: 10.1115/GT2021-58595. [Online]. Available: https://www.scopus.com/inward/record.uri?eid=2-s2.0-85115614279&doi=10.1115%2fGT2021-58595&partnerID=40&md5=763ac00e47918fd54ab49bf0382bad14.

[65] T. Burschyk, D. Silberhorn, J. Wehrspohn, M. Kühlen, and T. Zill, "Scenario-based implications of liquid hydrogen storage tank insulation quality for a short-range aircraft concept," in *AIAA Aviation Forum*, San Diego, California, USA, 2023. DOI: 10.2514/6.2023-3522. [Online]. Available: https://arc.aiaa.org/doi/abs/10.2514/6.2023-3522.

[66] C. Winnefeld, T. Kadyk, B. Bensmann, U. Krewer, and R. Hanke-Rauschenbach, "Modelling and designing cryogenic hydrogen tanks for future aircraft applications," *Energies*, vol. 11, Issue 1, Jan. 2018. DOI: 10.3390/en11010105. [Online]. Available: https://www.scopus.com/inward/record.uri?eid=2-s2.0-85040308847&doi=10.3390%2fen11010105&partnerID=40&md5=2a842f50bc7b2f68ffbce47fca4eab75.

[67] G. D. Brewer, *Hydrogen Aircraft Technology*, 1st ed. New York, USA: CRC Press, 1991.

[68] T. Burschyk, Y. Cabac, D. Silberhorn, B. Boden, and B. Nagel, "Liquid hydrogen storage design trades for a short-range aircraft concept," *CEAS Aeronautical Journal*, vol. 14, Issue 4, pp. 879–893, Oct. 2023. DOI: 10.1007/s13272-023-00689-4. [Online]. Available: https://www.scopus.com/inward/record.uri?eid=2-s2.0-85174740770&doi=10.1007%2fs13272-023-00689-4&partnerID=40&md5=0811b32bb7b0051b3b1bfb329d72facb.

[69] V. Osipov, M. Daigle, B. Muratov, M. Foygel, V. Smelyanskiy, and M. Watson, "Dynamical model of rocket propellant loading with liquid hydrogen," *Journal of Spacecraft and Rockets*, vol. 48, pp. 987–998, Nov. 2011. DOI: 10.2514/1.52587. [Online]. Available: https://c3.ndc.nasa.gov/dashlink/static/media/publication/LH2-AIAA.pdf.

[70] D. Silberhorn, G. Atanasov, J.-N. Walther, and T. Zill, "Assessment of hydrogen fuel tank integration at aircraft level," in *German Aerospace Congress (DLRK)*, Darmstadt, Germany, 2019. [Online]. Available: https://elib.dlr.de/129643/.

[71] P. Rompokos, A. Rolt, D. Nalianda, *et al.*, "Synergistic Technology Combinations for Future Commercial Aircraft Using Liquid Hydrogen," *Journal of Engineering for Gas Turbines and Power*, vol. 143, Issue 7, Mar. 2021. DOI: 10.1115/1.4049694. [Online]. Available: https://asmedigitalcollection.asme.org/gasturbinespower/article/143/7/071017/1095473/Synergistic-Technology-Combinations-for-Future.

[72] C. Xisto and A. Lundbladh, "Design and performance of liquid hydrogen fuelled aircraft for year 2050 eis," in *33rd Congress of the International Council of the Aeronautical Sciences (ICAS)*, Stockholm, Sweden, 2022. [Online]. Available: https://www.scopus.com/inward/record.uri?eid=2-s2.0-85159679664&partnerID=40&md5=8b8dcfe27e4a7d1a1153c1540176c47e.

[73] J. Huete, D. Nalianda, and P. Pilidis, "Propulsion system integration for a first-generation hydrogen civil airliner?" *Aeronautical Journal*, vol. 125, no. 1291, pp. 1654–1665, Sep. 2021. DOI: 10.1017/aer.2021.36. [Online]. Available: https://www.scopus.com/inward/record.uri?eid=2-s2.0-85111457345&doi=10.1017%2faer.2021.36&partnerID=40&md5=93180a0402f7ff499f0a1336890cccc0.

[74] D. Silberhorn, K. Dahlmann, A. Görtz, *et al.*, "Climate impact reduction potentials of synthetic kerosene and green hydrogen powered mid-range aircraft concepts," *Applied Sciences*, vol. 12, no. 5950, Jun. 2022. DOI: 10.3390/app12125950. [Online]. Available: https://www.mdpi.com/2076-3417/12/12/5950.

[75] B. M. H. J. Fröhler, S. Wöhler, T. Zill, and M. Iwanizk, "Increasing fuel efficiency for short to medium range market: A conceptual aircraft design study on unconventional configurations," in *AIAA Aviation Forum*, Las Vegas, Nevada, USA, 2024. DOI: 10.2514/6.2024-4325. [Online]. Available: https://arc.aiaa.org/doi/10.2514/6.2024-4325.

[76] S. Wöhler, G. Atanasov, D. Silberhorn, B. M. H. J. Fröhler, and T. Zill, "Preliminary aircraft design within a multidisciplinary and multifidelity design environment," in *Aerospace Europe Conference*, Bordeaux, France, 2020. [Online]. Available: https://elib.dlr.de/140902/.

[77] B. M. H. J. Fröhler, C. Hesse, G. Atanasov, and P. Wassink, "Disciplinary sub-processes to assess low-speed performance and noise characteristics within an aircraft design environment," in *Deutscher Luft- und Raumfahrtkongress*, Boon, Germany, 2020. DOI: 10.25967/530201. [Online]. Available: https://publikationen.dglr.de/?tx_dglrpublications_pi1%5Bdocument_id%5D=530201.

[78] P. Balack, T. Hecken, M. Petsch, G. Atanasov, D. Silberhorn, and B. Nagel, "Semi-physical method for the mass estimation of fuselages carrying liquid hydrogen fuel tanks in conceptual aircraft design," in *German Aerospace Congress (DLRK)*, Dresden, Germany, 2022. [Online]. Available: https://elib.dlr.de/203339/.

[79] T. Hecken, P. Balack, M. Petsch, and D. Zerbst, "Conceptual loads assessment of aircraft with fuselage integrated liquid hydrogen tank," in *German Aerospace Congress (DLRK)*, Dresden, Germany, 2022. [Online]. Available: https://elib.dlr.de/189171/.

[80] D. Zerbst, T. Hecken, P. Balack, *et al.*, "Preliminary design of composite wings using beam-based structural models," in *German Aerospace Congress (DLRK)*, Dresden, Germany, 2022. [Online]. Available: https://elib.dlr.de/188725/.

[81] M. Petsch, D. Kohlgrüber, C. Leon Munoz, *et al.*, "Analytical fuselage structure mass estimation using the pandora framework," in *German Aerospace Congress (DLRK)*, Dresden, Germany, 2022. [Online]. Available: https://elib.dlr.de/192843/.

[82] B. Boden, J. Flink, N. Först, *et al.*, "RCE: An Integration Environment for Engineering and Science," *SoftwareX*, vol. 15, no. 100759, Jul. 2021. DOI: 10.1016/j.softx.2021.100759. [Online]. Available: https://www.sciencedirect.com/science/article/pii/S2352711021000820.

[83] M. Alder, E. Moerland, J. Jepsen, and B. Nagel, "Recent Advances in Establishing a Common Language for Aircraft Design with CPACS," in *Aerospace Europe Conference*, Bordeaux, France, 2020. [Online]. Available: https://elib.dlr.de/134341/.

[84] DLR Smart Libraries. "CPACS Website." (2024), [Online]. Available: https://dlr-sl.github.io/cpacs-website/ (visited on 01/27/2024).

[85] RCE Development Team. "RCE Website." (2024), [Online]. Available: https://rcenvironment.de/ (visited on 01/27/2024).

[86] B. M. H. J. Fröhler, J. Häßy, and M. Abu-Zurayk, "Development of a medium/long-haul reference aircraft," *CEAS Aeronautical Journal*, vol. 13, pp. 693–713, Apr. 2023. DOI: 10.1007/s13272-023-00662-1. [Online]. Available: https://elib.dlr.de/195270/1/s13272-023-00662-1.pdf.

[87] EgyptAir. "A320 family maintenance training." (2024), [Online]. Available: https://training.egyptair.com/Maintenance/A320Family (visited on 07/02/2024).

[88] C. Bonnet and X. Barriola. "Airbus Safety: Understanding Weight and Balance." (2015), [Online]. Available: https://safetyfirst.airbus.com/understanding-weight-and-balance/1000/ (visited on 10/14/2024).

[89] "Final Report of the EXACT Project," DLR-SL, Hamburg, Germany, Tech. Rep., 2023, Not publicly available.

[90] D. P. Raymer, *Aircraft Design: A conceptual Approach*, 2^{nd} ed. Reston, Virginia, USA: American Institute of Aeronautics and Astronautics, 1992.

[91] M. Elangovan. "Typical fuselage structure." (Mar. 2024), [Online]. Available: https://www.linkedin.com/pulse/typical-fuselage-structure-elangovan-m-u6ojc (visited on 06/03/2024).

[92] Norebbo. "Boeing 737 max 8 blank illustration templates." (2024), [Online]. Available: https://www.norebbo.com/boeing-737-max-8-blank-illustration-templates/ (visited on 07/27/2024).

[93] SeatGuru. "Short-haul economy class comparison chart." (2024), [Online]. Available: https://www.seatguru.com/charts/shorthaul_economy.php (visited on 07/27/2024).

[94] C. Loh. "What is an aircraft tail stand and why is it needed?" (2023), [Online]. Available: https://simpleflying.com/aircraft-tail-stand/ (visited on 06/05/2024).

[95] "Which aircraft models need a tripod jack for tail support at airport?" (2016), [Online]. Available: https://aviation.stackexchange.com/questions/24569/which-aircraft-models-need-a-tripod-jack-for-tail-support-at-airport (visited on 07/29/2024).

[96] J. J. Rising, "Development of a Reduced Area Horizontal Tail for a Wide Body Jet Aircraft," NASA, Burbank, California, USA, Tech. Rep. Contractor Report 172278, 1984. [Online]. Available: https://ntrs.nasa.gov/citations/19870019131.

[97] J. Joseph L. Johnson, "A Study of the use of various High-Lift Devices on the Horizontal tail of a Canard Airplane model as Means of increasing the allowable center-of-gravity travel," NACA, Langley Field, Virginia, USA, Tech. Rep. NACA RN L52KL8a, 1954. [Online]. Available: https://ntrs.nasa.gov/api/citations/19930090589/downloads/19930090589.pdf.

[98] A. K. Kundu, M. A. Price, and D. Riordan, *Aircraft Design*, 1^{st} ed. New York, NY, USA: Cambridge University Press, 2010.

[99] M. Burnazzi and R. Radespiel, "Design and analysis of a droop nose for coanda flap applications," *AIAA Journal of Aircraft*, vol. 51, pp. 1567–1579, Sep. 2014. DOI: 10.2514/1.C032434. [Online]. Available: https://www.researchgate.net/publication/269568285_Design_and_Analysis_of_a_Droop_Nose_for_Coanda_Flap_Applications.

[100] EUROCONTROL. "Boeing 757-300 Performance Data." (2024), [Online]. Available: https://contentzone.eurocontrol.int/aircraftperformance/details.aspx?ICAO=B753 (visited on 10/14/2024).

[101] "TiXI (DLR - Institute for software technology)." (2024), [Online]. Available: https://www.dlr.de/sc/en/desktopdefault.aspx/tabid-12766/22301_read-50944/ (visited on 01/27/2024).

[102] LTH Executive Secretary, *LTH Aeronautical Engineering Handbook*, 7th. 2004–2020. [Online]. Available: https://www.lth-online.de/en/about-lth-aeronautical-engineering-handbook-information/lth-edition.html (visited on 07/21/2024).

[103] R. M. Granzoto, L. A. Algodoal, G. J. Zambrano, and G. G. Becker, "Horizontal tail local angle-of-attack and total pressure measurements through static pressure ports and kiel pitot," *The Aeronautical Journal*, vol. 123, no. 1268, pp. 1476–1491, Oct. 2019. DOI: 10.1017/aer.2019.68. [Online]. Available: https://www.cambridge.org/core/journals/aeronautical-journal/article/horizontal-tail-local-angleofattack-and-total-pressure-measurements-through-static-pressure-ports-and-kiel-pitot/DAD7DA03F4C63C872F7C945DA8A3CE2C.

[104] G. Brüning, X. Hafer, and G. Sachs, *Flugleistungen: Grundlagen, Flugzustaende, Flugabschnitte*, 1st ed. Heidelberg , Germany: Springer, 1993.

[105] F. Nicolosi, P. Della Vecchia, D. Ciliberti, and V. Cusati, "Fuselage aerodynamic prediction methods," *Aerospace Science and Technology*, vol. 55, pp. 332–342, Jun. 2016. DOI: 10.2514/6.2015-2257. [Online]. Available: http://wpage.unina.it/pierluigi.dellavecchia/pdf/publications/journals/AESCTE_11.pdf.

[106] D. Scholz, *Aircraft design: Wing design*, PDF, Aircraft Design. Lecture Notes by Prof. Dr. D. Scholz. Hamburg University of Applied Sciences. Available from: http://LectureNotes.AircraftDesign.org, 2015.

[107] Airbus, *Airport Planning Manual: Airbus A330*, Online, Nov. 2021. [Online]. Available: https://www.airbus.com/sites/g/files/jlcbta136/files/2021-11/Airbus-Commercial-Aircraft-AC-A330.pdf (visited on 01/15/2024).

A

Internship report: HTP sizing tool documentation and validation

This appendix includes an adapted and updated version of the internship report. A horizontal tailplane sizing analysis tool was developed during this period. The main goal was to improve the existing methodology for horizontal tailplane sizing used at the DLR-SL institute for their different conceptual aircraft design studies. The improvements made with respect to the previous methodology are summarized in four main points:

- Include more tail sizing requirements. The previous methodology only sized the horizontal tailplane for rotation at take-off and controllability of the aircraft at low speeds, based on the expressions from [5]. In this case, the stability requirement is also modeled. This requirement is sizing for the most aft center of gravity position [23], thus especially critical for LH2 aircraft with rear fuselage cryogenic tanks.

- Horizontal tailplane sizing is a complex process. Having a good estimate of the reference area requires good aerodynamic and engine models, as well as a good estimation of the aircraft mass distribution and center of gravity positions. This is complex, especially at a conceptual design stage. An effort was made during the development to include preliminary calculations and correction factors that account for aerodynamic effects, compressibility/Mach effects, sweep effects, or thrust effects.

- The flight condition also plays a major role. The different altitudes and Mach numbers affect the aerodynamics and engine thrust. Besides this, the aircraft´s angle of attack and the different settings for the high-lift devices affect the the flow-field at the tail and its effectiveness. The tool aims to analyze the sizing requirements among different flight points, corresponding to different flight conditions among the aircraft flight envelope. This is similar to the approach done in [10], where the different requirements were computed for several power and flap settings of the aircraft.

The appendix is divided in two main sections. Firstly the methods implemented for the analysis are described. The tool is structured in different modules that contain the functions for the calculation of the different parts of the analysis. These are:

- Input data functions module
- Center of gravity positions and range definition module
- Mass moment of inertia calculation module
- Flight envelope definition module
- Requirements calculation module
- Parameter calculation module

The second section showcases the validation procedure of the tool using different aircraft reference models.

A.1. Methodology

The tool is divided in different modules. The methods used to develop each of them and the calculations included inside are described in the following sections.

A.1.1. Input data functions module

The tool is able to read from XML-Files in the CPACS format [83] by using the TIXI library [101]. TIXI is a library to work with XML files. On the other hand, CPACS is an XML-based central data schema for the exchange of data in multi-disciplinary and multi-fidelity design environments. It can hold data from a variety of disciplines considered in an aircraft design process [83]. All DLR tools output their files in this format. Creating a tool that is able to read this kind of files facilitates the integration with the rest of the DLR-SL tools. All CPACS data is stored in a big Python Dictionary. Each dictionary entry is a data type used for the calculation of the tail sizing requirements.

The different entries in the dictionary can be classified into seven groups:

- **Configuration settings:** the tool includes a config.py file from which the user can define different values for the analysis. These include different methods for the calculation of the aerodynamic parameters, or the number of points analyzed inside the flight envelope.
- **Digitized plots:** these are plots found in the literature for the calculations of some parameters. They are digitized in an Excel file and loaded inside the tool as data frames.
- **Geometric parameters:** aircraft geometric values such as wing shape or the position of the different aircraft components. These are taken from the CPACS input file of the tool.
- **Mass values:** values for MTOM, OEM, fuel, or payload mass, which are also taken from the CPACS input file of the tool.
- **Aero and engine maps:** the aero and engine maps are CPACS data structures that contain the aerodynamic and engine information for different flight conditions and aircraft flap settings. The tool aims to use as much information as possible from these sources. Since the flight points studied might not be always included in the map, interpolation inside them is implemented in the tool.
  - Engine maps: there is an engine map for every aircraft flap setting. This also includes an engine map for hot and high take-off conditions or OEI conditions. The data is structured in the following way:
    - There are a series of flight altitudes. The range depends on the aircraft configuration.
    - For every altitude there is a range of Mach numbers, which depends also on the aircraft configuration.
    - For a given combination of Mach number and altitude, i.e. a flight point, a series of turbine entry temperatures (TET) are defined. These are the engine thrust settings and are ordered from low to high values of the temperature.

* For each of these temperatures, the corresponding value of thrust, mass flow, and NOx emissions is found. As logical, the higher the TET setting the bigger the thrust produced by the engine for a given flight point.

Normally, the value that has to be interpolated is the engine thrust for a given flight condition and an engine temperature setting. The *scipy.interpolate.griddata* function is used to perform this 4D interpolation. The interpolation method is linear, which is assumed to be sufficient with this data as showcased in the example plot in Figure A.1. Besides this, no other interpolation methods are available for 4D data structures.

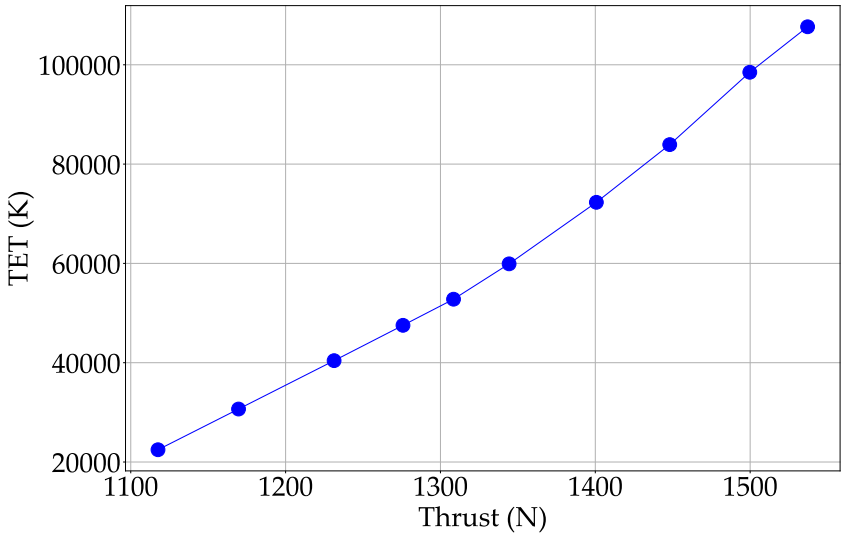

Figure A.1: Variation of thrust with turbine entry temperature (TET) for a given flight condition

– Aero maps: there is an aero map for every aircraft configuration. This also includes different flap deflections for take-off, landing, OEI... The data is structured in the following way:

* There are a series of flight altitudes that depend on the aircraft configuration.
* For every altitude there is a range of Mach numbers, which also depend on the aircraft configuration.
* For a given combination of Mach number and altitude, i.e. a flight point, a range of angles of attack is defined. The side-slip angle is set to zero by default.
* For each of these aircraft attitudes the corresponding value of the lift coefficient, drag coefficient, and zero-lift pitching moment coefficient are defined. These values correspond to the wing and fuselage combination.

The *scipy.interpolate.griddata* function is also used in this case to perform the 4D interpolation. The angle of attack/ lift coefficient is interpolated for a given combination of altitude and Mach number, and a value of lift coefficient/ angle of attack. The linear method for interpolation is used, assuming to be always inside the linear range of angles of attack. To interpolate the zero-lift pitching moment coefficient, only the flight point is needed. Its value is constant with the change of aircraft attitude.

- **Performance limits:** the maximum operating altitude, velocity, or Mach, are taken from the limits of the aero and engine maps. These are used to define the aircraft flight envelopes.
- **Maximum lift coefficient:** the aero maps taken from OpenAD (used to develop the tool), do not show a dependency of the maximum lift coefficient on the flight condition. They do not model the increase due to a Reynolds Number effect, or the decrease in its value at transonic regimes (due to compressibility effects and shock wave boundary layer interaction). The value stays constant for every flight point. Thus, only four values are defined for this coefficient. One value is defined for clean configuration, one for landing configuration, one for take-off at sea level, and another one for take-off at airport conditions.

A.1.2. Center of gravity positions and range definition

This module includes all the functions that calculate the center of gravity positions for different aircraft mass configurations. The different values for the masses (MTOM, OEM, fuel mass, payload mass . . .) are taken from the CPACS inputs, as well as the CG positions for MTOM, OEM, cargo, passengers and fuel masses. The following calculation methods are implemented for the estimation of the different CG positions along the x and z axis:

- Payload: two values for the CG position are calculated, taking always the maximum payload mass value. In one of them the payload CG is calculated assuming the maximum cargo capacity and the rest of the payload being passengers. The other assumes full passenger capacity.
- OEM + Payload: position of the aircraft center of gravity with empty mass and maximum payload. It is calculated for the two previously mentioned payload configurations. For a conventional kerosene aircraft this mass configuration has been observed to be the most aft center of gravity.
- OEM + Fuel: position of the CG of the aircraft empty mass with full fuel tanks. For a conventional kerosene aircraft this mass configuration has been observed to be usually the most forward position of the center of gravity.

The center of gravity position for a given configuration is calculated using a weighted average. The CG position of each mass component (CG Fuel, CG payload . . .) is multiplied by the mass (fuel mas, payload mass...). The products are then summed and the total is divided by the total mass. An example is shown for MTOM in equation (A.1).

$$x_{cg,MTOM} = \frac{x_{cg,OEM} OEM + x_{cg,fuel} m_{fuel} + x_{cg,payload} m_{payload}}{OEM + m_{fuel} + m_{payload}} \tag{A.1}$$

Among the CG positions for different weight configurations, a minimum and maximum are found. These two define the longitudinal travel for the in-flight center of gravity positions and are limited by the controllability and stability requirement respectively. As will be further discussed, the most forward center of gravity is also limited by another requirement, the take-off rotation requirement.

A.1.3. Mass moment of inertia calculation module

The value for the aircraft mass moment of inertia is required for the calculation of the take-off rotation requirement. A good estimate of the aircraft´s moment of inertia around the landing gear, and center of gravity position is needed. The previous method in OpenAD consists on an empirical method based on statistical aircraft data. It expresses the inertia as a function of the aircraft mass, fuel mass, and a series of coefficients. As a result, this method is useless to compute the moment of inertia of LH2 aircraft, where the fuel mass is positioned far away from the wing and thus its effect is not modeled in the formula.

To solve this problem, a small separate tool was developed. The code is able to read an aircraft´s geometry. Then, it models all aircraft components as simple volumes, i.e. the fuselage as a cylinder, or the wing as a series of boxes. The mass moment of inertia is calculated individually for each component. Lastly, all component moments of inertia are translated to the point of interest via Steiner's parallel axis theorem. Although it is a rather simple approach, it allows to model the different positioning of the fuel mass in an LH2 aircraft.

To obtain feasible results, the tool was calibrated and validated using data from different existing aircraft. The moment of inertia values were taken from the mass analysis section of LTH Handbook [102]. A factor was applied to each axis to correct for the inaccuracies of the method and the simplicity of the representation of the aircraft components. This method, although not perfect, allows to capture the main differences in the mass distribution of an LH2 aircraft compared to a kerosene one. The tank inertia is included together with the different positioning of the fuel mass.

A.1.4. Flight envelope definition module

This module contains 3 functions. Each of them is used to define each of the flight envelopes for the given aircraft configuration (clean configuration, take-off, and landing). The flight envelope resolution

is set by the user in the config.py file. It represents the number of points in which each of the bounds of the flight envelope is discretized. The following procedure was implemented in the tool to define each of the flight envelopes:

A.1.4.1. Clean configuration flight envelope

The points for the clean configuration flight envelope are defined in the following way:

- For the stall limit, the stall speed is calculated from the values of MTOM and maximum lift coefficient (A.2). Then, based on the altitude, the Mach number is calculated (A.3).

$$V_S = \sqrt{\frac{2gMTOM}{\rho C_{L,max} S}} \tag{A.2}$$

$$Mach = \frac{V_S}{a} \tag{A.3}$$

- For the altitude limit, the value is set to the maximum in the aero/engine map.
- For the maximum speed, the limit taken from CPACS is given as IAS. The value is firstly converted to TAS. For every altitude, it is compared to see if this Mach number is bigger or smaller than the maximum operating Mach number taken also from CPACS. This defines the kink in the right bound of the clean configuration envelope.

A.1.4.2. Take-off flap setting flight envelope/ landing flap setting flight envelope

- Aero maps show no variation in take-off maximum lift coefficient with altitude. For the stall limit, the same process is used as for the clean configuration.
- The maximum altitude is selected based on the maximum found in the aero/engine maps for take-off/landing (OpenAD sets it to 6000 m).
- The maximum Mach boundary is set based to the maximum value found in the aero/engine maps for take-off/landing (OpenAD sets the maximum speed for operating flaps at Mach 0.4).

A.1.5. Requirements module

The tool calculates three different tail sizing requirements. These are evaluated at multiple flight points along each of the three flight envelopes.

A.1.5.1. Stability Requirement

This requirement is not implemented in OpenAD. The aircraft should be longitudinally statically stable for all its center of gravity positions. This is ensured by the derivative of the pitching moment coefficient with respect to the angle of attack being negative [5]. For an aircraft with irreversible flight controls, the stick-fixed neutral point defines the position of the CG for which this derivative equals zero for a given constant elevator angle. Thus, for this condition to be fulfilled, the most aft CG position should be in front of this so-called neutral point. The neutral point position can be expressed as a function of the aerodynamic center position of the aircraft less tail (A.4) [24].

$$\overline{x}_{np} = \overline{x}_{ac_{wf}} + \frac{C_{L\alpha_h}}{C_{L\alpha_{wf}}} \cdot \left(1 - \frac{d\varepsilon}{d\alpha}\right) \cdot \frac{S_h l_h}{S\overline{c}} \cdot \left(\frac{V_h}{V}\right)^2 \tag{A.4}$$

The static margin (SM) is a measure of the degree of the static stability of an aircraft. It is defined as the distance of the center of gravity ahead of the neutral point, expressed as a percentage of the mean aerodynamic chord [5]. Expression (A.5) is obtained substituting the definition of the static margin in the previous equation [24].

$$\overline{x}_{cg} = \overline{x}_{ac_{wf}} + \frac{C_{L\alpha_h}}{C_{L\alpha_{wf}}} \cdot \left(1 - \frac{d\varepsilon}{d\alpha}\right) \cdot \frac{S_h l_h}{S\overline{c}} \cdot \left(\frac{V_h}{V}\right)^2 - SM \tag{A.5}$$

Rearranging expression (A.5) as a straight line to be plotted on the scissors plot, the final equation for the stability requirement results in (A.6).

$$\frac{S_h}{S} = \frac{C_{L\alpha_{wf}}}{C_{L\alpha_h} \cdot \left(1 - \frac{d\varepsilon}{d\alpha}\right) \cdot \frac{l_h}{\bar{c}} \cdot \left(\frac{V_h}{V}\right)^2} \cdot \overline{x}_{cg} + \frac{C_{L\alpha_{wf}}(-\overline{x}_{ac_{wf}} + SM)}{C_{L\alpha_h} \cdot \left(1 - \frac{d\varepsilon}{d\alpha}\right) \cdot \frac{l_h}{\bar{c}} \cdot \left(\frac{V_h}{V}\right)^2} \tag{A.6}$$

It is usually the case that this requirement is especially important for aircraft flying at high altitudes and speeds. The lift curve slope increases due to compressibility effects (see Prandtl-Glauert compressibility correction factor). This effect is combined with an expected forward shift of the neutral point with increasing speed (that can be interpreted as the aerodynamic center moving forward) [24]. As a result, high-speed conditions are usually the most critical for tail sizing from an stability point of view.

A.1.5.2. Low Speed Controllability Requirement

This is exactly the same requirement implemented in OpenAD for low speed controllability. The aircraft should be controllable at every flight point in its envelope. Given a certain aircraft configuration, a combination of wing + fuselage lift and tail lift must be obtained in a way that the resulting total aircraft moment coefficient obtained around the centre of gravity is zero. In this condition, the aircraft is said to be trimmed [24]. Taking moments around the CG of the aircraft, and rearranging the equation as a straight line, expression (A.7) is found. Note that (A.7) accounts also for the engine effect (defined in [23]), as the main difference w.r.t. to the equation from [5] implemented in OpenAD, or the expression from [24].

$$\frac{S_h}{S} = \frac{1}{\frac{C_{L_h}}{C_{L_{wf}}} \cdot \frac{l_h}{\bar{c}} \cdot \left(\frac{V_h}{V}\right)^2} \cdot \overline{x}_{cg} + \frac{\frac{C_{m,ac_{wf}}}{C_{L_{wf}}} + \frac{C_{m_E}}{C_{L_{wf}}} - \overline{x}_{ac_{wf}}}{\frac{C_{L_h}}{C_{L_{wf}}} \cdot \frac{l_h}{\bar{c}} \cdot \left(\frac{V_h}{V}\right)^2} \tag{A.7}$$

The most critical conditions for trimming are normally achieved with the aircraft flying at its maximum lift coefficient, and the CG in its most forward position, having some reserve available for maneuvering [5]. Thus, the landing configuration is the one that is usually sizing for this requirement, limiting the most forward CG position.

A.1.5.3. Take-Off Rotation Requirement

This requirement is also implemented inside OpenAD; however, the expression used is different. The expression used for the tool was taken from chapter 12 in [25] (see (A.8)). In this case, the moments are taken with respect to the main landing gear position. The forces acting on the aircraft during rolling are depicted in Figure A.2.

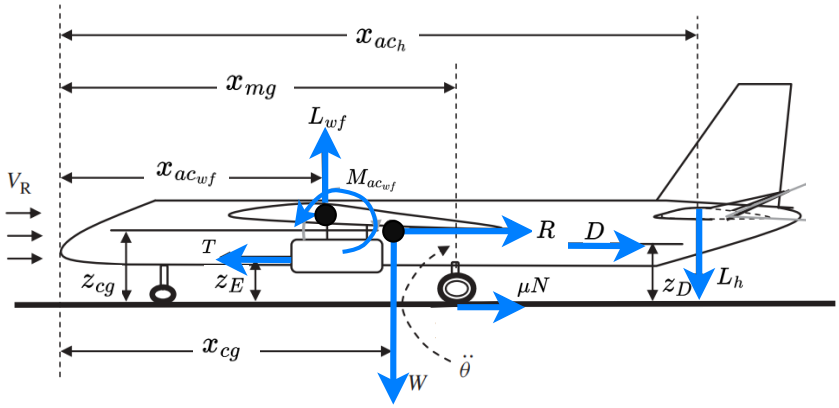

Figure A.2: Forces and moments during take-off rotation [25]

The resulting moment around the main landing gear position has to overcome the inertia of the aircraft, that needs to be able to reach a certain angular acceleration to rotate ($\ddot{\theta}$). Expression (A.8) depicts the balance of moments and forces with their corresponding signs

$$\begin{aligned} I_{yy,mg}\ddot{\theta} = &-W(x_{mg} - x_{cg}) - T(z_E) + D(z_D) \\ &+ L_{wf}(x_{mg} - x_{ac_{wf}}) + L_h(x_{ac_h} - x_{mg}) + M_{ac_{wf}} + R(z_{cg}) \end{aligned} \tag{A.8}$$

where the calculation for the wing and fuselage lift, tail lift, drag, and reaction force, follow from equations (A.9), (A.10), (A.11) and (A.12) respectively.

$$L_{wf} \cong \frac{1}{2}\rho V_R^2 S C_{L,r} \tag{A.9}$$

$$L_h = \frac{1}{2}\rho V_R^2 S C_{L,max_h} \frac{V_h^2}{V_R^2}\frac{S_h}{S} \tag{A.10}$$

$$D \cong \frac{1}{2}\rho V_R^2 S C_D \tag{A.11}$$

$$R \cong T - D - \mu N = T - D - \mu(W - L_{wf}) \tag{A.12}$$

The distances are defined in a way that the resulting arm is always positive. The direction of the moment in each case is given by the sign in front (being nose up positive). As a result, the inertia, weight, and thrust moments, are negative, going against the aircraft rotation.

In the stability requirement, the line drawn depicts the most aft CG position for a given tail size for the aircraft to be stable. In the low-speed control requirement, the line drawn depicts the most forward CG position for a given tail size for the aircraft to be controllable. However, in this case, neither forward nor aft aircraft total CG position limits are calculated. In the expression for take-off rotation, a certain mass and the corresponding center of gravity position are included. Then, when plotting the line, the method calculates the most forward CG position for this given mass for the aircraft to be able to rotate during take-off. Among all existing mass combinations, the following are considered:

- Maximum take-off mass (MTOM)
- Maximum operating empty mass (OEM)
- Maximum operating empty mass + payload and maximum operating empty mass + fuel. The payload includes maximum cargo and maximum pax. configurations (OEM + Fuel, OEM + Payload (max. pax.) and OEM + Payload (max. cargo).

For the above 5 weight configurations, the rotation requirement is computed, obtaining 5 straight lines that limit the most forward CG position for every weight configuration. This is shown in Figure A.3.

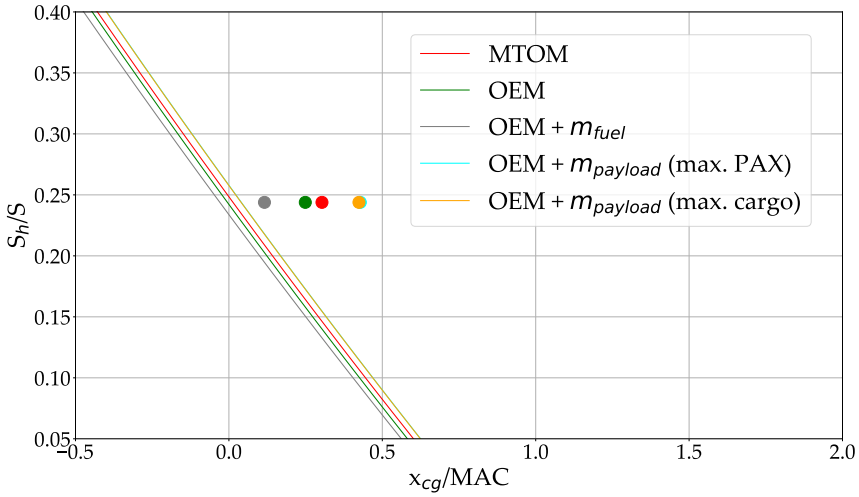

Figure A.3: Example of take-off rotation requirement limit for different aircraft weight configurations

Among all weight configurations, there will be one that is more critical, thus sizing for the HTP. Zooming into Figure A.3, results in the grey dot being the closest to the grey line among all weight combinations. This has been observed to be almost always the case, where the most critical weight for rotation is the one corresponding to the most forward center of gravity. Thus, it can be concluded that the take-off rotation requirement also limits the most forward position of the center of gravity of the aircraft. This calculation procedure will be repeated for two take-off conditions, at sea level (shown in Figure A.3) and at airport conditions.

A.1.6. Parameter calculation module

This section summarizes all the methods used to calculate the aerodynamic and geometric parameters needed to compute each of the tail sizing requirements. The tool aimed to find all available methods for tail sizing, encapsulating the existing knowledge inside a code. All methods were taken from the literature, so no new methods or models were defined. This section then does not explicitly include all equations implemented inside the tool. Some of them are lengthy and rely on numerous experimental plots.

Besides this, due to the uncertainties during the aircraft conceptual design phase, some values have been hard-codded in the tool. In this section, the values chosen are discussed and justified based on the literature.

To sum up, this section focuses more on showcasing the assumptions taken and the limitations that each of them implies. Nonetheless, all references to the equations and graphs used, including book, chapter, and page, are stated in the text, so the reader can still reproduce the work. Each parameter is calculated using an individual *calc* function. Every parameter calculation function can have one or multiple methods inside. The desired method can be selected by the user from the config.py file.

A.1.6.1. Aerodynamic parameters

- **Aircraft angle of attack (α):** its value is taken form the aero maps. A 4D interpolation is used, implementing the *scipy.interpolate.griddata* function. The angle will be interpolated inside the aero map data, providing a flight condition (that dictates the slope of the lift curve), and a lift coefficient.
- **Lift curve slope of a lifting surface ($C_{L\alpha_h}$ or $C_{L\alpha_w}$):** the calculation of the coefficient for the wing or horizontal tail uses a method taken from [17]. It can be found in section 4.1.3.2-49. The expression (A.13) relates the wing curve slope to its geometric parameters and corrects it for the compressibility effect with the Prandtl-Glauert β factor.

$$C_{L\alpha} = \frac{2\pi AR}{2 + \sqrt{\frac{AR^2\beta^2}{k^2}\left(1 + \frac{tan^2\Lambda_{c/2}}{\beta^2}\right) + 4}} \tag{A.13}$$

  The airfoil efficiency factor (k) is assumed to be equal to 0.95 [24]. For the calculation of β in the case of the tail, the local Mach number is corrected with the value of the dynamic pressure ratio at the horizontal stabilizer. A correction is also added in the case of the wing to account for the change in lift curve slope due to flap deflection. This method can be found in [5], Appendix G, equations G-3, G-4, G-23, and G-27. Two plots were digitized for the calculation procedure, shown in Fig. G-5 and Fig. G-13 from [5].

- **Dynamic pressure ratio at the tail (DPR or $(V_h/V)^2$):** this parameter is complex to estimate in the conceptual aircraft design phase. That is why most aircraft design books suggest fixed values or a range of values, normally between 0.8 and 0.9 [5] [23] [90]. However, these values do not account for the different flap settings and different flow conditions that are given at the tail.

  There are also methods in the literature to estimate this ratio. One example is section 4.4.1 in [17] from pages p.4.4.1-10 to p.4.4.1-22. It has to be considered that this method was initially

designed for fighter aircraft, so the outcome has to be treated carefully. To validate the results of this methodology, some values were found for a flight test experiment carried out on an Embraer E-190 aircraft [103]. The paper showcased the huge influence of the flap defection on the DPR value. For clean configuration, the values were no lower than 0.85 (Figure A.4). For the landing flap setting, much lower values were achieved of around 0.7 (see Figure A.6). Take-off values resulted somewhere in the middle (see Figure A.5).

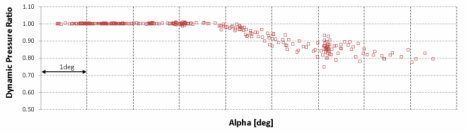

Figure A.4: DPR measurements for E-190 aircraft at cruise flap settings [103]

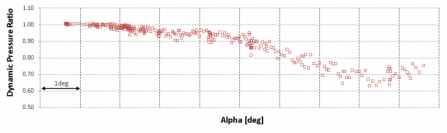

Figure A.5: DPR measurements for E-190 aircraft at take-off flap settings [103]

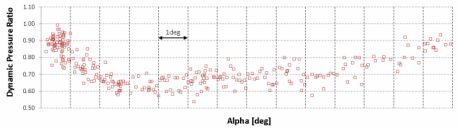

Figure A.6: DPR measurements for E-190 aircraft at landing flap settings [103]

Comparing the method from [17] with the results from the flight tests, yields the following conclusions:

- When applied to an A320-type aircraft, similar in size to the E-190, the values matched quite well the results from the paper. Values around 0.75 were obtained for landing flap settings, and around 0.9 for the aircraft in clean configuration, being the take-off values somewhere in the middle.
- When the method is applied to wide-fuselage aircraft (A330 or A350 type), the method always resulted in a DPR = 1, independently of the flap setting. An increase in tail effectiveness is expected, due to a lower wake influence. The wake thickness will decrease, as it depends on the C_{D0} value (lower due to a higher Reynolds Number). Besides this, a bigger lever arm is given. However, it is still expected some interaction between the wing wake and the tail.

In the end, it was decided to set a hardcoded value for the DPR, that was different for every flap setting. Also, a distinction will made based on the aircraft size. The parameter will serve at the same time as a calibration factor for the tool while being consistent with the values suggested in the literature, and the results from the DATCOM method [17] and from [103]. Values of 0.875, 0.825, and 0.75 were selected respectively for clean, take-off, and landing configuration in the case of a narrow fuselage aircraft. For a long-range aircraft, with a wide fuselage, the values taken were slightly increased, to 0.925, 0.875, and 0.85 respectively. Note that the angles of attack analyzed for the stability and control requirements are always close to the stall angle.

For the take-off rotation manoeuvre, the DPR is set to 1. At the start of the manoeuvre, the aircraft is still on the ground, with a zero angle of attack, and most of the weight is still supported by the landing gear. The wing lift force and down-wash are small, thus no wake is influencing the tail. This scenario can be observed also in the flight tests from [103].

For a T-Tail aircraft, the value is set to 1 [5] [24]. Literature considers that a T-tail is positioned high enough, so it is far away from any interaction with the wing wake. The method from DATCOM [17] also resulted in the tail being outside the influence of the wake.

- **Lift curve slope of the aircraft minus tail configuration ($C_{L\alpha_{wf}}$):** the wing curve slope calculated with the previous method is corrected with a geometric factor, to model the effect of the fuselage.

The method is found in Appendix E from [5] , shown in (A.14).

$$C_{L\alpha_{wf}} = C_{L\alpha_w}\left(\left(1 + 2.15\frac{b_f}{b}\right)\frac{S_{net}}{S} + \frac{\pi}{2C_{L\alpha_w}}\frac{b_f^2}{S}\right) \tag{A.14}$$

- **Lift coefficient increase due to flap deflection ($\Delta C_{L,flap}$):** the method described in section 6.1.1.3 from [17] has been implemented. Note that this method calculates the 2D increase in lift. When applied to a lifting surface a correction must be implemented for the result. The method includes 4 digitized plots. The steps followed are:

  1. Define the flap type. The tool supports the flap types available in OpenAD: plain, single slotted and fowler flaps.
  2. Obtain the base lift coefficient for a 25 % chord flap length and a given reference flap angle. See plot 6.1.1.3-12a [17] . The value of the airfoil thickness is taken as the average thickness of the wing.
  3. Obtain the correction factor for the flap chord length. See plot 6.1.1.3-12b in [17].
  4. Obtain the correction factor for the flap deflection angle. See plot 6.1.1.3-13a in [17].
  5. Obtain the correction factor for the flap system motion. See plot 6.1.1.3-13b [17].

  The resulting value is corrected for the 3D effects (10% reduction in lift) and the sweep angle of the flap/control surface (multiplying by the cosine of the sweep angle).

- **Horizontal tail lift coefficient (C_{L_h}):** the method implemented is based on expression (A.15) taken from [5]. The different flap settings, down-wash angles, and aircraft attitudes, have a big impact on the flow-field at the HTP, and thus its capability to generate lift. The influence of the different flight conditions is taken into account with this method.

$$C_{L_h} = C_{L\alpha_h} \cdot (\alpha - \varepsilon + i_h) + C_{L\delta_e}\delta_e \tag{A.15}$$

  The following values are calculated for each of the terms in expression (A.15):

  - $C_{L\alpha_h}$: lift curve slope of the HTP. The value is calculated using the previously defined function based on the flight conditions.
  - α: angle of attack of the aircraft, taken from the aero maps. In the case of take-off rotation, the angle of attack of the aircraft is equal to zero. At the moment of the start of the rotation, the aircraft is still with both nose and main landing gears touching the runway.
  - ε: the downwash angle. It is calculated using a method from Dubs (1987) shown in [23]. The result is corrected by an increase factor of 10% if flaps are deflected [23]. This method depends on the wing geometry and the lift coefficient for the given flight condition.
  - i_h: incidence angle of the HTP, considering an adjustable or trimmable stabilizer. A value of -10^o is suggested in [5] for the maximum incidence angle.
  - $C_{L\delta_e}\delta_e$: the increase in lift due to elevator deflection is calculated using the method showcased before for the change in lift due to flap deflection. The elevator is modeled as a plain flap, and the maximum upward deflection is considered. A default value is set at 30° for this parameter [25]. The calculated increase in lift due to flap defection is again corrected to account for the 3D effect and the sweep angle of the control surface.

  This method calculates the maximum lift coefficient achievable by the tail for a given flight condition. The flight condition will dictate the angles of attack and downwash, and the value of the lift curve slope. The elevator and incidence angles are set to their maximum, so the maximum tail download is produced for each case.

  The calculation method also considers the possible stall of the HTP. The angle of attack that the tail sees, is obtained by combining the angle of attack, downwash angle, and incidence of the tail. In some scenarios, this combination might lead to a really big negative angle at the tailplane, and

thus stall. To control this phenomenon, a limit has been set to -10^o for the maximum angle at the tail. If the combination of α, ε, and i_h surpasses -10^o, the latter value is adjusted reducing the incidence of the stabilizer to remain below the stall limit.

- **Calculation of the lift coefficient of the aircraft during rolling ($C_{L,r}$):** the expression is taken from [104], see (A.16). This is the lift coefficient of the wing at take-off at the moment of the start of the rotation. Thus, its value is used to calculate the wing downwash angle for the take-off rotation requirement.

$$C_{L,r} = \frac{\pi A R e \mu}{2} \tag{A.16}$$

The value for the runway friction coefficient, (μ), can be set by the user from the config.py file (default set to 0.03).

- **Pitching moment coefficient around the aerodynamic center or zero-lift pitching moment coefficient ($C_{m,ac}$):** to estimate the wing pitching moment coefficient, the value of the moment coefficient for the wing airfoil is corrected with a series of geometrical parameters, and a factor that accounts for the wing twist (A.17). This method is found in section 4.1.4.1- a in [17].

$$C_{m,ac_w} = \left[c_{m,ac} \cdot \frac{AR cos^2 \Lambda_{c/4}}{AR + 2cos\Lambda_{c/4}} \cdot \left(\frac{\Delta c_{m,ac}}{\varepsilon_t} \right) \varepsilon_t \right] \tag{A.17}$$

A value of -0.01 is assumed for the airfoil pitching moment coefficient around the a.c. in clean configuration [23]. There are also tabulated values in [17]. The correction factor due to wing twist ($\Delta c_m / \varepsilon_t$) is obtained from the plots in 4.1.4.1-5 [17]. On top of the clean airfoil pitching moment coefficient, a contribution is added due to deflected flaps. This increases the nose-down pitching moment of the airfoil. The change in pitching moment coefficient due to flap deflection is directly related to the change in the lift coefficient due to flap deflection by equation (A.18) [23].

$$\Delta c_{m,ac_{flap}} = \Delta c_{L,flap} \left(\frac{x_{ac}}{\overline{c}} - \frac{x_{CP}}{\overline{c}} \left(\frac{c'}{c} \right) \right) \tag{A.18}$$

This expression can be applied to fowler and slotted flaps, where the dimensionless position of the center of pressure ($x_{CP}/\overline{c}$) equals 0.44 [23]. A similar expression is also found for plain flaps in [23]. Once the contribution due to flap deflection is obtained, the final airfoil moment is obtained adding the clean configuration coefficient to the increment in moment due to flap deflection. However, the values cannot be added directly. The flaps do not extend for the full span of the wing, so not every wing section experiences the $\Delta c_{m,ac_{flap}}$. A weighted average is done using the $S_{flapped}$ value, which represents the fraction of the wing area that is affected by the trailing edge flaps (A.19). The expression to roughly approximate this area can be found in appendix G, equation G-26 from [5].

$$c_{m,ac} = c_{m,ac_{clean}} \frac{S - S_{flapped}}{S} + (c_{m,ac_{clean}} + \Delta c_{m,ac_{flap}}) \frac{S_{flapped}}{S} \tag{A.19}$$

The slat effect on the pitching moment is neglected. Slats improve stall behavior by extending the lift curve to higher angles of attack, but they do not generate additional lift. Thus, their contribution to a change in pitching moment is neglected.

Equation (A.17) only considers the wing contribution. The fuselage contribution has to be added on top, which makes the value even more negative. The method used is taken from [105], using for simplification the plot from Fig. 8 on p.338 in [105]. This plot shows the pitching moment coefficient of the cabin part of the fuselage, as a function of the fineness ratio, around different points along the fuselage length (35%, 50%, and 60%). It was observed that for a given fineness ratio, the fuselage pitching varies linearly with the position of the reference point. Thus, the value of the pitching moment coefficient is calculated first at the 35%, 50% and 60 % locations. Based on these results

and the position of the aerodynamic center along the fuselage, the final value is interpolated linearly.

Lastly, both wing and fuselage values are added and corrected by a compressibility factor to account for the change with Mach number, (A.20). The compressibility effect factor $((C_{m,ac})_{Mach}/(C_{m,ac})_{Mach=0})$ is obtained from plot 4.1.4.1-6 in [17].

$$C_{m,ac_{wf}} = \left[C_{m,ac_w} + C_{m,ac_f}\right] \cdot \frac{(C_{m,ac})_{Mach}}{(C_{m,ac})_{Mach=0}} \tag{A.20}$$

- **Wing downwash gradient, or change in downwash angle due to changes in the angle of attack ($d\varepsilon/d\alpha$):** there are two calculation methods implemented
  - The first method is found in section 4.4.1, p-4.4.1-6, from [17], and also described in [23] . The method approximates the downwash gradient for angles in the linear range of angles of attack. It only depends on geometric parameters, so no control surface deflection effect is modeled. A correction factor for the compressibility effect is included based on the lift curve slope.
  - The second method is stated in slide 42 from chapter 7 of [24]. It is also based on geometric parameters of the wing shape and its position with respect to the horizontal tail.

  Both expressions model the wing downwash gradient considering the lifting surface in clean configuration. Thus, they do not include the effect of flap or slats. This value is only used for the stability requirement, where usually high Mach number and altitude combinations are sizing. As a result, the sizing condition will always be a flight point from the clean configuration flight envelope, so this inaccuracy will not affect the outcome of the analysis.

- **Stall speed and the rotation speed for the aircraft with take-off flap setting (V_R and V_S):** the take-off Mach is calculated based on the maximum lift coefficient for take-off and the aircraft mass in each case (MTOM, OEM + fuel . . .). Based on the Mach value, and the altitude of the airport, the speed is calculated. The value of the rotation speed of the aircraft is directly obtained from the stall speed, multiplying its value at the given take-off condition times a factor (usually a factor from 1.05 - 1.1 is used, see p. 325 [5] and [25] respectively).

A.1.6.2. Geometric parameters

Some geometric parameters need to be estimated as they are not directly included in the CPACS values taken from the OpenAD.

- **Angular acceleration for rotation at take-off ($\ddot{\theta}$):** the aircraft has to achieve a certain angular acceleration when rotating around the main landing gear at take-off. The acceleration depends on the size of the aircraft and its design purpose. The tabulated values in table 12.9 from [25] have been taken as reference. A value of $6°/s^2$ has been taken for a 30 m fuselage aircraft and $4°/s^2$ for an aircraft longer than 50 m. Between these values, a simple linear expression has been implemented, that calculates the value based on the aircraft size.

- **Extended airfoil chord due to flap deflection (c'):** the calculation follows from the method used in [5], Appendix G, equation G-12. The ratio of the airfoil chord extension to the flap chord is obtained from the plot in figure G-7 in [5]. Knowing this ratio, and the flap chord to airfoil chord ratio, expression G-12 in [5] is evaluated.

- **Sweep angle calculation (Λ):** this expression allows to get the sweep at any position (x) of a lifting surface, given the value of the leading-edge sweep angle. Equation (A.21) is taken from [106].

$$tan\Lambda_x = tan\Lambda_{LE} - \frac{4}{AR}\left[\frac{x}{100} \cdot \frac{1-\lambda}{1+\lambda}\right] \tag{A.21}$$

- **Wing twist (ε_t):** a value is needed for the wing twist between the tip and the root stations. The method assumes a linear twist distribution. The twist value is negative if the incidence angle reduces towards the wing tip. The method can be found in [106] and is shown in equation (A.22).

$$\varepsilon_t = i_{w,tip} - i_{w,root} \tag{A.22}$$

- **Position of the wing-body aerodynamic center w.r.t to the mean aerodynamic chord ($\overline{x}_{ac}$)**: two different methods are implemented. Both methods are from [5] and can be chosen from the config.py file.
  - The position of the aerodynamic center is set to be at 25% of the mean aerodynamic chord.
  - A more complex calculation method is also available, which refers to Appendix E in [5], from pages p.476 to p.481. This method accounts for the different contributions of the wing and the fuselage on the position of the aerodynamic center. The expression also applies corrections that account for the effect of the wing geometry and Mach number [5].

A.1.6.3. Engine parameters

Some parameters that are related to the aircraft engines are used in the tail sizing requirements. The following methods and assumptions are taken.

- **Pitching moment due to engine thrust (C_{m_E}):** its calculation can be switched "on" and "off" from the config.py file. To calculate the value, expression (A.23) is used [23]

$$C_{m_E} = \frac{n_E(z_{cg} - z_E)T}{qS\overline{c}} \tag{A.23}$$

  The thrust value is interpolated inside the engine maps for a given aircraft configuration. The *scipy.interpolate.griddata* function is used, knowing the flight point (altitude and Mach number) and the thrust setting based on the turbine entry temperature (maximum or minimum setting depending on the engine position).
  For engines mounted under the wing, the resulting moment has a positive contribution (nose-up pitching moment). Thus, the bigger this moment, the smaller the tail size (assuming a negative tail load). To study the most critical condition, i.e. the biggest tail surface required, the lowest thrust setting is selected.
  On the other hand, when engines are mounted above the center of gravity, the thrust produces a nose-down pitching moment. It acts in the opposite direction of the tail moment. Trimming the aircraft in this case will have its more critical scenario when the engines are operating at their highest thrust setting.

- **Minimum available thrust at take-off rotation (T):** the process to get the thrust value uses the *scipy.interpolate.griddata* function, inputting the flight point (altitude and mach number) and the thrust setting based on the turbine entry temperature (maximum or minimum setting depending on the engine position).
  The expression (A.8) is used in this case to compute the take-off rotation requirement. As can be deduced, when the aircraft rotates around the main landing gear position, the engine always produces a pitch-down moment that opposes the aircraft´s motion. The bigger the thrust, the bigger the nose-down moment and thus the bigger the HTP. On the other hand, the engine thrust also contributes to the reaction force during the aircraft rotation (see expression (A.12)). This force generates a nose-up moment, helping during the rotation manoeuvre. In this case, the bigger the thrust the bigger the nose-up moment and thus the smaller the HTP.
  Both maximum and minimum thrust settings will be simulated to see which moment is dominating. This will set the critical sizing condition for the HTP for take-off rotation.
  For wing-mounted engines, the rotation moment due to the reaction force is bigger mainly due to the longer arm. Consequently, the critical rotation condition happens when the engine is at its lowest thrust setting, i.e. lowest turbine inlet temperature. The opposite effect is observed for fuselage mounted engines, which have a longer arm with respect to the landing gear position.

A.2. Validation results

The tool has been validated with existing aircraft data. For this purpose, DLR-SL reference aircraft models developed for previous projects were used. These files consist of accurate representations of existing aircraft that were used as reference for the design of other aircraft concepts. The information to recreate these models was mostly extracted from the different airport planning manuals available [48], [49], and [107]. The tail size was known beforehand for every case.

One of the goals of the validation is to justify the assumptions taken for some of the parameters in the code. These parameters were in part calibrated throughout the validation process. In the end, the goal is to obtain a solid set of assumptions that are justified by the results obtained with the tool when existing aircraft models are tested. For the validation of the tool, the following settings were applied:

- A value of 0.03 is chosen for the runway friction coefficient.
- The static margin (SM) value is set to 10% of the mean aerodynamic chord length for the analysis. This value is above the minimum 5% suggested in the literature [5] [24].
- Down-wash gradient is calculated using the method from [17].
- A rotation speed of 1.05 times the stall speed of the aircraft at the take-off flap setting is assumed for the analysis [5].
- The pitching moment produced by the engine is considered in the control at low speeds requirement.
- The method from [5] is used for calculating the position of the aerodynamic center of the aircraft. This accounts for the wing geometry and compressibility effects, as well as for the fuselage contribution.
- Calculation of the dynamic pressure ratio at the tail: the values have been calibrated with the flight test data from [103]. This approach seemed to be more conservative when comes to predicting the DPR at the tail for wide-fuselage aircraft. The method from DATCOM [17] gives really good results for small aircraft, like the A320 or A319. The values are really close to the flight test data in [103]. However, it seems to over-predict the DPR for bigger aircraft.

  Values of 0.875, 0.825, and 0.75 were chosen for narrow fuselage aircraft for cruise, take-off, and landing flap settings respectively. For wide fuselage aircraft, 0.925, 0.875, and 0.85 were selected. For take-off rotation, a DPR = 1 was chosen.
- A value of -0.01 is assumed for the aircraft airfoil pitching moment coefficient around the aerodynamic center. This is based on [23], and the tabulated values from [17]
- For the calculation of the maximum horizontal tail lift coefficient ($C_{L_{h,max}}$), a maximum incidence angle for the THS of -10 ° and a maximum elevator deflection of 30 ° (upwards) are assumed respectively.

The tool has been tested for two different aircraft family types:

- A330 family: this family has been chosen as the example for a wide fuselage long-range family.
- A320neo family: this family has been chosen as the example for a narrow fuselage short-medium-range family. It is also the reference aircraft used for the thesis study.

The final scissors plots for the various members of the two aircraft families are presented below. The most critical conditions for aircraft control, calculated using Equation (A.7), stability assessed with Equation (A.6), and take-off rotation determined by Equation (A.8), are included in the scissors plot. The control and stability lines establish the limits for the most forward and aft CG positions respectively. The take-off rotation limits the most forward CG for on-ground operations.

Please note that the plots presented are derived from using the tool as an analysis instrument. The expected outcome of the validation is that the tool accurately predicts the horizontal tailplane size for the different aircraft. The quality of the results will be assessed based on the distance between the boundaries of the scissors, which are calculated by the tool, and the actual fixed values for S_h/S and the CG range of the aircraft.

A.2.1. Airbus A330 family

The scissors plots are shown in Figure A.7 for the *-200* and in Figure A.8 for the *-300*. Both aircraft feature identical horizontal tail sizes. The geometric values, along with the ground center of gravity limits, were sourced from the airport planning manual for the family [107]. Note that the green line corresponding to the take-off rotation requirement at sea level (SL) in both figures coincides with the take-off rotation requirement at airport conditions (AP).

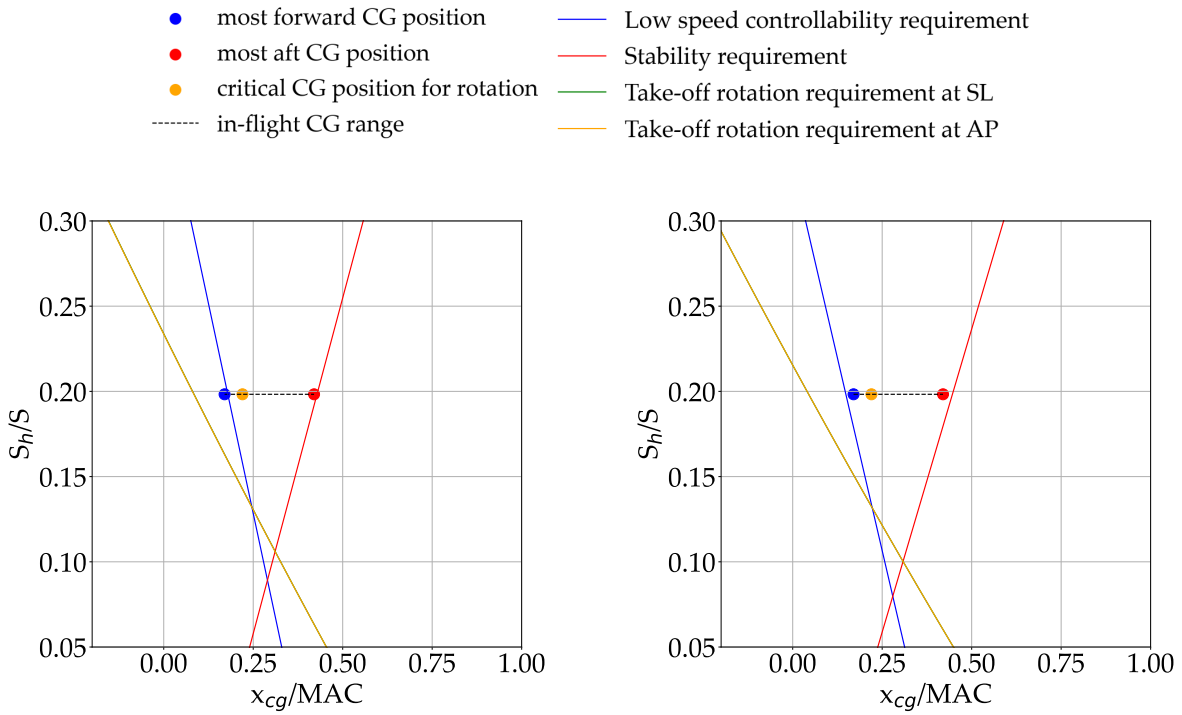

Figure A.7: Scissors plot for the A330-200

Figure A.8: Scissors plot for the A330-300

The actual horizontal tail size for the family is 72 m^2. As expected, the shorter member of the family is more critical for the HTP size. The tool provides a good prediction for the tail size, as the scissor boundaries closely align with the actual center of gravity range of the A330-200, as demonstrated in Figure A.7.

However, for the A330-300, the tail appears slightly oversized. This is expected, as both family members share the same tailplane due to commonality benefits. Based on Figure A.8, the tail area could be reduced by up to 65 m² (approximately 10 %).

A.2.2. Airbus A320neo family

For the A320neo family, only the A319neo and A320neo aircraft were tested. The scissors plots are shown in Figure A.9 for the A319neo, and in Figure A.10 for the A320neo. The take-off rotation requirement lines at both SL and AP coincide.

Again, both aircraft have the same HTP size. The shorter member of the family sizes the HTP, being the tail for the A320neo oversized. The same hypothesis as for the A330 is confirmed, with the aircraft with the shortest lever arm being sizing for the horizontal tail. The geometry values and the CG range have also been taken from the airport planning manuals of the A320 [48] and A319 [49].

The results from the tool analysis shown in Figure A.9 match perfectly the actual values for the CG range of the A319neo family member. The tail for the A320neo is oversized by around 7 %, observing the same trend as above. In this case, shifting the wing further aft could help to reduce the tail size.

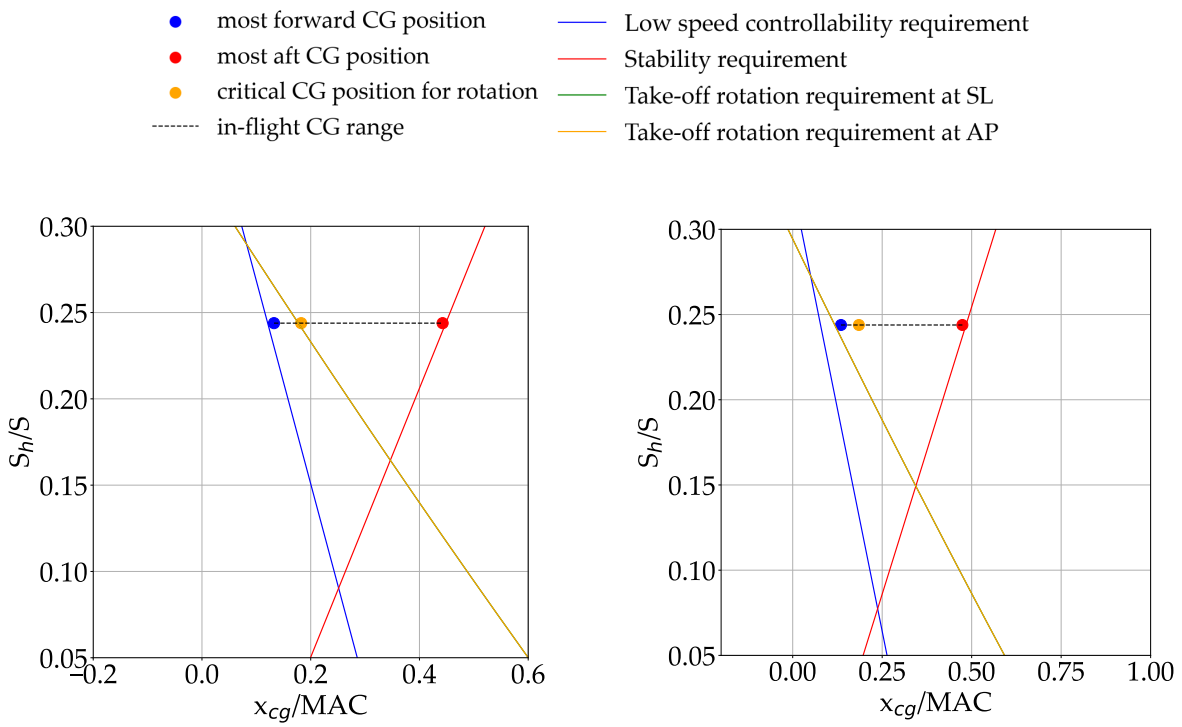

Figure A.9: Scissors plot for the A319neo

Figure A.10: Scissors plot for the A320neo

A.3. Conclusions

The results stated above show that the tool can perform accurately in multiple scenarios, regarding different aircraft geometries and sizes. The tool also predicts the expected oversized horizontal stabilizer in the case of the big family members, as discussed in the previous section. The computing time for a tailplane sizing analysis, in which the flight envelopes are discretized in 12 points, is around 15 seconds.

It can also be concluded that the set of assumptions taken, and justified during the methodology description, are a valid simplification of reality.

On the other hand, there is still room for improvement. Although the tool results have improved substantially OpenAD current status, the tool still relies on some roughly approximations of reality. These are mostly hardcoded values that imply an extra degree of uncertainty in the results. Better methods are needed to have a more reliable analysis. Two examples could be for instance having a better way to estimate the pitching moment coefficient of the airfoil, or improving the current status of the DATCOM method for the estimation of the dynamic pressure ratio at the tail for large transport aircraft.

B

Three-Dimensional Views D239, D250 and D250-LH2 final family conceptual designs

The appendix provides the three standard views—plan, front, and side—of the main aircraft concepts resulting from the thesis study. The main aircraft dimensions, including maximum length, width, and height, are provided alongside key parameters relevant to the study. These include the landing gear position and the locations of the lifting surfaces, mainly wing and horizontal tailplane. The following illustrations are included:

- D239 family: the D239 and D239-short family designs are shown in Figures B.1 and B.2, respectively. The designs correspond to the results from Section 4.2.2.2, with the tail sized for the D239-short variant and shared among family members.
  The first figure provides a visual representation of the geometry of the reference aircraft concept from the study. The second figure highlights how the shortened version, the D239-short, compares to the main D239 family member.

- D250 family: the final D250 concept (long family member) is depicted in Figure B.3. This design features wing-integrated landing gear. The views provided correspond to the family design, with the tail sized for the D250-short variant as discussed in Section 5.1.3.

- D250-LH2 family: the final D250-LH2 concept (long family member) is depicted in Figure B.4. In contrast to the kerosene baseline above, the design features fuselage-integrated landing gear. The views provided correspond again to the family design, with the tail sized for the D250-LH2-short variant as discussed in Section 5.2.3.
  By comparing this Figure with Figure B.3 above, the main differences between the baseline design and the liquid hydrogen D250 concept are highlighted. Key distinctions include variations in fuselage length, wing position, landing gear integration, and tailplane size.

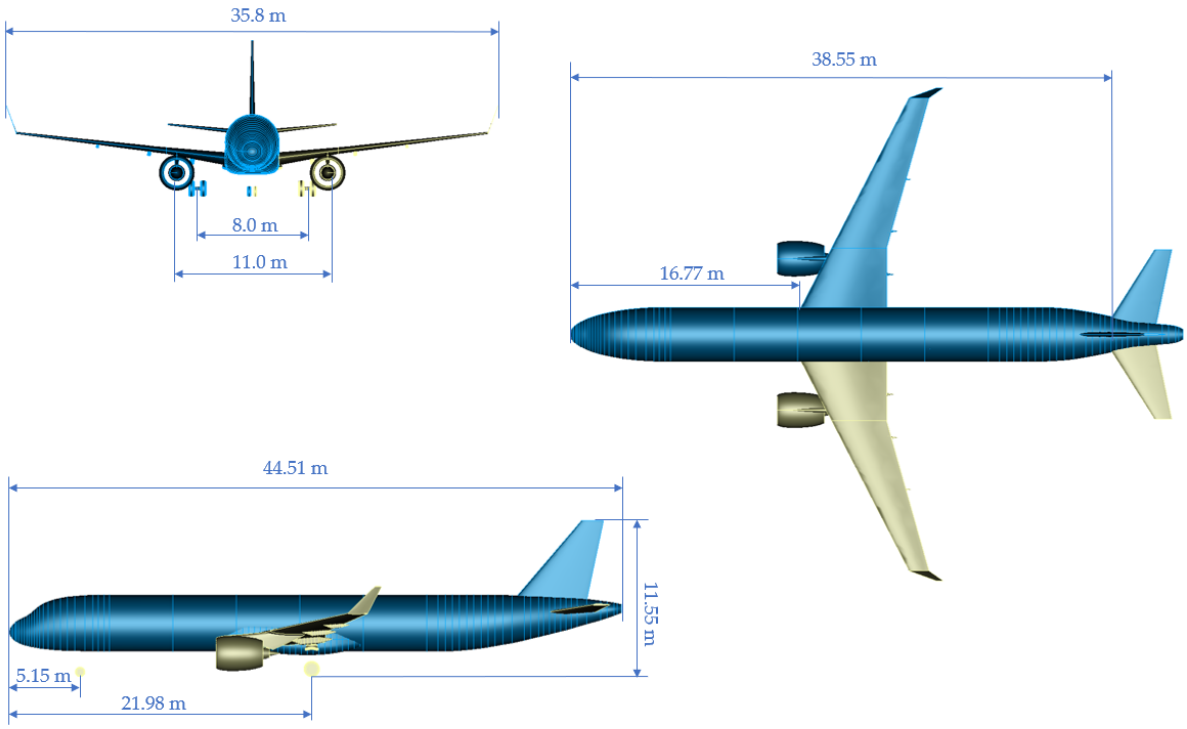

Figure B.1: Three standard views for the D239 final concept

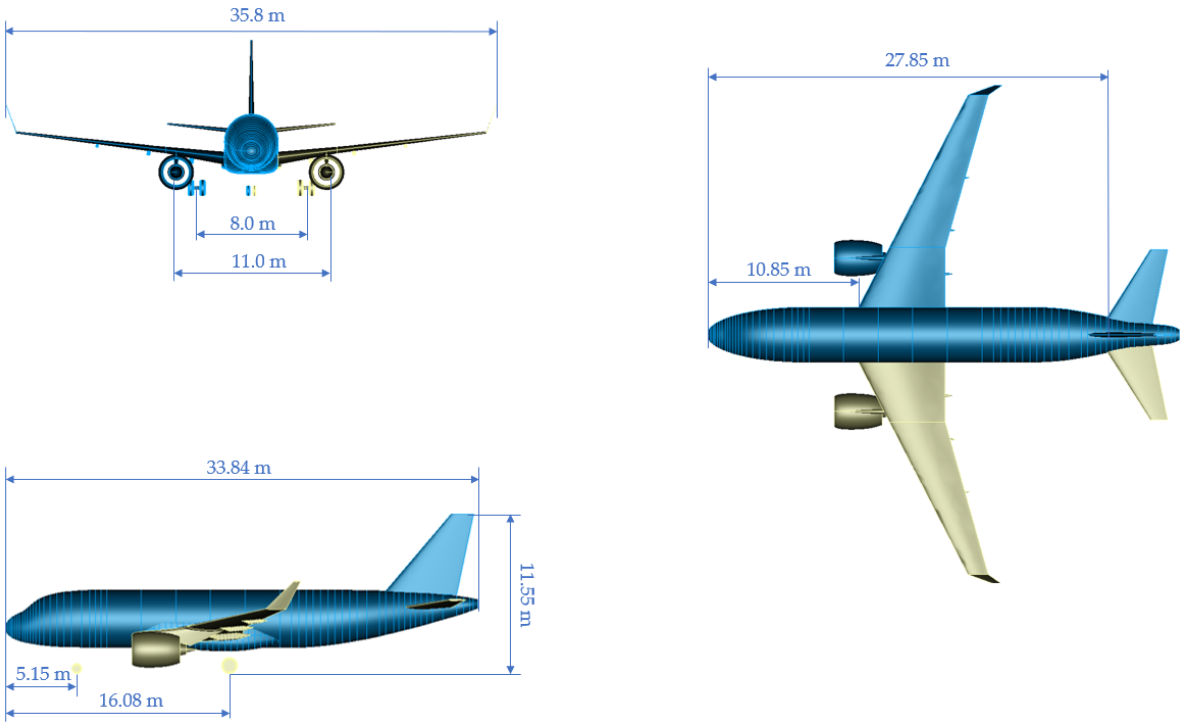

Figure B.2: Three standard views for the D239-short final concept

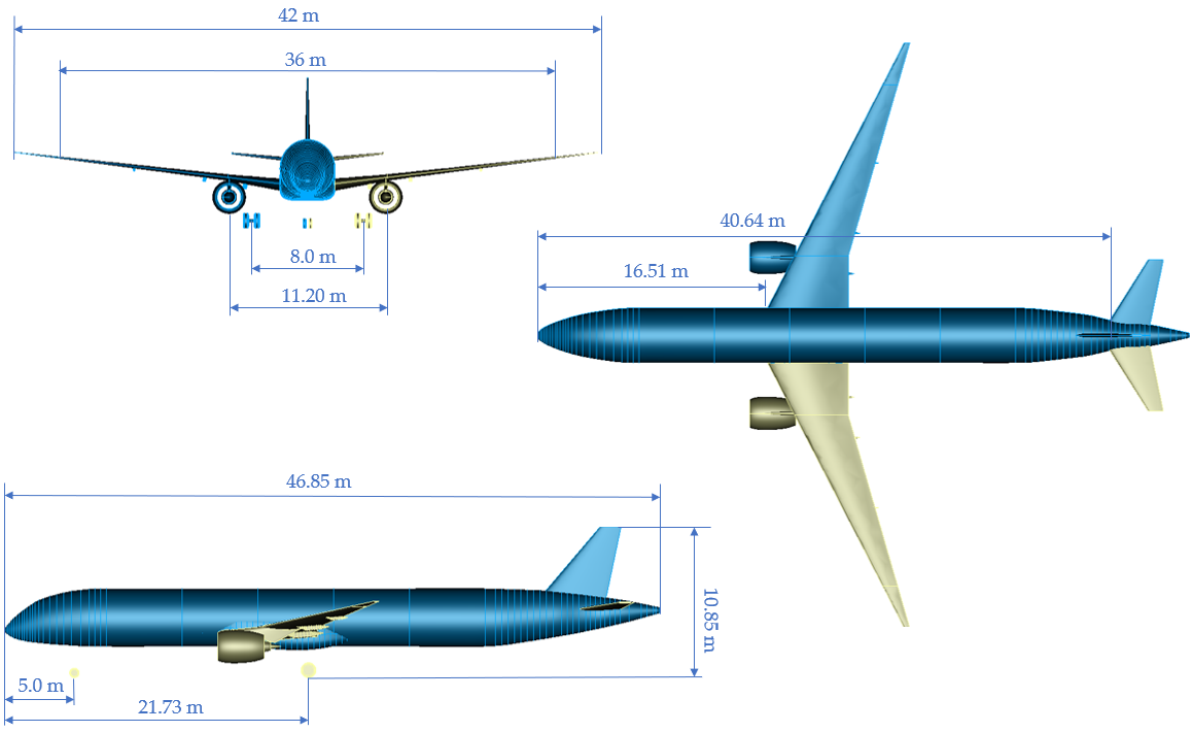

Figure B.3: Three standard views for the D250 final concept

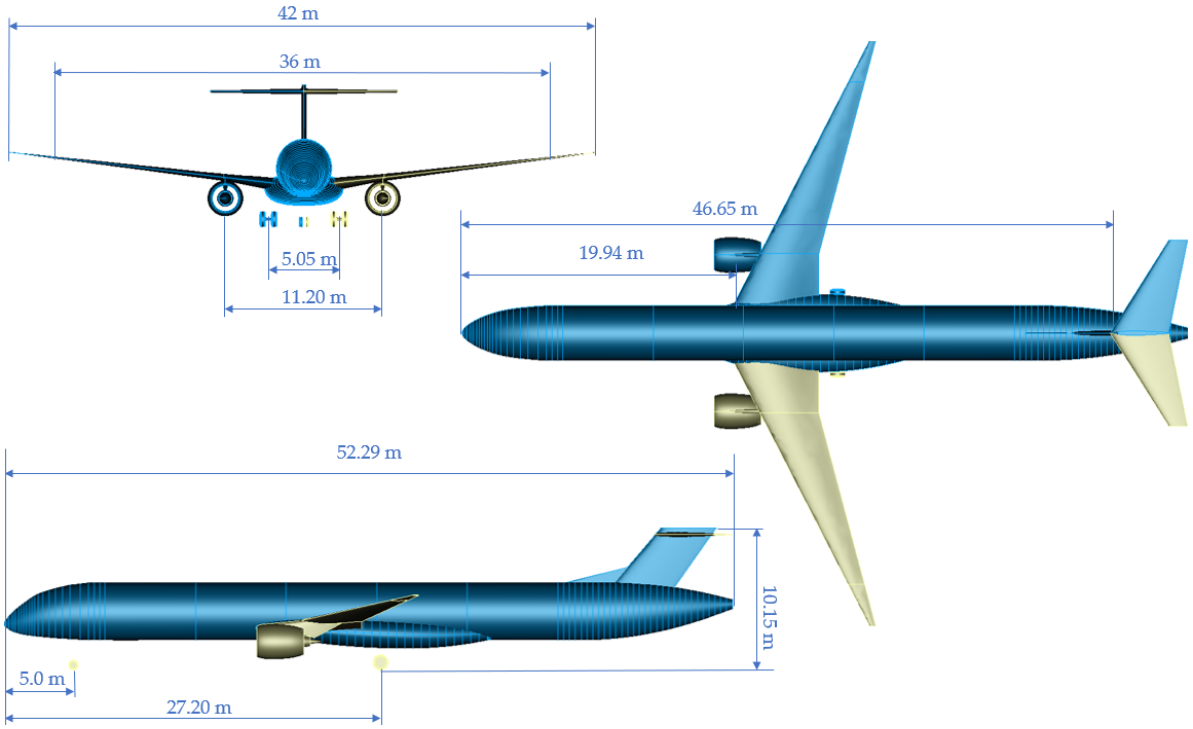

Figure B.4: Three standard views for the D250-LH2 final concept